HYDROLOGIC PROCESSES

IN UNSATURATED WASTE ROCK PILES

IN THE CANADIAN SUBARCTIC

by

STEVEN ALEXANDER MOMEYER

B.Sc. Simon Fraser University, 2003

A THESIS SUBMITTED IN PARTIAL FULFILLMENT OF
THE REQUIREMENTS FOR THE DEGREE OF

MASTER OF SCIENCE

in

THE FACULTY OF GRADUATE AND POSTDOCTORAL STUDIES

(Geological Sciences)

THE UNIVERSITY OF BRITISH COLUMBIA
(Vancouver)

July 2014

Abstract

Hydrologic processes occurring within waste rock situated in a semi-arid continuous permafrost environment at the Diavik Diamond Mine waste rock research project, located in Northwest Territories, Canada, were studied. Characterization of water flow through, and hydrologic properties of, waste rock is complicated by the heterogeneous clast composition, the spatial arrangement of these clasts, internal structures, and the unsaturated nature. Results are presented from experiments on six active zone lysimeters (AZLs), each with an approximate 5 cubic metre volume, along with three instrumented test piles, each with an approximate 3,000 square metre footprint and approximate 15 metre height. A basal drain collection system and individual basal collection lysimeters underlie each test pile to monitor water discharge. The test piles and AZLs were instrumented with monitoring devices designed to collect geochemical, thermal and hydrological data including moisture content, pore-water samples, pore-gas samples, temperature, thermal conductivity, air permeability, matric potential, and microbiology samples.

Results indicate that infiltration into the waste rock was dependent on the magnitude and timing of rainfall. Rainfall received after net radiation peaked in June permitted greater infiltration. Once infiltrated, water flow through the matrix was observed to be the dominate transport mechanism under average rainfall conditions despite a grain size distribution with less than 18% of the waste rock composed of the finer than 5-mm fraction. Only in response to large storm events was water flow through preferential flow paths observed. Continuous monitoring of water discharge at the base of the test piles indicated the rate of initial wetting front advancement under average precipitation was about 7.5 $m \cdot yr^{-1}$ and under drier conditions was about 6 $m \cdot yr^{-1}$. Based on solute transport determined from a tracer test at the AZLs, the average advective velocity during the active flow period was between 1.0 and 1.4 $m \cdot yr^{-1}$. Through the first three years of study, the active layer of the uncovered test piles extended the entire depth of the pile, although frozen areas within the core may remain. Each year the discharge period was shorter and less pile volume thaws, consistent with an overall cooling of the lower central core of the test piles.

Preface

The Diavik Diamond Mine Waste Rock Research project is a collaborate research project with researchers from the University of Alberta (UA), University of British Columbia (UBC) and the University of Waterloo (UW). To put this work in the broader context of the research project, theses and dissertations have been completed on the following topics:

Matthew Neuner (UBC) – Documents hydrology from years 1 and 2 predominantly concerning Type I and Type III piles as well as the active zone lysimeters (AZLs) along with laboratory derived hydrologic analyses (e.g., porosity, permeability, and soil water characteristic curves) (Neuner, 2009).

Liana Smith (UW) – Documents test pile construction, physical waste rock characterization and initial geochemistry (Smith, 2009).

Xiaotong Chi (UW) – Presents image analysis methodology for characterizing grain-size of constructed waste rock piles and wind-induced gas transport analyses (Chi, 2011).

Stacey Hannan (UW) – Explores the geochemistry/mineralogy of the waste rock test piles focussing on the 2010 to 2011 AZLs dataset and the correlation between the operational waste rock pile mineralogy and Type III waste rock test pile geochemistry (Hannam, 2012).

Nam Pham (UA) – Documents the thermal regime of the waste rock test piles and operational waste rock piles through an extensive dataset and numerical modelling (Pham, 2013).

Nathan Fretz (UBC) - Documents hydrology from years 1 through 6 as the waste rock test pile approached or entered a state of hydrogeological dynamic equilibrium (Fretz, 2013).

Brenda Bailey (UW) – Documents the geochemistry of the waste rock test piles from year 1 through 5 ((Bailey, 2013)).

This research builds upon the work of Mr. Matthew Neuner by adding data from years 3 and 4 for the Type I and Type III piles as well as the AZLs. This thesis extends these research efforts to include the results of the Covered test pile for years 1 through 4, set-up by various research group members, and to

report on additional experimental studies conducted. Data collected by Mr. Neuner, and automated monitoring systems, are relied upon to present the test pile evolution following construction in 2006 through the end of the 2009/2010 active season. In all cases, raw data from Mr. Neuner has been reprocessed to be seamlessly integrated with new data.

Mr. Mike Gupton, from UBC, collected data related to the covered test pile for years 1 and 2. This data has not been previously published. Again, this raw data was processed to be seamlessly integrated with new data from years 3 and 4 to evaluate the evolution of hydrologic processes in the covered waste rock test pile. Other researchers will report on surface hydrological processes in the cover material of the Covered test pile.

Mr. Nate Fretz, from UBC, continued this research project collecting and analyzing data through 2010 and 2011 field seasons and Mr. Andrew Krentz, from UBC, continues for the 2012 and 2013 seasons. There is some duplication of data presented in this thesis for years 3 and 4, since to understand the evolution of the waste rock test pile hydrology it was necessary for Fretz to rely upon to the complete dataset, and the work presented herein had not yet been formally documented. This independent review of the same data provides support to one another's conclusions as often the methodology or interpretation follows a different framework, but ultimately produces similar conclusions.

In Chapter 5, thermal data are reported from thermistors installed within the test piles, which was provided by Dr. Nam Pham from the University of Alberta. This data was used to compare the effect of the thermal regime on hydrologic process. Processed temperature readings provided by Dr. Pham were relied upon. Calculated areas of the unfrozen portion of the instrumented tip face on a daily scale provided by Dr. Pham were used to estimate the unfrozen volume of the Type I and Type III test piles to allow test pile discharge to be normalized to unfrozen volume.

Table of Contents

List of Tables

List of Figures

Acknowledgements

To all those who came before me and to all those who will come after me.

The author would like to thank the following individuals for support along the way: Dr. Leslie Smith, Dr. David Blowes and Dr. Dave Sego for the insight, patience and the opportunity to work on this project. The assistance of Diavik staff including Liana Smith, Dave Mohler and Clarence Choban was greatly appreciated, as was the food from the amazing kitchen staff. Matthew Neuner and Michael Gupton for their assistance at the start of the program. And Brenda Bailey, Jeff Bain, Richard Amos. For the work of all the co-op students who participated in the research project. Danny Bay for getting me started with Matlab.

To JB for the needed distractions, and for not letting school get in the way of our education. In addition, to Ellie who appeared along the way and finally forced me to complete this.

The author is thankful for financial support provided to the project by: Rio Tinto, NSERC, INAP, MEND, and CFI.

To all the teachers in my life; in whatever form they take.

1 INTRODUCTION

1.1 Literature Review

1.1.1 Background and Significance

Proponents of mine projects, regulators and society as a whole, each have motives to ensure that modern mine developments extract valuable resources while minimizing effects to the environment below thresholds where they are considered significant and adverse. The uneconomic waste rock and processed tailings generated at mine sites frequently contain a significant mass of sulphide minerals (such as pyrite and pyrrhotite) which can generate drainage of deteriorated quality. When not managed appropriately, weathering of these mine wastes can produce drainage of mine-impacted waters which at sustained loading to the receiving environment contaminate surface water and groundwater resources, potentially leading to regulatory non-compliance or environmental and socio-economic effects, or both. This acid mine drainage (AMD) generated from oxidation of these sulphide-bearing minerals proceeds by a bacterially mediated reaction in the presence of oxygen and water and is characterized by high sulphate concentrations, low pH and elevated concentrations of metals or metalloids (e.g., Arsenic) (equation 1-1) (Blowes et al., 2003).

$$2FeS_2\,(s) + 7O_2\,(g) + 2H_2O \rightarrow 2Fe^{2+} + 4SO_4^{2-}\,(aq) + 4H^+\,(aq) \qquad 1\text{-}1$$

Neutral mine drainage (NMD) is generated if there is sufficient acid buffering potential, usually in the form of readily soluble carbonates from minerals such as calcite, to neutralize the acidity and although characterized by near neutral pH, can also have elevated metals concentrations (Blowes and Ptacek, 1994; Heikkinen et al., 2009).

Impacts from AMD creates large liabilities for mining companies (Tremblay and Hogan, 2009). Operating mines can face post-closure liabilities of tens to hundreds of million dollars for remediation and treatment if issues related to drainage quality are not properly managed during the mine's life (INAP, 2011). The remediation cost of AMD related issues at abandoned mines in North America has been estimated in the tens of billions of dollars (INAP, 2011).

Therefore, mine planning requires reasonably accurate prediction of the drainage quality emanating from mined material. Likewise, mine development requires proper management of this drainage. Ultimately, mine closure requires design and implementation of a sound closure plan to manage effects from mine-impacted drainage on the receiving environment. Prediction and management of mine drainage requires an understanding of its geochemical generation, and evolution, along with fluid flow and transport processes. The research documented in this thesis characterizes and investigates fluid flow and transport processes in stockpiled mine generated waste rock.

Uneconomic rock removed to access ore is stored in waste rock piles which can have footprints covering hundreds of hectares and reach hundreds of metres in height (Blowes et al., 2003). The potential environmental risks and liabilities posed by reactive sulphide minerals in mine wastes can persist for decades to centuries (Nordstrom and Alpers, 1999; Meldrum et al., 2001; Price, 2003; Moncur et al., 2005; Kuipers et al., 2006; Slater and Moodie, 2008). Effects of mining on the environment by oxidation of sulphide minerals has been documented since the mid-16th century (Agricola, 1556); however, only over about the last three decades has significant attention been placed on improving mining practices to limit effects to the environment from AMD (Price, 2003;Tremblay and Hogan, 2009). Less attention has been directed towards waste rock, particularly with respect to characterization of hydraulic properties and fluid flow and solute transport mechanisms. Since about the mid-1990's studies quantified net infiltration to waste rock (Harries and Ritchie, 1983) or characterized unsaturated hydrogeologic properties of waste rock (Diodato and Parizek, 1994; Morin et al., 1994) but comprehensive data sets quantifying hydrologic properties of waste rock piles including discharge rates, fluid potential and volumetric water balances were limited (Morin et al., 1991; Smith et al., 1995). The research and datasets on hydrologic processes in waste rock continue to grow, including those from specifically designed research projects on larger-scale experiments designed for the purpose of quantitative assessments of hydrologic properties and fluid flow and transport mechanisms in heterogeneous waste rock, including the use of well instrumented test piles (e.g., University of Saskatchewan et al., 1999; Bellehumeur, 2001; Nichol, 2002; Wagner, 2004; Fines, 2006; Stockwell et al., 2006; Corazao Gallegos, 2007; Marcoline, 2008; Andrina et al., 2009; Bay, 2009; Rohde and Williams, 2009; Fretz, 2013, and Neuner et al., 2013). Studies of sites under different climatic conditions, and of different waste rock compositions, help to further our understanding of the

behaviour of water movement within waste rock piles and the processes influencing drainage quality (Smith and Beckie, 2003). From these studies, factors that influence the hydrology, and hydrologic properties, of waste rock include the heterogeneous clast composition, the spatial arrangement of these clasts, the internal structures created during, or post, deposition, and the variably saturated nature of the rock piles.

1.1.2 Heterogeneous Clast Composition

Waste rock piles have a heterogeneous clast composition which include a range of grain sizes, from clay-sized fraction to boulders (Nichol et al., 2005; Chi, 2011; Neuner et al., 2013). The grain size distribution contained in a waste rock pile is determined by the geological properties of the material, the mining technique used, and the waste rock deposition method (Smith and Beckie, 2003). Waste rock piles, or zones within a pile, can be classified as being soil-like or rock-like (Smith and Beckie, 2003). Waste rock with a large content of fines (greater than 20% sand-sized grain fraction and finer) is visualized as a fine-grain matrix supporting larger clasts and therefore the material can be considered soil-like with hydraulic properties reflective of the fine-grained matrix. Rock-like waste rock is visualized as having matrix free zones with rock-to-rock point contacts and therefore the fluid flow mechanisms and hydraulic properties are reflective of the coarse-grained material. The difference in the connected fine-grained matrix fraction and pore-space created by areas of adjacent larger clasts without intervening matrix affects unsaturated water flow.

1.1.3 Internal Structures

Internal structures arise from the construction method used to place the waste rock but are also created by variation in material type properties and generated post-construction. Internal structures include angled layers, stratified layers or pockets of fine-grained material or coarse-grained material, coarse-grained toes, pavement surfaces (i.e., compacted layers created by mine vehicle traffic during deposition), and low-permeability layers created as a result of weathering and downward migration of particles (Morin et al., 1991; Smith and Beckie, 2003; Stockwell et al., 2006; Andrina et al., 2009).

1.1.4 Waste Rock Stockpile Construction

Waste rock can be placed by end-dumping, push-dumping, free dumping or dragline spoiling (Morin et al., 1991). The internal structures and distribution of grain size fractions are affected by the method used to place the material. End-dumping creates piles with finer particles concentrated near the dump crest grading to coarser particles at the dump toe (Golder Associates Ltd., 1989). Alternatively, instead of progressive grading, distinct zones may develop, following a similar pattern of finer particles concentrated near the dump crest and coarser particles accumulated at the dump toe (Nichols, 1986). Push-dumping forms piles with coarse-grained material accumulating at the toe, but does not generate the concentrated fine particles near the crest (Nichols, 1986). Segregation of the coarse-grained material occurs to a lesser extent during push-dumping than from end-dumping. Free-dumps are deposited from a haul truck and then spread-out into a lift, or layer, on a flat surface of the waste rock pile. Limited segregation of different grain-sizes occurs during free-dumping, however compaction of the deposited material occurs from vehicle and equipment traffic. The upper-most layer of a free-dump may not be spread-out and instead, be left as an uncompacted, hummocky deposit. Dragline spoils are deposited directly to the dump surface and result in little compaction or grain-size separation (Morin et al., 1991).

1.1.5 Unsaturated Waste Rock

The unsaturated nature of waste rock piles affect the hydraulic properties of the material as changes in moisture content, and matric suction, will change the hydraulic conductivity of the material. Functions are needed to describe the relationship between matric suction and volumetric soil moisture, and both of these to hydraulic conductivity, instead of single values used to represent material when saturated. Material properties may also be characterized differently if the material is wetting or drying due to hysteresis. The soil water characteristic curve presented in **Figure 1-1**, relates matric suction to volumetric soil moisture, and demonstrates how the fine-grained soil with an air entry value that occurs at a higher value of matric suction will begin to desaturate later than a coarse-grain soil under drying conditions. Under wetting conditions the lower matric suction water entry value of the coarse-grained material results in the coarse material not allowing flow to occur through the pores until a larger pressure is achieved than for the finer-grained material.

In saturated porous material, a coarse-grained material has higher hydraulic conductivity than a finer-grained material, but as the materials desaturate there is a matric suction above which the finer-grained material becomes more permeable than the coarse-grained material (**Figure 1-2**). The result, is that at high values of matric suction and low moisture content, water will occupy, and flow through, the fine-grained matrix material, whereas larger pores will be air filled.

Infiltration to waste rock will be spatially variable, reflecting the variation in the hydraulic conductivity and spatial arrangement of the materials on the surface. Water flow will predominantly occur through the fine-grained matrix material in response to infiltration rates that are less than the saturated hydraulic conductivity value of the fine-grained material (Nichol, 2002; Okane Consultants, 2004). Areas of a waste rock pile composed of coarse-grained material will only transport water under higher infiltration events; which will have an effect on solute transport. Since larger pores are air filled under dry conditions, accumulation of high-solubility efflorescent evaporite minerals and weathering products may occur on the pore walls. These accumulated minerals will be dissolved and mobilized during infiltration events that follow dry periods producing discharge that contains relatively high dissolved loads (Nordstrom and Alpers, 1999).

1.1.6 Infiltration

Further external factors related to climate, underlying soil/rock, and topography influence the hydrology of waste rock piles. Precipitation received on the surface of a waste rock pile, may infiltrate, evaporate or run-off. Water infiltration through the surface of a waste rock pile is affected by the rainfall intensity, infiltration capacity of the material at the surface, the surface texture and topography, antecedent moisture content and vegetation cover, if present (Smith and Beckie, 2003). At the start of a rainfall event both gravity and capillarity draw water into the pile. If the surface layer approaches near-uniform moisture content, the infiltration rate stabilizes at a rate approximately equal to the hydraulic conductivity. At the surface of a heterogeneous waste rock pile, when the rainfall rate exceeds the infiltration capacity of fine-grained material, infiltration through coarse-grained pathways will be activated. Ponding and surface runoff occur when the rainfall rate exceeds the infiltration capacity of the surface. Evaporation from the pile surface, will affect the net infiltration and is dependent on the energy received at the surface and on

the hydrologic properties of the surface. The spatial and temporal variation in mass loadings from a waste rock pile is linked to these local climatic dependent processes.

1.1.7 Water Flow Mechanisms

The mechanism of water flow through the heterogeneous unsaturated material following infiltration will affect the geochemical signature of the drainage. Two main types of water flow mechanisms through waste rock piles are: matrix flow and preferential flow (Elboushi, 1975; Beven and Germann, 1981; Eriksson et al., 1997; Newman et al., 1997; Smith and Beckie, 2003; Nichol et al., 2005; Neuner et al., 2013). Water flow through the fine-grained matrix material is under capillary tension and gravity. Water flow through the matrix can be described by Richards equation, written in one dimension as:

$$\frac{\partial\theta(\psi)}{\partial t} = \frac{\partial}{\partial z}\left[K(\psi)\left(\frac{\partial\psi}{\partial z} + 1\right)\right] \qquad 1\text{-}2$$

Where the rate of change in soil moisture content (θ) with time results from a change in hydraulic conductivity ($K(\psi)$) with changes in matric potential (ψ) with depth (z) and the change in hydraulic conductivity with changes in depth.

Water flow through preferential pathways includes macropore flow (Beven and Germann, 1981), and film flow (Tokunaga and Wan, 1997). The term preferential flow, encompasses flow mechanisms that move water through localized pathways and at rates greater than average velocity (Nichol et al., 2005).

Capillary barrier flow (Fala et al., 2005) could be included as a preferential flow mechanism because the flow path is restricted along a specific route, however it differs the from the rest of the group because it does not result in faster water transit the way the other preferential flow mechanism do and it is governed by the Richards flow equation. Capillary barrier flow occurs where fine-grained material overlying coarse-grained material creates a break at which infiltrating water will not enter the coarse-grained material because the water entry value of the coarse-grained material occurs at comparatively lower matric suction and therefore the water flow occurs in the fine-grained material at the interface between the two materials.

Water flow through macropores occurs in connected pore-spaces created between clasts with greater than about a 5 mm diameter (i.e., corresponding to fine gravels in the Unified Soil Classification System) which are matrix free. Flow of water through macropores is gravity driven (non-capillary) and is activated under high infiltration events (Bellehumeur, 2001; Nichol et al., 2005).

Modeling studies of fluid flow and solute transport in waste rock often rely on representation of separate matrix and macropore domains to capture these two flow mechanisms or the non-uniform characteristics of the material. Dual porosity models (Van Genuchten and Wierenga, 1976; Decker and Tyler, 1999) or dual permeability models (Gerke and van Genuchten, 1993) both describe solute exchange between the domains, but dual porosity models consider fluid in the matrix domain is immobile. These differences in matrix and preferential flow lead to differences in residence time and drainage quality. Preferential flow is attributed as one possible explanation for the disagreement at some waste rock piles between mass loading rates calculated from laboratory humidity cell tests and those rates observed from field measurements (Velbel, 1993; Eriksson and Destouni, 1997). As non-capillary flow moves water more rapidly through the pile, and in matrix free areas, there is less interaction with exposed mineral surfaces. Water flow through the matrix material moves at a slower rate and interacts with a larger surface area of potentially reactive minerals within the pile (Smith and Beckie, 2003).

Displacement flow through the matrix can occur by propagation of a pressure wave downwards through the porous media in response to infiltrating water. This response has been observed to occur at velocities significantly greater than the velocity of a particle of water (i.e., average velocity of a conservative tracer) and is described by kinematic wave equation (Rasmussen et al., 2000; Neuner et al., 2013). Therefore rapid changes in discharge at the base of waste rock, may represent a response to the wetting front or the presence of preferential flow (Nichol et al., 2005).

Transport of dissolved solids will occur by advection, dispersion and diffusion.

When waste rock is deposited in a stockpile, the moisture content is generally less than its field capacity. Water initially infiltrating will be retained in the matrix due to capillarity. Significant time may be required for waste rock to reach its field capacity and drainage to occur (Swanson et al., 2000). The time required

is dependent upon initial moisture content, net infiltration, volume of fine-grained material in waste rock pile and the field capacity (Smith and Beckie, 2003).

1.1.8 Cold Regions Considerations

In cold regions, AMD is affected by annual freeze–thaw cycles that influence mineral weathering rates, fluid flow, and aid physical weathering. Prediction and mitigation performance from mined material at northern mines need additional consideration. From a rock drainage quality perspective, the following climatic features are important: temperature, humidity, rainfall, total spring snow-pack, number of days that ground temperature exceeds 0°C and the presence and type of permafrost (Indian and Northern Affairs, 1993). Geochemical processes in cold regions are also affected (SRK Consulting and Mehling Environmental Management Inc., 2006). Oxidation rates of sulfide minerals are temperature dependent and the Arrhenius equation provides a relationship for the temperature dependence of the reaction rate. Different types of bacteria can be active at sub-zero temperatures and can adapt to low temperature conditions. Further, solubility limits of oxygen and many metals will be greater at lower temperatures. Fluid flow may occur at temperatures below zero due to freezing point depression. Physical exposure of minerals due to freeze-thaw processes has potential implications for the exposure of reactive minerals to oxidizing conditions.

Although mines sites in cold regions can potentially use thermal controls advantageously, it may not be sufficient to rely upon the thermal regime alone to mitigate potential effects (Holubec, 2004). Covers utilized in cold climates need different consideration than in warmer climates (Rykaart and Hockley, 2009; Rykaart and Hockley, 2010). Regardless of the long-term outcome, drainage quality of the material until the onset of freezing needs to be predicted and mitigated. A cover may delay freezing by providing insulation initially, which could allow reactions and drainage to occur year-round. For example, in Rankin Inlet, Nunavut, after 30 years of acidic drainage from the tailings, the material was buried in the abandoned open-pit and are predicted to require 15 years before freezing (Meldrum et al., 2001). Future climatic conditions also need to be considered. If sulphide-bearing materials freeze, attention to drainage from the active layer is still required. If future conditions are warmer than current conditions an increase in the thickness of the active layer in mined materials will increase the volume of reactive material and

therefore increase the mass loadings. Freeze-thaw conditions need to be considered in the design of a cover.

1.1.9 Scale-Dependence

Prediction of drainage quality from mine wastes has proven challenging (Velbel, 1993; Malmström et al., 2000; Kuipers et al. 2006). Waste rock characterization and drainage chemistry prediction occurs from data collected on a range of different scales that includes laboratory studies (e.g., analytical analyses, humidity cells and column experiments), field studies (e.g., field cells, lysimeters, and test piles) and full-scale waste rock piles. Laboratory studies and to an extent, field studies, have the limitation of not being capable of testing, in a holistic manner, the full range of heterogeneity or internal structures that would be present in a full-scale waste rock pile and therefore may not accurately predict drainage quality. Waste rock test piles provide an opportunity to study a smaller-scale version of a full-scale waste rock pile capable of including the full range of clast sizes, and some of the internal structures that are created during deposition (Nichol et al., 2005; Neuner et al., 2013). Although it may be possible to recreate internal structures by mimicking construction methodologies and inclusion of the full range of material that would be deposited in a waste rock pile, limitations still exist from their scaled-down nature (e.g., proportion of batter area to inner volume or proportion of active zone development compared to pile depth). Boundary conditions, specifically the batters of the piles, can overestimate the influence that these boundaries have on water, and air, flow along with geochemical and thermal patterns when compared to the larger full-scale waste rock pile. Despite these limitations, hydrologic processes occurring within waste rock test piles and field cells are studied to gain information for mine planning and mine closure. Exposure to field conditions and testing of a representative range of material lessen but do not remove the dependence on scaling corrections. Experiments designed to study the scale-dependence from prediction at the laboratory-scale to field-scale to full-scale are needed to develop and assess scaling approaches and relationships for better long-term drainage quality management from mine wastes.

The following presents on overview of the collaborative Diavik Diamond Mine waste rock research project and details the experiments and data set with respect to hydrologic processes observed over the initial four-year study, 2006 through 2009.

1.2 Overview: Diavik Diamond Mine Waste Rock Research Project

1.2.1 Waste Rock Test Pile Set-Up

The Diavik Diamond Mine, located about 300 kilometers (km) northeast of Yellowknife in Northwest Territories, Canada (**Figure 1-3**), is host to a collaborative waste rock research project between the University of Alberta (UA), University of British Columbia (UBC), and University of Waterloo (UW). Results from the project provide insight to the relationship between the geochemical, hydrological, and thermal regime on the behaviour of waste rock piles situated in a semi-arid continuous permafrost environment. The research presented in the following thesis contributes to our understanding of waste rock pile hydrology and the interaction of processes (e.g., effect of thermal regime) by relying on new data collected in 2008 and 2009 and supplementing with data previously collected on the project in 2006 and 2007.

The research project consists of three instrumented test piles, each with an approximate 3,000 square metres (m^2) footprint and approximate 15 metre (m) height, constructed by end-dumping and bulldozer push-dumping. The run-of-mine waste rock at Diavik is segregated based on total sulphur content into three classes as follows: Type I contains average total sulphur (S) concentration of less than 0.04% by weight, Type II between 0.04 and 0.08% S by weight, and Type III greater than 0.08% S by weight (Smith et al., 2013). The multi-pile experimental design allows data collection from two of these rock classes and inclusion of a potential closure strategy. One test pile is composed of Type I rock (containing an average concentration of 0.035% S by weight); a second test pile is constructed of Type III rock (containing an average concentration of 0.053% S by weight); and a third test pile consists of a core of Type III rock (containing an average concentration of 0.082% S by weight), which has been re-graded and covered with a compacted till layer and thermal cover of Type I rock (Smith et al., 2013) (**Figure 1-4**). Although the waste rock contains low S concentrations there is a comparative lack of neutralizing potential (Smith et al., 2013). Type III rock is classified as potentially acid generating by standard acid base accounting methods, due the sulphide mineralogy in the biotite schist.

The grain-size distribution on the surface of the Type I and Type III test pile batters was analysed photographically (Chi, 2011). As is typically with end-dumping construction methods, this analyses

demonstrated that the finer-grain size fraction was retained near the crest of the pile and the grain-size fraction graded to coarser particles non-linearly from the crest to the toe of the pile. The grain-size fraction finer than 100 mm comprises the greatest surface area while the fraction greater than 100 mm makes up the greatest mass.

Test pile construction details are provided in Neuner (2009), Smith et al. (2013), and reiterated in Fretz (2013). A brief summary is provided here to aid in the subsequent discussion of results. A high density polyethylene (HDPE) liner was placed on top of a graded base to form the basis of a basal drain collection system (**Figure 1-5a**). This drainage collection system consists of a basal drain and individual basal collection lysimeters. The basal drain consists of a perforated 152 mm nominal diameter polyvinylchloride (PVC) pipe on top of the HDPE liner, which directs drainage to an instrumentation trailer. The PVC drain lines are heat-traced with temperatures set to maintain between about 5 and 10 degrees Celsius (^{o}C). The basal perimeter of the piles consists of a 0.5-m high berm, which the HDPE liner extends over, to contain all water seeping from the base of the piles. In addition to the basal drain collection system, individual lined basal collection lysimeters were constructed at the base of the test pile under the central portion of the test pile and a portion of the batters. These basal collection lysimeters are either 4m^2 or 16 m^2 and direct infiltration to separate flow and geochemistry monitoring instruments inside an instrumentation trailer (**Figure 1-5b**). The test piles were constructed on top of the basal drainage systems by end-dumping and bull-dozer push-dumping from a constructed ramp (**Figure 1-5c**). These construction methods result in tip faces at about 38 degrees (^{o}), the angle of repose for the waste rock. The Covered test pile was subsequently re-graded to 18.4^{o} prior to covering with 1.5 m of compacted till and 3 m of Type I waste rock. Construction of the Type I and Type III waste rock test was completed between August and September 2006. Construction of the Covered test pile was completed in the winter of 2007.

Four tip faces were instrumented with a series of monitoring devices designed to collect geochemical, thermal and hydrological data including moisture content, pore-water samples, pore-gas samples, temperature, thermal conductivity, air permeability, and microbiology samples (**Figure 1-5d**). Specific instrumentation installed within the piles to collect hydrology related data included: custom built time

domain reflectrometry (TDR) probes for volumetric moisture content determination; commercial TDR ECH_2O probes (Decagon Devices Inc.) also for determining volumetric moisture content as well as temperature, and bulk soil electrical conductivity (EC); and tensiometer probes for monitoring matric potential (soil tension) (Soil-moisture Equipment Corporation). Outflow discharge rates and geochemistry parameters (pH, EC, temperature) are continuously monitored in instrumentation trailers from infiltration reaching the base of the test piles via the basal drain collection system and basal collection lysimeters (**Figure 1-6**). As reported by others (Fretz, 2013; Smith et al., 2013), instrumentation leads were excavated from the surface of the test piles which disturbed any traffic surface created during pile construction, and as might be expected to develop during construction of a full-scale pile. Further, an excavator placed a 0.5 m cover over the instruments to add a layer of protection, which may influence the internal structure when compared to placement of material by standard end-dumping or push-dumping.

Included in the continuum of scales used to predict the quantity and quality of the drainage from waste rock between laboratory experiments and full scale waste rock piles, as well as to study active zone processes, the experiment also consists of six collection lysimeters with an approximate volume of 5 m^3. These active zone lysimeters (AZLs) are constructed from HDPE tanks and situated adjacent to the test piles (**Figure 1-7**). Two of the AZLs are filled with Type III rock and two filled with Type I rock. Two were also filled with Type III rock then covered with compacted till, and Type I waste rock, similar to the construction of the Covered test pile. Construction of the AZLs was completed in September 2006 (Neuner 2009). **Figure 1-7** shows AZLs construction. The AZLs extend to a depth of 1.70 m (Type III) or 1.45 m (Type I) and therefore are designed to represent processes occurring in the active zone of the waste rock. An excavator placed waste rock in the AZLs and therefore the surface was not compacted by heavy machinery as would occur on a typical full-scale pile. The AZLs containing Type III material have a surface area opening of 2.09 m^2 and the AZLs containing Type I material have a surface area opening of 3.60 m^2. The volume of each AZLs is approximately equivalent at 5.24 m^3 for the Type III and 5.22 m^3 for the Type I. Observations of the surface of the AZLs indicate a distinct difference in the grain size that appear on the surfaces (**Figure 1-8**). Numerous boulders (clasts greater than 256 mm) are clearly visible on the surface of the western Type I AZLs along with cobbles and gravels. Uncompacted fine-grained material predominantly covers the surface of the eastern Type I AZLs. The Type III lysimeters both show

a range of grain sizes on the surface. The depth to which these differences extend is not known, however the variation between eastern and western Type I lysimeters is noted as this grain size distribution may affect infiltration rates. Maximum clast size placed into the AZLs was between about 1 m (Neuner et al., 2013) and less than 2 m (Smith et al., 2013).

Additionally, hydraulic properties of the waste rock have been characterized with a 32 m^3 field scale permeameter, constructed in 2009.

Neuner (2009), Smith et al. (2013), and to a lesser degree Fretz (2013), provide instrumentation details for the Type I and Type III piles along with for the AZLs. Smith et al. (2013) reports instrumentation location information for the Covered test piles. For reference and clarity a table of instruments and their location within each test pile which provided data used in this thesis is included in **Appendix A**. Instrumentation type and function for the Covered test pile is the same as those reported in Neuner (2009), however specific calibration information, not reported by Neuner is provided in **Appendix A.** Similarly, any new calibration data, not reported by Neuner, for instruments utilized in years 3 and 4, is also provided in **Appendix A.**

A naming convention exists for all instruments installed at the test piles and AZLs. In general, the following attempts to provide a 'clear language' descriptive location for the area of the test pile that the data were obtained. However, in some places the instrument identification label has been used to specify the location. The following provides the naming convention for all the instrumentation installed within the test piles and AZLs, using 12E2tdr03 as an example.

The first character indicates the test pile (e.g., '1' represents the Type I test pile), the second character indicates the tip face (e.g., '2' represents the 2nd tip face), the third and fourth characters describe the sensors location with respect to the centre line of the test pile (e.g., 'E2' represents 2 m east of the centre line), the fifth through seventh characters indicate the instrument type (e.g., 'tdr' indicates a TDR probe), and the eighth and ninth characters indicate the depth the sensor is located beneath the crown of the test pile (e.g. '03' indicates 3 m below the crown).

1.2.2 Regional Setting

The Diavik Diamond Mine is located on the 20 km^2 island (East Island), within in Lac de Gras, in the Canadian subarctic, in a zone of continuous permafrost. Based on the derived regional analyses for Diavik between 1959 and 2006 the mean annual temperature is -10.1 ºC and ranges from a minimum mean monthly temperature of -29.4ºC in January to a maximum mean monthly temperature of 12.0ºC in July (Golder Associates, 2008). The climate is characterized by long cold winters and short warm summers, with eight months of the year having a mean monthly temperature less than 0ºC. This limits the period when infiltration occurs to between May and October. Long-term mean annual precipitation based on regional analyses is 350.9 mm, with 163.9 mm (47%) occurring as rainfall (Golder Associates, 2008).

The area is part of the Canadian Precambrian Shield; locally identified geology includes greywacke-mudstone metaturbidites, biotite and hornblende tonalite to quartz diorite, and mica or potassium feldspar porphyritic granite and granodiorite (Roscoe Postle Associates Inc., 2005). The diamond deposits are hosted in kimberlite pipes and the country rocks have been identified as metamorphosed turbidites composed of muscovite-biotite granites intruded by pegmatite and biotite schist. Sulphide minerals are present in the biotite schist in the form of pyrrhotite ($Fe_{(1-x)}S$), along with lesser amounts of chalcopyrite ($CuFeS_2$) and sphalerite (Zn,FeS) (Smith et al., 2013). The area was glaciated by the Laurentide Ice Sheet during the Pleistocene glaciation and surface deposits consist of a veneer of till or glaciofluvial deposits.

As described in the following subsection, this research aims to provide additional field characterization, to add to the growing body of research to assist in the characterization, prediction, performance evaluation and closure implementation of mined material, specifically waste rock situated in semi-arid continuous permafrost regions.

1.2.3 Thesis Scope and Organization

This research documented the evolution of test pile hydrology and thermal interaction through the four year dataset by synthesizing hydrology data from 2006 (year 1) through 2009 (year 4) for the Covered test pile and between 2008 (year 3) and 2009 (year 4) for the Type I and Type III test piles along with the AZLs. For Type I and Type III test piles, data from 2006 and 2007 (year 2) was also incorporated to

facilitate an understanding of the hydraulic evolution of these test piles. Additional experimentation included testing on a 27 m^3 field permeameter and conducting a conservative tracer experiment on the AZLs. Data obtained from the experiment was incorporated into the understanding of water movement through waste rock and evidence identified to support different flow mechanisms occurring within this unsaturated waste rock was presented.

Specific research objectives of the research as outlined below include:

- To determined mean residence time and mean advective velocity of a conservative tracer at the AZL scale.
- To characterize porosity and saturated hydraulic conductivity from a 27 m^3 field permeameter.
- To provide an accounting of infiltration, evaporation, storage and drainage to understand the water balance components.
- To quantify net infiltration to the waste rock under a range of precipitation conditions.
- To evaluate the application of the extended Penman-Monteith model to estimate evaporation from this waste rock surface.
- To document the evolution of test pile hydrology from changes in storage and drainage over the four-year period between 2006 and 2009.
- To quantify the range of wetting front velocities generated in response to different infiltration rates.
- To evaluate flow mechanisms from the relationship between electrical conductivity and discharge.
- To quantify changes in the hydrologically active volume of piles with changes in the depth of active layer.
- To assess the effect of high solutes concentrations on pore-water freezing by using the EC from samples collected in SWSS with VMC.
- To assess the effect of freezing front migration on test pile hydrology.

This thesis is composed of six chapters including an overview of the current literature on hydrology of waste rock piles, an introduction to the Diavik Waste Rock Research Project, including the study area and along with background information on the experimental design and construction, needed for interpretation in the subsequent chapters (Chapter 1). Chapter 2 describes and presents the results and analyses of a tracer test initiated in 2008 at the AZL, while Chapter 3 describes and presents the results of a 27 m^3 field permeameter experiment conducted in 2009. Chapter 4 presents an accounting of water balance components: infiltration, evaporation, storage, and discharge. Chapter 5 focuses on flow mechanisms by tracking the discharge in response to rainfall events and explores the relationships between the hydraulic regime and thermal regime. Chapter 6 summarizes the key findings and conclusions of this research. Chapter 2, 4, and 5 are written as mostly stand-alone reports, with the exception that a separate abstract and site details are not repeated. Chapter 3 documents work completed and observations from the data, but does not form the bulk of this work. Chapter 4 and 5 describe and interpret aspects of the research that overlap with some discussion provided by Fretz (2013), however focus on a shorter timeframe covering the initial four years of the experiment.

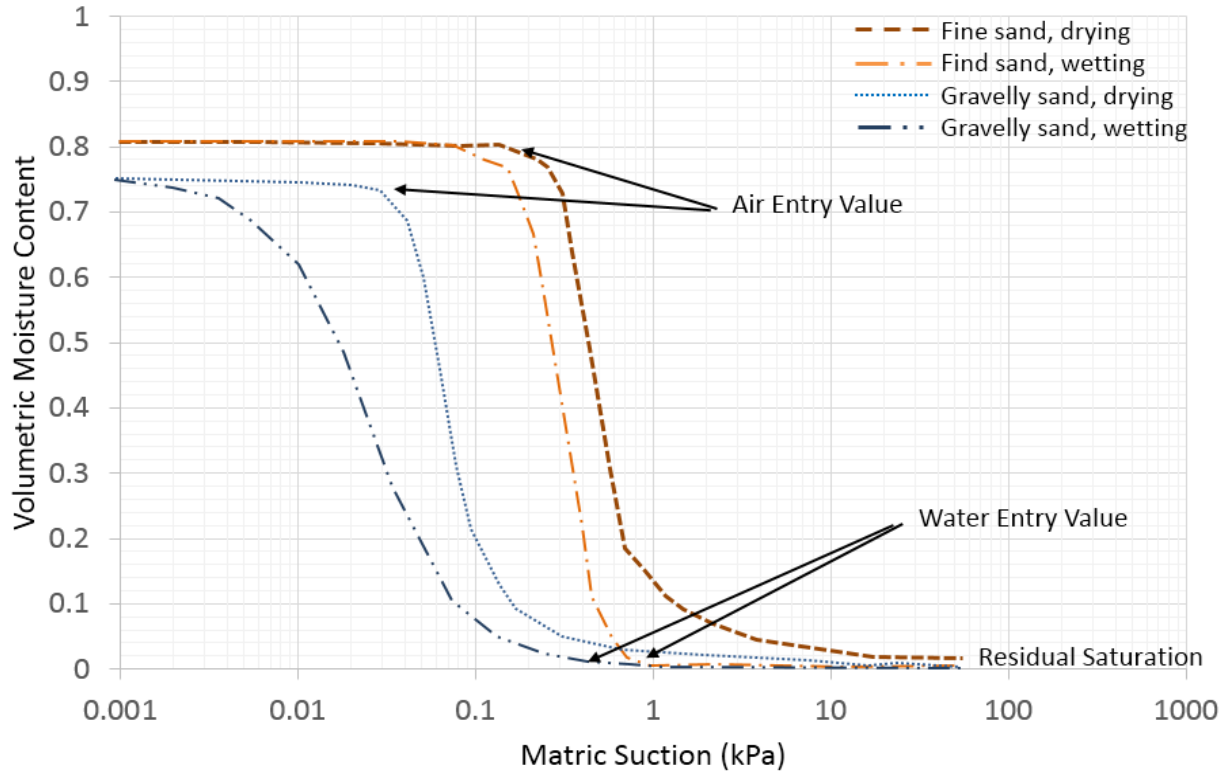

Figure 1-1: Example of soil water characteristic curve to illustrate important differences between a coarse and fine-grain soil (adapted from Tami et al., 2004).

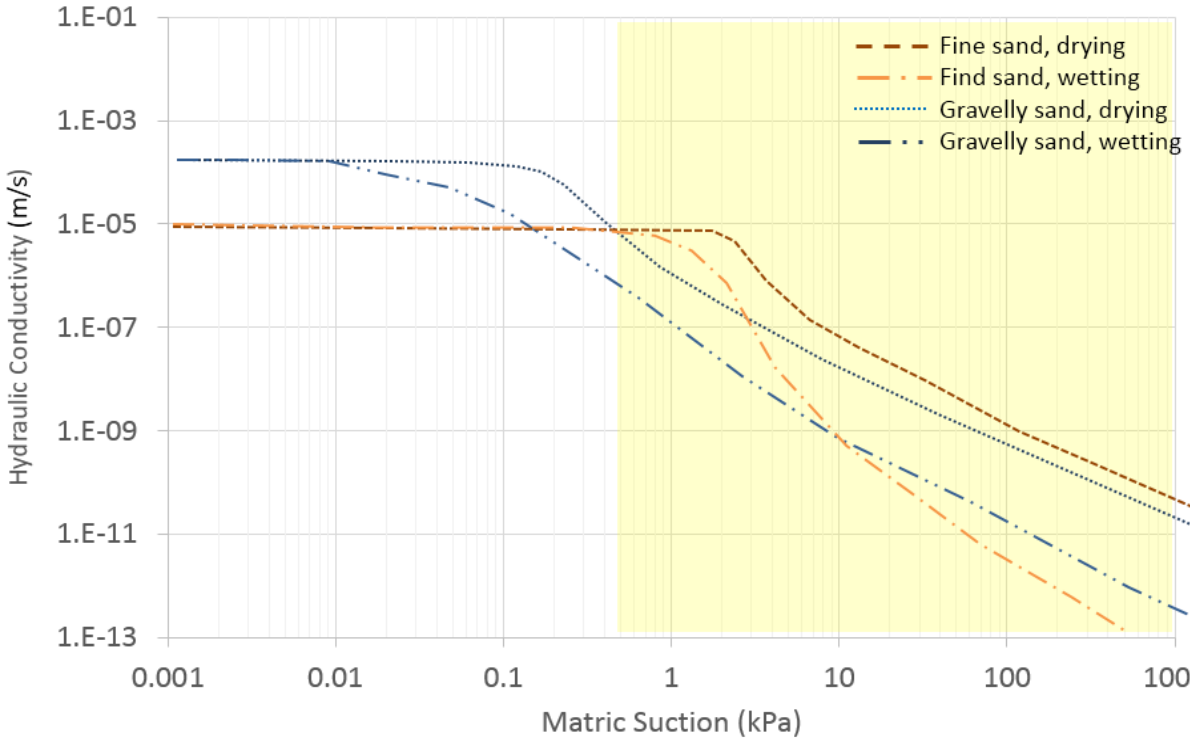

Figure 1-2: Example of hydraulic function to illustrate important differences between a coarse and fine-grain soil (adapted from Tami et al., 2004).

Figure 1-3: Diavik Diamond Mine location (64.5°N, 110.3°W), Northwest Territories, Canada. Modified from: Brock University Map Library. Canada. St. Catharines, ON: Brock University Map Library. 2004.

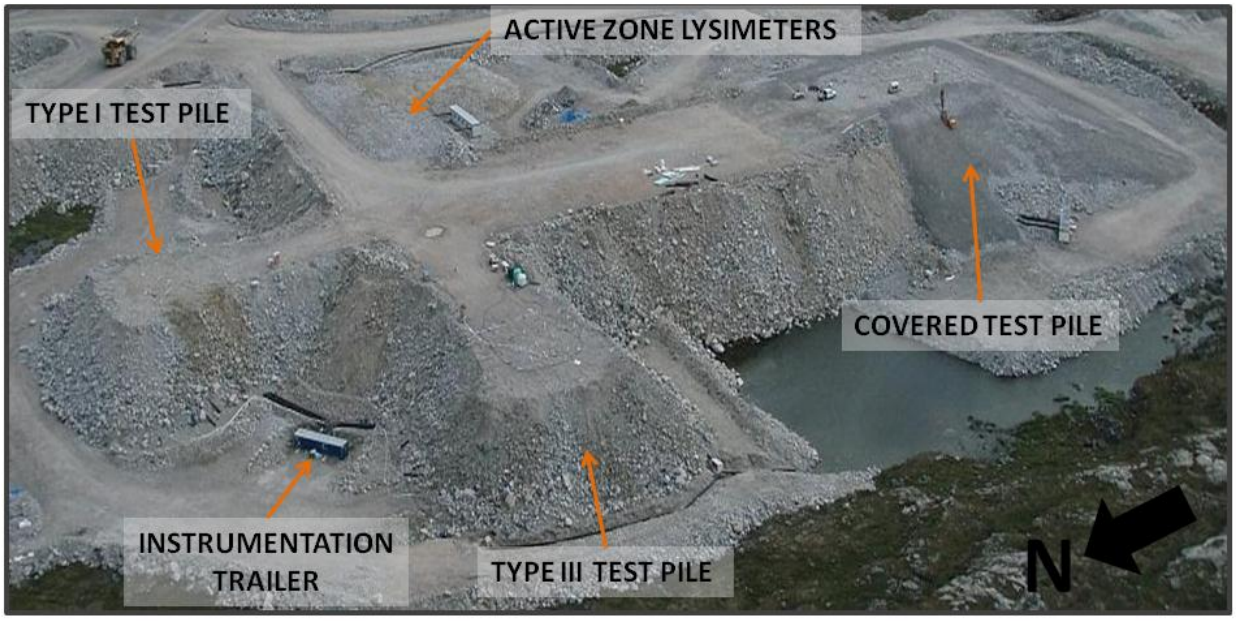

Figure 1-4: Waste rock research test pile field site, Diavik Diamond Mine. Photograph provided by M. Gupton.

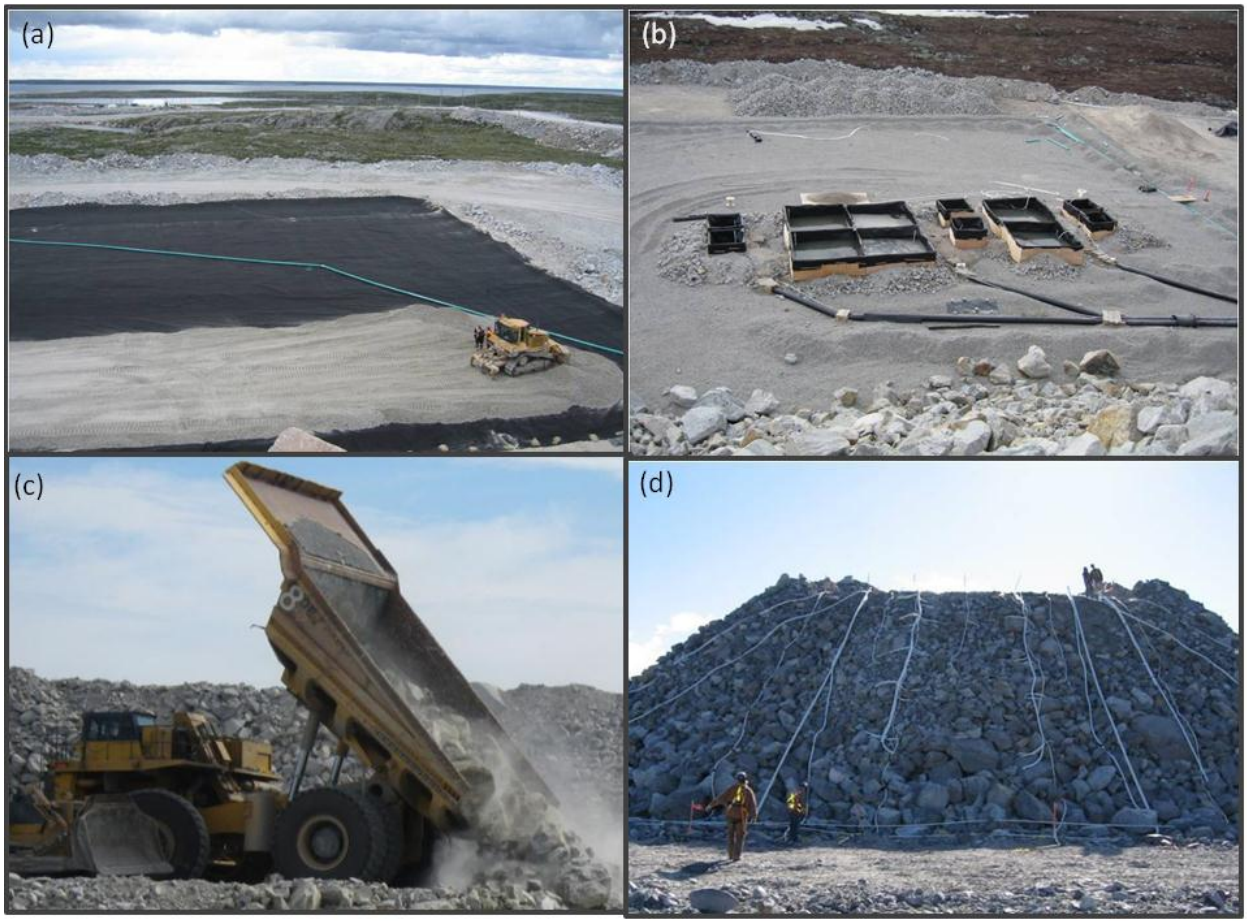

Figure 1-5: a) HDPE linear and drain pipe composing the basal drain collection system; b) Construction of the basal collection lysimeters; c) End dumping and push dumping of run-of-mine rock from the ramp; d) Instrument installation on face of test pile. Photographs provided by M. Gupton and N. Neuner.

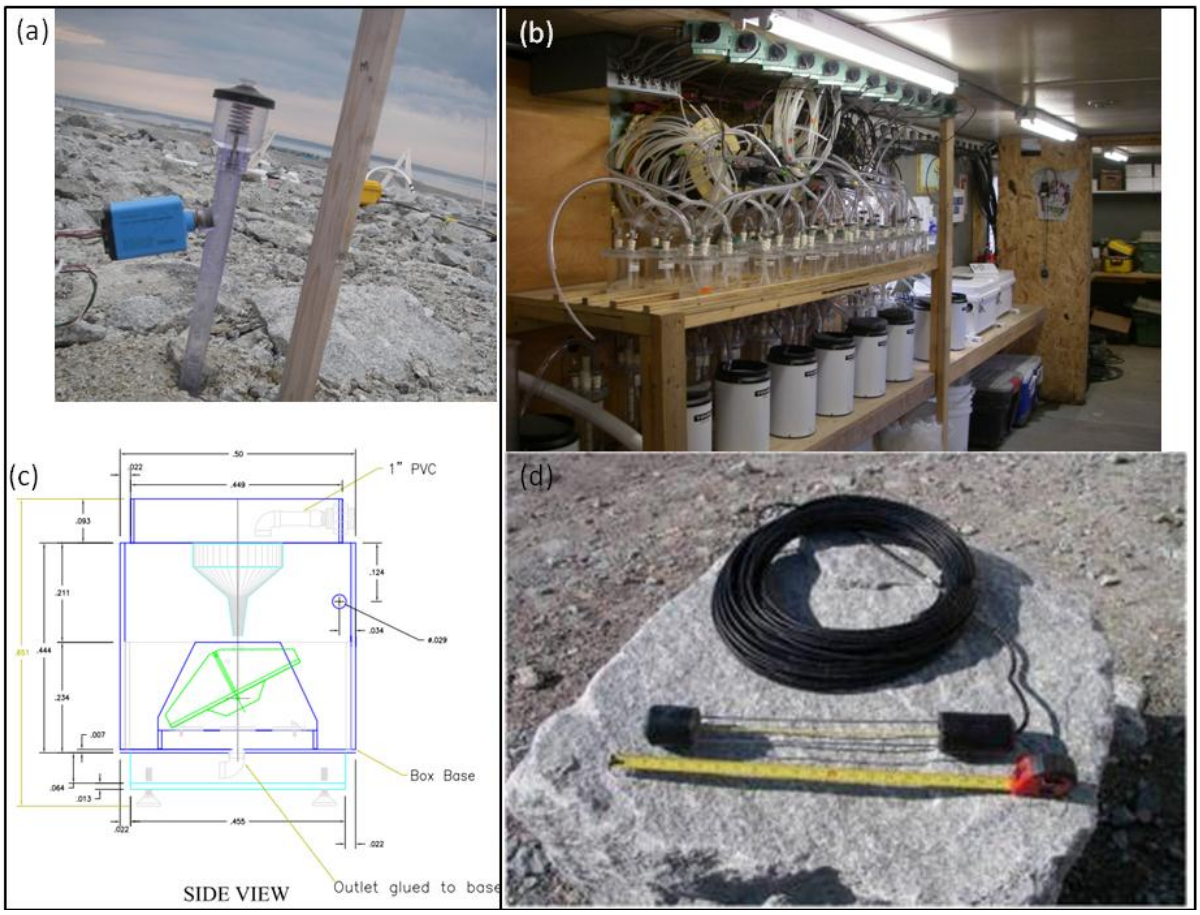

Figure 1-6: a) Tensiometer for measuring matric potential; b) sample cells and cells for continuous pH, EC and temperature monitoring along with commercially manufactured RM Young model tipping buckets for discharge measurement from the basal collection lysimeters; c) Design schematic of large custom built tipping bucket for the basal drain; d) Custom built TDR using shielded three-rod design.

Figure 1-7: a) Construction of AZLs (July 2006); b) AZLs constructed of approximate 5000 L HDPE tanks with tops cut off; c) Placement of waste rock by excavator; d) Waste rock fill placed around AZLs. Photographs provided by M. Neuner.

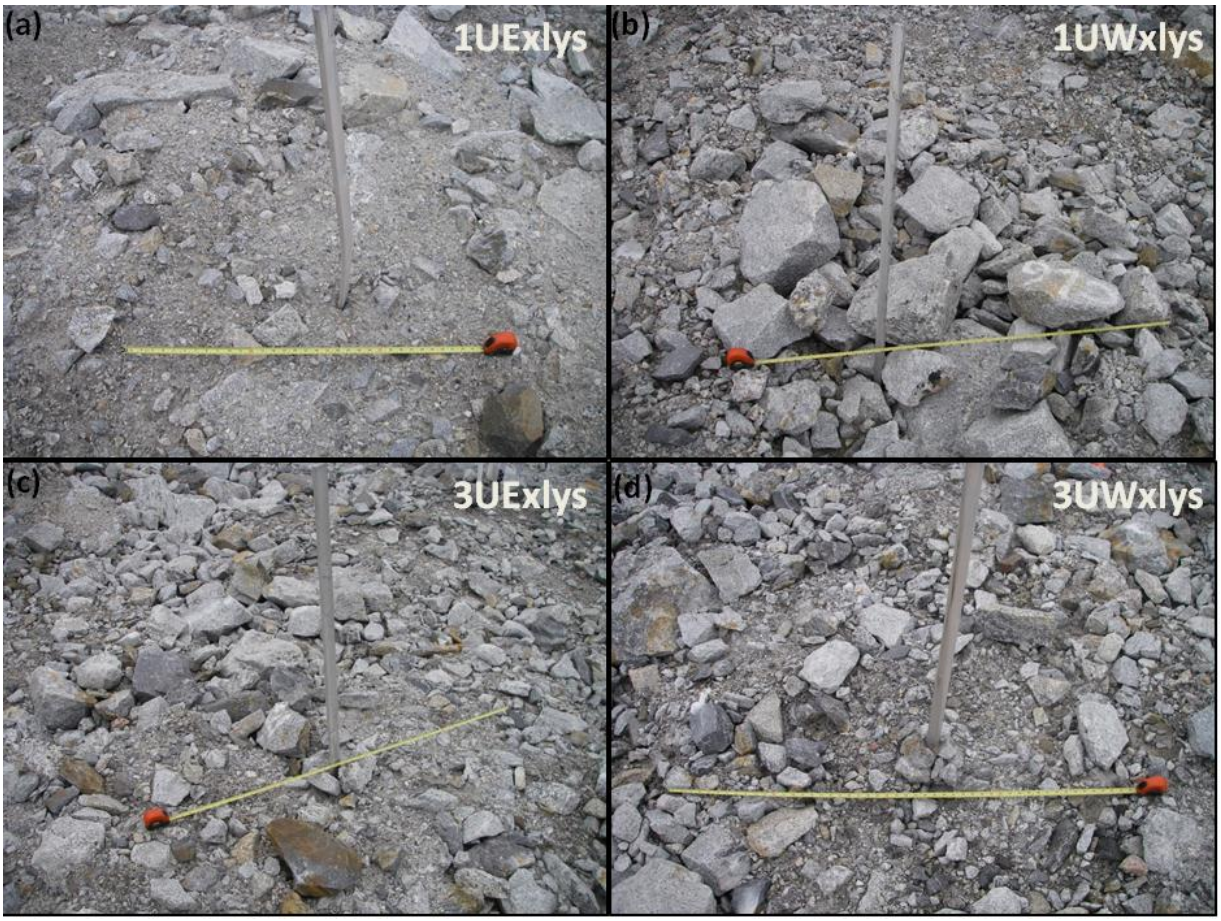

Figure 1-8: Photograph of the surface of the two Type I and two Type III AZLs showing the difference in grain size distribution on surface.

2 AZLs TRACER TEST

Tracer tests are used to characterize hydraulic and geochemical properties of porous media. Tracer's can be applied as a continuous source or as a pulse injection (e.g., Bellehumeur, 2001; Nichol et al., 2005). Tracer movement can be observed in response to natural gradients or to a forced gradient (e.g., applied flow rate or in response to pumping), either of which can be conducted in the field or under laboratory conditions (Ptak, et al, 2004). Applied tracers are either non-reactive, conservation substances or reactive substances. The following section presents the methodology, results, analyses and discussion of a natural gradient, pulse injection, conservative tracer applied to the Type III AZLs at the Diavik waste rock research project. The objective of this tracer test was to estimate residence time at the AZL-scale and to help understand water flow and solute transport processes in unsaturated waste rock located in an arctic environment.

Tracer response is described by a break-through curve, which plots concentration versus time at a specified location. A simple model to describe and conceptualize tracer response is by advective transport only using a piston-flow model. A break-through curve of solute transport represented by the piston-flow model describes the solute advancing uniformly across an entire cross-section through a soil column or lysimeter; new infiltrating water pushes resident water downwards and the concentration in the effluent will be 0 until one pore-volume has discharged, at which time the concentration in the discharge increases to the applied concentration (**Figure 2-1a**).

In an ideal homogeneous porous media, solute transport can be better described by a model which includes hydrodynamic dispersion as well as advection (advection-dispersion model). Hydrodynamic dispersion includes both molecular diffusion and mechanical spreading. Dispersion of the solute, generated by molecular diffusion and from spatial variation in the flow field, results in solute break-through ahead of the peak concentration (or mean velocity) (**Figure 2-1b**).

In a heterogeneous porous media, such as waste rock, solute transport may be better described by a dual-porosity model (Van Genuchten and Wierenga, 1976; Decker and Tyler, 1999) or a dual-permeability model (Gerke and van Genuchten, 1993; Gerke, 2006; Van den Daele et al., 2007). Dual-porosity models

include a mobile and immobile domain for water flow. The dual-permeability model allows interaction between a coarse-grain and fine-grain domain and provides for water flow and solute transport in each domain. The coarser-grained domain describes flow in a higher permeability domain where water flow occurs under capillary tension and gravity (Gerke and van Genuchten, 1993) or where water flow occurs under gravity alone (Van den Daele et al., 2007). The dual-permeability model includes a water transfer term to describe water flow between the two domains based on head (pressure) differences and a first-order transfer coefficient (Šimůnek and van Genuchten, 2008). To introduce solute transport in the dual permeability model, the advection-dispersion equation is applied to both domains and a mass transfer term describing the exchange of solute between the domains is required.

In addition to macropore and matrix domains between which the solute exchanges, there could also exist preferential flow paths which provide connected conduits that do not interact with the matrix domain and provide for rapid transport to the base of the AZL, or at least to by-pass significant portions of the macropore and matrix domains (Bellehumeur, 2001). Water flow in preferential flow paths is non-capillary, gravity driven and solute would be assumed to move at the same rate as the water flow.

Analysis of the transport of the applied Chloride (Cl^-) tracer through the AZLs is performed by observation of the discharge at the base of the AZL, as well as through instrumentation installed between the two Type III AZLs in the upper portion of the rock column. This instrumentation includes tensiometers to measure soil matric suction at 0.3, 0.6 and 0.9 metres below grade (mbg) and co-located commercial ECH_2O probes to measure moisture content, electrical conductivity (EC) and temperature.

The objectives of the tracer test were to:

- Estimate the mean residence time along with peak and mean velocity of a conservative ion tracer through the unsaturated waste rock;
- Estimate the proportion of the Cl^- mass that moved through the matrix domain versus the macropore domain; and
- Estimate wetting front velocity in response to the applied rainfall events.

Neuner (2009) described an unlabelled irrigation event (14.8 mm total) applied to the Type III AZLs on September 1, 2007 at an intensity of 8.4 millimetre per hour ($mm \cdot hr^{-1}$). An event at this rate is estimated to have a recurrence of between 5 to 10-years (Golder, 2008) and a 2 to 5-years (Meteorological Service of Canada (MSC), Environment Canada (EC) Government of Canada (GC), 2009). The response was used to estimate the water flux through the waste rock by observing the wetting front detected by changes in moisture content and matric potential, as well as lysimeter outflow. This applied event was not labelled with a tracer and observations of the advance of the wetting front cannot be distinguished between the velocity of a particle of water and pore-water displacement in response to a pressure wave. Pore-water displacement describes the downward movement of pre-event pore-water in response to infiltration.

Based on the unlabelled irrigation event, Neuner concluded that flow in the Type III AZLs was dominated by displacement of pore-water and not a preferential flow mechanism. In comparison, this chapter describes the response of a conservative Cl^- tracer applied at the Type III AZLs at a rate of 16.3 $mm \cdot hr^{-1}$ for a total of 14.9 mm; an event with between a 10 to 20-year return period (Golder, 2008) and a 2 to 5-year return period (MSC EC GC, 2009). Both of these estimates of rainfall event frequency are based on rainfall intensity and duration. This labelled irrigation event allows tracking of pore-water with the tracer signature through the waste rock and response to a higher applied infiltration rate. No ponding or run-off was observed during the application of either event.

2.1 Overview of Chloride Tracer Test Experiment

In August 2008, a natural gradient conservative tracer test, using Cl^-, was initiated on the two Type III AZLs. These AZLs are 1.7 m high HDPE containers with a volume of approximately 5,240 litres (L) filled with Type III waste rock. Flux and normalized outflow calculations for the Type III lysimeters are calculated using the basal area of the lysimeter, 3.14 square metres (m^2), instead of the surface opening area of 2.09 m^2. The basal area is used for these calculations as only at the immediate surface opening of the container is the cross-sectional area 2.09 m^2. Below the opening, the sidewalls slope outwards, to a vertical depth of 0.2 mbg, from which point the remainder of the container has a cross-sectional area of 3.14 m^2. Infiltration occurs across the 2.09 m^2 surface opening cross-sectional area, but below this, it is

assumed that there is a lateral water flow component which results in the entire cross-sectional area accommodating downward vertical water flow, and ultimately, discharge.

Following initial discharge at the end of June 2008, which continued into early July, no additional discharge occurred from either Type III AZLs in the weeks prior to tracer application. In an effort to initially wet-up the waste rock contained in the Type III AZLs to field capacity, following lower than average precipitation over the beginning of the summer in 2008, a water-only irrigation event was applied with garden-variety sprinklers prior to the labelled irrigation event. On August 6, an unlabeled 10.6 mm simulated rainfall event with an intensity of 15.2 $mm \cdot h^{-1}$ was applied. Field capacity of the matrix was estimated between 0.10 and 0.15 cubic metre per cubic metre ($m^3 \cdot m^{-3}$) from the laboratory derived soil water characteristic curves and approximately 0.06 $m^3 \cdot m^{-3}$ by observations of water balance before initial flow at the AZLs (Neuner et al., 2013). VMC from ECH_2O probes averaged over all depths recorded was 0.11 $m^3 \cdot m^{-3}$ immediately prior to the application of the tracer. The average VMC following application of the tracer, until discharge ceased in 2008 was 0.15 $m^3 \cdot m^{-3}$. During the below average rainfall conditions in 2009, the average VMC during periods of outflow was 0.12 $m^3 \cdot m^{-3}$.

On August 12, following the unlabelled irrigation event, a labelled 14.9 mm simulated rainfall event, with an intensity of 16.3 $mm \cdot hr^{-1}$ and an average Cl^- concentration of 1,880 milligrams per litre ($mg \cdot L^{-1}$) was applied. A total Cl^- mass of approximately 58.5 grams (g) was delivered during the event which lasted for 55 minutes and applied a total of 31.1 L to each Type III lysimeter. Wind speed during the tracer application was variable between 5 and 10 kilometre per hour ($km \cdot hr^{-1}$) from the north.

The applied rainfall events in 2008 increased the total amount of rain received at the Type III AZLs to 110% of the annual average rainfall, up from the 94% that was delivered by natural rainfall events. Applied rainfall was delivered using two garden-variety oscillating sprinklers on opposite sides of the test area, based on trial results that demonstrated more uniform coverage than a single sprinkler located in the middle of the test area (**Figure 2-2**). The trade-off of achieving better coverage with two sprinklers was higher application intensity. During application of the tracer, the simulated rainfall event achieved a Christiansen uniformity coefficient (Christensen, 1942) of 80.4%, which is within the range of other researchers who have performed applied rainfall events on waste rock (Nichol, 2002; Neuner, 2009). This

uniformity coefficient represents the consistency of rainfall received on the ground across the coverage area of the oscillating sprinklers via rainfall collection cups placed on a 1 m by 1 m grid (**Figure 2-2**).

Intensity Duration Frequency (IDF) curves were created from data presented in Golder (2008) (**Figure 2-3)**. Golder uses eight years of site data (1999 to 2006) to estimate extreme events based on a Gumbel extreme value distribution. As noted in Golder (2008), recurrence intervals beyond this range have greater uncertainty due to the small data set and the required extrapolation. As a check, site data were compared to regional stations with longer records. As the period of record presented by Golder covers a limited duration, the meteorological station in Yellowknife, NWT is also considered to provide additional perspective on the applied irrigation intensity. The IDF curves prepared for the Yellowknife station are based on a 34-year record between 1963 and 1996. A rainfall intensity of 16.3 $mm \cdot hr^{-1}$ applied for 55 minutes has between a 10 to 20-year return period (Golder, 2008), and a 2 to 5-year return period (MSC EC GC, 2009). The recurrence interval appears high, based on the intensity and duration of natural events that have fallen over the study period. This work did not undertake the preparation of new IDF curves incorporating the most recent site-specific data to better reflect climate trends observed at site.

On August 25 and 26, about two weeks after the tracer application, a 35.8 mm rainfall event occurred. Over the 24.8 hour duration of the event, the average rainfall intensity was 2.9 $mm \cdot hr^{-1}$; based on the IDF curves, an event of this intensity and duration has a recurrence interval of less than once in 100 years (Golder Associates, 2008), or between 25 and 50-years (MSC EC GC, 2009). After this, individual rainfall events delivered less than 2 mm, except for an event on September 23 when 15.9 mm was recorded. Rainfall occurred on 31 of the 54 days between tracer application and when air temperature decreased to less than $0^{o}C$ in 2008.

Following tracer application, sampling of the outflow water initially consisted of multiple daily samples and the frequency decreased to every day or two depending on whether water was reporting to the drain and the availability of onsite personnel. Background Cl^- concentrations sourced from the blasting residues provided interference with the applied Cl^- tracer. The accelerant perchlorate (ClO_4^-) used as a blasting agent, provides the source of the Cl^- following detonation (Bailey et al., 2013). This background contribution decreases with time as these residues are removed with flushing. A correction was applied to

the Cl^- concentrations measured in the discharge to separate Cl^- sourced from the tracer test and Cl^- from blasting agents. This was done by describing a relationship between the Cl^- and nitrate (NO_3^-) concentration in the discharge, which was also contributed from the blasting residues from the mixture of ammonium nitrate and fuel oil used in blasting.

2.1.1 Corrected Chloride Concentrations

Isolating Cl^- concentrations sourced from the tracer test required correction for Cl^- concentrations derived from blasting agents. A relationship exists between Cl^- and NO_3^- (**Figure 2-4),** both components of the blasting residues. At the Type I AZLs, where no tracer was applied, there was generally a linear relationship between Cl^- and NO_3^-. At the Type III AZLs there are two distinct linear relationships between Cl^- and NO_3^-, one prior to application of the tracer; and one that applies after tracer application beyond the end of August. The change in slope evident for the Type III AZLs in **Figure 2-4** between the period before tracer application and the following several weeks after tracer application, is consistent with an increase in Cl^- concentrations relative to NO_3^- concentration, which has no new source. Following the large storm event at the end of August, the NO_3^- concentration decreased, as if this pulse of water flushed some of the remaining residual blasting residue. Following the large storm event, the NO_3^- concentration is between 30 and 40% of the concentration immediately preceding the event for both AZLs. This contrasts with the observed increase in Cl^- concentration in the discharge from the Type III AZLs. At the Type I AZLs, the concentration of both Cl^- and NO_3^- decreased following this large storm event to between 20 and 40% of the concentration immediately prior to the rainfall event. The constant linear relationship between Cl^- and NO_3^- at the Type I AZLs, which did not receive a Cl^- tracer, supports the validity of the relationship for the Type III AZLs.

The concentrations of Cl^- and NO_3^- have a strong linear relationship from when discharge began, until the application of the tracer, and then there was a distinct change in the relationship following August 27 when the Cl^- concentration increased relative to the NO_3^- concentration (**Figure 2-4**). Bailey et al., (2013) suggested that the initial flush of the blasting residuals (NO_3^-, NH_3, and ClO_4^-) initially present in the Type III AZLs coincided with the large storm event on August 25 and 26. This was based on the change in concentration in the discharge of AZL, noted above, along with a calculated volume of discharge which

was equivalent to 91% of the matrix porosity volume. Between application of the tracer on August 12, and August 27, the relationship shifted slightly but remained close to the linear regression line from prior to the tracer application. These data are not included in the correction, to remove any influence of the tracer test by earlier Cl^- arrival. The linear regression has a strong correlation with a coefficient of determination (R^2-value) for the western and eastern lysimeters of 0.88 and 0.93, respectively. Corrected Cl^- concentrations are reported for Type III western and eastern lysimeter following application of the tracer by dividing the western and eastern NO_3^- concentration by the slope of the fitted line, 19.04 and 13.88, respectively, to estimate the Cl^- concentration attributed to background. Then this value was subtracted from the measured Cl^- concentration in the sample collected from the drain, as indicated below (equation 2-1 and 2-2).

$$\text{Western lysimeter: } Cl^-_{corrected} = Cl^-_{measured} - (NO_3^-{}_{measured}/19.04) \qquad 2\text{-}1$$

$$\text{Eastern lysimeter: } Cl^-_{corrected} = Cl^-_{measured} - (NO_3^-{}_{measured}/13.88) \qquad 2\text{-}2$$

A check was made on the predicted Cl^- concentrations by applying equation 2-1 and 2-2 to the dataset prior to tracer addition. Residuals of predicted concentration and actual concentration during the period before the tracer was applied appear to be randomly distribution and standard error is 4 $mg \cdot L^{-1}$. This check provides confidence that the corrected Cl^- concentration dataset can be used to interpret the tracer response.

2.2 Observed Response – Results

Data from the tracer test are considered by reviewing the Cl^- concentration in the discharge (**Figure 2-5**), the daily Cl^- mass loading (**Figure 2-6**) and the proportion of Cl^- in the discharge relative to the initial applied concentration (**Figure 2-7**). Both Figure 2-5 and Figure 2-6 present precipitation and normalized daily outflow, the figures differ in the presentation of Cl^- concentration and Cl^- mass loading shown on the middle two plots. Temporal moment analyses is used as a descriptor of mean velocity and to estimate residence time (**Figure 2-8**). Data to support these analyses are based on the corrected Cl^- concentration from the discharge at the base of the lysimeters. When discharge occurred but no measured concentration was available, the dataset was populated with values estimated by linear interpolation.

Instrumentation installed within the upper 0.9 m of the waste rock between the AZLs were used to further review the results of the tracer response. Observations of matric potential (**Figure 2-9**) recorded at the tensiometers, along with moisture content (**Figure 2-10**) and EC (**Figure 2-11**) recorded at the ECH_2O probes, are used to provide additional information about the initial tracer response in the upper portion of the waste rock and to bound estimates of tracer velocity through the waste rock.

2.2.1 Observed Response – Concentrations, Mass Loading, Proportional Discharge

Volumetric discharge has been similar in both quantity and timing from the east and west Type III lysimeters (**Figure 2-5**). Through 2009, an additional 10 L discharged from the eastern lysimeter. Following the application of the tracer, outflow began on August 14, coincident with a natural rainfall event of 16.9 mm. Chloride was first observed in the discharge on August 16, when the measured concentration was 14.1 $mg \cdot L^{-1}$. As noted by Nichol (2002), samples collected from the base of a lysimeter provide flux-averaged concentrations over the spatial scale of the lysimeter; the saturated, zero-tension, base of a lysimeter results in water mixing which would not have occurred in the absence of the lysimeter. Flux-averaged concentrations are representative of average discharge per sample at the western lysimeter (would be similar for the eastern lysimeter) in 2008 of 2.9 L/sample and 0.5 L/sample in 2009.

If the tracer test had been performed in a column of uniform sand, and the event water concentration was 1,800 $mg \cdot L^{-1}$, then hydrodynamic dispersion will result in the solute spreading through the column creating a leading edge of the tracer arrival at the base. Assuming a Fickian model of dispersion, the peak concentration will discharge at the mean advective velocity and will be less than the initial input concentration. Following this peak, concentrations will decrease until the entire applied mass is recovered, minus any residual tracer retained by immobile pore-water (**Figure 2-1b)**.

In a lysimeter containing heterogeneous waste rock, hydraulic conductivity differences are created from the grain size and pore-space variation, and water flow and solute transport may occur in matrix and preferential domains. Additionally, heterogeneity will be present within either domain. The normal distribution of concentration observed at the base of the column described above (**Figure 2-1b)** will be overprinted by multiple leading edges, peaks and tails as solute is transported through different flow paths in each flow domain in response to precipitation events.

By comparing the proportion of the conservative tracer in the discharge to the source input concentration, the percentage of tracer event water contained in the discharge is evaluated (**Figure 2-7**).

In the absence of dispersion and diffusion, if discharge from the lysimeter consisted only of event water, the concentration of Cl^- should be about 1,800 $mg \cdot L^{-1}$ (i.e., the applied tracer concentration). If discharge consists of 50% pre-event water (or by-passing flow) and 50% event water, the Cl^- concentration in the discharge should be about 900 $mg \cdot L^{-1}$. Discharge reporting to the base of the lysimeter potentially consists of pre-event water, event water, or by-passing flow from different parts of the cross-sectional area that result in flux averaged concentrations measured in the total discharge sampled (equation 2-3).

$$Cl^-_{mass} = C_{Flux\ avg\ Cl^-} \times Q_T = (C_{pre\text{-}event\ Cl^-} \times Q_{pre\text{-}event}) + (C_{by\text{-}pass\ Cl^-} \times Q_{by\text{-}pass}) + (C_{event\ Cl^-} \times Q_{event}) \quad 2\text{-}3$$

Where $C_{Flux\ avg\ Cl^-}$ is the flux averaged discharge concentration, $C_{pre\text{-}event\ Cl^-}$ is the pre-event Cl^- concentration (0 $mg \cdot L^{-1}$), $C_{by\text{-}pass\ Cl^-}$ is the by-pass Cl^- concentration (0 $mg \cdot L^{-1}$), and $C_{event\ Cl^-}$ is the event Cl^- concentration (1,800 $mg \cdot L^{-1}$). Q_T is the total discharge, $Q_{pre\text{-}event}$ is the proportion of discharge carrying pre-event discharge concentrations, $Q_{by\text{-}pass}$ is the proportion of discharge carrying by-pass concentrations, and Q_{event} is the proportion of discharge carrying event concentrations. Although the proportions of outflow are not known, the $C_{pre\text{-}event\ Cl^-}$ and $C_{by\text{-}pass\ Cl^-}$ are 0 $mg \cdot L^{-1}$and therefore the above equation can be reduced to:

$$\frac{C_{\text{Flux avg Cl}-}}{C_{\text{event }Cl-}} = \frac{Q_{\text{event}}}{Q_{\text{T}}} \quad 2\text{-}4$$

The proportion of event water in the discharge ($\frac{Q_{\text{event}}}{Q_{\text{T}}}$) equals the proportion of flux averaged Cl^- concentration in the discharge to the event Cl^- concentration ($\frac{C_{\text{Flux avg Cl}-}}{C_{\text{event }Cl-}}$).

This method of describing outflow relies on a mass balance formulation with the following assumptions:

- The initial applied event water has a concentration of 1,800 $mg \cdot L^{-1}$. This discussion assumes no diffusion or dispersion, which would reduce maximum concentration detected from the applied concentration. Instead for the basis of this relative comparison, event water at the applied Cl^- concentration is assumed to move through the lysimeter.

- Initial Cl^- concentration in the AZL is equal to about 0 $mg \cdot L^{-1}$. This is a reasonable assumption after the correction of initial background concentrations based on NO_3^- is applied.
- Following the tracer application there is no secondary source of Cl^-, therefore the Cl^- concentration in any by-pass flow is 0 $mg \cdot L^{-1}$. This assumption is reasonable for the lysimeters since the HDPE containers provide mass balance control as the only input is through the top surface and the only output is through the drain at the base of the container.

The value of looking at the data in this manner is the information it provides on flow contribution. Since hydrodynamic dispersion will result in attenuation of peak concentrations along with earlier arrival of some tracer mass, the actual percent values indicated from this analyses are meaningless, but the relative contributions are of interest. Mass discharge and mean position of mass based on load recovered are also considered. The daily mass load of Cl^- is also reported and discussed (**Figure 2-6**).

The following describes the response observed at the eastern AZLs; the western response was similar, and in general lagged by up to two days. Additional differences in the response of the western lysimeters are noted following the description of the observed response at the eastern lysimeter (**Figure 2-5**).

- On August 16, 92 hours after application of the tracer, about 1% (14.1 $mg \cdot L^{-1}$) of the discharge appears to be sourced from tracer test event water.
- The Cl^- concentration in the discharge remained low over the following 10-days, but began to increase following the significant rainfall event that began on August 25. The concentration of the Cl^- in the discharge was 162.4 $mg \cdot L^{-1}$ following the rainfall event and increased to 212.1 $mg \cdot L^{-1}$ by September 4, or 11% of the discharge attributed to tracer event water. The Cl^- concentration in the discharge declined after this.
- On September 22, the Cl^- concentration in the discharge spiked to 251.1 $mg \cdot L^{-1}$ or 13% of the discharge attributed to tracer event water. This peak occurs during a six day period when minimal outflow (0.5 L) is recorded. Following this abrupt increase, the Cl^- concentration in the discharge declined, as discharge increased in response to a 15.9 mm rainfall event that occurred on September 23.

- On October 20, the Cl^- concentration in the discharge sharply increased to 620.5 $mg \cdot L^{-1}$ or 33% of the discharge attributed to tracer event water. Discharge receded and about 0.1 L was recorded on October 20. During the preceding two weeks approximately 0.2 mm of rain fell. The advancing freezing front reached 0.3 mbg, as recorded by the ECH_2O probe, at 1700 on October 19.
- The Cl^- concentration in the discharge declined until discharge ceased for 2008 on October 23 (eastern lysimeter) and on October 26 (western lysimeter).

Several notable differences were observed in the discharge from the western lysimeter, as compared to the eastern lysimeter:

- On September 25, the contribution of event water in the discharge abruptly spiked to 202.0 $mg \cdot L^{-1}$, along with discharge at 5.5 L. The Cl^- concentration in the discharge continued to gradually increase until September 30, when it peaked at 254.6 $mg \cdot L^{-1}$ or 14% attributed to event water. The initial increase on September 25 followed a reduced outflow period that lasted 7 days (during which 1.4 L was recorded). This increase in Cl^- concentration in the discharge occurred after a total of 634 minutes of rainfall, delivered in four separate events between September 21 and 23. A total of 18.6 mm of rain fell during these four events (15.9 mm of this fell on September 23) at an average intensity of 1.5 $mm \cdot hr^{-1}$. This is the most rainfall since the storm event that began on August 25.
- This was followed by a gradual decrease until October 14, when the Cl^- concentration in the discharge sharply increased to 220.4 $mg \cdot L^{-1}$ or 12% of the discharge attributed to tracer event water. No precipitation occurred on this day, or in the preceding seven days and discharge was 0.6 L. Air temperature ranged from a low of -4.5 degrees Celsius (ºC), to a high of 0.9 ºC though temperature at 0.3 mbg did not drop below 0 ºC. This was the coldest night to occur in October to this date in 2008.

As a result of dispersion, diffusion, and mass transfer into lower permeability zones following application, and particularly after the 2008/2009 winter, the maximum Cl^- concentration measured in the water draining from the lysimeter will be less than the applied concentration. Therefore the calculated proportion

of event water in the discharge from equation 2-4, will underestimated the true proportion. To account for diffusion and dispersion, the denominator value, $C_{\text{event } Cl-}$, should be represented by a temporally-varying concentration that decreases with time. The proportion of event water estimated in the discharge for 2009 is reported to provide a relative comparison. As was done for 2008, the response of the eastern lysimeter is described, and notable differences from observations at the western lysimeter are provided afterwards. Several key observations include:

- Initial discharge slowly increased to a peak concentration of 145.7 $mg \cdot L^{-1}$, or 8% of the discharge attributed to tracer event water, on July 11 (two weeks after discharge began). However, the outflow at the eastern lysimeter was not sampled during the first three days of discharge, and therefore the Cl^- concentration in the initial discharge is not known. The peak concentration observed on July 11 followed a rainfall event of 5.2 mm which occurred on July 10, and 11.8 mm of rainfall occurred over the preceding 5 days; this is relative to a total 20.3 mm of rainfall which occurred to this date in 2009.
- A predominately-steady increase continued until August 2, when the Cl^- concentration in the discharge peaked at 283.6 $mg \cdot L^{-1}$ or 15% of the discharge attributed to event water. This follows a rain event of 9.2 mm, which began on July 24 when VMC at 0.3 m was 0.11 $m^3 \cdot m^{-3}$.
- For the 45-day period between August 12 and September 25 no discharge occurred except on August 28 when about 0.5 L of discharge was recorded.
- On September 25, the Cl^- concentration in the discharge spiked at 382.5 $mg \cdot L^{-1}$ or 20% of the discharge attributed to event water. This follows a rainfall event on September 24, having 135-minute duration and an average intensity of 13.3 $mm \cdot hr^{-1}$, the second highest event recorded during this experiment based on intensity and duration.
- After September 25 the Cl^- concentration in the discharge steadily decreased until outflow stopped on October 15 (eastern lysimeter) and October 16 (western lysimeter).

The response in 2009 at the western lysimeter demonstrated a similar response however there were several notable differences which include:

- The Cl^- concentration in the initial discharge on June 28, was 193.3 $mg \cdot L^{-1}$ or 10% of the discharge attributed to event water. This initial peak Cl^- concentration in the discharge decreased as outflow from the lysimeter continued.
- On July 23, the Cl^- concentration peaked at 249.0 $mg \cdot L^{-1}$, or 13% of discharge was attributed to event water. This response occurred following an 18-day period when there was no discharge, and during which low magnitude infrequent rainfall events occurred, which together delivered about 20.4 mm to the surface of the AZL.
- On July 24, following the previously mentioned 9.2 mm rainfall event, the Cl^- concentration was 141.2 $mg \cdot L^{-1}$ or 8% of the discharge was attributed to event water. The abrupt decrease in concentration at the western lysimeter is distinct from the steady response at the eastern lysimeter.

The response follows several similar patterns. There are about 9 events when a peak Cl^- concentration is observed in the discharge from the lysimeter following application of the tracer. These concentration peaks occur under three main conditions. One, in response to large (magnitude or intensity) rainfall events (e.g., September 4, 2008, September 25, 2008, and August 2, 2009); or two, in response to moderate cumulative rainfall volumes following dry periods (e.g., June 28, 2009, July 11, 2009, July 23, 2009, and September 25, 2009); or three, during recession from peak discharge (e.g., September 22, 2008, October 14, 2008 and October 20, 2008). Two events occur coincident with the onset of freezing conditions (i.e., October 14, 2008 and October 20, 2008), however at the same time the discharge was receding and the controlling factor is unknown.

The response to large (magnitude or intensity) rainfall events is conceptualized as events with sufficient magnitude to trigger flow paths that were not otherwise active and mobilized otherwise stagnant water, however the increase in the concentration of Cl^- in the discharge could also be attributed, at later times, to mobilization of matrix water by pore-water displacement in response to the pressure wave generated from the wetting front.

The Cl^- concentration in the discharge was also observed to decrease in response to high magnitude or intensity events (e.g., August 26, 2008 and July 24, 2009). But more frequently, gradually declining Cl^-

concentrations are coincident with low magnitude and infrequent precipitation, and the drain down of water released from the finer-grained portions of the matrix.

Initial Cl^- concentrations were observed in the discharge 92 hours after tracer application from both lysimeters. This yields a maximum velocity of the Cl^- through the unsaturated waste rock of $5.1x10^{-6}$ $m \cdot s^{-1}$ (0.44 $m \cdot d^{-1}$). It is assumed that the solute transport, in part, occurred through preferential flow paths or through coarser matrix fraction, in consideration of the average velocity (Section 2.4.1). However, if the solute transport occurred through the matrix fraction, the average moisture content of the matrix during this period (0.15 $m^3 \cdot m^{-3}$), could be used to provide an estimate of average unsaturated hydraulic conductivity. The measured gradient (i) in the upper 0.9 m during this period is about 1.7 $m \cdot m^{-1}$. Based on the initial estimate of Cl^- arrival the bulk average unsaturated hydraulic conductivity of the most permeable flow paths within the matrix material is $4x10^{-7}$ $m \cdot s^{-1}$ ($5.1x10^{-6}$ $m \cdot s^{-1}$ x 0.15 $m^3 \cdot m^{-3}$ ÷ 1.7 $m \cdot m^{-1}$). Gradient varies through the depth of the lysimeter and temporally, between a plausible range of bulk average values 0.1 and 10 $m \cdot m^{-1}$, bulk average unsaturated hydraulic conductivity would be expected to range from 10^{-6} $m \cdot s^{-1}$ to 10^{-8} $m \cdot s^{-1}$. This range of values can be compared to the saturated hydraulic conductivity of the matrix estimated by Neuner et al. (2013) as $9x10^{-6}$ $m \cdot s^{-1}$.

A mass loading calculation shows that to the end of 2009 at the eastern lysimeter, approximately 29.8 g of Cl^- (51% of applied) was recovered (**Figure 2-6**). In terms of water volumes attributed to event water, based on the proportion of event water in the discharge, approximately 15.4 L or about half of the total volume supplied during the applied event (51%). At the western lysimeter, approximately 24.0 g of Cl^- (41% of applied) has been recovered (**Figure 2-6**). In terms of water volumes attributed to event water, based on the proportion of event water in the discharge, approximately 12.7 L or just under half of the total volume supplied during the applied event (41%).

The relatively high proportion of the flow mobilized from the tracer event at the western lysimeter when outflow began in 2009 is of note. As no sample was collected when outflow began at the eastern lysimeter it cannot be determined if each lysimeter behaved similarly. However, VMC data from the ECH_2O probes installed between the two Type III lysimeters were inspected to support the observation. No snow cover remained on the top surface of the AZLs by the end of May, and after May 30 the

temperature at 0.3 mbg remained greater than 0°C. The ECH$_2$O probes capture the movement of the wetting front. Between 0.3 and 0.9 mbg the wetting front was moving at an average velocity of 0.07 m·d^{-1}; at this rate, the front should reach the base of the drain after approximately 23 days. The first discharge arrived after closer to 28 days. The relevant comparison is not the numeric values, but the relationship; the first outflow from the lysimeters arrived as matrix flow and displacement of resident pore-water. This is consistent with the observation that no snow cover remained by the end of May and therefore there was no rapid snowmelt infiltration.

The 14.9 mm applied tracer, delivered at a rate equivalent to between a 2 and 20 year recurrence interval, to waste rock with an average antecedent matrix VMC of 0.11 resulted in a small fraction of flow traveling in preferential flow paths, which terminated in discharge at the base of the 1.7 m tall lysimeter. Up to 1% of the outflow may have moved as preferential flow arriving as discharge 92 hours after application. After about 185 days of active water flow (i.e., excluding periods when temperature was less than 0 ºC) between 41 and 51% of the initial mass, or volume, of the applied tracer has been observed to discharge at the base of the Type III AZLs. These observations were made during a two year period, 2008 and 2009, when rainfall was equivalent to 110% and 43% of the annual average, respectively.

2.2.2 Observed Response - First Moment (Mean Average Velocity)

Temporal moment analysis, the statistical description of the measured distribution of the mass of the applied tracer, is used as a descriptor of mean average velocity (Freyberg, 1986; Garabedian et al., 1991; Adams and Gelhar, 1992; Eriksson et al., 1997).

The nth temporal moment of concentration at a specified location is defined as (Harvey and Gorelick, 1995).

$$M_{n,t} = \int_0^\infty t^n C dt \qquad 2\text{-}5$$

Therefore, the zeroth moment describes the total mass of tracer to pass a specified location; in this case it represents the total mass recovered from the base of the lysimeter and the area under the break-through curve. And the first moment describes the centre of mass and when normalized to the zeroth moment, describes the mean break-through time. The second moment describes the spreading of the

tracer around the centre of mass. Equation 2-6 and 2-7 provide the analytical solution for the zeroth and first moments, which have the units of concentration • time and concentration • time squared, respectively. The effective velocity ($\bar{v}_{eff}$) is then described by the transport distance (*d*) divided by the normalized moments (equation 2-8).

$$\mathrm{M}_{0,t} = \sum_{n=1}^{\infty} \left[\frac{C_n + C_{n-1}}{2}\right](t_n - t_{n-1}) \qquad 2\text{-}6$$

$$\mathrm{M}_{1,t} = \sum_{n=1}^{\infty} M_{0,n}(T_n) \qquad 2\text{-}7$$

Where T_n is the elapsed time between tracer application the current time step.

$$\bar{v}_{eff} = \frac{d}{(M_1/M_0)} \qquad 2\text{-}8$$

As only a portion of the tracer mass has been recovered, a simplified analysis is used. The total mass applied at each AZL was 58.5 g. Cumulative mass load discharged from the eastern lysimeter was 29.8 g (51%) and 24.0 g (41%) at the western lysimeter at the end of October 2009. By definition, the first normalized moment is the time when 50% of the injected mass has been recovered. By October 3, 2009, 50% of the applied Cl^- mass had been recorded in the discharge from the eastern drain (**Figure 2-8**). On October 16, at the end of the outflow season in 2009 approximately 41% of the mass had reported to the western drain (**Figure 2-8**).

Cumulative discharge over the period the AZLs were active, following the application of the tracer test, was used to represent an average rate of future discharge to estimate the arrival of the central moment of mass for the western drain. The arrival time for the centre of mass is 169 days for the eastern lysimeter and is projected to be recovered after 229 days for the western lysimeter. These durations consider all days in the active season beginning from the first seasonal discharge and ending on the day of the final seasonal discharge in each of 2008 and 2009 and excluding intervening days when the temperature was less than 0 ºC and water flow was not occurring. For the western lysimeter, the additional projected time is determined from the average cumulative normalized outflow based on this active season, and therefore projects that 50% recovery will occur during the 2010 active flow season. The period for the western

lysimeter is extrapolated from a plot of normalized cumulative tracer recovery against normalized cumulative discharge (**Figure 2-8**). A best-fit line projected to 50% tracer mass recovery predicts that the centre of mass will discharge after 0.079 $m^3 \cdot m^{-2}$ cumulative normalized outflow has occurred. This amount is predicted to occur after an additional 38 days of active season, based on the average cumulative normalized outflow per day in 2008 and 2009 (0.0002 $m^3 \cdot m^{-2} \cdot d^{-1}$ at the western lysimeter).

Based on the estimated time required to recover 50% of the tracer mass, the average velocity of the Cl^- tracer through the unsaturated waste rock in the Type III AZL is 0.010 $m \cdot d^{-1}$ ($1.2 \times 10^{-7} m \cdot s^{-1}$) for the eastern lysimeter and 0.007 $m \cdot d^{-1}$ ($8.6 \times 10^{-8} m \cdot s^{-1}$) for the western lysimeter. The average moisture content of the matrix material over this period is 0.15 $m^3 \cdot m^{-3}$. The average specific discharge through the unsaturated waste rock at the long-term moisture content is estimated at between 1.3×10^{-8} and 2.6×10^{-8} $m \cdot s^{-1}$ (e.g., 0.007 $m \cdot d^{-1}$ x 0.15 $m^3 \cdot m^{-3}$) for the western and eastern lysimeter, respectively.

The case of plug flow through the lysimeter is considered to help bound the estimate of residence time. The case of plug flow provides an averaged estimate for residence time, as it assumes that the solute moves with water until one pore-volume has been displaced. The pore volume of the matrix material in the Type III AZLs is estimated to be between 240 L and 470 L of water, based on the calculated matrix porosity of 0.05 $m^3 \cdot m^{-3}$ (Neuner et al., 2013) and 0.09 $m^3 \cdot m^{-3}$ by Fretz (2013), with the noted adjustment in Chapter 3. Assuming plug flow, the tracer will reach the base of the lysimeter after between 115 and 225 mm of infiltration over the 2.09 m^2 surface opening area. Based on calculated infiltration for 2008 and 2009 at the AZLs (**Section 4.2.2**) this predicts between two and three year residence time although this is dependent the amount of precipitation received during this period.

Since application of the tracer, between approximately 0.5 and 0.9 pore volumes have reported to the lysimeters. This response compares with that observed by Nichol (2002) during a tracer test at the Cluff Lake, Saskatchewan waste rock experiment, where after approximately 0.5 pore volumes reported to the drain, approximately 0.35 normalized cumulative tracer had been recovered. The Cluff Lake experiment observed flow through a waste rock test pile 5 m high with an 8 m by 8 m footprint. Mean residence time through this test pile was estimated as 3.0 to 3.9 years or estimated average pore-water velocity was 1.5 $m \cdot yr^{-1}$ (Nichol, 2002).This residence time compares to the residence time at the Diavik AZLs. Mean

residence time of the solute was estimated to be between 169 and 229 days or if corrected to the active water flow period (average of 137 days/year) the mean residence time is between 1.2 and 1.7 years (e.g., 169 days/137 days/year). For an equivalent height of the Cluff Lake experiment this would equate to between 3.6 and 4.9-year residence time. This includes the influence of the drier than average, lower drainage, conditions that occurred in 2009.

Cumulative mass load discharged from the lysimeters was between 41 and 51% of the applied load at the end of October 2009. The arrival time for the centre of mass is between 169 and 229 days, when the temperature was greater than 0 ºC, under the conditions experienced in 2008 and 2009, which included one year which received 110% of mean annual rainfall and the other year received less than 50% of the mean annual rainfall. The plug-flow model predicts a similar mean residence time, which suggests the majority of the solute transport occurs as diffuse matrix flow.

The presence of background Cl^- concentrations from blasting residues have been accounted for by establishing a relationship with NO_3^- concentrations. Other instrumentation installed at the AZLs are used to support the results of the tracer response. Observations of matric potential, moisture content and EC are used to confirm, or at least bound, the movement of conservative tracer through the waste rock in the following sections.

2.2.3 Flux Measured by Matric Potential

Nested tensiometers installed at depths of 0.3, 0.6 and 0.9 m between the two Type III lysimeters monitor matric potential within the matrix component of the waste rock. Along with VMC measured by co-located ECH_2O probes, it is possible to calculate the pore-water flux in the upper portion of the waste rock. An unsaturated hydraulic conductivity curve (equation 2-9) was produced with the Fredlund et al. (1994) relationship and a water retention curve relating moisture content to matric suction (ψ) as described by Neuner (2009):

$$\mathrm{K}(\psi) = 4x10^{-7}e^{-0.29\psi\,(kPa)} \qquad 2\text{-}9$$

The hydraulic conductivity for the equivalent matric potential ($K(\psi)$) can be used to calculate specified discharge (q) in upper portion of waste rock with the gradient (i) determined from the tensiometers and

based on Darcy's Law formulated for unsaturated conditions [$q = -K(\psi)i$]. **Figure 2-9** presents the specified discharge calculated past the co-located tensiometer and ECH$_2$O probe nest following tracer application. Average specified discharge to the peak wetting front arrival following the application of the tracer, determined by this method is 7.0 mm·d^{-1} at 0.45 m and 4.8 mm·d^{-1} at 0.75 m.

To determine the average velocity of the wetting front, the specified discharge is divided by the average moisture content of the matrix fraction.To compare to velocity estimates calculated in the previous section based on the recovery of Cl^- in the discharge, the specific discharge is divided by the average matrix VMC to estimate a velocity. Velocity of the wetting front is 0.4 m·d^{-1} at 0.45 m and 0.2 m·d^{-1} at 0.75 m, approximately an order of magnitude faster than that determined by movement of the tracer through the entire height of the lysimeter. Wetting front velocities in response to large rainfall events up to three to four orders of magnitude faster than the median water velocity have been also observed by others (Rasmussen et al., 2000; Nichol et al., 2005; Neuner et al., 2013). The average flux (discharge/ basal area) from the outflow over the same period was about 1 mm·d^{-1}.

2.2.4 VMC Response Following Applied Tracer

Following the applied rainfall event labeled with the tracer, the change in moisture content observed at the ECH$_2$O probes at depths of 0.3, 0.6 and 0.9 m, record a wetting front velocity of 30, 0.4 and 0.5 m·d^{-1} (**Table 2-1**). To calculate this, the depth to the sensor was divided by the time to peak change in moisture content. The peak change in moisture content is used to track the movement of the wetting front, as opposed to the initial response, which was harder to distinguish (**Figure 2-10**). Similar to the wetting front velocity determined based on the flux from the gradient measured at the tensiometers (**Section 2.2.3**), the initial wetting front advance estimated directly from a change in VMC is faster than the advance of the solute. The rate of advance of the wetting front was recorded to be slowing as it moves deeper. Again, these velocities are consistent with the response expected from a moderate rainfall generating a propagating pressure wave through porous media that mobilizes antecedent pore-water at velocities several orders of magnitude faster than the velocity of a particle of water.

2.2.5 VMC Response Following Applied Irrigation Event

The advance of the wetting front in response to the applied irrigation event, which was performed prior to the tracer application, provides insight to the effect of rainfall intensity on infiltration and antecedent moisture content (**Figure 2-10**). The applied rainfall on August 6, 2008 to increase the VMC of the matrix material to field capacity prior to initiating the tracer test occurred at an intensity of 15.2 $mm \cdot hr^{-1}$. The average velocity of the wetting front, based specified discharge, in response to the irrigation event was 0.01 $m \cdot d^{-1}$ at 0.45 m and 0.002 $mm \cdot d^{-1}$ at 0.75 m. Tracking the wetting front movement by the moisture content measured by the ECH_2O probes shows the peak VMC response to this applied rainfall was 0.2, 0.1, and 0.1 $m \cdot d^{-1}$ at 0.3, 0.6 and 0.9 m, respectively (**Table 2-1**). The wetting front from surface to 0.3 mbg moved approximately one order of magnitude slower when the lower intensity rainfall event was applied to the drier soil. From surface to 0.9 mbg, the wetting front moved at a rate 40% slower to two orders of magnitude faster than the rate of the wetting front following the applied tracer. The compounding effects of antecedent moisture content and intensity of applied rainfall are difficult to separate with this experimental design.

2.2.6 ECH2O Probe Response – Electrical Conductivity

In addition to moisture content changes, the ECH_2O probes record bulk soil electrical conductivity (EC) of surrounding medium, which can be converted to pore-water EC (Hilhorst, 2000). A higher EC represents increased concentrations of ions, which enhance the waters ability to conduct an electric current. Following the application of the Cl^- tracer, EC was used as a surrogate to track the tracer movement, assuming that sudden increases in EC are the result of the applied Cl^- as opposed to coincident changes resulting from increased mineral release through weathering or flushing previously weathered products. This assumption seems reasonable, as there was no change beyond the natural variation in EC following the applied unlabeled rainfall on August 6 (**Figure 2-11**). An EC spike first appeared at the 0.3 m probe 0.08 days after the tracer was applied. It peaked after 1.9 days and moved past the probe after 13.4 days. This EC front was logged at 0.6 m after 1.8 days, peaked after 2.2 days and moved past after 13.7 days. The probe at 0.9 m initially detected an increase in EC after 2.3 days, and a peak was recorded after 13.4 days and moved past after 14.7 days (**Figure 2-11**). The EC signal observed at all probes sharply

declined on the recession of the wetting front generated from the large rainfall event that began on August 25. Velocity of the EC front is determined by dividing the probe depth by the time until the peak EC was recorded. Velocity of the peak EC front at each depth varies between 0.2, 0.3 and 0.1 $m \cdot d^{-1}$ for 0.3, 0.6, and 0.9 m, respectively (**Table 2-2**). Although the estimated velocity at 0.6 m is not consistent with the velocity slowing with depth, signal noise may obscure the true peak (**Figure 2-11**). EC response at each depth is approaching an order of magnitude slower than observed from changes in matrix potential and VMC as reported in the previous sections. EC response at 0.9 m is about an order of magnitude faster than the average velocity observed from the projected centroid of the tracer at the discharge point. The EC response is useful to track solute transport in the upper portion of the waste rock and to confirm solute movement given the interference of the applied tracer with Cl^- present from the blasting agents.

The velocity of the wetting front advance estimated from measurements of gradient and matric potential, VMC and the advance of the EC front, allowed comparison to the response from the recovered tracer at the base of the AZL. The wetting front moved through the waste rock material as a pressure wave and provided the fastest indication of flow. The EC response in the upper portion of the waste rock was used a surrogate for the Cl^- response. Average Cl^- movement appeared slower than EC. The insight provided by the EC response at an internal location does not replace an accounting of mass and only accounts for transport that directly passed the probe location. Although the EC response allowed confirmation of the Cl^- movement and observation in the upper portions of the waste rock material, flow and concentration measurement at the base of the AZL provided full accounting of the mass of the solute that has migrated through the AZL.

2.3 Observed Response – Discussion

The majority of solute transport occurring through the matrix material at a site located in a semi-arid environment is consistent with the expectation that under drier conditions fluid flow will be confined the finer-grained matrix materials. Three response classes, fast, medium and slow, were reported in Nichol (2002) for the analyses of a tracer test for which discharge reported to a basal drain and 16 basal lysimeters underlying a constructed waste rock pile. Generally, flow was characterized as: (1) following

preferential flow paths (fast); (2) exchanging between macropores and matrix (medium); or (3) matrix flow (slow). The evolution of the tracer movement within the Type III rock at the AZLs appeared to demonstrate components of each of these flow classes. The initial response within 92 hours of application, in consideration of the mean average flow (see Section 2.2.2), demonstrated activation of preferential flow paths. In these paths there is no or little interaction of water in the flow path and water in the matrix. Spikes in tracer recovery in response to the significant rainfall events (e.g., August 25/26, 2008 and September 24, 2008), suggests exchange between the slower moving water in the matrix and faster moving pathways or macropore domain (i.e., a dual permeability model (Gerke and van Genuchten, 1993) or mobilization of Cl^- in flow paths that are only active under high moisture content and infiltration rates. Decreasing concentrations corresponding to low flow and minimal rainfall are interpreted to be matrix flow, initially releasing resident pore-water, followed by discharge contributing slow moving matrix water supplied by the tracer event.

The recovery ratio, normalized cumulative tracer recovery ($mg \cdot mg^{-1}$) divided by the normalized cumulative volumetric discharge ($m^3 \cdot m^{-2}$), was calculated as a means of describing dispersion (Nichol, 2002) and comparing the differences in response between the western and eastern lysimeters. Higher recovery ratios indicate greater dispersion since dispersion acts to spread the plume in front of the mean position of mass, generating a leading edge. Following similar discharge volumes at the AZLs, a higher recovery ratio indicates more Cl^- reported to the AZL drain by dispersion. The eastern lysimeter has a recovery ratio of 6.9, whereas the western recovery ratio is 5.9. Greater dispersion at the eastern lysimeter is evident, as the two lysimeters have otherwise been exposed to the same conditions with respect to tracer delivery, rainfall, and temperature. The western lysimeter has reported 95% of the discharge that has reported to the eastern lysimeter, however normalized tracer recovery is 81% of that at the eastern lysimeter. Variation in the grain size distribution included in each of the Type III AZLs is expected and greater dispersion related to large scale compositional heterogeneity, and variation in hydraulic conductivity (Adams and Gelhar, 1992) could explain the resultant differences, as could velocity variations in response to variable precipitation leading to increases in solute spreading (Zinn and Harvey, 2003). Preferential flow and mass transfer between mobile and low permeability domains will also contribute to dispersion, particularly under lower VMC conditions (Eriksson et al., 1997). Differential

spreading could also result from internal structure (Zhang et al., 1998) within the AZLs, however as the AZLs were constructed from material placed by excavator, few or no internal structures are anticipated. Density differences between the resident pore-water and the applied tracer (at least initially) may also drive (vertical) dispersion (in this case vertical dispersion is aligned with longitudinal dispersion) (Schincariol et al., 1994). The instabilities created by the density differences will diminish as dispersion acts to remove the differences in fluid density and create a smooth transition zone.

Non-Fickian dispersion (i.e., dispersion with a non-Gaussian distribution) is indicated by the arrival of concentration peaks prior to the arrival of the first moment (**Figure 2-5**). More likely there is a component of dispersion, rate-limited mass transfer and preferential flow paths.

The heterogeneous waste rock material produces a large range of hydraulic conductivity values which vary over short distances. This creates mobile and immobile zones, or higher and lower permeability zones, between which rate-limited mass transfer of Cl^- likely occurs. Some mass is likely stored in immobile, or low permeability, zones (Harvey and Gorelick, 2000).

A slower than expected tracer response has been observed by other researchers when the tracer sat after application (Jury et al., 1982). Upward gradients created by evaporation and the advance of the freezing front, transport the solutes in the water towards the surface (Gray and Granger, 1986; Flerchinger et al., 2004). The solutes will be excluded from the water as it freezes and will accumulate higher in the waste rock profile in the remaining unfrozen water. During the thawing sequence and the active period, the solutes within the upper portion of the rock profile may also be transported towards the surface by evaporation, particularly during periods of low infiltration and high solar radiation (Gray and Granger 1986). The conditions required to promote upward movement of the applied tracer resulting in a longer residence time are prevalent in the Canadian arctic and during 2009 when lower than average precipitation conditions occurred. For example, Section 5.4 documents one instance of upward moisture flux in response to the advancing freezing front.

Following the application of the tracer at the AZLs, the majority of water contained in the outflow in response to any individual rainfall event was pre-event water or by-passing flow post-event water. This

observation is similar to Nichol et al. (2005) where the pre-event water contained in the outflow to any individual rainfall event composed the majority of the discharge. By the end of the active season in 2009, between 41 and 50% of the initial mass of the applied tracer discharged from the base of the Type III AZLs.

Water and solute transport processes through the waste rock following application of the tracer included matrix flow, preferential flow, and exchange between these two domains. Solute transport occurs by both advection and dispersion and the heterogeneities encountered in the waste rock increase dispersion. Transport through the matrix results in a long residence time, transport is further slowed by processes that cause the solute to accumulate in the surface.

2.4 Conclusion

A natural gradient, pulse injected conservative tracer was applied at the AZL on August 12 at a rate of 16.3 $mm \cdot hr^{-1}$. Tracer response was observed by sampling the discharge at the base of AZL as well as by instrumentation for measuring VMC, matric potential and EC installed within the matrix of the upper waste rock profile. Solute transport in the unsaturated Type III waste rock at the Diavik Diamond Mine occurs at a slow rate, predominantly through the matrix material. Velocity estimates based on unlabeled moisture movement overestimate the rate of movement as the pressure wave response mobilizing resident pore-water in advance of the applied event is recorded. The majority of the water movement in the waste rock from the mine occurs through the matrix domain, and can be conceptualized by two or more flow and transport domains, with water flow and solute transport occurring in both domains. Except for the events on October 20/21, 2008 following the onset of freezing conditions and September 25/26, 2009 following both a period with minimal outflow and high intensity rainfall, pre-event water or by-passing flow composed the majority of the discharge on any individual day. The 14.9 mm tracer event delivered to waste rock with an average antecedent matrix VMC of 0.11 resulted in a small fraction of flow traveling in preferential flow paths. Discharge 92 hours after the application of the tracer included about 1% of the tracer, which suggests activation of preferential pathways, in consideration of the mean velocity, however the average movement of the tracer was through the matrix domain. Mean residence time was 169 days at the eastern lysimeter and was projected to be 229 days at the western lysimeter, this is equivalent to

between 1.2 and 1.7 years residence time, when corrected for the 137 days annual active period. Infiltration conditions during this response included one year which received 110% of mean annual rainfall (2008) and one year which received less than 50% of the mean annual rainfall (2009). The average advective velocity, during the active flow period is 7 to 10 $mm \cdot d^{-1}$. These results further support the conclusion reached by Neuner et al., (2013), and Fretz (2013) that the majority of water flow in response to moderate intensity rainfall moves through the matrix fraction and is therefore controlled by capillary forces. The significance of this is, that the longer residence time in contact with the finer-grain-sized fracture will allow greater reaction time and dissolution of weathering products.

As is expected, the advancing wetting front moves faster (300 to 50 $cm \cdot d^{-1}$) than the flux to 0.75 m (which occurs at a rate of 40 to 20 $cm \cdot d^{-1}$). The response of the EC front was 30 to 10 $cm \cdot d^{-1}$.

2.5 Recommendations for Tracer Test

The tracer test initiated in summer 2008 observed through fall 2009 provides useful data to allow characterization of residence time and flow processes in the Diavik waste rock. Future repetition of this experiment may be useful to provide variation of the application rate and antecedent moisture content, or to perform further correction for interference with residual Cl^- concentration from blasting agents, or to document the response in the absence of rare (100-year recurrence) rainfall events. Additional considerations for any future tracer test include:

- Identify potential sources of interference (e.g., background concentrations) prior to tracer application to inform tracer selection. Select a conservative tracer based on testing to confirm that the tracer will not be reactive in the material to be tested. Ideally, more than one tracer would be identified to provide a second conservative tracer to support results and interpretation.
- Determine sampling interval on flux-determined basis instead of a temporally determined basis;
- Recalculate IDF with the most current site specific data to better define event ranking; and
- Improve method for application of applied rainfall to allow lower intensity rainfall rates while maintaining uniform coverage.

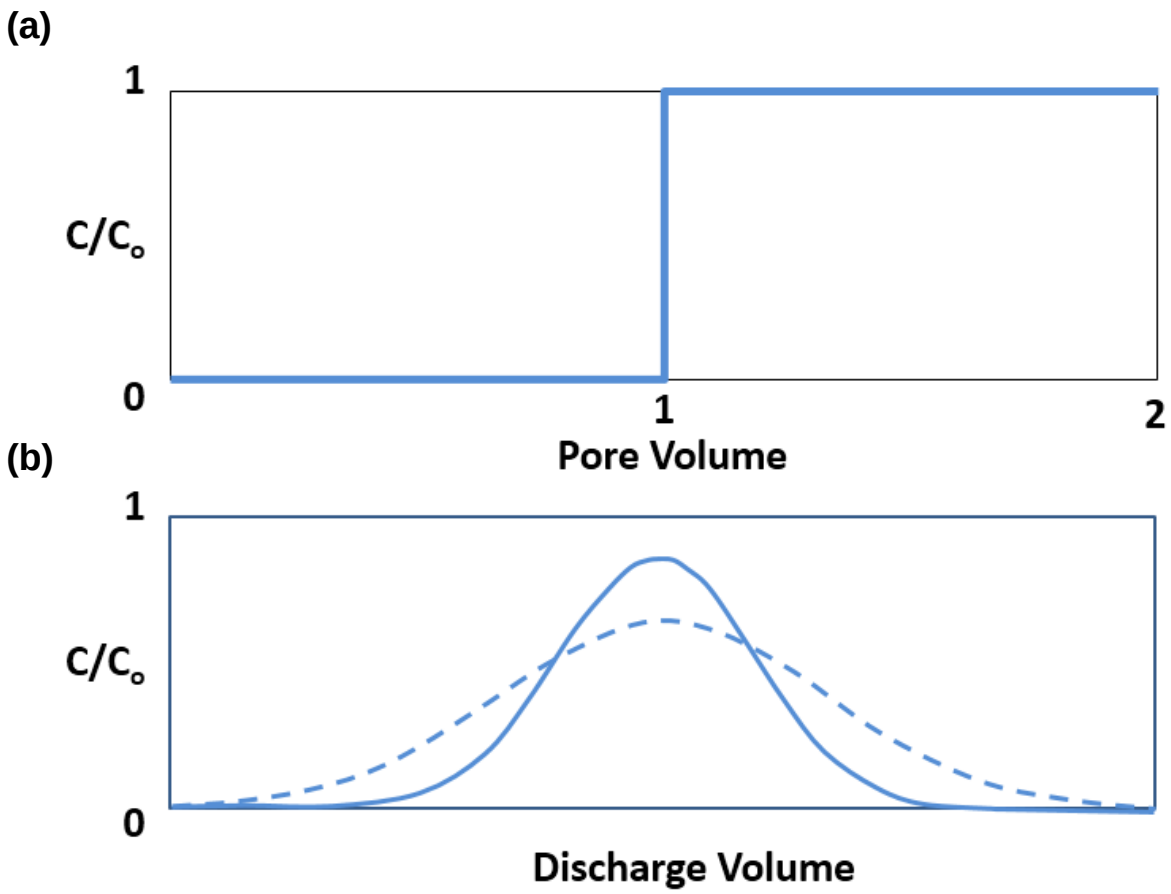

Figure 2-1: Conceptualized tracer concentration in discharge. Where C is the concentration at time, t, and C_o is the initial input concentration. (a) Advective transport only (piston-flow model). Tracer break-through occurs after 1 pore volume of discharge; (b) Solute transport by advection and dispersion results in tracer break-through ahead of the centre of mass. Dashed line represents tracer response to greater dispersion or rate-limited mass transfer, which reduces peak concentration, results in earlier arrival and longer tail.

Figure 2-2: Tracer test set-up showing two sprinkler configuration over the Type III AZLs. To record the magnitude and intensity of the applied rainfall, cups were positioned on the ground in an approximate 1 m by 1 m grid. Note, cups are visible in the photographs by the orange flagging tape.

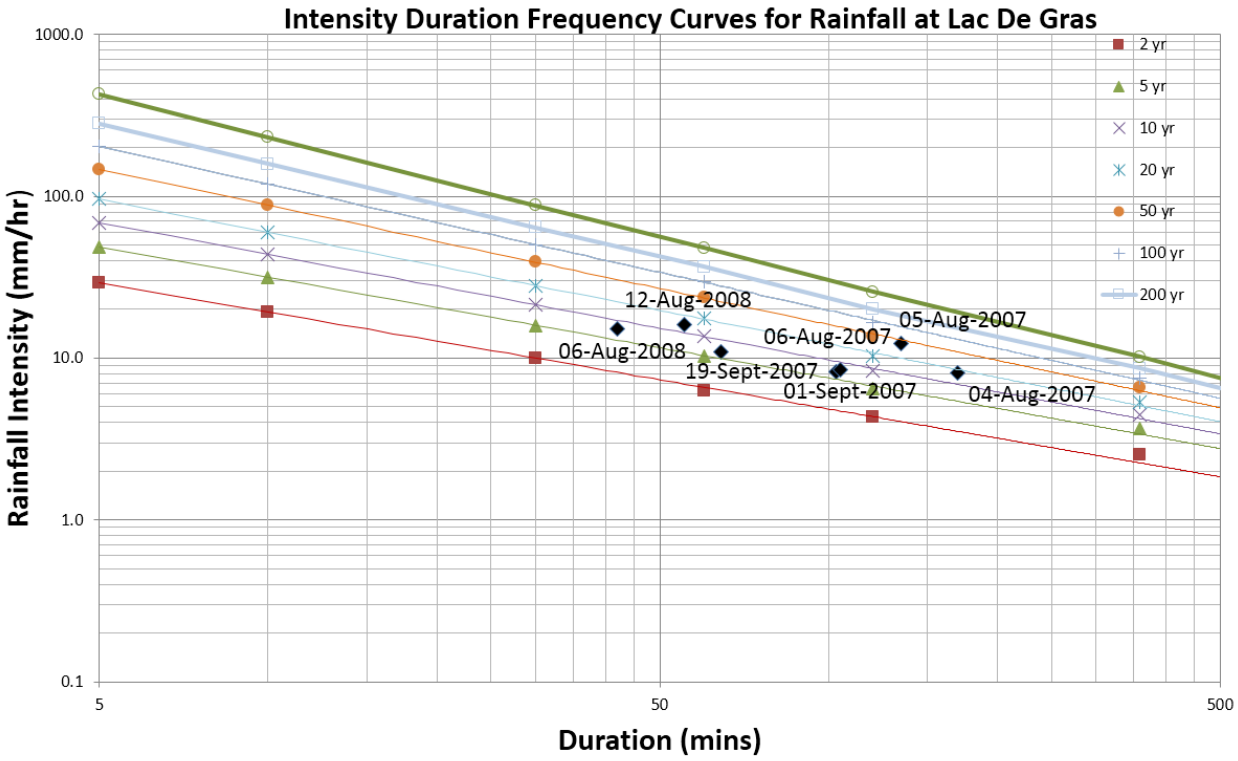

Figure 2-3: Applied rainfall events at the Type IIII AZLs plotted with respect to intensity and duration against intensity duration frequency curves for rainfall at Lac De Gras by Golder (2008).

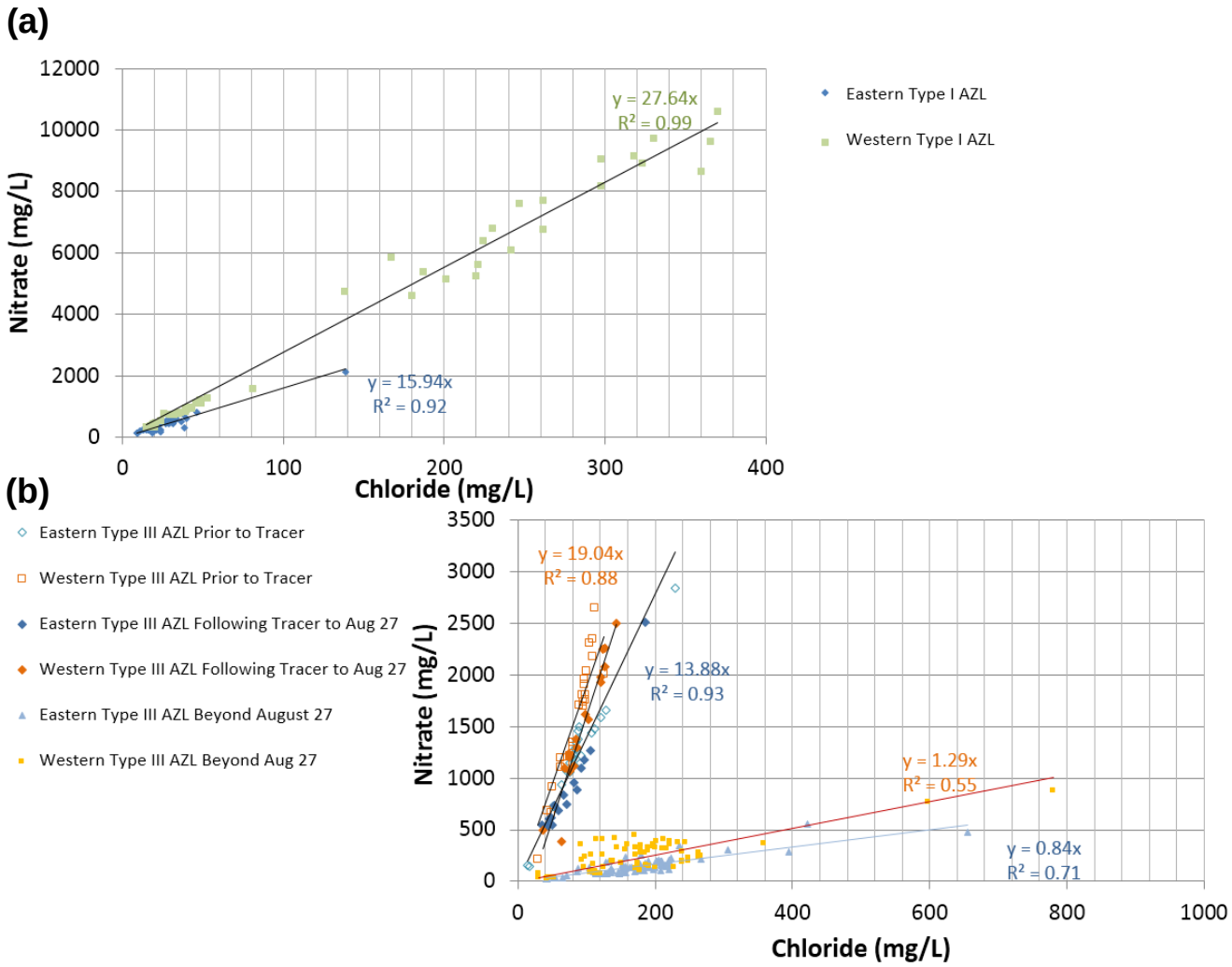

Figure 2-4: Relationship between nitrate and chloride at (a) Type I AZLs and (b) Type III AZLs.

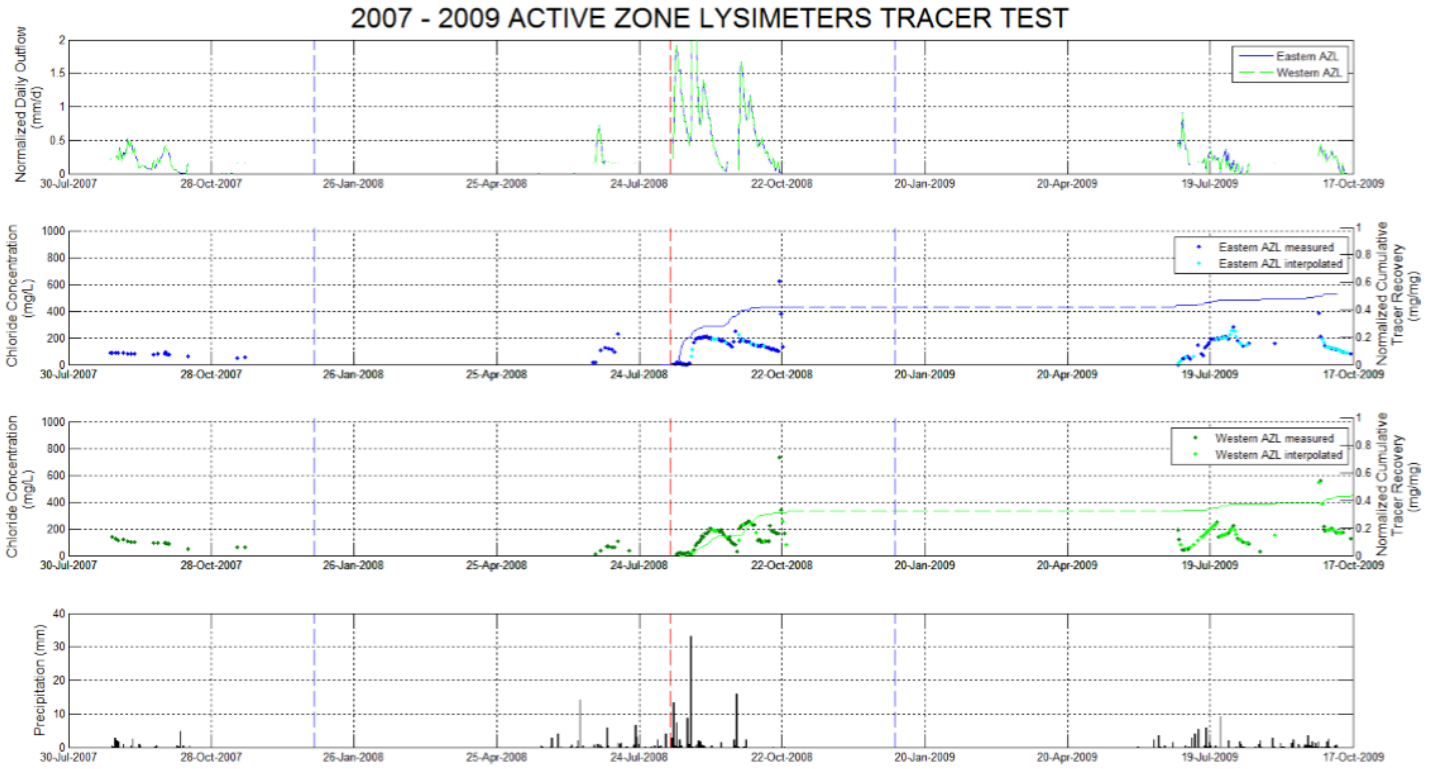

Figure 2-5: Comparison of normalized daily outflow, chloride concentration and precipitation prior to application of tracer and response for both the eastern and western Type III AZLs. Solid blue and green lines report normalized cumulative tracer recovery, vertical blue dashed lines mark January 1 of 2008 and 2009, and red dashed line denotes date tracer applied (August 12, 2008). Plotted chloride concentrations following tracer application are corrected for background concentration as described in the text.

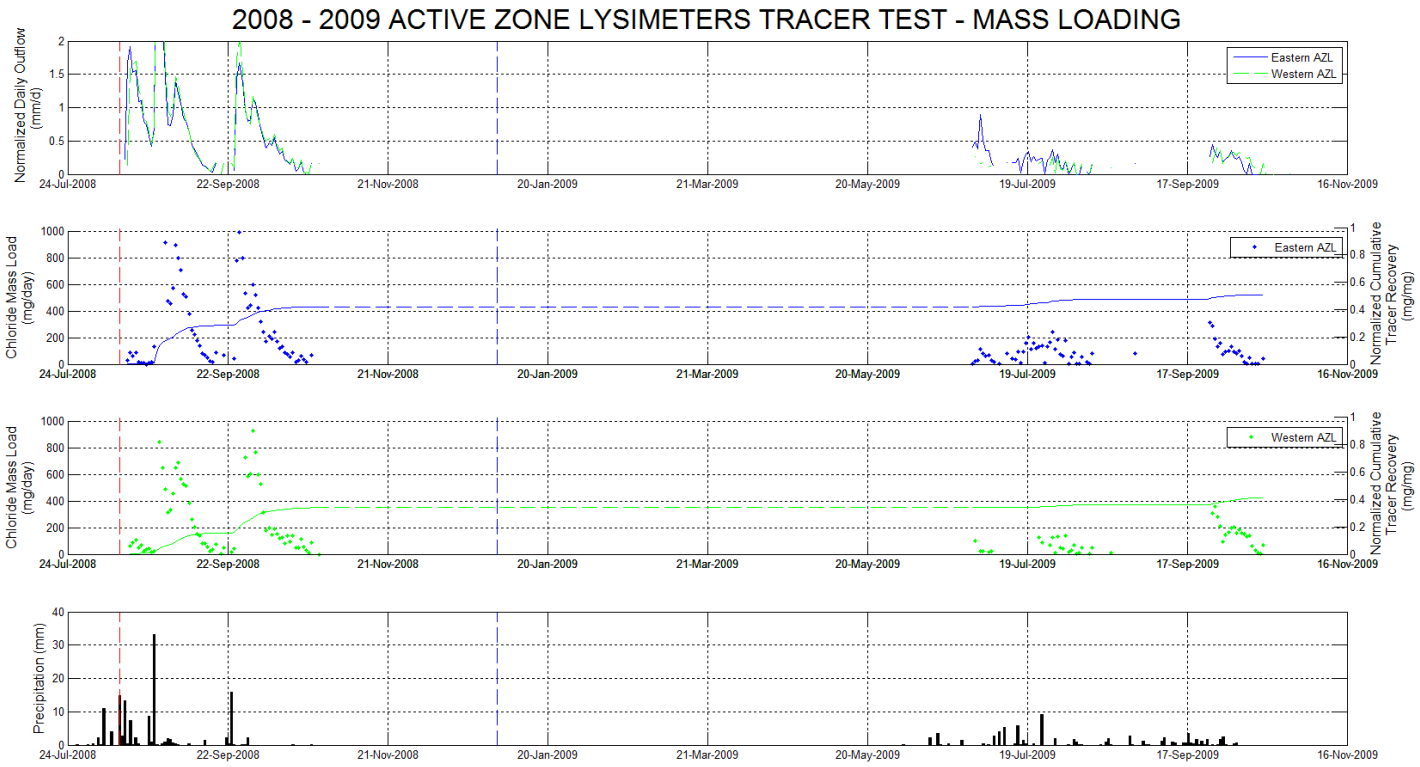

Figure 2-6: Comparison of normalized daily outflow, chloride daily mass loading and precipitation prior to application of tracer and response for both the eastern and western Type III AZLs. Solid blue and green lines report normalized cumulative tracer recovery, vertical blue dashed line marks January 1, 2009, and red dashed line denotes date tracer applied (August 12, 2008).

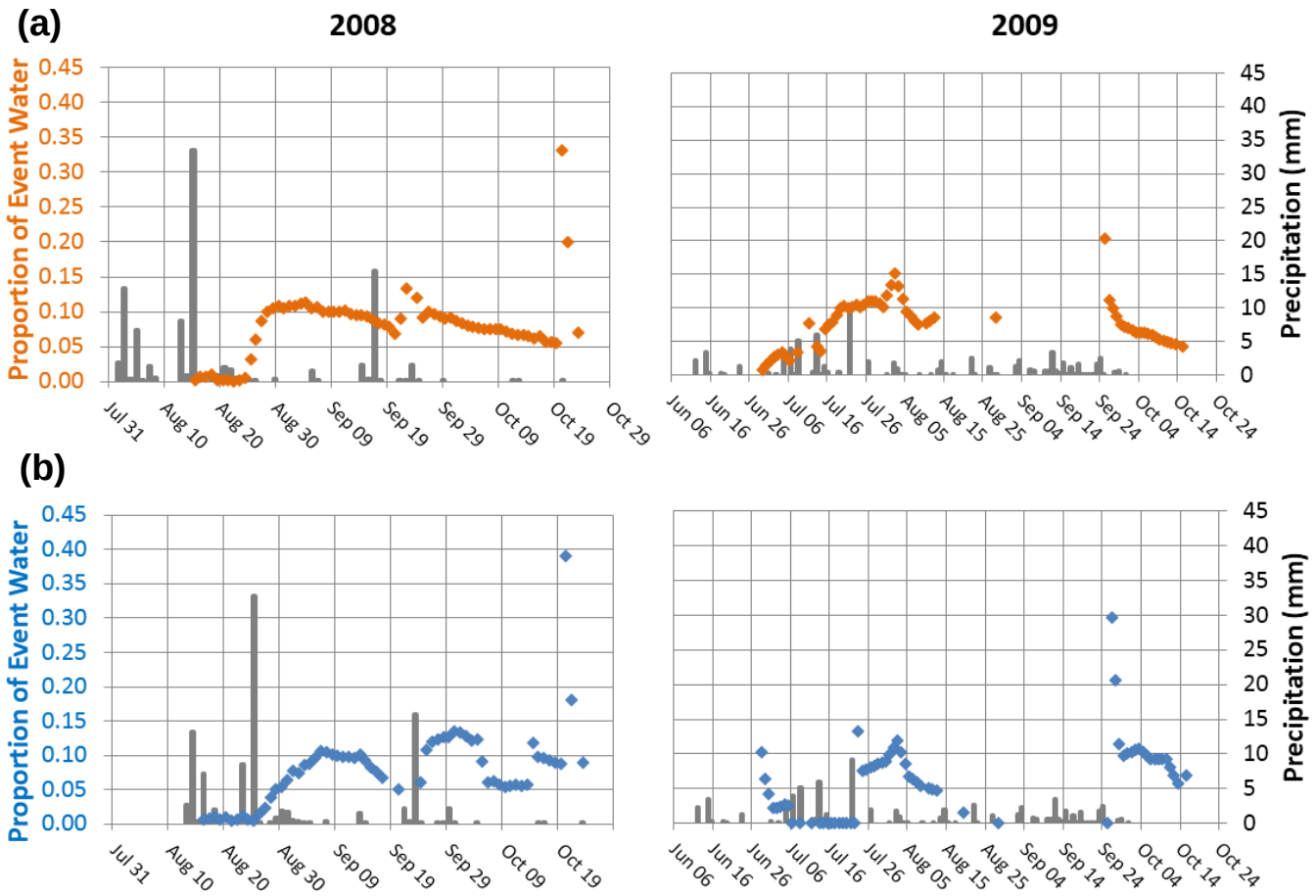

Figure 2-7: Percentage of tracer event water contained in the discharge by comparing the proportion of the conservative tracer in the discharge as compared to the source concentration for (a) Type III eastern AZL and (b) Type III western AZL. Precipitation shown by gray bars.

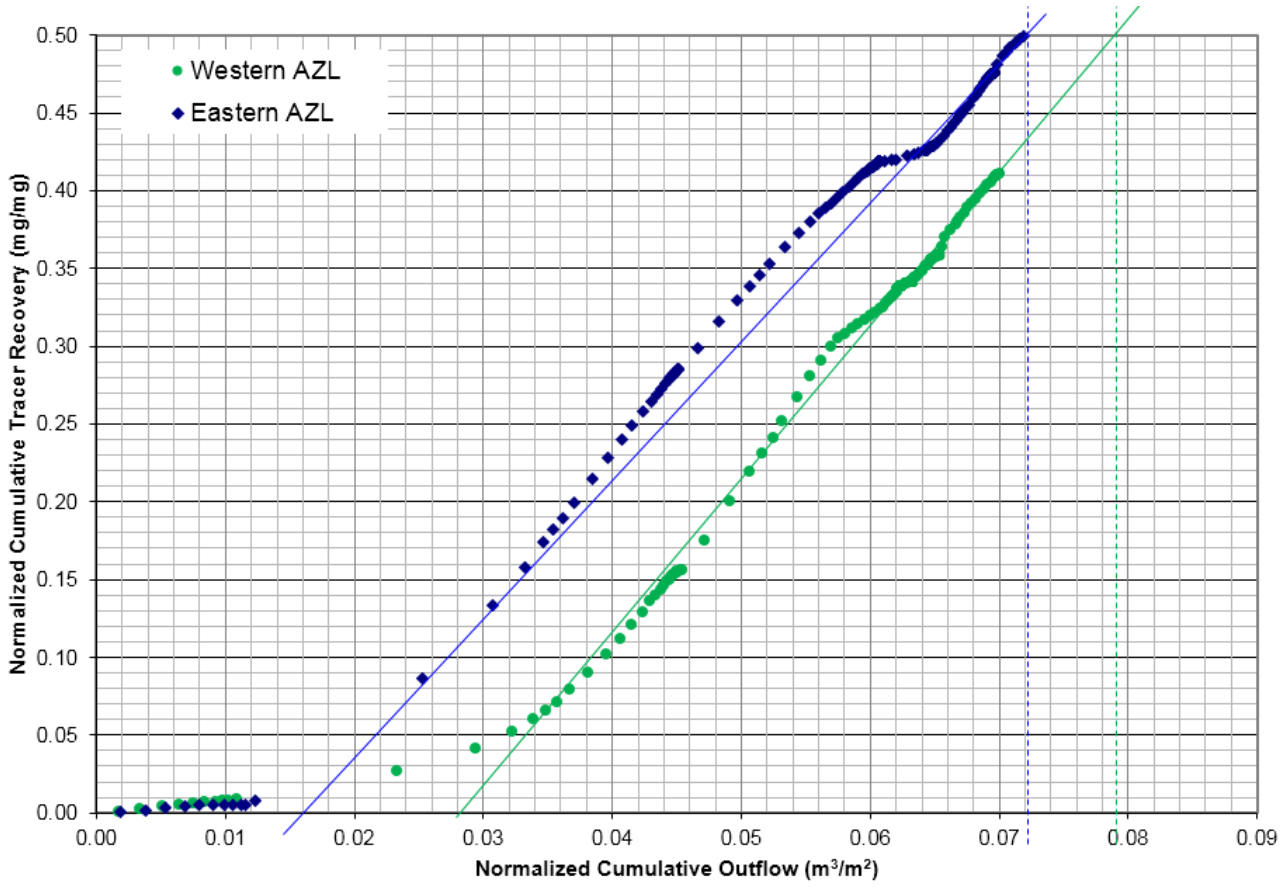

Figure 2-8: Normalized cumulative tracer recovery ($mg \cdot mg^{-1}$) versus normalized cumulative outflow ($m^3 \cdot m^{-2}$) for both the eastern and western Type III AZLs. Centre of mass indicated by 50% recovery.

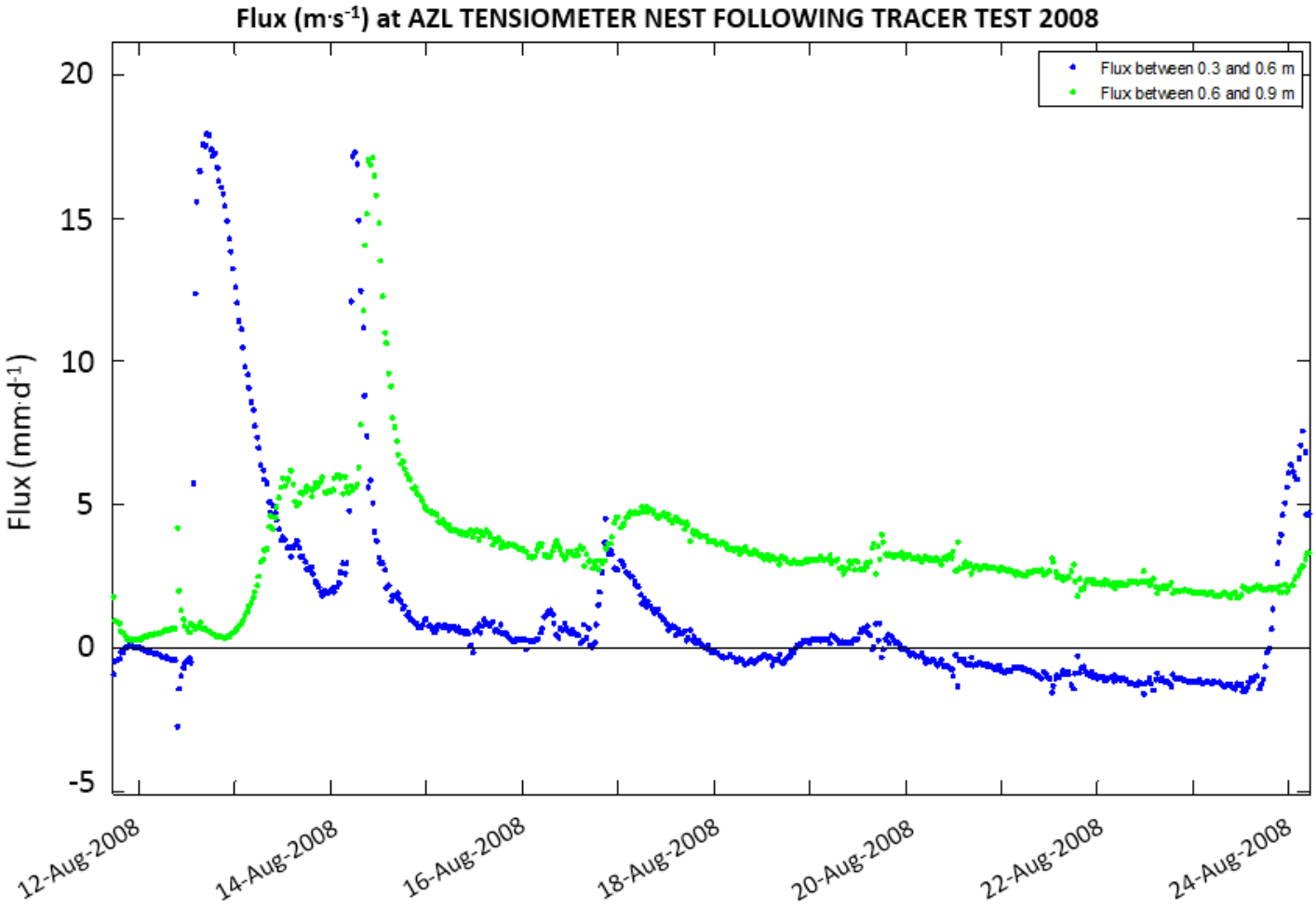

Figure 2-9: Flux ($m \cdot s^{-1}$) calculated at the co-located tensiometer and ECH2O nest between the Type III AZLs following tracer application in 2008. Positive flux indicates downward flow.

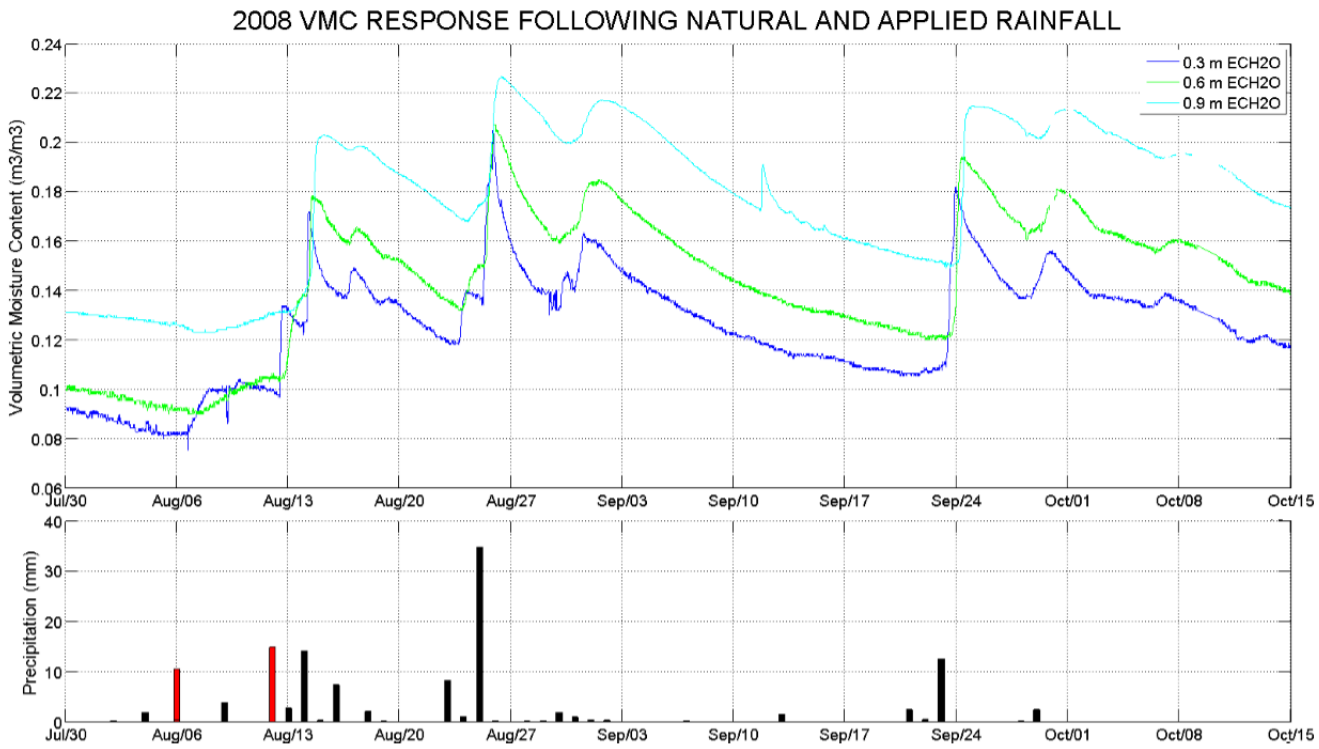

Figure 2-10: VMC response recorded by ECH₂O probes at the Type III AZLs (upper plot) following natural (black bars) and applied (red bars) rainfall.

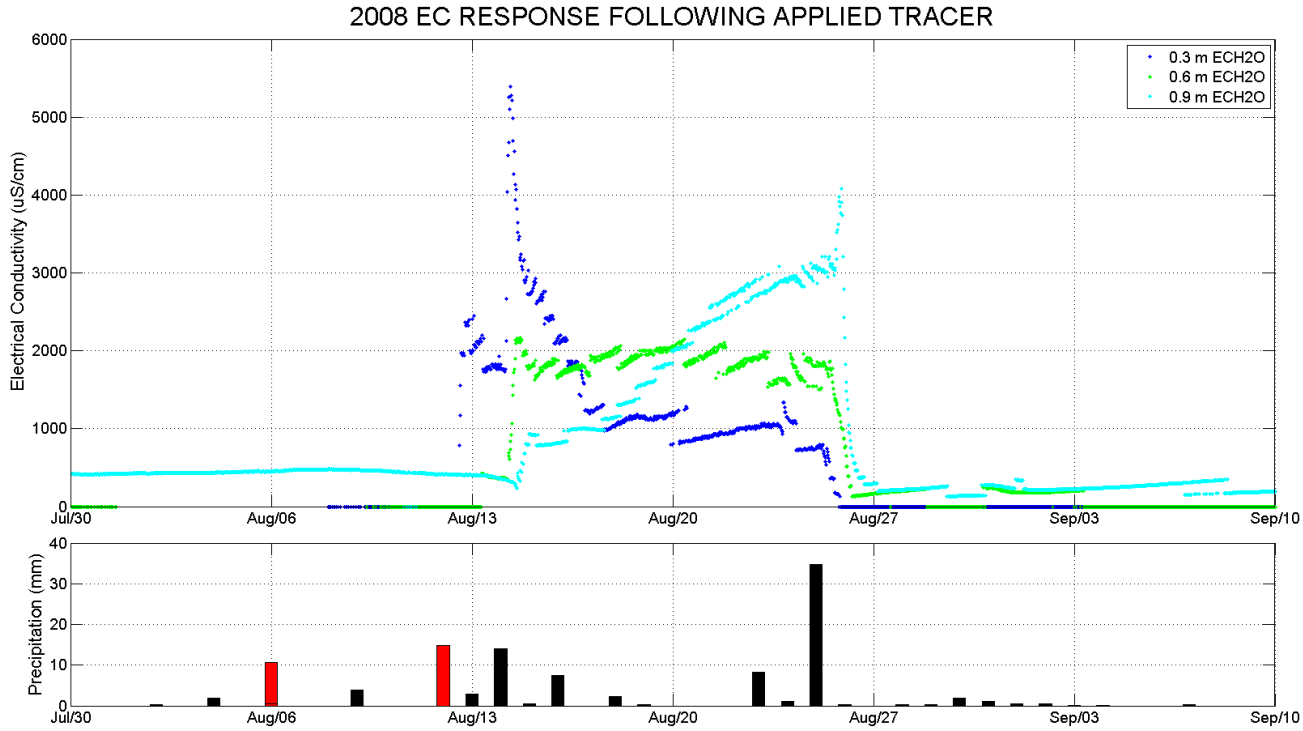

Figure 2-11: EC response recorded by ECH₂O probes at the Type III AZLs (upper plot) following natural (black bars) and applied (red bars) rainfall.

VMC by ECH2O Probes

Peak Response to Aug. 6 Applied Rainfall (06/Aug/2008 16:20:10)

Location (m)	Time of Response	Elapsed Time (hr)	Infiltration Rate (m/s)	Infiltration Rate (m/d)	Residence Time (days)
0.3	07/Aug/2008 21:30:00	29.2	2.9E-06	0.2	6.9
0.6	11/Aug/2008 04:30:00	108.2	1.5E-06	0.1	12.8
0.9	11/Aug/2008 18:00:00	121.7	2.1E-06	0.2	9.6

Initial Response to Aug. 12 Applied Tracer (12/Aug/2008 11:35:00)

Location (m)	Time of Response	Elapsed Time (hr)	Infiltration Rate (m/s)	Infiltration Rate (m/d)	Residence Time (days)
0.3	12/Aug/2008 13:00:00	1.4	5.9E-05	5.1	0.3
0.6	12/Aug/2008 19:00:00	7.4	2.2E-05	1.9	0.9
0.9	13/Aug/2008 12:00:00	24.4	1.0E-05	0.9	1.9

Peak Response to Aug. 12 Applied Rainfall (12/Aug/2008 11:35:00)

Location (m)	Time of Response	Elapsed Time (hr)	Infiltration Rate (m/s)	Infiltration Rate (m/d)	Residence Time (days)
0.3	12/Aug/2008 14:00:00	2.4	3.4E-05	3.0	0.6
0.6	13/Aug/2008 22:00:00	34.4	4.8E-06	0.4	4.1
0.9	14/Aug/2008 11:30:00	47.9	5.2E-06	0.5	3.8

Table 2-1: VMC response to applied rainfall and tracer test recorded by ECH_2O probes.

EC by ECH2O Probes

Peak Response to Aug. 12 Tracer Application (12/Aug/2008 11:35:00)

Location (m)	Time of Response	Elapsed Time (hr)	Infiltration Rate (m/s)	Infiltration Rate (m/d)	Residence Time (days)
0.3	14/Aug/2008 08:30:00	44.9	1.9E-06	0.2	10.6
0.6	14/Aug/2008 16:30:00	52.9	3.1E-06	0.3	6.2
0.9	25/Aug/2008 21:30:00	321.9	7.8E-07	0.1	25.3
		Average	**1.9E-06**		**14.1**

Initial Response to Aug. 12 Tracer Application (12/Aug/2008 11:35:00)

Location (m)	Time of Response	Elapsed Time (hr)	Infiltration Rate (m/s)	Infiltration Rate (m/d)	Residence Time (days)
0.3	12/Aug/2008 13:30:00	1.9	4.3E-05	3.8	0.5
0.6	14/Aug/2008 07:30:00	43.9	3.8E-06	0.3	5.2
0.9	14/Aug/2008 19:30:00	55.9	4.5E-06	0.4	4.4
		Average	**1.7E-05**		**3.3**

Table 2-2: EC response to tracer test recorded by ECH2O probes.

3 WASTE ROCK CHARACTERIZATION

This chapter documents the construction of a 32m^3 field permeameter and presents waste rock characterization parameters derived from the tests conducted. Similar to a laboratory permeameter (ASTM International, 2010a), the field permeameter allows measurement of porosity, and saturated hydraulic conductivity; except scaled-up to accommodate a representative waste rock sample. The design volume of the field permeameter was 32 m^3; however, the as-built dimensions are 3.96 by 3.96 m (15.68 m^2) with a waste rock sample height equal to 1.72 m to accommodate a coarse grain gravel base and as required to allow discharge from the upper drain. Therefore, the total volume of the waste rock sample in the field permeameter is 27.0 m^3.

3.1 Overview of Field Permeameter Experiment

Over the summer of 2009, a field permeameter was constructed to conduct controlled experiments on a waste rock sample to determine bulk material values for porosity and saturated hydraulic conductivity (K_{sat}). The maximum clast size included in the sample placed into the permeameter was 0.5 m^3. A brief description of the construction details follows. A plywood box supported by a wooden crib structure was constructed on a base of 50.8-mm minus crush material in which a lower drain, constructed of 50.8-mm inner diameter (ID) polyvinyl chloride (PVC) pipe, was installed (**Figure 3-1**). Geotextile fabric was placed on top of the crush material (Figure 3-1d). The plywood box was lined with a custom sized prefabricated one-piece polyethylene liner, Enviroliner 4040 (40-mil, or about 1-mm, thickness) manufactured by Layfield Geosynthetics & Industrial Fabrics Ltd. Prior to filling the lined permeameter with waste rock, an approximate 0.25-m thick layer of 9.5-mm crushed gravel was placed over the floor of the lined permeameter to provide a high permeability base to evenly distribute inflowing water from the lower drain and protect the lower PVC drain (**Figure 3-2**). An upper drain constructed of 50.8-mm ID PVC pipe, reports the outflow back to the main supply tank during K_{sat} measurement. Rubber gasket compression fittings on the upper and lower drains maintain a watertight seal (**Figure 3-2**). The final height of the waste rock sample above the crushed gravel to the upper drain is 1.72 m. Prior to placement of the waste rock, manometers consisting of 25.4-mm ID PVC pipe with a 50-mm hand slotted section at the base were positioned within the permeameter. The permeameter was filled on September 10, 2009 with

mined material from a September 6, 2009 blast from the A418 pit on the 360-040 bench that was reported to be classified as Type I material. This material was placed in the permeameter by free-dumping from an excavator bucket (Figure 3-2d). As a result of this method of material placement there was no compaction of the rock and less segregation of the clasts would occur as compared to end-dumping or push-dumping. Saturation of the waste rock sample was performed through the lower drain on September 13, 2009 and hydraulic conductivity testing was performed on September 15, 2009. This experiment was intended to replicate the one conducted by Neuner (2009) but at a larger scale, as the dimensions the previous permeameter were 4 by 4 by 1 m. The field permeameter and maximum sample size, were modelled after the 16 m^3 field permeameter by Neuner (2009). The permeameter constructed by Neuner was filled with Type III rock. Based on grain size analyses reported in Neuner (2013) and Smith et al., (2013), the Type III rock is typically slightly finer than Type I. The purpose of replicating the experiment conducted by Neuner was to generate greater hydraulic head differences across the sample than was achieved when conducted on the 1-m high permeameter. **Appendix B** provides the work plan created prior to conducting the experiment. The work plan includes further construction details and a complete methodology of the testing procedure.

Initial moisture content was determined on five matrix samples sieved to less than 5 mm fraction and an additional five hand samples sieved to less than 100 mm fraction collected from the waste rock prior to placement in the permeameter. These grab samples were split by cone and quarter methodology. Sieves, manufactured by Endecotts Ltd., serial no. 24-8-1-68, constructed of stainless steel mesh with a brass frame, were used to separate samples into the grain sizes. Equipment from the onsite grain-size lab was utilized to perform moisture content determination. Methods of moisture content determination followed ASTM D2216 (ASTM International, 2010b). The sample weight was determined with a calibrated Sartorious brand scale, model number LE340015, with 0.1 g accuracy prior to drying and following 24 hours in an oven at about 120^{o}C. Gravimetric moisture content measurements to volumetric moisture content determinations assume a bulk density of the waste rock equal to 2,040 $kg \cdot m^{-3}$ and density of water at 10^{o}C.

Bulk porosity of the field permeameter sample was determined by recording the volume of water required to saturate the waste rock sample contained in the permeameter. Water was pumped into the sample from the base until free water was just visible at the upper surface.

Saturated hydraulic conductivity (K_{sat}) from the field permeameter is determined by Darcy's Law (equation 3-1) by supplying water at a constant flow rate through the waste rock sample, with the water level at a measured head and known height of the sample (hydraulic gradient).

$$K_{sat} = \frac{Q}{iA} \qquad 3\text{-}1$$

Where the flow rate, Q, was controlled, the gradient, i, was measured over the height of the sample by the water table expression at the upper drain and the water level in the manometers, and the cross-sectional area, A, 15.7 m^2, was known, allowing calculation of K_{sat}. The flow rate, Q, was controlled by maintaining a constant head in a barrel set on a narrow rock bench adjacent to the top of the permeameter, which was supplied water from a storage tank (Figure 3-3). The upper drain returned water to the storage tank.

Seven trials were performed. Between each trial the flow rate was adjusted. The flow rate was increased between trial 1 and trial 4, then the flow rate was reduced between trial 4 and trial 6. The last trial repeated the experiment at approximately the same flow rate as the initial trial. The flow rate was checked during each trial, prior to measuring the hydraulic heads in the manometers and following the measurements to confirm that the flow rate remained constant through the trial.

Results from the field permeameter experiment are presented in **Section 3.2**.

Neuner (2009) reported on a drain down test conducted on the 16 m^3 permeameter to estimate the portion of drainage sourced from the coarse-grained and fine-grained portions of the sample for determination of the proportion of matrix porosity to free-draining porosity. The drainage plumbing of the 27 m^3 permeameter was sized too small to allow unobstructed drain down testing. The drainage plumbing was reduced from a nominal 50-mm diameter PVC pipe to a nominal 13-mm diameter flexible PVC tubing to accurately measure discharge volume (**Figure 3-3**). Analyses of the drain down testing

was not conducted as a result and also since cumulative discharge data on its own would likely have produced a non-unique solution if used to attempt to calibrate a model used to describe the outflow. Similar types of laboratory based drain down (one-step pressure outflow) experiments rely on internal measurements of matric suction or moisture content along with cumulative outflow (Zachmann et al., 1981; Kool et al., 1985, Van Dam et al., 1992). The purpose of the field permeameter experiment at Diavik did not have this type of modelling and data fitting in mind at the onset and no pressure head or water content data are available, except from the manometers screened in waste rock at the base of the permeameter.

3.2 Field Permeameter Experiment

As described in the preceding section a 27m^3 field permeameter experiment was established. Initial moisture content was determined for two sets of samples collected from the waste rock prior to placement in the permeameter. These samples were collected on September 10, 2009, five days after the material was blasted. Over these five days about 3.6 mm of rainfall occurred and 1.1 mm is estimated to have evaporated (Chapter 4). Therefore initial moisture content may be biased high, and overestimate run-of-mine material, but provides accounting of the initial moisture occupying pore-space from the material placed into the permeameter. The mean value of the initial volumetric moisture content of the five matrix samples, less than 5 mm screened fraction, collected from the material placed into the field permeameter is 6.2% ± 0.5% (**Table 3-1**). The fraction of material less than 5 mm is understood to exhibit capillarity and therefore retain water (Yazdani et al., 2000) and comprises approximately 18% of the waste rock (Neuner et al., 2013). Based on the less than 5 mm fraction, the initial bulk VMC of the full waste rock sample emplaced into the permeameter is 1.1% ±0.1% (0.062 x 0.18). However, the mean value of the initial VMC of five hand samples, less than 100 mm sieved fraction, is 3.7% ± 0.7% (**Table 3-1**). The less than 100 mm fraction comprises approximately 50% of the waste rock (Neuner, 2009). Based on the 100 mm fraction, the initial bulk VMC of the full waste rock sample emplaced into the permeameter is 1.8% ± 0.4% (0.037 x 0.5). These values provide similar estimates of initial VMC. An initial VMC of 1.8% was used to calculate porosity.

Saturation of the permeameter through the lower drain required 8.02 m^3 of water and occurred over a period of 160 minutes. Therefore including pore-space occupied by water initially held within the waste rock the bulk porosity of the waste rock sample is calculated as 31.5 ± 0.3% ([8.02 m^3+ 0.49 m^3]/27.0 m^3) (**Table 3-2**). This is higher than the estimate of about 24% (Neuner et al., 2013) but within a comparable range to estimates of waste rock porosity (Lefebvre et al., 2001; Martin et al., 2004; Azam et al., 2007; Yilmaz, 2011). As this larger permeameter is still not at the representative elementary volume, it is not inconsistent that two tests would differ by about 24%. For example, if two 0.5 m^3 boulders (or four 0.25 m^3 clasts) in the 16 m^3 permeameter were instead replaced with matrix material, the porosity would increase to 30%, given that large clasts have zero porosity.

The calculated saturated hydraulic conductivity of the sample is $5x10^{-3}$ $m{\cdot}s^{-1}$, the geometric mean of seven repetitions conducted at different flow rates. The saturated hydraulic conductivity ranged from $3x10^{-3}$ to $1x10^{-2}$ $m{\cdot}s^{-1}$ (**Table 3-3**). The upper estimate of this range is equal to estimates of saturated hydraulic conductivity presented in Neuner (2009) from testing on the 16 m^3 constant head permeameter ($1x10^{-2}$ $m{\cdot}s^{-1}$). Further these values are comparable to air permeability estimates made on the test piles reported in Amos et al., (2009) which were estimated as an average of $1x10^{-9}$ m^2 with a range between $2x10^{-10}$ and $3x10^{-9}$ m^2. As a permeability, the mean saturated hydraulic conductivity determined from the field permeameter is about $5x10^{-10}$ m^2, within the lower bound of the range reported by Amos.

Checks were made to ensure at the maximum flow rate, the Reynolds number for flow through porous media (Bear, 1988) was less than between 1 and 10, so that laminar flow was maintained and viscous forces predominant and as such Darcy's Law applied.

Results from the drain down test do not represent natural conditions due to a restriction on the drainage system and therefore are not reported.

Table 3-4 compares values from this work to values determined by Neuner et al., (2013) on a 16 m^3 permeameter, and replication of the experiment by Fretz (2013) on the same 27 m^3 permeameter described above.

3.3 Field Permeameter Experiment Conclusion

A field permeameter containing a 27 m^3 waste rock sample was constructed and tested to provide characterization of porosity and saturated hydraulic conductivity. Due to restrictions in the tubing during drain down, estimates of drainable porosity are inconclusive. The methodology used to conduct the field permeameter experiment, including maximum clast size included, was similar to that of Neuner (2009). The purpose of performing a similar experiment as that conducted by Neuner was to generate greater hydraulic head differences across the sample than could be achieved when conducted on the smaller 16 m^3 field permeameter, which accommodated a waste rock sample 1 m high. The 27 m^3 field permeameter contains a waste rock sample that is 1.72 m high. The initial bulk volumetric moisture content of the waste rock sample emplaced into the permeameter was 1.8% ± 0.4%. The bulk porosity of the waste rock sample was determined to be 31.5% ± 0.3%, which is higher than the value determined on the 16 m^3 field permeameter of about 24% (Neuner et al., 2013) but within a comparable range to other published estimates of waste rock porosity (Lefebvre et al., 2001; Martin et al., 2004; Azam et al., 2007; and Yilmaz, 2011). The mean saturated hydraulic conductivity of the sample is $5x10^{-3}$ $m \cdot s^{-1}$, and ranged from $3x10^{-3}$ to $1x10^{-2}$ $m \cdot s^{-1}$ between repeated trials at different flow rates. This range is less than, but comparable to estimates of saturated hydraulic conductivity determined on the 16 m^3 constant head permeameter ($1x10^{-2}$ $m \cdot s^{-1}$) (Neuner et al., 2013).

Figure 3-1: Field permeameter construction: (a) Lower drain constructed of 50.8-mm diameter PVC pipe and protected by rigid, thick-walled HDPE piping; (b) 50.8-mm minus crush pad placement; (c) Constructed plywood box with crib structure for support; and (d) Installation of the geotextile over crush material and one-piece polyethylene liner.

Figure 3-2: Field permeameter construction: (a) Filling box with 0.25-m thick layer of 9.5-mm crush gravel base; (b) Installation of 25.4-mm diameter manometers with 50-mm long hand slotted section at base; (c) Installation of rubber gasket compression fitting for lower and upper drain; and (d) Placement of Type I rock within and around the exterior of the permeameter for support.

Figure 3-3: Field permeameter final set-up: (a) For saturated hydraulic conductivity testing, water pumped from storage tank to constant head barrel; (b) water saturates permeameter from base to surface and flows through the upper drain back to the storage tank; (c) T-valve to allow water to drain from saturated permeameter; and (d) Discharge measurement during drain-down.

	Sample	Sample Date	Mass Sample + Pan, wet (g)	Mass, wet (g)	Pan #	Time in oven	Time out oven	Sample + pan mass, Dry (g)	Pan Mass (g)	Mass Dry (g)	Water Mass (g)	Gravimetric Moisture Content (w)	Volumetric Moisture Content (q)
< 5 mm screened fraction	MC-1	Sept. 12/09	226.2	219.9	7	9/11/09 20:05	9/12/09 20:10	219.2	6.3	212.9	7.0	3.3%	6.7%
	MC-2	Sept. 12/09	161.5	156.9	8	9/12/09 20:05	9/13/09 20:10	157.4	4.6	152.8	4.1	2.7%	5.5%
	MC-3	Sept. 12/09	105.0	97.8	1	9/13/09 20:05	9/14/09 20:10	101.9	7.2	94.7	3.1	3.3%	6.7%
	MC-4	Sept. 12/09	232.0	223.8	9	9/14/09 20:05	9/15/09 20:10	225.3	8.2	217.1	6.7	3.1%	6.3%
	MC-5	Sept. 12/09	198.7	188.9	10	9/15/09 20:05	9/16/09 20:10	193.4	9.8	183.6	5.3	2.9%	5.9%
<100 mm screened fraction	MC-6	Sept. 12/09	394.4	386.2	5	9/16/09 20:05	9/17/09 20:10	386.1	8.2	377.9	8.3	2.2%	4.5%
	MC-7	Sept. 12/09	461.3	447.6	3	9/17/09 20:05	9/18/09 20:10	454.8	13.7	441.1	6.5	1.5%	3.0%
	MC-8	Sept. 12/09	414.7	404.1	4	9/18/09 20:05	9/19/09 20:10	406.3	10.6	395.7	8.4	2.1%	4.3%
	MC-9	Sept. 12/09	341.0	330.1	2	9/19/09 20:05	9/20/09 20:10	335.2	10.9	324.3	5.8	1.8%	3.6%
	MC-10	Sept. 12/09	945.3	931.1	6	9/20/09 20:05	9/21/09 20:10	931.7	14.2	917.5	13.6	1.5%	3.0%

Table 3-1: Initial moisture content determination on Type I rock placed in field permeameter.

Volume of waste rock in permeameter	27.0 m^3
Volume of water to saturate waste rock	8.0 m^3
Initial volumetric moisture content	1.8%
Porosity	31.5 %

Table 3-2 Porosity determination from field permeameter.

	Test 1	Test 2	Test 3	Test 4	Test 5	Test 6	Test 7
Qavg (m^3/s)	1.1E-04	1.3E-04	1.3E-04	4.3E-04	2.4E-04	1.1E-05	1.2E-04
dh at manometer 1 (mm)	2	1	2	2	3	2	1
dh at manometer 2 (mm)	-3	-1	0	1	2	0	-1
dh at manometer 3 (mm)	9	12	10	7	14	0	8
dh average (mm)	3	4	4	3	6	1	3
dh/dL (m/m)	0.0015	0.0023	0.0024	0.0019	0.0036	0.0003	0.0015
Ksat (m/s)	**4.6E-03**	**3.5E-03**	**3.6E-03**	**1.4E-02**	**4.3E-03**	**2.5E-03**	**4.8E-03**

Notes:

Test 1: constant head at 0.9 m above box, valve opened 0.75 turns
Test 2: constant head at 0.6 m above box, valve opened 0.75 turns
Test 3: constant head at 1.2 m above box, valve opened 0.75 turns
Test 4: constant head at 1.2 m above box, valve opened 1.25 turns
Test 5: constant head at 1.2 m above box, valve opened 1 turn
Test 6: constant head at 1.2 m above box, valve opened 0.375 turns
Test 7: constant head at 1.2 m above box, valve opened 0.75 turns

Table 3-3 Bulk saturated hydraulic conductivity determination from field permeameter.

	16 m^2 Permeameter (Neuner et al., 2013)	27m^2 Permeameter (this work)	27 m^2 Permeameter (Fretz, 2013)
Bulk Porosity (%)	24	31.5	31.5[a]
Mean Saturated Hydraulic Conductivity (m/s)	1×10^{-2}	5×10^{-3}	6×10^{-3}
Estimated Matrix Porosity (%)	7	-	9
Estimated Free-draining Porosity (%)	18	-	22

Notes:

a. Fretz reported porosity values from an earlier version of this work. Values of estimated matrix porosity and free-draining are reported here, based on the updated porosity value but relying on the same estimated proportions.

Table 3-4: Comparison of waste rock properties determined on field permeameters at site.

4 WASTE ROCK WATER BALANCE

Water balances are needed in planning, development and closure of mining projects to enable water management. Understanding the hydrological components and processes in waste rock allows more accurate representation of the water balance. In this chapter, data from the well-instrumented AZLs at the Diavik Diamond Mine located in a semi-arid arctic environment are used to develop a water balance. The methods used to evaluate the collected dataset, which includes meteorological, VMC and discharge information, are presented in **Section 4.1.** Data available between 2007 and 2009 were considered. A water balance was not performed for the test piles, but the data components for storage changes in terms of moisture content, and drainage from the pile between 2007 and 2009 are documented. The water balance requires accounting for all water inputs and outputs to the waste rock piles; this includes precipitation, evaporation, run-off, discharge and changes in internal storage. Rainfall was recorded at three locations on the test piles and at other areas around the island (**Section 4.1.1**). Near continuous moisture content was recorded by custom-built TDR probes installed within the test piles (**Section 4.1.2**). A change in moisture content tracks redistribution and storage changes occurring within the test piles. Drainage from the piles was tracked by tipping buckets monitoring outflow from the base of the test piles and AZLs **(Section 4.1.2**). Evaporation was modelled based on meteorological information from a near-by monitoring station (**Section 4.1.3**). Evaporation was not directly recorded and the water balance was used to confirm estimates of modelled evaporation across the surface of the waste rock. Gradients measured at the tensiometers are also used to evaluate evaporation estimates. **Section 4.2** presents the results of the various water balance components and **Section 4.3** summarizes key observations from review of the water balance components and the development of the water balance.

The objectives of describing individual components and performing a water balance were to:

- produce a water balance for the AZLs to understand hydrologic processes in waste rock in an northern environment;
- assess the application of the extended Penman-Monteith model (Granger and Gray, 1989; Granger, 1999; Carey et al., 2005) to estimate evaporation from the Diavik waste rock test piles; and

- further develop a dataset of the temporal variations in net percolation and evaporation from waste rock surfaces in a cold semi-arid environment.

4.1 Water Balance Accounting - Methods

A water balance was produced for the AZLs to provide an accounting of the water movement within waste rock. The water balance was calculated by the following:

$$E = P – R - \Delta S - NP \quad (4\text{-}1)$$

Where:

E = evaporation
P = precipitation
R = runoff
ΔS = change in storage of moisture content (increase in storage is positive value)
NP = net percolation

The term net percolation is used instead of net infiltration consistent with the usage of Marcoline (2008) to distinguish from infiltration that occurs across the surface but in turn, may be subject to evaporation. For the AZLs, net percolation is measured as discharge at the base. Water received at the top surface of the waste rock test pile or AZLs may pond or runoff locally, but there is no loss from the pile. If surface runoff occurs, it is localized, and this water is conserved by the test pile. Ponding has been observed on the tops of the piles, but has generally been limited to traffic surfaces (i.e., areas of the ramp utilized for end-dumping material) from which water either seeps into the waste rock or is lost to evaporation. Therefore, R in the water balance equals zero. Precipitation includes rainfall plus snow-water-equivalent available when snowmelt begins, however, there were no snow surveys conducted between 2006 and spring 2010 and therefore the water balance only accounts for rainfall as precipitation. No transpiration occurs from the waste rock test piles and AZLs, as there was no vegetation.

4.1.1 Precipitation and Other Meteorological Data

A rain gauge located on the top of each of the Type I, Type III and Covered test piles recorded rainfall. The rain gauge on the Type III test pile became operational on September 16, 2006; the rain gauge on

the Type I test pile on May 5, 2007; and the rain gauge on the Covered test pile on June 14, 2008. A meteorological station operated by Diavik Diamond Mines Inc. (DDMI) recorded temperature, wind speed, wind direction, precipitation, average solar radiation, net solar radiation and relative humidity on an hourly basis since 1994. The meteorological station is located at approximately 2.1 km northwest of the test piles. The station is located at 2 m above a waste rock surface, at an elevation within 10 m of that of the test piles (Neuner et al., 2013). To further complement climate data the regional precipitation analyses performed by Golder (2008), was reviewed.

Snow surveys have not been completed at the waste rock test piles between 2006 and spring 2010. Visual observations of snow cover on the test piles have been periodically recorded. Depth of snow was measured at the manual DDMI climate station; however, due to processes of sublimation, ablation and redistribution and the importance of aspect, test pile alignment and the effect of the surrounding topography on wind patterns, these data are not useful to apply to the test piles. Snow density data are reported from snow surveys conducted between 2003 and 2007 (Golder Associates, 2008). Snow density ranged from 0.19 to 0.50 mm snow water equivalent (SWE) per mm depth of snow, with an average value of 0.30 $mm \cdot mm^{-1}$.

Ablation processes, including wind scour and sublimation, result in redistribution and outright removal of the snowpack from the test piles. Neuner (2009) estimated average snow depth on the batters of the test piles at the end of the snow accumulation cycle as 1.3 m for 2007 based on visual observation. At 0.30 $mm \cdot mm^{-1}$ SWE, this snow depth is equivalent to 390 mm of water available to infiltrate. Snow depth on the test piles is variable on each batter and not equal on the batters of each test pile due to different test pile centre-line orientations, as well as difference in roughness, and the slope angle between the Type I, Type III and Covered test piles. On the flat surfaces on top of the test piles and AZL, minimal snow remains at the end of the snow accumulation cycle as these surfaces are exposed to wind scour and sublimation. Neuner (2009) estimated a snow depth of less than 10 cm on the top flat surface of the test piles. Fretz (2013) considered the snowpack on these top flat surfaces to be negligible. Neuner's observation provides an upper estimate of the potential contribution of snowmelt infiltration (30 mm water equivalent) on the top surface of the test piles and AZL for an average year.

4.1.2 Storage/Redistribution

Moisture content storage and drainage components of water balance are documented in **Chapter 5**. In **Section 4.2.2**, moisture content changes and drainage from the AZLs is used to constrain and evaluate evaporation and net percolation estimates. Soil moisture within the matrix material component of the waste rock was monitored with TDR and commercially manufactured ECH_2O probes (Decagon Devices Inc.) (**Chapter 5**). These instruments allow changes in soil moisture to be tracked. **Section 5.2.1** covers the evolution the volumetric moisture content within the test piles, whereas in this section, VMC is used to identify periods during which there was no change in moisture storage within the AZLs to constrain evaporation/net percolation estimates.

Commercially manufactured ECH_2O probes were used to monitor temperature and electrical conductivity, in addition to soil moisture, and reside in the upper 0.9 m of the waste rock between the Type III AZLs. This location is instrumented with ECH_2O probes and co-located tensiometers at 0.3, 0.6 and 0.9 mbg. In 2009, a fourth temporary ECH_2O probe was installed at 0.06 mbg. This instrument set of co-located ECH_2O probes and tensiometers provides soil-moisture and matric potential data, which allows development of in-situ soil water characteristic curves and the calculation of moisture flux. VMC from the ECH_2O is used to develop a small-scale water balance to evaluate modelled evaporation in **Section 4.2.2.1**. **Section 4.2.2.3** reports infiltration estimates from flux calculations using the gradients recorded at the tensiometers.

4.1.3 Evaporation

Actual evaporation from natural non-irrigated soil surfaces is less than potential evaporation (Hillel, 1980; Wilson et al., 1994). Three stages of evaporation have been identified which are dependent on the degree of saturation of the soil and the available solar energy. The first stage occurs while the surface is saturated. The solar radiation received at the soil surface is the limiting factor and actual evaporation is approximately equal to potential evaporation. The second stage occurs as the soil dries, available moisture becomes the limiting factor and actual evaporation is less than potential. In the third stage, soil moisture is spatially discontinuous and movement of moisture restricted to movement by vapour diffusion.

Actual evaporation from a natural soil surface is limited by both climatic conditions and soil properties (e.g., hydraulic conductivity, and vapour diffusivity) (Wilson et al., 1994).

The Penman-Monteith equation (equation 4-2) has become a standard method for estimating evaporation in agricultural sciences (Allen et al., 1998) and is intended to be used for determination of evaporation from a well-irrigated surface which remains near saturation. Potential evaporation from a non-saturated surface can be calculated by:

$$ET_o(t) = \frac{0.408\Delta(R_n - G) + \gamma\left(\frac{37}{T_{hr}+273}\right)\mu_2(e^o(T_{hr}) - e_a)}{\Delta + \gamma(1 + 0.34\mu_2)} \qquad 4\text{-}2$$

Where Δ is the slope of the saturation vapour pressure temperature curve, at a given temperature (dimensionless), γ is the psychometric constant (kPa·ºC^{-1}); R_n is the net radiation (W·m^{-2}·hr^{-1}), G is the ground heat flux density (W·m^{-2}·hr^{-1}), T_{hr} is mean hourly air temperature (ºC), μ_2 is mean hourly wind speed (m·s^{-1}), $e^o(T_{hr})$ is the saturation vapour pressure at air temperature T_{hr} (kPa), e_a is the actual vapour pressure *(*kPa*)*.

This formulation is known as a combination equation. The component, $0.408\Delta(R_n - G)$*,* accounts for the energy balance, and provides the evaporation into saturated air caused by the addition of energy (Carey et al., 2005). Whereas the component, $\left(\frac{37}{T_{hr}+273}\right)\mu_2(e^o(T_{hr}) - e_a)$, accounts for the aerodynamic process, and provides evaporation into unsaturated air based on the humidity gradient between surface and atmosphere.

Adaptation is required to estimate actual evaporation from a surface that is variably saturated. The Penman-Monteith equation has been applied to calculate evaporation from waste rock surfaces by: (1) applying a constant to reduce potential evaporation to estimate actual evaporation (Bay, 2009); (2) applying a correction based on infiltration depth following the last rainfall (Neuner et al., 2013); and (3) applying a two-step correction (dual crop coefficient (Allen et al., 1998)) for water loss from the upper layer of waste rock based on deeper percolation and evaporation (Fretz, 2013). In the latter approach, evaporation from the layer near the waste rock surface is limited by the depth subject to evaporation (Z_e), the total evaporable water (TEW); and the readily evaporable water (REW). Fretz determined the REW

and Z_e by calibration with net percolation estimated from site data. The following describes an alternative method for determining evaporation from a waste rock surface using an extension of the Penman-Monteith model presented by Granger and Gray (1989), Granger (1999), Carey et al. (2005). Evaporation estimated by the method used in this work are compared to the calculated evaporation based on a water balance completed for the AZL. The estimates are also compared to estimates of flux across the upper waste rock surface determined from the measured gradients and VMC. Finally, the evaporation estimates by this method are compared to the evaporation estimates by Fretz (2013) and Neuner et al., (2013).

The advantage of the method presented here, as compared to the method employed by Fretz (2013), is the absence of field-based calibration of the terms for Z_e and REW. Although at Diavik, the AZLs and tensiometers allow coefficients to be determined for these parameters this may not be feasible at other sites of interest.

Granger and Gray (1989) modified the Penman-Monteith equation to develop a general equation describing evaporation from a non-saturated surface to estimate actual evaporation for different non-saturated land surfaces, which requires no prior estimation of potential evaporation and follows the complementary feedback approach. In the complementary feedback approach (Bouchet, 1963; Morton 1983), atmospheric conditions reflect surface parameters, and remove the need for measured surface parameters (i.e., calculation relies only on measured atmospheric parameters).

The eddy covariance method allows for direct measurement of evaporation from soil surfaces (Carey et al., 2005). The eddy covariance method requires continuous measurement of sensible heat flux, latent heat flux and ground heat flux about the surface. In Carey et al. (2005), evaporation modelled by the extension of the Penman-Monteith model (Granger and Gray, 1989; Granger, 1999) provided good agreement with evaporation directly measured by the eddy covariance method. This extension of the Penman-Monteith equation, relying on atmospheric data alone, predicted actual evaporation to within 10% of the value measured by eddy covariance method (Carey et al., 2005). The extension of the Penman-Monteith model was developed for surfaces with crops (Granger and Gray, 1989), extended to forest and alpine settings (Granger, 1999) and has been successfully applied to a waste rock pile (Carey et al., 2005). This extension of the Penman-Monteith equation is applied to the data collected at Diavik to

estimate evaporation from the top surface of the waste rock test piles and AZLs. Evaporation estimates are not calculated for the test pile batters as the energy balance part of the formulation, which is based on evaporation from the net radiation into saturated air, is expected to vary for different aspects (faces) of the waste rock test pile, but can be reasonably assumed to be equivalent to that received at the top surface of the test piles and AZLs. Equations 4-3 through 4-8 provide the equations used to estimate evaporation. The approach described here differs from that performed by Fretz (2013) and Neuner et al, (2013) as described in the following.

The general equation describing evaporation from a non-saturated surface formulated by Granger and Gray (1989) is:

$$E_{A-m} = \frac{\Delta E_R (R_n - G) + \gamma E_R \mathrm{Ea}}{\Delta E_R + \gamma} \qquad 4\text{-}3$$

Where $E_{R,}$ the relative evaporation parameter (dimensionless) (equation 4-4) and E_a is the drying power of air (equation 4-6). The difference between the Penman-Monteith formulation and the extension to the Penman-Monteith model is found in this relative evaporation parameter, which allows evaporation to be estimated from non-saturated surfaces. Formulated for different land use and vegetation cover, E_R is provided in Granger 1999 as:

$$E_R = \frac{1}{0.793 + 0.20e^{4.902\mathrm{D}}} + 0.006D \qquad 4\text{-}4$$

Where D, is the relative drying power of air (dimensionless) and determined by:

$$D = \frac{Ea}{(Ea + R_n - G)} \qquad 4\text{-}5$$

As noted by Granger (1999) characteristics of different surfaces are accounted for in the parameters for surface roughness and albedo, needed to determine E_a and R_n, respectively. The value for the ground heat flux density, G, was determined as 0.31 x R_n. This determination of the ground heat flux density is based on the observation in Pham (2013) that on an annual basis G/R_n for the Diavik waste rock piles is 0.31 (4.1 W/m^2/13.4 W/m^2). This relationship between the ground heat flux density and net radiation, R_n, is similar to the ratio reported by Carey et al. (2005) based on data from the Key Lake, Saskatchewan site

which has similar thermal and surface conditions. In that work, the ratio of the ground heat flux density to net radiation was equal to 0.28 for Rn less than 25 $W \cdot m^{-2}$.

A correction was also applied to periods when D was negative, so that actual evaporation is only determined for hourly periods when net radiation is positive (Granger, 1999). This correction excluded all negative values of D from total daily actual evaporation estimates.

The drying power of air *(*E_a*),* which is an estimate of the potential evaporation, is defined as:

$$E_a = f(u)(e_s(T) - e_a) \qquad 4\text{-}6$$

Where e_a is the actual vapour pressure of air (kPa), e_s (T) is the saturated vapour pressure of the air (kPa), at temperature (T) in ºC and $f(u)$ is the vapour transfer coefficient, which is determined by:

$$f(u) = \frac{0.622K^2pu}{P \ln\left(\frac{z_1-d}{z_{0m}}\right) ln\left(\frac{z_2-d}{z_{0h}}\right)} \qquad 4\text{-}7$$

Where P is atmospheric pressure (kPa), the von Karman's constant, K, is equal to 0.4, ρ is air density ($kg \cdot m^{-3}$), μ is wind speed ($m \cdot s^{-1}$), z_1 and z_2 are measurement heights for wind speed, humidity and temperature (m), z_{0m} is the roughness length governing momentum transfer, z_{0h} is the roughness length governing heat and vapour transfer (Han et al., 2011), and *d* is the zero-plane displacement height for vegetation surfaces (Granger and Gray, 1989). Equations for z_0 and *d* are provided in Allen et al., (1998) and are based on mean height of a vegetation surface. To apply to waste rock, the input for the mean height of a vegetation surface was replaced with one-half of the mean grain size of the waste rock surface, 0.1 m, as described by (Granger and Gray, 1989). The assumed roughness height of the waste rock was based on the mean grain size of the test pile exposed at the surface of the pile (Chi, 2011).

Following the approach taken by Neuner et al., (2013) and Fretz (2013), when the surface of the test pile, or AZLs, is frozen, evaporation is inhibited by the frozen surface and therefore the following condition is applied:

$$E_{A\text{-}m} = C_{temp} * E_{A\text{-}m} \qquad 4\text{-}8$$

Where C_{temp} is a temperature dependent coefficient and determined by the average daily temperature (T_{avg}) and is equal to one or zero, as follows:

if daily $T_{avg} < 0$, then $C_{temp} = 0$; and

if daily $T_{avg} \geq 0$, then $C_{temp} = 1$.

The difference between the Penman-Monteith formulation and the extension of the Penman-Monteith equation can be observed in equation 4-4, in the dimensionless relative evaporation parameter, E_R, and in equation 4-6, the drying power of air, E_a, which relates to the boundary layer and surface roughness conditions.

The Penman-Monteith equation, $ET_o(t) = \frac{0.408\Delta(R_n - G) + \gamma\left(\frac{37}{T_{hr}+273}\right)\mu_2(e^o(T_{hr}) - e_a)}{\Delta+\gamma(1+0.34\mu_2)}$, is presented next to the extension to Penman-Monteith equation used to calculate evaporation, $E_{A-m} = \frac{\Delta E_R(R_n - G)+\gamma E_R \mathrm{Ea}}{\Delta E_R+\gamma}$, for comparison.

Data required for the evaporation calculation includes temperature, mean wind speed, albedo, relative humidity, net solar radiation, barometric pressure, and latitude. **Table 4-1** presents the parameters required in the evaporation calculations. Following the approach of Neuner (2009) and Fretz (2013) from these hourly values, an estimated daily actual evaporation rate ($mm \cdot d^{-1}$) is determined.

An assumption for the waste rock test piles research site was that the meteorology data collected at the station location approximately 2.1 km northwest of the test piles were representative of the conditions at the test piles. The relative humidity may provide the greatest variation between the waste rock test piles and meteorological station. This discrepancy will affect all estimates of evaporation relying on recorded measurements not collected immediately above the test pile surface.

Using these formulations, the daily evaporation was estimated and compared to evaporation estimated by a water balance created for the Type III AZLs for several different periods in 2008 and 2009 during which there was no net change in storage at the 0.3, 0.6 and 0.9 m probes recording VMC located between the eastern and western Type III AZLs (**Section 4.2.2.1**). Evaporation was estimated by lysimetry on the Type I AZLs for the same periods in 2009. In 2008, evaporation could not be estimated for the Type I AZLs by lysimetry since the application of the two rainfall events described in **Section 2.1**, created VMC conditions recorded by the ECH_2O probes that did not represent conditions at the Type I AZL. In 2009, no applied rainfall events were performed and therefore the recorded VMC was assumed to reasonably

represent the conditions at the Type I AZLs. It was also assumed that (1) the moisture content between the lysimeters was representative of the moisture content within the lysimeters, and (2) that equivalent VMC at the recorded depths can be used to indicate the conditions at depths that lack VMC recording instruments, and (3) that changes are linear. Total rainfall during the period was compared to cumulative discharge over the same period; as there was no change in storage during these periods, and run-off from the surface of the AZLs has not been observed, the total rainfall was assumed to either evaporate, discharge or push existing pore-water to discharge.

There are two pairs of tensiometers installed at the Type III test piles, at 0.3 and 0.6 mbg, located north and south of the pile centre line. There are three tensiometers installed between the Type III AZLs, at 0.3, 0.6 and 0.9 mbg. The tensiometers installed at the AZLs and Type III test pile are used to determine the hydraulic gradient in the upper portion of the waste rock. The gradient is then used to calculate the flux in the upper portion of the waste rock to aid in the quantification of evaporation and net percolation. To prevent freezing, the tensiometers cannot be installed (i.e., filled with water) until nighttime temperatures are consistently greater than 0^{o}C, therefore they are not used to record snowmelt infiltration.

4.2 Water Balance Accounting - Results

This section presents the data and results of the individual water balance components and the water balance generated for the AZL used to evaluate evaporation estimates from the extended Penman-Monteith model. Rainfall or snow melt infiltration on the test piles (**Section 4.2.1**) infiltrates and evaporate across the surface of the waste rock (**Section 4.2.2**).

4.2.1 Precipitation

Rainfall recorded from rain gauges located on top of the test piles are supplemented with data from regional stations to confirm precipitation amounts since site stations have limited historical records. Rainfall recorded at the three stations located on the test piles over the course of the experiment (2007 through 2009) has been less than the annual average rainfall (163.9 mm), with the amounts of 84.6 mm in 2007, 154.1 mm in 2008, and 71.6 mm in 2009 (**Table 4-2**). Total rainfall in 2006 from the rain gauge located on the Type III test pile is unknown because the rain gauge was not installed and reliably operating until September 16.

As documented by Neuner (2009), several irrigation (applied rainfall) events have been carried out at the Type III test pile in 2006 and 2007. A total of 118.2 mm was delivered to the surface of the Type III test pile by these irrigations events. In 2007, the addition of the applied rainfall events to the naturally received rainfall on the Type III test pile resulted in approximately annual average rainfall. Applied rainfall events have also occurred at the Type III AZLs in 2007 (91.3 mm) and 2008 (25.5 mm) (**Table 4-3**).

Long-term mean annual precipitation for Diavik estimated from regional data between 1959 and 2006 is 350.9 mm (288.0 mm without correction for undercatch), which is partitioned to 163.9 mm rainfall (146.3 mm without correction for undercatch) and 187.0 mm snowfall (141.7 mm without correction for undercatch) (Golder Associates, 2008). This value of mean annual rainfall can be compared to the meteorological station maintained by Environment Canada at Yellowknife (located approximately 300 km southwest at an elevation of 206 m), which reports a mean annual rainfall of 161.5 mm from the period 1969 to 2009 (MSC, EC GC, 2010). Other regional stations include Ekati (located approximately 26 km north at an elevation of 469 m) and Lupin (located approximately 145 km north at an elevation of 490 m) which receive 164.9 mm and 158.3 mm mean annual rainfall, respectively. Environment Canada has records for the station at Ekati from 1998 through 2007 and for Lupin from 1982 through 2001. Data from the Diavik maintained meteorological station indicates a mean annual rainfall of 159 mm based on records from 2000 to 2003 and from 2006 to 2009 (**Table 4-4**).

Accumulation of snow on the surface of the test piles and AZLs is minimal (i.e., less than 10 cm) due to scour (redistribution) as well as sublimation on top of the piles (**Figure 4-1 and 4-2**). The average moisture content recorded at three ECH$_2$O probes installed between the Type III AZLs over the active period (from about the end of May to the end of October) was 13%. The difference in moisture content between the end of the previous season and the start of the next season provides a maximum bound on estimates of snowmelt infiltration. It is a maximum estimate as infiltrating rainfall that fell prior to the end of the previous season, may not have had time to penetrate to the depth of the sensor before the onset of freezing conditions. This water, rather than snowmelt infiltration, may cause the increase in moisture content following the onset of thawing conditions. Between the fall 2008 and spring 2009 there is a net loss in VMC. Between the fall 2009 and spring 2010 there is an estimated net gain of about 65.8 L or 31.5

mm infiltrated. This would be equivalent to a 10.5 cm snowpack, similar to the snowpack observed on the pile crowns by Neuner (2009).

4.2.2 Evaporation and Net Percolation

The components of the water balance: precipitation (**Section 4.2.1**), changes in soil moisture content (**Section 5.2.1**) and discharge (**Section 5.2.3**), are used to generate a small scale water balance at the AZL, to help assess the application of the extended Penman-Monteith model for estimating evaporation from the waste rock at the northern latitude of the research site (**Section 4.2.2.1**). The extended Penman-Monteith model is then used to estimate daily evaporation for the AZLs and Type I and III test pile for 2007 through 2009 (**Section 4.2.2.2**). Lastly, gradients measured by the tensiometers installed at the Type III test pile and AZL are used to further evaluate evaporation estimates (**Section 4.2.2.3**).

4.2.2.1 Comparison of Evaporation by lysimetry to Modelled at AZL

A small-scale water balance for the AZLs is presented to generate estimates of evaporation and net percolation, which are then used to evaluate estimates of evaporation calculated from the extended Penman-Monteith model (**Table 4-5)**. Seven different periods were identified during which no net change in moisture content was recorded at each of the three ECH_2O probes, or the change was minimal and was calculated. This analyses relies on the assumption that the zero net change in moisture content at the probe locations is equivalent to there being no change in storage throughout the AZLs, and the volume of net percolation can be determined from rainfall minus discharge. The fraction of rainfall that did not contribute to discharge is assumed to be evaporation, that is, equation 4-1 reduces to E = P – NP.

The AZL are closed-sided containers, and since there was no recorded change in storage during these periods, the underlying assumption in the following discussion is that the recorded discharge is linked to the precipitation that occurred. Although the same water is unlikely to contribute to discharge (Chapter 2), the discharge is a direct response to the rainfall. For example, if 3.5 mm discharges over a period with 18.9 mm of rain and no change in storage, then the infiltrating rainfall displaced 3.5 mm of water from pore-space within the lysimeter, which discharged at the base. The response could be described as a piston-flow, where the infiltrating water, or pressure wave generated in front of the infiltrating water,

pushes an equal amount of water out through the base; or the response may be coincidental and an equivalent volume of net percolation has drained over the same period.

Three of these periods provide a snapshot of evaporation over shorter durations extending over:

- 17-days in 2008 between June 13 and June 30
- 28-days in 2008 between September 5 and October 3
- 29-days in 2008 between September 6 and October 5

Two of these periods span the majority of the active season extending over:

- 124-days in 2008 between May 31 and October 16
- 67-days in 2009 between July 9 and September 19

Two additional periods span long portions of multiple active seasons through 2008 and 2009 over:

- 383-days between July 31, 2008 and August 18, 2009
- 485-days between May 28, 2008 and September 25, 2009

In the following summary, the eastern Type III lysimeter was selected to review, rather than report evaporation estimates from both lysimeters for all periods. As discussed in Section 2.2.1, discharge volumes from both the Type III AZLs have been similar. For the periods that span the 2009 active season and multiple years, the water balance was calculated for both Type III lysimeters for comparison and since the volume of discharge between the two lysimeters began to diverge in 2009.

In 2008, irrigation events were applied to the surface of the Type III AZL. Moisture content recorded by the ECH_2O probes are therefore unique to the area around the Type III AZL that received the applied rainfall and cannot be extend to the Type I AZL. However, in 2009, no irrigation events were applied; therefore, the water balance was also performed on the Type I AZLs.

The following documents these analyses, which are summarized in **Table 4.5**.

For the period between June 13 and June 30, 2008, 18.9 mm of rain fell and 7.4 L discharged from the eastern lysimeter. Net percolation estimated from the lysimeter is 3.5 mm (19% of the rainfall) and 15.4

mm evaporated for an average of 0.9 $mm \cdot d^{-1}$. Based on the calculated actual evaporation for this period using the extended Penman-Monteith model, net percolation equals 3.7 mm (20% of the rainfall) and 15.2 mm evaporated, also about 0.9 $mm \cdot d^{-1}$. For this period, the absolute difference in the modelled evaporation and evaporation estimated by lysimetry is 0.2 mm (1% of rainfall).

Over the late season response observed for the period between September 5 and October 3, 2008, 23.5 mm of rain fell and 43.2 L discharged from the eastern lysimeter. Net percolation estimated from the lysimeter is 20.6 mm (88% of the rainfall) and 2.9 mm evaporated for an average of 0.1 $mm \cdot d^{-1}$. Based on the calculated actual evaporation using the extended Penman-Monteith model, for this period net percolation equals 21.7 mm (92% of the rainfall) and 1.9 mm evaporated or about 0.07 $mm \cdot d^{-1}$. For this period, the absolute difference in the modelled evaporation and evaporation estimated by lysimetry is 1.0 mm (4% of rainfall). This is similar to the observation for the period between September 6 and October 5. For this latter period, the absolute difference in modelled evaporation and evaporation estimated by lysimetry is 0.2 mm (1% of rainfall).

For these shorter duration periods in June and September/October, at the beginning and end of the active season respectively, there was good agreement (i.e., 1 mm or less difference) between evaporation estimates calculated at the lysimeters and the modelled actual evaporation calculated by the extended Penman-Monteith model.

These two periods, at the beginning and end of the active season, are insightful to support the previous statement that there is an energy-limited stage, later in the active season. As noted above, the evaporation rate in June (about 0.9 $mm \cdot d^{-1}$) was greater than in the fall, when it was estimated as less than 0.1 $mm \cdot d^{-1}$.

In 2008, between May 31 and October 16, 176.4 mm of rain fell and 199.4 L discharged from the eastern Type III AZL, therefore 95.4 mm (54% of the rainfall) infiltrated, whereas 80.9 mm evaporated. This is an average of 0.7 $mm \cdot d^{-1}$ of evaporation. Using the extended Penman-Monteith model for actual evaporation, calculated net percolation is 107.6 mm (61% of the rainfall), whereas 68.8 mm evaporated, for an

average of 0.6 $mm \cdot d^{-1}$ over the same 124-day period. For this period, the absolute difference in the modelled evaporation and evaporation estimated by lysimetry is 12.2 mm (7% of rainfall).

The amount of natural rainfall received at the test piles in 2008 was approximately equivalent to the mean annual rainfall; however, with the two applied events the total rainfall received at the Type III AZL was 110% of the mean annual value. In addition, a large storm event occurred in 2008, delivering 35.8 mm over 24.8 hours. During this wet summer, net percolation was greater than 50% of the rainfall received. Although greater than 50% net percolation in a wet summer may appear high in relation to southern sites and native material (e.g., LeBlanc et al., 1991), rainfall received beginning in about early July, occurred after net radiation has peaked, and the available energy is the limiting factor for evaporation, which facilitates greater infiltration. In 2008, about 106 mm of precipitation fell between August 1 and October 16, which was approximately 70% of rainfall that was received between May 31 and Oct 16. In 2007 and 2009, about 85 and 45% of the rainfall occurs between August and October, respectively.

For comparison, over an 81-day period between June and August at Key Lake uranium mine in northern Saskatchewan, located at about 57.2^{o} N, 236 mm of rain fell; 145 mm was measured as evaporation (61% of rainfall) by the eddy covariance method and net percolation to the waste rock pile was 91 mm (39%) (Carey et al., 2005). Although net percolation at this northern site is not as high as during the period identified in 2008 at Diavik, the observed period at Key Lake only includes a portion of the period of declining net radiation following the peak in the early summer.

Over the 67-day period in 2009 between July 9 and September 19, 46.2 mm of rain fell, and 14.5 L discharged from the eastern Type III AZL. Net percolation is 6.9 mm (15% of the rainfall) and 39.2 mm evaporated for an average of 0.6 $mm \cdot d^{-1}$. Based on the modelled actual evaporation for this period, net percolation equals 10.5 mm (23% of rainfall) and 35.6 mm evaporated for 0.5 $mm \cdot d^{-1}$. For this period, the absolute difference in the modelled evaporation and evaporation estimated by lysimetry is 3.6 mm (8% of rainfall). Performing the same accounting for the western Type III AZL and both the eastern and western Type I AZLs indicates a range in the absolute difference between modelled evaporation and evaporation estimated by lysimetry of 1.5 to 7.9 mm (3 to 17% of rainfall). The low net percolation as compared to

2008, is a result of the low rainfall (i.e., less than half the mean annual average rainfall occurred in 2009), and the timing and magnitude of rainfall events that occurred during the energy limited stage.

Two longer-term durations spanning the 2008/2009 active seasons (or parts thereof) were also noted to experience no net change in storage. Although there is strong seasonal variation in net percolation/evaporation, consideration of these longer durations is informative for two key reasons: (1) they provide a longer duration average value for comparison; and (2) they help to define the amount of snowmelt infiltration.

Between July 31, 2008 and August 18, 2009, 153 days for which the lysimeters were active (unfrozen), 178.5 mm of rain fell and 215.8 L discharged from the eastern Type III lysimeter. Net percolation was 103.3 mm (58% of the rainfall) and 75.3 mm evaporated, for an average of about 0.5 $mm \cdot d^{-1}$. Based on the calculated actual evaporation for this period, infiltration was 104.9 mm (59% of rainfall) and 73.7 mm evaporated or about 0.5 $mm \cdot d^{-1}$. For this period, the absolute difference in the modelled evaporation and evaporation estimated by lysimetry was 1.6 mm (1% of rainfall). The same accounting is performed for the western Type III lysimeter for comparison. The absolute difference in the modelled evaporation and evaporation estimated by lysimetry was between 7.3 mm (4% of rainfall).

Between May 28, 2008 and September 25, 2009, there were 243 days when the lysimeters were active (unfrozen). This spans much of the 2008/2009 experiment during which outflow occurred. There was less than 0.003% net change in VMC recorded at any depth in the lysimeter over this period for a calculated total change of -2.8 L. During this period, 245.4 mm of rain fell and 225.4 L of discharge occurred from the eastern Type III lysimeter or was lost to change in moisture storage. Therefore, approximately 107.8 mm (44% of the rainfall) was observed to infiltrate and report as drainage and 137.6 mm evaporated, for an average of 0.6 $mm \cdot d^{-1}$. The modelled actual evaporation over this period was 136.0 mm (55% of rainfall) and 109.4 mm infiltrated. For this period, the absolute difference in the modelled evaporation and evaporation estimated by lysimetry was 1.6 mm (1% of rainfall). Performing the same accounting for the western Type III lysimeter indicates an absolute difference in the modelled evaporation and evaporation estimated by lysimetry of 9.9 mm (4% of rainfall).

A check of net percolation estimates from this longer period that spans two active seasons against estimates of net percolation reported for periods within 2008 and 2009 was performed. In 2008 net percolation by lysimetry was calculated as 95.7 mm, and 7 mm in 2009 for a total of 102.7 mm. Note that in 2009 the observed period with no change in storage was between July 9 and September 19, and therefore shorter than the period considered in the preceding paragraph. Net percolation calculated based on the modelled evaporation was 109.6 mm in 2008 and about 0 mm in 2009. This is an absolute difference of 13.9 mm in 2008 (7% of rainfall) and 7 mm in 2009 (11% of rainfall).

For these periods that span multiple active seasons, the calculated net percolation may underestimate evaporation (calculated as one minus net percolation as percent of rainfall) which neglects infiltration supplied by snowmelt. At 30% snow water equivalent (Golder Associates, 2008) a snowpack not greater than 10 cm thick, at the end of the snow accumulation cycle, on top of the AZLs could supply up to 30 mm of snowmelt infiltration. However, the agreement between the modelled actual evaporation and the evaporation calculated based on the lysimeter water balance would suggest that minimal infiltration is supplied through the tops of the AZLs by snowmelt. This is consistent with observed snow redistribution processes including scour and sublimation (**Figure 4-1 and 4-2**) and observations by other (Fretz, 2013; Neuner et al., 2013).

The proceeding comparison between evaporation and net percolation estimates based on observed conditions at the AZLs and the extended Penman-Monteith model suggests the method as a valid technique for estimating evaporation at waste rock piles in northern environments and an alternative to the method applied by others (Fretz, 2013; Neuner et al., 2013). **Table 4-6** provides a comparison of estimated net percolation for the Type I and Type III AZLs between the method presented here and the approach by Fretz (2013). These net percolation estimates are within 1 mm for 2008 and 6 mm for 2009. In 2009, net percolation was the same for the Type I and Type III AZLs since they received the same rainfall, as opposed to 2008 when irrigation events were applied at the Type III AZLs.

This method has employed assumptions regarding the ground heat flux density, G, and roughness height, h, however it has been applied with success to other waste rock surfaces (Carey et al., 2005) and based on this work, it appears suited to use at different sites.

For these periods that range between 17 and 243-days when the lysimeters were active, there was good agreement between observed evaporation at the lysimeters and evaporation modelled by the extended Penman-Monteith equation. In this case, good agreement was defined as having an absolute difference between 0.2 and 12.2 mm, or less than 17% of rainfall (**Table 4-7**). The absolute difference as a percentage of rainfall was less than 10% except during the 67-day period in 2009 between July and September from the western Type III lysimeter (17% of rainfall) and the eastern Type I lysimeter (15% of rainfall). The absolute difference was less than 8 mm for both of these locations. Further improvement on evaporation estimates may be achieved by determining a calibration coefficient for site data and applying the temperature correction factor (equation 4-8) on an hourly time-step instead of a daily. As demonstrated over the shorter periods, there is strong seasonal variation; the usefulness of determining evaporation over annual periods was to allow comparison of the model estimates to observed data. Seasonality, at a monthly or finer scale, should be taken into account when determining and applying evaporation estimates to waste rock piles in an arctic environment. Another important observation from these analyses is that the net percolation/evaporation as a percentage of annual rainfall varied significantly with variation in annual rainfall.

4.2.2.2 Modelled Evaporation at AZL and Test Piles

Since there was good agreement of evaporation estimated by the extended Penman-Monteith model with evaporation estimated by the water balance at the AZLs, the model was used to calculate evaporation on a daily basis between 2007 and 2009 for the AZLs as well as for the Type I and Type III test piles. Daily actual evaporation calculated by the extended Penman-Monteith model is presented on **Figures 4-3 through 4-5** as cumulative annual evaporation. These figures also provide a comparison of the modelled actual evaporation to the calculated potential evaporation. **Table 4-7** presents cumulative annual estimates of actual evaporation using the extended Penman-Monteith model for evaporation from the surface of the AZLs and from crowns of the test piles. Estimates of evaporation through batters are not provided as the energy balance and water balance will vary for different aspects (faces) of the waste rock test piles.

In 2007 and 2008, evaporation at the Type III AZLs was estimated to be 41% (73.0 mm) and 42% (75.1 mm) of rainfall; applied rainfall bought the rainfall received to approximately 110% of the long-term average for both of these years. In 2009, evaporation was estimated to be 94% (67.0 mm) of rainfall and rainfall was less than 50% of the average annual. Evaporation estimates are the same for the Type I AZLs and Type I test pile, since both have been exposed to the same conditions.

For test piles which received close to the mean annual average rainfall (i.e., Type III test pile in 2007, and Type I and Type III test piles in 2008), it was estimated that approximately 50% of the rainfall evaporated (75.1 mm). In 2009, when less than half of the mean annual rainfall occurred, evaporation was estimated to be 94% of the received rainfall from all the test piles (67.0 mm). The monthly average evaporation rate was 0.1, 0.8, 0.8, 0.5, 0.1 and 0.01 $mm \cdot d^{-1}$ in May, June, July, August, September and October.

Using the data collected by Neuner (2009), evaporation was calculated by the extended Penman-Monteith model for the waste rock test piles for 2007. Evaporation from the Type III test pile was estimated as 50% of rainfall (73.0 mm) in 2007 and as 85% of rainfall (73.0 mm) from the Type I test pile. Neuner (2009) calculated evaporation in 2007 at the Type III test pile as 61% of rainfall (93 mm) and at the Type I test pile as 102% of rainfall (95 mm). To calculate evaporation Neuner used the FAO-56 Penman-Monteith formulation (Allen et al., 1998) to determine the reference evaporation and then applied a soil moisture-dependent coefficient and a temperature-dependent coefficient to determine actual evaporation.

4.2.2.3 Evaporation Estimates Based on Gradient at the Tensiometers

The tensiometers installed at the AZLs and Type III test pile were used to determine the hydraulic gradient in the upper portion of the waste rock. The gradient is then used to calculate the flux in the upper portion of the waste rock to aid in the quantification of evaporation and net percolation.

The gradient is influenced by the volume and frequency of rainfall events. In 2007, the applied events on Type III test pile and Type III AZLs created wetter conditions, resulting in a persistent downward gradient for the majority of the active season (Neuner, 2009). In 2008, an upward gradient, representing upwards flux between the tensiometer at 1.2 and 0.6 mbg at the Type III test pile was recorded during the majority

initial part of the active season between July and mid-August (**Figure 4-6**). This is consistent with the expected higher input of solar radiation received during this part of the summer, which will promote evaporation as described in **Section 4.2.2**. This is also consistent with the expectation that during periods with lower magnitude precipitation events, evaporation will dominate over infiltration, and an upward gradient would be expected. During the latter part of the active season, beyond about mid-August when higher magnitude precipitation events and wetter conditions were more prevalent, in conjunction with declining solar radiation, the gradient reverses, and was predominantly downwards (**Figure 4-6**). Downward flux past the tensiometers during this period is consistent with the greater infiltration estimates during this period discussed in the preceding section.

At the Type III AZLs in 2008, the overall pattern was similar to that observed at the Type III test pile, although there was greater short-duration fluctuation between upward and downward gradients.

In 2009, at both the Type III test pile and Type III AZLs, the recorded gradient was predominantly upwards (**Figure 4-6**), which was consistent with the expectation during an active season with low magnitude precipitation events and infrequent periods of infiltration.

The flux was calculated to estimate infiltration at the AZLs based on the gradient recorded at the tensiometers, and the K(ψ) relationship developed by Neuner (2009).

$$\mathrm{K}(\psi) = 4x10^{-7}e^{-0.29\psi\,(kPa)} \qquad 4\text{-}9$$

From this approach, net percolation past 0.75 m in 2007 was 77.6 mm and in 2008 was 77.7 mm. In 2009, the deeper tensiometer was not functioning for most of the summer, and therefore infiltration was not estimated. In 2007, there were 73 days over which the tensiometers were active, operating from August 2 until October 15. For the same period in 2007, 133.4 mm of rain fell, or 58% (77.6 mm/133.4 mm) of the rainfall infiltrated into the waste rock and past 0.75 m. In 2008, there were 99 days that the tensiometers were active, operating from June 28 until October 19. Over the same period in 2008, 153.6 mm of rain fell, or 51% (77.7 mm/153.6 mm) of rainfall infiltrated into the waste rock based on the flux observed past 0.75 m. In 2009, there were 84 days that the tensiometers were active, operating from June 20 until October 7. In 2009, 64.4 mm of rain fell and net percolation was inferred to be negligible,

based on the predominant upward gradient observed and the low precipitation received. Over the same periods, net percolation by the extended Penman-Monteith model, was 116.4 mm in 2007, 105.7 mm in 2008, and 8.7 mm in 2009. That is an absolute difference between observed and modelled infiltration of 38.8, 28.0, and 8.7 mm in 2007, 2008 and 2009, respectively.

The difference between observed and modelled net percolation may be a result of a change in moisture content. The average change in moisture content in the upper 0.9 m rock column in 2008 was a gain of 33.2 mm and a loss of 3.0 mm in 2009. Change in moisture content could not be calculated for 2007 from the available dataset. In other words, of the 105.7 mm calculated to infiltrate across the surface by the extended Penman-Monteith model in 2008, it is possible that 33.2 mm went into storage, and 72.5 mm contributed to infiltration past 0.9 m. In 2008, cumulative normalized discharge (normalized to discharge area) for the western AZL totals 64.5 mm (64.3 mm from the eastern AZL); and 63.8 mm during the period the tensiometers were active, suggesting minimal infiltrated moisture was stored between 0.9 and 1.7 m. In 2009, cumulative normalized discharge for the western AZL totals 7.2 mm (12.1 mm from the eastern AZL), that amount of moisture could be sourced from drainage of stored moisture by a 0.004 $m^3 \cdot m^{-3}$ change in VMC over the entire AZL (0.007 $m^3 \cdot m^{-3}$ from the eastern AZL). A 17.3 mm (0.01 $m^3 \cdot m^{-3}$) change in moisture content (loss) between June 20 and October 7 was recorded at 0.9 m ECH_2O probe; and only a gain of 1.3 mm (0.00001 $m^3 \cdot m^{-3}$) in VMC was recorded at 0.3 m probe. The 0.6 m probe recorded a gain of 0.13 mm (0.001 $m^3 \cdot m^{-3}$) in VMC between June 20 and September 26, and then stopped working.

Comparison of evaporation and infiltration relying on the gradient and calculated $K(\psi)$ with estimates by the extended Penman-Monteith model lack full constraint on changes in storage and only allow general confirmation of the method.

As discussed in **Section 4.1.2**, the available solar energy was indicated to be a key driver to evaporation. At the Type III AZLs, seasonal differences in the evaporation rates were noted between summer and fall based on estimates derived during periods of zero change in storage. Additional support for this observation is illustrated on **Figure 4-7**, which presents the net radiation calculated from 2007 through 2009. On **Figure 4-7**, negative values of net radiation indicate that longwave radiation (out) is greater

than net solar radiation (in). In 2008, for example, modelled daily net evaporation (and daily net radiation) reaches about 0.2 $mm \cdot d^{-1}$ (0.6 $W \cdot m^{-2}$) in April, peaks between June 19 and 28 at about 1.1 $mm \cdot d^{-1}$ (2.0 $W \cdot m^{-2}$), then steadily decreases through July and August before dropping below 0.1 $mm \cdot d^{-1}$ (-0.5 $W \cdot m^{-2}$) after September 28. Evaporation was energy-limited by September. In 2007, 2008 and 2009 between 35 and 50% of the rainfall fell from August 20 to when freezing conditions set-in, coincident with declining or limited solar energy availability to drive evaporation and allowing significant rainfall infiltration to occur during this period. These percentages of rainfall after August are greater when applied events are included.

Modelled evaporation provides good agreement with estimates from the water balance developed for the AZLs. There is strong seasonal variation in evaporation rates related to the availability of solar radiation and the frequency and magnitude of individual rainfall events. For example, in 2008 when the amount rainfall (natural and applied) received at the Type III AZL was 110% of the mean annual value, evaporation was estimated to be between 39 and 46% of the rainfall. About 106 mm of precipitation fell between August 1 and October 16, which was approximately 70% of rainfall that was received and included four large storm events delivering 14.9, 13.3, 33.2 and 15.9 mm. Rainfall received after net radiation has peaked in June, and energy is a limiting factor for evaporation, permits greater net percolation. In 2007 and 2009, about 85 to 45% of the rainfall occurs between August and October and mean annual evaporation was estimated to be 41 and 94%, respectively. This seasonal variation occurs on a monthly, or finer, time scale reflective of the variable and short duration peak in, solar radiation at this northern latitude. In very generic terms, annual average evaporation rates are 0.6 $mm \cdot d^{-1}$ and for a year with mean average precipitation, approximately 50% evaporates. However, as noted above, the evaporation rate peaks in June and July at slightly greater 1 $mm \cdot d^{-1}$ and declines from August (average of 0.5 $mm \cdot d^{-1}$) through the fall, when it was estimated at less than 0.1 $mm \cdot d^{-1}$. Therefore, to accurately account evaporation, and net percolation, for a waste rock water balance in northern environments it is important to consider the data on a fine time-step (e.g., daily). Over the course of the experiment, annual evaporation between 41 and 94% of rainfall has been determined; further net percolation/evaporation as a percentage of annual rainfall varied significantly with variation in annual rainfall. These values are within a similar range to estimates at other cold/arid regions (Nichol, 2002; Marcoline, 2008; Janowicz et

al., 2008; Fretz, 2013). At the Faro Mine Complex in Yukon, the north, east and west facing slopes experienced the lowest evaporation due to lower energy received at the surfaces; whereas on the south-facing slope competing factors of rapid snowmelt infiltration played against increased energy directed at the surface leading to higher seasonal evaporation (Janowicz et al., 2008). These factors are likely a controlling mechanism at Diavik, but no monitoring data to isolate the effect of aspect was available to support or further develop this relationship. However, the highest evaporation is likely experienced from flat surfaces and south/west facing batters and the greatest net percolation is likely experienced across the other batters.

4.3 Water Balance Accounting - Conclusions

A water balance was created at the Type III AZLs to help constrain estimates of evaporation and net percolation into the waste rock stockpiled in a northern, semi-arid environment. Evaporation determined from the extended Penman-Monteith model was compared to evaporation estimated by the water balance on the AZLs. The comparison between these two methods suggests the model as a valid technique to estimate evaporation and therefore net percolation, in the absence of run-off. There was good agreement between estimated evaporation based on recorded data at the Type III AZLs and modelled by the extended Penman-Monteith model, with an absolute difference less than 8 mm or 10% of the rainfall. Comparison of evaporation and infiltration relying on the gradient and calculated $K(\psi)$ with estimates by the extended Penman-Monteith model provided reasonable agreement when changes in storage were accounted.

In 2007 and 2008, evaporation at the Type III AZLs was estimated to be 41% (73.0 mm) and 42% (75.1 mm) of rainfall; applied rainfall bought the rainfall received to approximately 110% of the long-term average for both of these years. In 2009, evaporation was estimated to be 94% (67.0 mm) of rainfall and rainfall was less than 50% of the average annual.

These modelled evaporation estimates indicate that for a year with mean average precipitation approximately 50% evaporated. Over this study period, annual net percolation determined with the model was between about 0 and 60%. The monthly average evaporation rate in May, June, July, August, September and October was 0.1, 0.8, 0.8, 0.5, 0.1 and 0.01 $mm \cdot d^{-1}$, respectively.

Net percolation/evaporation in northern waste rock piles is influence by seasonal changes with respect to solar radiation and the timing and magnitude of individual rainfall events. Water movement across the waste rock surface is restricted to between May and October, and by late August or early September, evaporation is energy-limited. Rainfall received after net radiation has peaked in June, and energy is a limiting factor for evaporation, permits greater infiltration. In 2007, 2008 and 2009 between 35% and 50% of the rainfall fell between August 20 and when freezing conditions set-in, in mid-October, coincident with declining or energy-limited evaporation stage therefore allowing significant rainfall infiltration to occur during this period.

As demonstrated over the shorter periods considered in the preceding section, there is strong seasonal variation on net percolation/evaporation. Seasonality, at a monthly or finer scale, should be taken into account when determining and applying evaporation estimates to waste rock piles in an arctic environment. Another important observation from this analysis is that the net percolation/evaporation as a percentage of annual rainfall varied significantly with variation in annual rainfall.

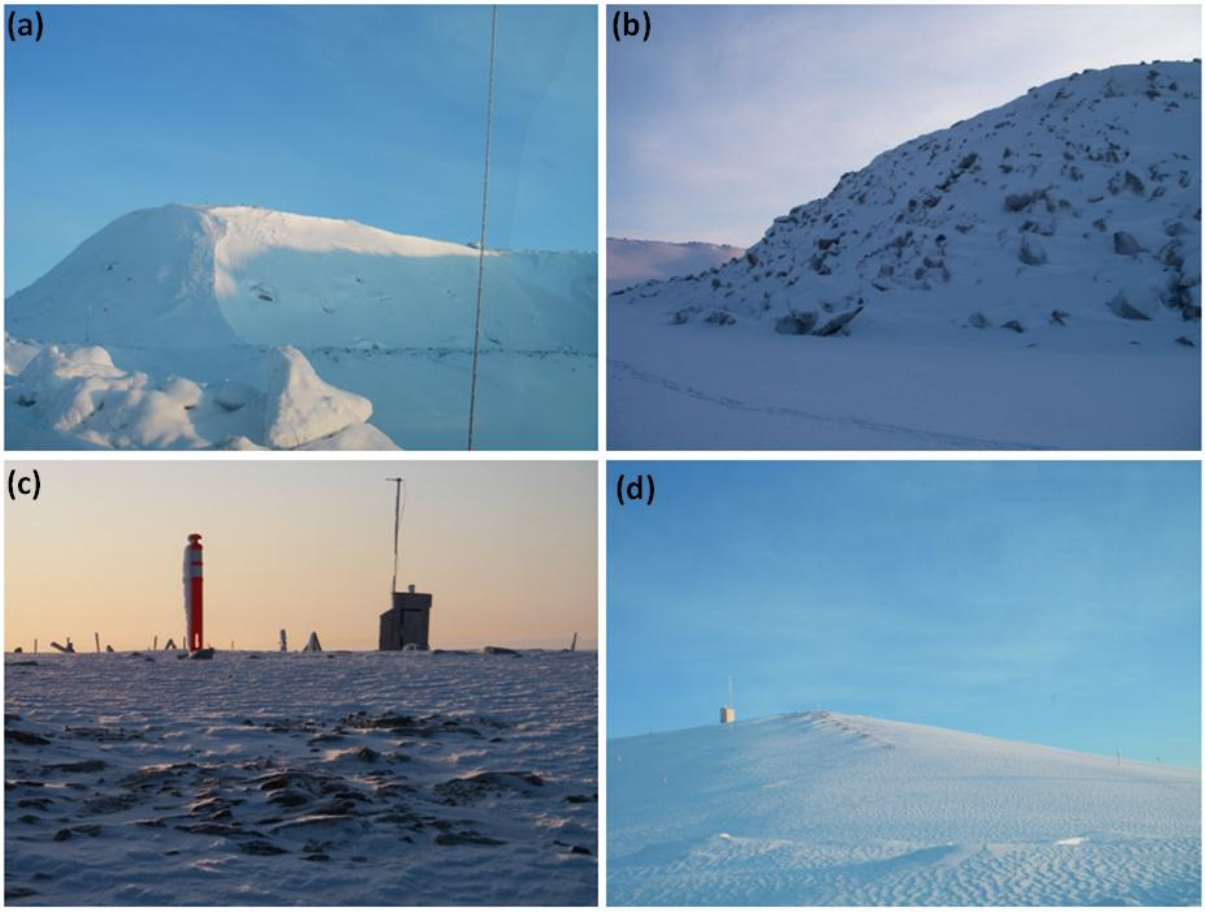

Figure 4-1: (a) Wind loading on west and south facing slope of Type III pile; (b) Wind scour on north facing slope on Type I pile ; (c) Wind scour on top of Covered pile; (d) Scour on the south and west facing slope of the Covered Pile. All photos from January 24, 2010.

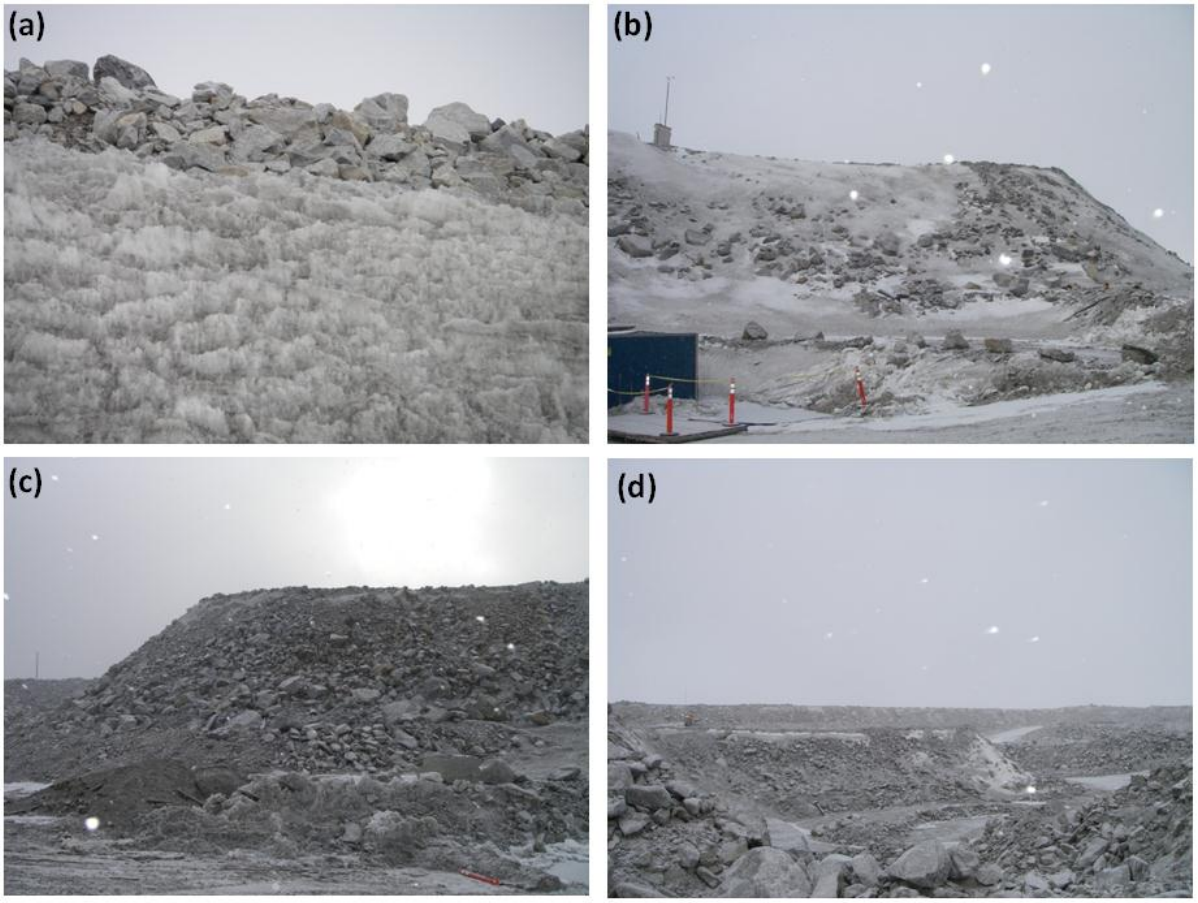

Figure 4-2: a) Sublimation of snow near pile crest; b) looking south at north face of the Type III pile at unequal areas of snow distribution; c) looking east at west face of the Type I pile, minimal snow accumulation; d) looking northwest at the east face of the Type I at unequal areas of snow. All photographs from early spring 2009.

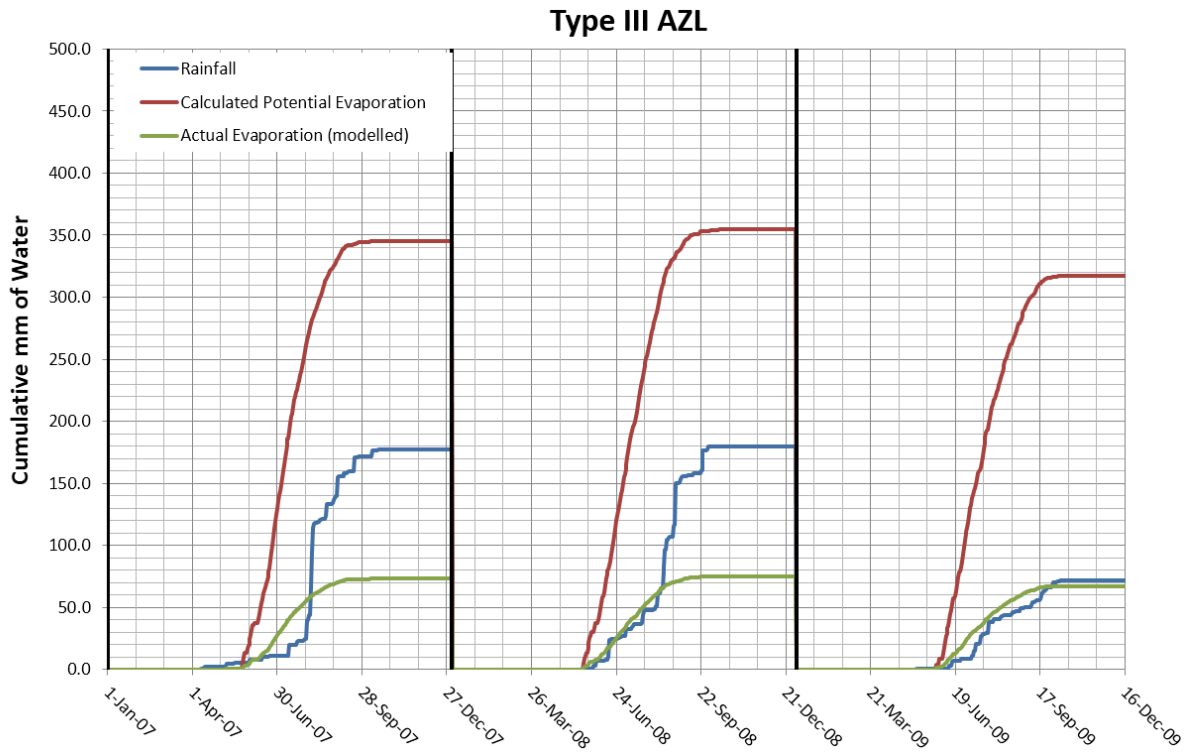

Figure 4-3: Comparison of calculated annual cumulative potential evaporation and actual modelled evaporation, presented along with cumulative annual rainfall for the Type III AZLs. The term actual evaporation (modelled) indicates evaporation from a non-saturated surface.

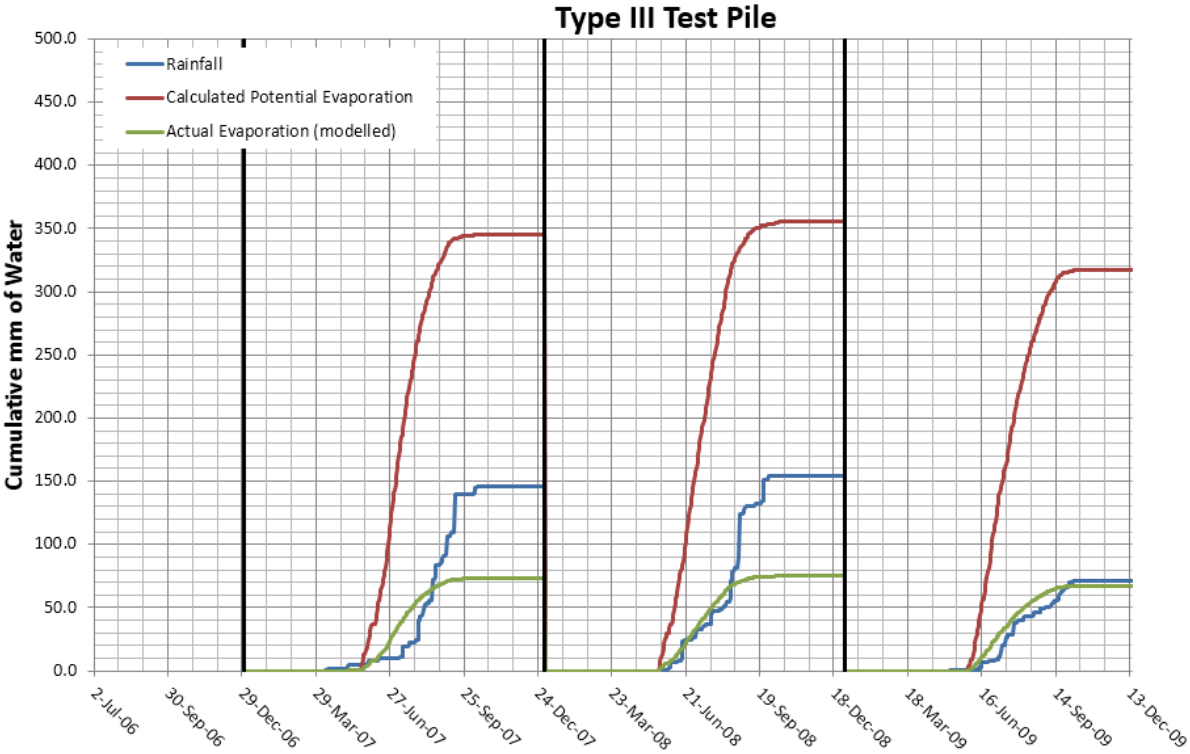

Figure 4-4: Comparison of calculated annual cumulative potential evaporation and actual modelled evaporation, presented along with cumulative annual rainfall for the Type III test pile. The term actual evaporation (modelled) indicates evaporation from a non-saturated surface.

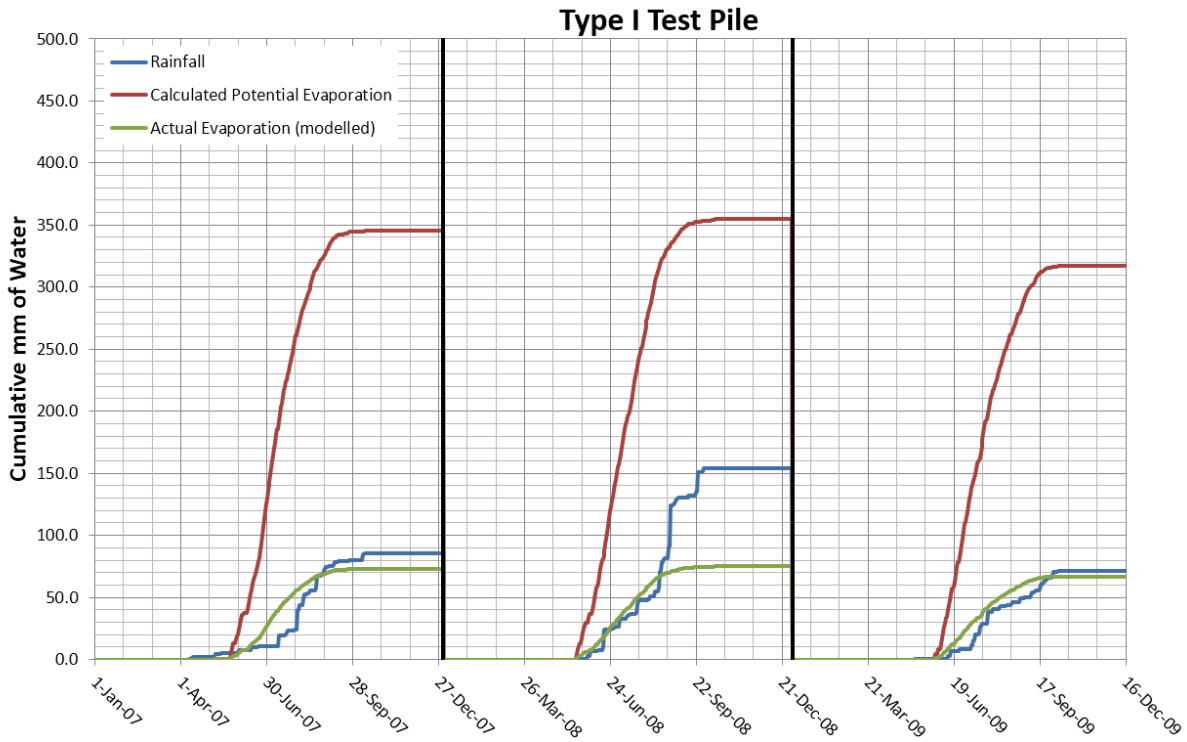

Figure 4-5: Comparison of calculated annual cumulative potential evaporation and actual modelled evaporation, presented along with cumulative annual rainfall for the Type I test pile. The term actual evaporation (modelled) indicates evaporation from a non-saturated surface.

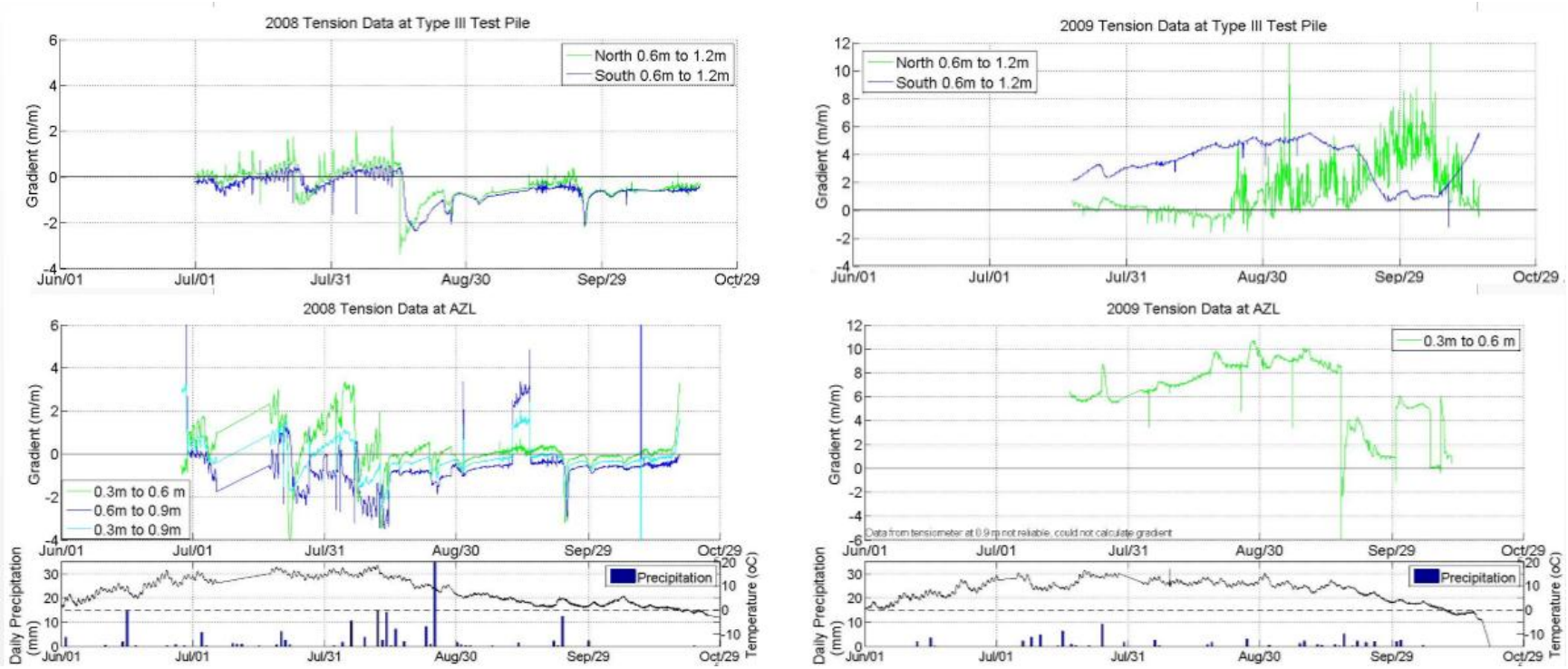

Figure 4-6: Hydraulic gradient near the surface of the Type III test pile (upper plots) and Type III AZLs (middle plots) measured at installed tensiometers. Positive gradient values indicate upward flow. Blue bars on lower plots indicate daily precipitation, black line reports daily temperature.

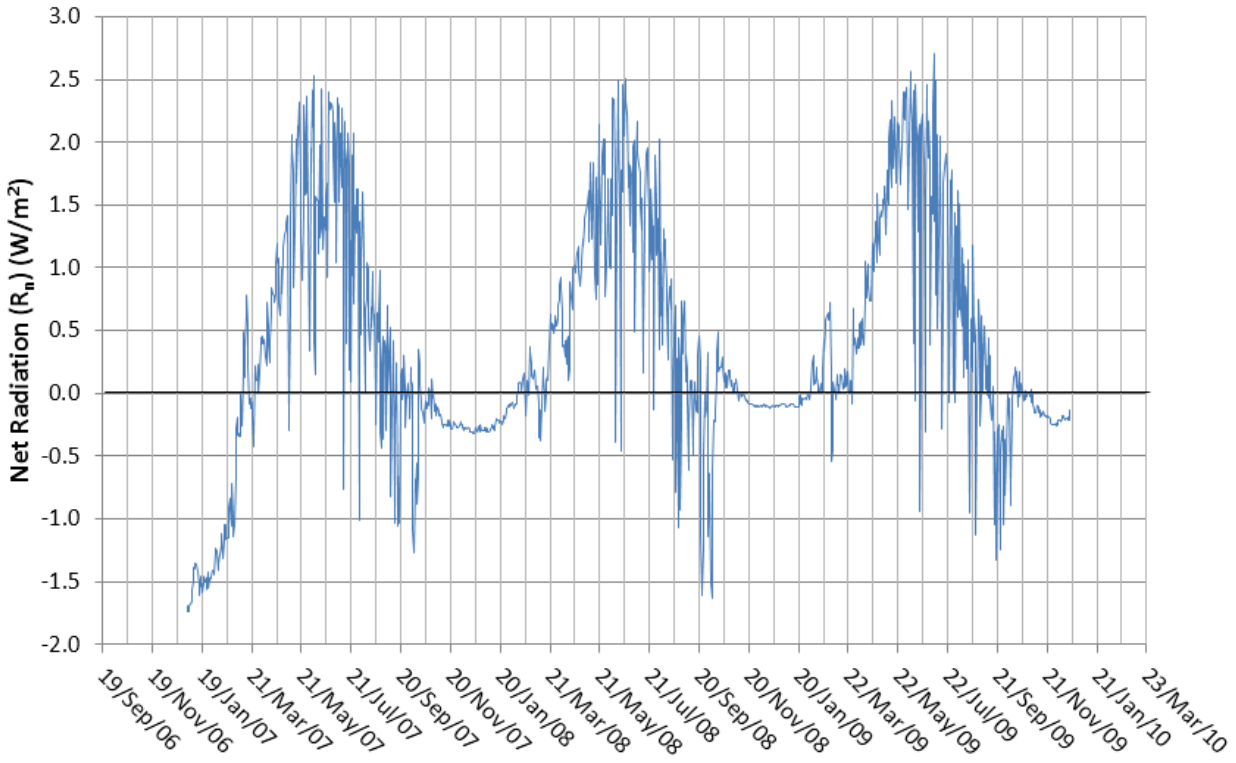

Figure 4-7: Net radiation (R_n) calculated from 2007 through 2009. Negative values indicate that net longwave radiation (out) is greater than net solar radiation (in).

Parameter	Units	Source
Von Karman Constant (K)		0.4, Constant
Pressure (P)	kPa	$101.3 \times \left[\frac{293-0.0065*Elevation}{293}\right]^{5.26}$ (*ASCE ,2003*)
Temperature (T)	°C	Measured
Wind Speed (μ)	$m \cdot s^{-1}$	Measured
Air density (ρ)	$Kg \cdot m^{-3}$	Ideal gas law, $\rho = P/R \cdot T$
Zero plane displacement of vegetation (d_o)	M	0.67*h (*Granger and Gray, 1989*)
Roughness length governing momentum transfer (z_{oh})	m	h/0.735 (*Granger and Gray, 1989*)
Roughness length governing heat and vapour transfer (z_{om})	m	0.1x z_{oh} (*Allen et al. 1998*)
Mean height of waste rock (h)	m	0.1 (Chi, 2011)
Measurement height (z_1 and z_2)	m	2, Measured
Saturated Vapour Pressure [$e_s(T)$]	kPa	$0.6108 \times \exp\left[\frac{(17.27xT)}{(T+237.3)}\right]$ (*Reid, 2005*)
Actual Vapour Pressure (e_a)	kPa	$e_s(t) \times \frac{\text{Relative Humidity}}{100}$
Net Radiation (R_n)	$W \cdot m^{-2}$	Net Solar Radiation – Net Longwave Radiation
Soil heat flux (G)	$W \cdot m^{-2}$	Rn x 0.31 (*Pham, 2013*)
Net Solar Radiation (R_{ns})	$W \cdot m^{-2}$	(1-albedo) x Shortwave Radiation (measured)
Albedo	-	0.48 (*Carey et al. 2005*)
Net Longwave Radiation (R_{nl})	$W \cdot m^{-2}$	
Slope of the saturation vapour pressure temperature curve (Δ)	$kPa \cdot C^{-1}$	$4098 \times \left[\frac{0.6108 \times EXP\left[\frac{17.27*T}{T+237.3}\right]}{(T+237.3)^2}\right]$
Psychometric constant (γ)	$kPa \cdot C^{-1}$	$\frac{1.013*10^{-3}*P}{0.622*2.45}$

Table 4-1: Parameters required for evaporation calculation.

Station	Annual Rainfall (mm)												Average Annual Rainfall (mm)
	1998	1999	2000	2001	2002	2003	2004	2005	2006	2007	2008	2009	
Ekati	143.5	224.0	154.9	136.7	191.3	107.0	179.4	144.7	250.3	116.8	-	-	164.9
Lupin[a]	173.0	208.6	111.0	104.2	-	-	-	-	-	-	-	-	158.3
Yellowknife[b]	195.0	122.7	211.5	228.1	207.7	153.8	65.3	239.6	193.2	189.2	249.7	219.6	161.5
Diavik Meteorological Station	-	-	134.6	132.6	214.6	134.6	-	-	175.5	117.5	203.4	-	159.0
Diavik Type III Test Pile [c]	-	-	-	-	-	-	-	-	6.4[d]	79.4	151.7	73.7	101.6
Diavik Type I Test Pile	-	-	-	-	-	-	-	-	-	87.6	156.6	72.5	105.6
Diavik Covered Test Pile	-	-	-	-	-	-	-	-	-	-	146.3	61.8	104.1

Notes

a. Average annual rainfall between 1982 and 2001.

b. Average annual rainfall between 1961 and 2009.

c. Amount of natural rainfall recorded by rain gauge installed on the top surface of the Type III test piles. Does not include applied events. See Table 4-4 for applied rainfall amounts.

d. Reflects rainfall received after September 16 only.

Table 4-2: Annual rainfall for regional and site maintained meteorological stations between 1998 and 2009.

Type III Test Pile

Event	Rainfall (mm)	Duration (hr)	Rainfall Intensity (mm/hr)	Recurrence Interval (yrs)	Relative Christiansen Uniformity	Tracer Applied
20-Sep-06	24.2	2.4	10.2	30	0.73	-
24-Sep-06	19.0	2.0	9.5	17	0.83	-
26-Sep-06	14.7	1.5	9.8	9	0.90	-
17-Aug-07	16.1	2.1	7.6	9	0.72	D_2O
04-Sep-07	15.0	1.8	8.6	8	0.68	-
13-Sep-07	29.2	3.8	7.7	35	0.75	Cl^- and Br^-
2006	57.9					
2007	60.3					
Total	**118.2**					

Type III AZL

Event	Rainfall (mm)	Duration (hr)	Rainfall Intensity (mm/hr)	Recurrence Interval (yrs)	Relative Christiansen Uniformity	Tracer Applied
04-Aug-07	23.1	2.8	8.2	20	0.90	-
05-Aug-07	27.7	2.3	12.3	50	0.96	-
06-Aug-07	14.1	1.7	8.2	8	0.92	-
01-Sep-07	14.8	1.8	8.4	8	0.82	-
19-Sep-07	11.6	1.1	10.8	7	0.90	-
6-Aug-08	10.6	0.7	15.2	5 to 10	0.82	-
12-Aug-08	14.9	0.9	16.3	10 to 20	0.80	Cl^-
2007	91.3					
2008	25.5					
Total	**116.8**					

Table 4-3: All applied rainfall events to Type III test pile and Type III AZLs between 2006 and 2009.

	Annual Average Rainfall (mm)	Precipitation (mm)	UTM Coordinates		UTM Zone	Elevation (m)	Period of Record
			Northing (m)	Easting (m)			
Ekati	164.9	265.0	7,175,081	518,994	12W	469	1998 to 2007
Lupin	158.3	298.0	7,292,068	488,542	12W	490	1982 to 2001
Yellowknife	161.5	275.0	6,927,126	632,358	11W	206	1961 to 2009
Diavik – regional analyses[a]	163.9	350.9	-	-	-	-	1959 to 2006
Diavik Meteorological Station	159.0		7,152,045	531,550	12W	440	2000 to 2009[b]
Diavik Test Piles[c]	104.9		7,151,082	533,442	12W	454	2007 to 2009

Notes:
a. Regional analyses by Golder Associates (2008)
b. Does not include data from 2004 and 2005 due to equipment malfunction
c. Average rainfall recorded by the three gauges installed on top of the test piles

Table 4-4: Climate normals for regional and site maintained meteorological stations.

					Observed										Modelled							
					Δ Storage	Total Rain		Discharge	Net Percolation			Evaporation			Net Percolation		Evaporation from E_{A-M}			Modelled vs Estimated		
			Date From	Date To	(L)	(mm)	(L)	(L)	(mm)	(%)	(mm/d)	(mm)	(%)	(mm/d)	(rain) (mm)	(rain) (%)	(mm)	(%)	(mm/d)	Evaporation Difference (mm)	% of Rainfall	Days Unfrozen
2008	1[a]	3UExlys	13-Jun-2008 08:30	30-Jun-2008 04:30	0	18.9	39.5	7.4	3.5	19	0.2	15.4	81	0.9	3.7	20	15.2	80	0.9	0.2	1	17
	2	3UExlys	05-Sep-2008 02:30	03-Oct-2008 04:00	0	23.5	49.2	43.2	20.6	88	0.7	2.9	12	0.1	21.7	92	1.9	8	0.07	1.0	4	28
	3	3UExlys	06-Sep-2008 01:00	05-Oct-2008 00:00	0	23.6	49.3	45.4	21.7	92	0.8	1.8	8	0.1	22.0	93	1.6	7	0.06	0.2	1	29
	4	3UExlys	31-May-2008 23:00	16-Oct-2008 08:30	0	176.4	368.6	199.4	95.4	54	0.8	80.9	46	0.7	107.6	61	68.8	39	0.6	12.2	7	124
2009	5	3UExlys	09-Jul-2009 22:00	19-Sep-2009 18:30	0	46.2	96.5	14.5	6.9	15	0.1	39.2	85	0.6	10.5	23	35.6	77	0.5	3.6	8	67
		3UWxlys			0	46.2	96.5	5.5	2.6	6	0.0	43.5	94	0.7	10.5	23	35.6	77	0.5	7.9	17	67
		1UExlys			0	46.2	96.5	7.5	3.6	8	0.1	42.6	92	0.6	10.5	23	35.6	77	0.5	6.9	15	67
		1UWxlys			0	46.2	96.5	18.8	9.0	20	0.1	37.1	80	0.6	10.5	23	35.6	77	0.5	1.5	3	67
2008 - 2009	6[b]	3UExlys	31-Jul-2008 00:00	18-Aug-2009 16:00	0	178.5	373.2	215.8	103.3	58	0.7	75.3	42	0.5	104.9	59	73.7	41	0.5	1.6	1	153
		3UWxlys			0	178.5	373.2	204.0	97.6	55	0.6	80.9	45	0.5	104.9	59	73.7	41	0.5	7.3	4	153
	7[b]	3UExlys	28-May-2008 14:30	25-Sep-2009 18:30	-2.8	245.4	512.9	225.4	107.8	44	0.4	137.6	56	0.6	109.4	45	136.0	55	0.6	1.6	1	243
		3UWxlys			-2.8	245.4	512.9	208.0	99.5	41	0.4	145.9	59	0.6	109.4	45	136.0	55	0.6	9.9	4	243

Notes:

a. Includes 1 day with 14 mm rainfall.

b. Assuming no infiltration from snowmelt.

Table 4-5: Water balance for AZLs during periods when no change in storage was observed or minimal storage was calculated.

		Net Percolation (mm)		
		2007	2008	2009
Type III AZL	Momeyer	104.3	104.7	4.3
	Fretz	-	105	10
Type I AZL	Momeyer	12.7	76.2	4.3
	Fretz	-	83	10

Table 4-6: Comparison of modelled actual evaporation estimates for AZLs by Momeyer and Fretz (2013).

	2007	2008	2009
Type III AZL			
Evaporation (mm)	73.0	75.1	67.0
Rainfall (mm)	177.3[a]	179.6[a]	71.3
Net Percolation (mm)	104.3	104.7	4.3
Net Percolation (%)	59	58	6
Days active[b]	114	126	118
Evaporation rate (mm/d)	0.6	0.6	0.6
Type III Test Pile			
Evaporation (mm)	73.0	75.1	67.0
Rainfall (mm)	146.0[a]	154.1	71.3
Net Percolation (mm)	73.0	79.2	4.3
Net Percolation (%)	50	51	6
Days active[b]	114	126	118
Evaporation rate (mm/d)	0.6	0.6	0.6
Type I Test Pile and Type I AZL			
Evaporation (mm)	73.0	75.1	66.9
Rainfall (mm)	85.7	154.2	71.3
Net Percolation (mm)	12.7	76.2	4.3
Net Percolation (%)	15	51	6
Days active[b]	114	126	118
Evaporation rate (mm/d)	0.6	0.6	0.6

Notes:

a. Includes applied rainfall. Amount of applied rainfall indicated on Table 4-4.

b. Days active are calculated when the average daily temperature is greater than 0°C, and is consistent with the temperature dependent coefficient applied in the modelled evaporation estimates

Table 4-7: Net Percolation and evaporation from extended Penman-Monteith Model (Granger and Gray, 1989; Granger, 1999; Carey et al., 2005).

5 FLOW MECHANISMS

Rainfall received on the surface of a waste rock pile, may infiltrate, evaporate or run-off. Infiltration of water through the surface of a waste rock pile is affected by the rainfall intensity, infiltration capacity of the material at the surface, surface texture and topography, antecedent moisture content and if present, vegetation (Smith and Beckie, 2003). At the start of a rainfall event both gravity and capillarity draw water into the pile. In response to infiltration rates lower than the saturated hydraulic conductivity value of the fine-material water flow will predominantly occur through the fine-grained matrix material (Nichol, 2002; Okane Consultants 2004). At high values of matric suction (low moisture content), water will reside in, and flow will occur in, the fine-grained matrix material and larger pores will be air filled. Areas of a waste rock pile composed of matrix free coarse-grained material will only transport water under higher infiltration events. The heterogeneous clast composition, the spatial arrangement of these clasts and the internal structures created during deposition influence the manner in which water flow moves through the variably saturated waste rock (Bellehumeur, 2001; Nichol, 2002; Smith and Beckie, 2003; Stockwell et al., 2006; Marcoline, 2008; Andrina et al., 2009; and Neuner et al., 2013). Two main types of water flow mechanisms through waste rock are: matrix flow and preferential flow (Elboushi, 1975; Beven and Germann, 1981; Eriksson et al., 1997; Newman et al., 1997; Smith and Beckie, 2003; Nichol et al., 2005; Neuner et al., 2013). Flow of water through the fine-grained matrix material occurs under capillary tension and gravity and is described by Richards flow equation. Flow of water through preferential pathways includes macropore flow (Beven and Germann, 1981), and film flow (Tokunaga and Wan, 1997). Flow of water through macropores occurs in connected pore-spaces created between clasts with greater about 5 mm diameter, which are matrix free and is gravity driven (non-capillary) and is activated under high infiltration events (Bellehumeur, 2001; Nichol et al., 2005).

Displacement flow through the matrix can occur by propagation of a pressure wave downwards through the porous media, described by kinematic wave equation, in response to infiltrating water. Fretz (2013) concluded that the dominant flow mechanism through the waste rock at the test piles and AZLs was in response to propagating pressure waves resulting in pore-water displacement and not preferential flow.

This response has been observed to occur at velocities significantly greater than the velocity of a particle of water (i.e., average velocity of a conservative tracer) (Rasmussen et al., 2000; Neuner et al., 2013).

The flow mechanisms within these two domains are explored in this chapter. The following section synthesizes four years of moisture content, discharge and thermal data from three 15-m high waste rock piles (test piles), and four 2-m high lysimeters focusing on wetting front migration and flow mechanisms in the active zone, to document the evolution of test pile hydrology.

The moisture content of waste rock when stockpiled is generally less than its field capacity; therefore, the water that initially infiltrates will be retained in the matrix due to capillarity. Significant time may be required for waste rock to reach its field capacity and drainage to occur (Swanson et al., 2000). The time required is dependent upon initial moisture content, net percolation, volume of fine-grained material in waste rock pile and the field capacity (Smith and Beckie, 2003). Neuner et al., (2013) and Fretz (2013) estimated in-situ field capacity of the bulk waste rock between 0.04 and 0.06 $m^3 \cdot m^{-3}$ based on the change in moisture content between being placed and initial drainage at the AZLs. **Section 5.2.1** documents the changes in moisture content within the test pile between 2007 and 2009. Whereas **Section 5.2.2** documents the wetting front response to different magnitude rainfall events at the test piles and AZLs as recorded by changes in moisture content. The wetting front is defined as the boundary between the advancing region with higher moisture content and fluid velocity and the region beneath with lower moisture content and fluid velocity (Smith and Beckie, 2003).

Discharge reporting to the basal drain may have traveled the height of the test pile, or more commonly, the water has moved along shorter flow paths after infiltrating through the sloping surface of the pile batters (Fretz, 2013). **Section 5.2.3** documents the discharge occurring from the test piles and AZLs between 2007 and 2009.

The mechanism that infiltrating water flows through the heterogeneous unsaturated material will affect the geochemical signature of the drainage. The differences in matrix and preferential flow lead to differences in residence time and drainage quality. Preferential flow is attributed as one possible explanation for the disagreement at some waste rock piles between mass loading rates calculated from laboratory humidity

cell tests and those rates observed from field measurements (Velbel, 1993; Eriksson and Destouni, 1997). As non-capillary flow moves water more rapidly through the pile, and in matrix free areas, there is less interaction with exposed mineral surfaces. Water flow through the matrix material moves at a slower rate and interacts with a larger surface area of potentially reactive minerals within the pile (Smith and Beckie, 2003). Conditions that may influence preferential flow and can be observed include antecedent moisture content and rainfall intensity. Conditions which may influence the flow mechanism but are more difficult to observe include internal structure created by clast arrangement (e.g., stratified layers or pockets of fine-grained or coarse-grained material). By studying the outflow response, and changes in internal pile moisture conditions, it may be possible to infer preferential flow. For example, signs of macropore flow would include, faster rate of wetting front movement with greater depth, and wetting front velocity greater than infiltration rate. Discharge from the basal collection lysimeters allow characterization of water that has moved through the full height of the test pile. **Section 5.2.4** utilizes the geochemical signature, characterized by the EC, to assess flow mechanisms. Conditions that induced preferential flow are documented.

The latter part of this chapter provides a discussion on the effect of thermal controls on test pile hydrology. **Section 5.3** quantifies changes in depth of the active layer, which controls the hydrologically active volume of piles and presents discharge normalized to this active volume. **Section 5.4** provides an assessment of the effect of freezing front migration on the hydrology of the piles. An upward flux towards the drying soil in response to the state change of moisture at the freezing front is documented at the AZLs.

5.1.1 Storage/Redistribution

Soil moisture within the matrix material component of the waste rock was monitored with TDR probes and commercially manufactured ECH_2O probes (Decagon Devices Inc.). These instruments allow movement of the wetting front to be tracked as it passes functioning instruments and provide a near-continuous (in time, not space) record of matrix moisture content. Instrumentation to measure moisture content were installed in a matrix of fines derived from the waste rock and held in a nylon mesh bag. During installation of the instruments, attempts were made to position the instrumentation in areas where they would be in

contact with fine-grained material within the test pile (Neuner, 2009). Due to the heterogeneous nature of the material, water may by-pass the location of the probes and specific observations of the passing wetting front may not be recorded. Alternatively, active flow paths may promote the movement of water in certain areas of the test pile to a specific probe that would show as an advancement of the wetting front, which was actually isolated to a unique conduit. This issue was particularly a concern for the Type I test pile since there was limited spatial coverage as only four TDR probes are functioning. TDR have been installed through-out the piles, however as reported by Neuner (2009), survival in some areas (i.e., Type I and Type III piles) was less than 50%.

TDR probes are located from 1 to 9 mbg and provide an estimate of VMC of the matrix material in contact with, and in a small zone of influence of, the probe at internal test pile locations. The TDR probes installed within the waste rock piles are custom-built instruments based on the shielded three-rod design of Nichol (2002). Detailed construction and operational theory is provided in Nichol et al. (2003) and Neuner (2009). Of note, the response recorded by the TDR probes for either frozen conditions or air filled pores is similar due to comparable dielectric permittivities of ice (~3) and air (~1) as opposed to water (~80). Site-specific calibration of the TDR probes was performed and reported by Neuner (2009). **Section 5.2.1** documents the evolution the volumetric moisture content within the test piles. Whereas **Section 5.2.2** relies on the VMC data to review the response of the wetting front to the rainfall events.

5.1.2 Drainage

The instruments for monitoring soil moisture content track water movement through internal locations in the test pile to its ultimate discharge recorded by the basal drain and basal collection lysimeters. Moisture migrating through the test pile is stored within the test pile or reports to either the basal drain or smaller basal collection lysimeters. The base of each test pile is lined with a 1.0 mm (40 mil) HDPE liner to collect all drainage which discharges to a series of flow-through cells in an instrumentation trailer (the basal drain) where sample collection took place and automated EC, pH, temperature and flow rate was recorded. Details on instrument set-up and design are provided in Neuner (2009) and Smith et al., (2013).

Basal drain outflow is tracked by custom-built tipping buckets (**Figure 5-1**) and recorded by datalogger. A calibration equation has been determined for each tipping bucket that relates time between tips to flow

rate (Neuner, 2009). Calibration was performed again in 2009 to confirm and revise the relationships of tip time to flow rate and to check that each tipping bucket was properly balanced (**Appendix A**). Each tip causes a magnetic reed switch to signal the datalogger. Datalogger programs are found in Neuner (2009) except that the revised program for the Covered test pile basal drain datalogger (CBa) is provided in **Appendix C.** This location was upgraded from a Campbell Scientific CR10X model datalogger to a CR1000 model datalogger and therefore the program was rewritten in the appropriate software language (i.e., CRBasic).

Commercially manufactured tipping buckets (R.M. Young model 52202) are utilized to record discharge from the basal collection lysimeters (**Figure 1-4b**). Basal collection lysimeters consist of either 16 m^2 or 4 m^2 HDPE lined cells filled with waste rock located under the central portion of the test pile or under the batters of the test pile. Each test pile has eight central lysimeters (four 16 m^2 and four 4 m^2) and four lysimeters located beneath the batters (two 16 m^2 and two 4 m^2). Specific locations are documented in Smith et al. (2013). Basal collection lysimeters assist in identifying regions of the test pile that are active by isolating areas and flow paths located above the cell. They allow characterization of flow that has traveled the full height of the test pile, rather than potentially moving through or mixing with water that has traveled through shorter flow paths beneath the test pile batters. Even locations indicated to be located under the batters represent a longer flow path as these underlie portions of the batter that are relatively close to the pile crest.

At the AZLs, pore-water movement was tracked below 0.9 m through the discharge recorded from the lysimeter drain at the base of the container. Each of the Type I and Type III AZLs have a drainage collection system in place to record discharge (R.M. Young model 52202 tipping bucket) and, as with the test piles, a series of flow-through cells for automated measurement of EC, pH, and temperature, as well as sample extraction. **Section 5.2.3** documents the drainage that occurs from the test piles and AZLs, whereas **Section 5.2.4** relies on the discharge data to review the response of outflow to the rainfall events.

5.2 Moisture Content Storage and Evolution

5.2.1 Storage/Redistribution

A review of the change in storage through-out the test piles provides insight to the progression of the wetting front. **Table 5-1** presents a summary of the annual average VMC and active season VMC from the TDR probes installed within the three test piles. The VMC is also presented in terms of percent matrix saturation, based on measured matrix porosity (Neuner et al, 2013). Matrix porosity determined by laboratory analyses of seven samples averaged 0.25 ±0.02. **Figure 5-2 through 5-4** present the VMC recorded at the Type III, Type I and Covered piles, respectively and **Figure 5-5** presents the VMC recorded adjacent to the Type III AZLs.

Year to year active season VMC at the Type III test pile, increased between 2007 and 2008, and declined slightly between 2008 and 2009. In conjunction with 2009 outflow from the basal lysimeters, it appears that the Type III test pile was approaching a state of dynamic equilibrium. TDR probes at the Type I test pile show a year to year increase in the matrix moisture content between 2007 and 2008 active season and a relatively stable average VMC between 2008 and 2009. The Type I test pile is in the process of 'wetting-up' through 2009. The TDR at the Covered test pile were not operational until 2008. Between 2008 and 2009, the average matrix moisture content increased.

Within the Type III test pile there are four instrument string locations including two on Face 1 and two on Face 3, located north and south of the centre line respectively (**Figure 5-2**). Each string has a different number of instruments functioning (as shown on **Figure 5-2**); the response of probes at approximately equivalent depths, regardless of which face they are located on, was similar. The instrument string on Face 1 is reviewed in the following as these instruments provide the most coverage but all data are presented on **Figure 5-2**. The shallow TDR probes in the Type III test pile begin recording moisture content when the temperature at the probe location was greater than 0°C which generally occurs in July, when air temperature peaks. There was a lag corresponding with depth for deeper TDR probes to begin recording moisture content as it takes longer for the 0°C isotherm to move deeper into the pile. As ice has a much lower dielectric permittivity than water, the TDR probes record an abrupt decrease in moisture content in reverse order as the freezing front passes. TDR probe readings at all depths indicate moisture

in the matrix was in a solid state by January. Further discussion on thermal effects is presented in **Section 5.3**. As described in **Section 5.1.1**, the TDR probes provide a similar reading in the presence of ice or air, due to the similar dielectric permittivities. TDR probe readings recorded over the winter are not considered in the analyses, however when temperatures reach greater than 0°C the following spring/summer and soil moisture was recorded again, there was generally higher VMC recorded, indicative of redistribution supplying water to the regions around the probes between when the probes stop recording moisture at the end of the season and start recording moisture the following season. This observation is further reviewed in **Appendix D**. In 2007, the wetting front advanced to 5 m (Neuner et al., 2013). Depending on the TDR location considered, the wetting front reached 7 m by the end of 2007 or at the beginning of the 2008 active season, and by August 2008, the wetting front arrived at 9 m. Here the wetting front is defined by the TDR probes recording a sharp increase in VMC, reaching near saturation. For example, the TDR probes at 9 m recorded less than 5% VMC in 2007. In August 2008, the VMC sharply increased to approximately 25%, defining the arrival of the wetting front.

There are no TDR below 9 m to detect the progression of the wetting front through to the base of the test pile, however as reported in **Section 5.2.3** drainage began to report to two of the eastern 16 m^2 basal collection lysimeters located under the central portion of the test pile on August 16 and 31, 2008 and to a third central 16 m^2 basal collection lysimeter on September 6.

An additional observation on the progression of water through the test pile is provided by a tracer test initiated at the Type III test pile in 2007 (Neuner et al, 2013). Based on preliminary results, flow did not reach the base of the test pile in 2007. The tracer was traveling at 0.05 to 0.7 $m \cdot d^{-1}$ based on tracer concentrations observed in soil water solution samplers installed within the test pile. At 0.05 $m \cdot d^{-1}$, it would take about 300 days for the tracer to reach the base of the 15 m high pile. As the Type III test pile has been active for between 154 and 182 days each year (**Section 5.2.3**), at this rate, tracer residence time would between 1.6 and 1.9 years. Under lower precipitation and infiltration conditions, the response will be slower.

The wetter conditions prevalent in 2008 were evident in the VMC recorded by the TDR probes at all depths, as throughout the active period these locations fluctuate but record VMC near saturation,

between 20 and 25%, whereas in 2009 VMC readings peak early in the active season and continuously drain through the remainder of the season (**Figure 5-2**).

Limited data points for the Type I test pile make interpretation of VMC trends speculative (**Figure 5-3**). However, the wetting front progresses at a much slower rate at the Type I test pile than compared to the Type III test pile, possibly reaching 6 m by November 2008. There is little evidence that the wetting front advanced in 2009. As will be seen in **Section 5.2.3**, some discharge did occur from a basal collection lysimeter; however, this appears to be related to preferential flow paths rather than uniform water flow through the matrix.

At the Covered test pile there are three instrument string locations; one is located west of the centre line on Face 2; one is located east of the centre line on Face 2; and one is located west of the centre line on Face 3 (**Figure 5-4**). In the fall/winter of 2007/2008, average moisture content of the matrix at 6 m and 8 m depth on Face 2 was between 20 and 25%. After peaking, the moisture content decreases, over the winter months. By the fall of 2008, on the eastern side of the test pile, moisture content again peaks slightly higher than the previous season at 6 m and 7 m. On the western side, there was a both a lag and attenuation of the peak moisture content as compared to the eastern side. The wetting front arrived at 10 m in the winter of 2008/2009 on the second face east of the centre line, moisture continued to drain over the spring and by summer, the probes were measuring residual moisture content. On both the second and third face, the probes at 10 m on the eastern side of the Covered test pile recorded the passage of the wetting front, arriving in fall of 2009 and passing over the winter/spring of 2010. Wetting front on the third face lagged the arrival on the second face. Unlike the Type III and Type I test pile, the VMC recorded by the TDR probes in the Covered test pile does not abruptly decrease over the winter indicating the frozen or drier conditions. TDR probes in the Covered test pile appear to reside in areas of the test pile that remain unfrozen year round. As noted by Pham (2013) through 2010, areas of the Type III rock underlying the till cover have remained thawed by internal heat sources (i.e., heat trace used in the basal collection lysimeters). These TDR probes record a generally rapid increase in moisture content in the fall, with a lag at greater depths and then after reaching a peak moisture content slowly drain to lower moisture contents over the remainder of the water year.

The initial advance of the wetting front in the Covered test pile appeared to advance at approximately 5 $m \cdot yr^{-1}$ and in the Type III test pile appeared to advance at approximately 7.5 $m \cdot yr^{-1}$. Although limited data are available from the Type I test pile, the initial advance of the wetting front appeared to be moving at approximately 6 $m \cdot yr^{-1}$, but during 2009, the advance has stalled due to drier conditions. Note, despite the cover on the Covered test pile, the wetting front has advanced at a rate similar to that at the Type I test pile and has advanced to a greater depth.

5.2.2 Wetting Front Velocity

Recorded VMC are used to provide insight to the advancing wetting front in response to infiltration events, however since the in-situ VMC measurements are from the matrix material in immediate vicinity of the probe location, only a small snapshot is available from which to base conclusions. These measurement on the matrix material will not detect passage of fluid flow in preferential flow paths. Nichol (2002) found that in-situ measurements of wetting front propagation were a poor predictor of the timing and volume of outflow. Nichol observed that discharge from the base of the 5 metre high pile often increased when TDR probes indicated that the wetting front had reached between 1.75 and 3 m depth. Fretz (2013) found TDR probes recording matrix wet-up corresponded with the initiation of drainage from the basal collection lysimeters at the Type III pile, as was also presented in the previous section. This suggests that the TDR sensors can be used to accurately monitor wet-up of the matrix fraction of waste-rock piles. Although, as noted in **Section 5.2.4,** drainage from the basal collection lysimeters at the Type I test pile occurred in 2008 and 2009 while moisture content indicated that the wetting front had not reached below 9 m.

In Fretz's (2013) compilation of data from between 2007 and 2011, the response to an August, 2008 large magnitude and intensity duration rainfall event was presented. The following review of rainfall events that occurred in 2008 and 2009 includes this same August 2008 rainfall event along with other smaller magnitude and intensity events. Fretz's observations of the hydrologic response to this large magnitude rainfall event concluded that preferential flow occurred. Discharge from the basal collection lysimeters located below the crown of the test piles was observed following the rainfall event; based on sulphate concentrations, he concluded the geochemical signature of the discharge indicated matrix flow.

This discussion begins by quantifying the range of wetting front velocities observed at site (**Table 5-2**). The wetting front velocity was determined by dividing the depth of the probe location by the time required to reach a peak change in moisture content following the initiation of a rainfall event. This method of determination for wetting front velocity assumed that the first peak increase in moisture content is a result of the most recent rainfall event of significant magnitude. It is recognized that the increase in VMC may not be due to the most recent event particularly at deeper depths; therefore these estimates of wetting front velocity are considered as maximum velocity (i.e., if the response was due to an earlier event the velocity would be reduced).

Seven rainfall events that represented six different recurrence intervals and the greatest rainfall events based intensity-duration during the study period were identified. The average velocity of the wetting front in response to each of these rainfall events was determined based on the recorded changes in moisture content at the TDR probes within the pile and by tensiometers and ECH_2O probes at the AZLs. Over August 25 and 26, 2008, an event ranked as having the least frequent recurrence based on the intensity and duration during this study delivered the largest rainfall recorded during this study (**Figure 5-6 and Figure 5-7**). This event had a magnitude of 35.8 mm rainfall and an average intensity of 2.9 $mm \cdot hr^{-1}$ (maximum intensity of 6.7 $mm \cdot hr^{-1}$). In response to the event that occurred between August 25 and 26, the average wetting front velocity observed by the peak response detected by TDR probes within the Type III test pile ranged from 11.0 $m \cdot d^{-1}$ at 2.4 m (31S2 3m) to 0.8 $m \cdot d^{-1}$ at 1.2 m (31S2 1m), however generally the velocity decreased with depth (**Figure 5-8**). The average measured velocity of the advance of the wetting front was 3.5 $m \cdot d^{-1}$. As shown on **Figure 5-8**, wetting front velocities were spatially variable. Results from Neuner et al. (2013) suggest that spatially variable wetting front velocity indicate macropore flow. This is the only rainfall in between 2008 and 2009 that has a directly distinguishable wetting front signal in the TDR data that also corresponds to a distinct change in the observed rate of discharge from the basal drain and basal collection system. At other times, increases in daily outflow following rainfall illustrate the shorter flow paths available through the batters, particularly the coarser material accumulated at the pile toes.

The advance of the wetting front following this rainfall recorded by the ECH_2O probes at the AZLs indicated an average velocity of 1.1 $m \cdot d^{-1}$. As recorded by the ECH_2O probes the velocity increased with depth from 0.8 $m \cdot d^{-1}$ at 0.6 m, to 1.3 $m \cdot d^{-1}$ at 0.9 m. This increase in wetting front velocity with depth is interpreted to be due to the increasing rainfall rate onto wetter soil later in the storm event, and not a reflection on a flow mechanism. If the start time of the event is considered to be 03:29 on August 25, 2008 (i.e., the time when the rainfall intensity remains at a rate greater than 1 $mm \cdot hr^{-1}$ for the remainder of the storm), the wetting front velocity, recorded by ECH_2O probes, decreases with depth from 2.9 $m \cdot d^{-1}$ at 0.6 m, to 2.3 $m \cdot d^{-1}$ at 0.9 m.

In response to a rainfall event on September 24, 2009, having an average intensity of 13.3 $mm \cdot hr^{-1}$, TDR probes within the Type III pile recorded a response to 9 m. As noted in **Section 2.2.1**, a total of 12.6 mm of rainfall had been recorded over a 7-day period concluding with this event, and the wetting front response may reflect response to the cumulative rainfall. A response was not observable at all of the TDR probes. The wetting front velocity was estimated as 2.0 $m \cdot d^{-1}$ at 0.7 mbg, but below this depth, the velocity was relatively uniform and averaged 0.2 $m \cdot d^{-1}$. The advance of the wetting front following the September 24, 2009 rainfall recorded by the ECH_2O probes at the AZLs indicated an average velocity of approximately 1.0 $m \cdot d^{-1}$.

Rainfall events, based on intensity duration, that occur at more frequent recurrence intervals, did not produce a readily discernable response in the TDR within the Type III test pile. A response was observed by the ECH_2O probes at the AZLs following the rainfall in response to 4 of the 5 other events (**Table 5-2**).

In response to a rainfall event on August 14, 2008, delivering 16.9 mm with 4.7 $mm \cdot hr^{-1}$ intensity the wetting front advanced at an average rate of 0.1 $m \cdot d^{-1}$. On July 10, 2009, 5.0 mm fell at a rate of 9.8 $mm \cdot hr^{-1}$ and on July 24, 2009, 6.3 mm fell at a rate of 26.3 $mm \cdot hr^{-1}$. Following the 9.8 $mm \cdot hr^{-1}$ event, the wetting front advanced at 2.2 $m.d^{-1}$ at 0.3 m, and 0.9 $m.d^{-1}$ at 0.6 m. The response at the 0.9 m probe was difficult to discern from the natural variation. Following the 26.3 $mm \cdot hr^{-1}$ rainfall, the wetting front advanced at 3.2 $m \cdot d^{-1}$ at 0.3 m and decreased to 2.0 $m \cdot d^{-1}$ at 0.9 m. The less than 2-year recurrence event evaluated occurred on June 6, 2008 and delivered 7.1 mm at a rate of 4.9 $mm \cdot hr^{-1}$. The advance of the wetting front moved at approximately 1.0 $m \cdot d^{-1}$ at each of 0.3, 0.6 and 0.9 m.

Antecedent moisture content measured at 0.3 m prior to these rainfall events ranged from about 0.11 to 0.13 $m^3 \cdot m^{-3}$. The limited difference is antecedent moisture content along with the limited number of large magnitude rainfall events does not present a large enough sample size to allow comment on the influence of initial moisture conditions.

This review of the wetting front response to different magnitude and intensity rainfall events reveals that only the largest events produce a discernible response at depth over the immediate timeframe following the event; however, there is limited data to draw this conclusion, only one of each type of event. Based on this data, it appears that individual rainfall events have minimal effect on advancing the wetting front beneath the top surface of the pile, nor do they lead to a change in the observed rate of discharge from the basal drain and basal collection system. Individual rainfall will events contribute to the moisture content of the pile, dependent on seasonal climatic conditions that may result in evaporation of any initial infiltration retained within the upper evaporative layer (**Section 4.2.2**). For example, in 2009 there was an initial increase in VMC at the start of season, apparently sourced from snowmelt infiltration or possibly from the previous year's infiltration that froze before reaching the TDR probes. VMC decreases thereafter; with the exception that rainfall appears to slow the decline. Consider the rainfall event on July 10, when 5 mm of rainfall occurred at 9.8 $mm \cdot hr^{-1}$, through the central portion of the pile (i.e., excluding batter flow patterns) a change in moisture content in response to this event was not observed. Only the largest two events based on intensity and duration, demonstrated an immediate response to rainfall events (August 25/26, 2008 and September 24, 2009) in the Type III test pile.

5.2.3 Drainage

The final advance of the wetting front results in drainage at the base of the test pile, collected by either the basal drain or the basal collection lysimeters. Normalized discharge as outflow flux ($m^3 \cdot s^{-1} \cdot m^{-2}$) is a useful means of reporting outflow for comparison when discharge areas are different. This was done in the tracer test analyses for the Type III AZLs (**Section 2.2.1**) and can be readily determined for the lysimeters that have a known basal drainage area. For the test piles the proportion of the basal area that contributes to discharge changes as the pile freezes or thaws. In this section, volumetric discharge is summarized to continue to track the advance of the wetting front and moisture migration through the pile.

In the discussion on thermal controls, (**Section 5.3**) discharge is normalized to unfrozen volume ($m^3 \cdot s^{-1} \cdot m^{-3}$) as a means of comparing discharge originating from piles with different active volumes.

Discharge from the test piles between 2007 and spring 2010 is summarized in **Table 5-3** (basal drains) and **Table 5-4** (basal collection lysimeters). Discharge from the AZLs is summarized in **Table 5-5**. Of note, in 2008 at both the Type I and Type III test piles the greatest amount of volumetric discharge has been recorded during this study period. This is coincident with 2008 having the greatest rainfall of the study period and the most days with a daily mean temperature greater than 0°C (126 days) or approximately 10 to 14 days more than 2007 and 2009.

5.2.3.1 Drainage Differences for Type I and Type III Test Piles

The cumulative volumetric discharge recorded at the Type III test pile in 2008 and 2009 is 3.8 times greater than the discharge recorded at the Type I test pile (**Table 5-4)**. The volume of water applied through irrigation events to the Type III test pile total 70 m^3. The difference in the discharge volume between the two test piles, 170 m^3, is 2.4 times the volume accounted for directly by applied rainfall events. In each of 2008 and 2009, only a fraction (38.5% and 10%) of the volume of outflow that reported to the basal drain at the Type III test pile reported to the basal drain at the Type I test pile. These differences and several possible reasons for the differences are discussed in **Appendix E**.

5.2.3.2 Drainage Differences Between Eastern and Western Type I AZLs

The cumulative volumetric discharge recorded at the western Type I AZL is 1.7 times greater than the discharge recorded at the eastern Type I AZL (**Table 5-6)**. This difference in volumetric discharge and several possible reasons for the difference are discussed in **Appendix E**.

5.2.4 Outflow Response and Rainfall

Figures 5-9 and 5-10 present the discharge hydrograph from the basal drain of the Type I and Type III piles. Volumetric discharge from the basal drain at both the Type I and Type III piles generally peaks in May or late June and again in late August or September. The early peak is interpreted to be a result of melting of the snowpack and dominated by flow through the batters. The peak discharge observed later in the summer interpreted as the result of mobilization of water upon thawing after being frozen over the

winter as the ambient air temperature warms the test pile interior and infiltration from precipitation over the active season mobilizes antecedent pore-water. As discussed in **Section 5.2.2**, changes in outflow through the central portion of the pile in response to individual precipitation events was not generally observed, instead thermal changes resulting in melting pore ice, and discharge of slow moving water contained within the matrix and replenished by rainfall, particularly later in the season when solar energy is limited, appear to dominant annual discharge.

Snowmelt and rainfall infiltration through the batters is surmised to dominate basal discharge since: (1) the batters present shorter flow paths to the base of the pile; and (2) the surface area of the batters are larger than the surface area of the crown for each test pile. As noted by Fretz (2013) the proportion of the basal area that underlies the test pile crowns is 45%, whereas 55% underlies the batters.

The shape, and thus the control on the hydrograph, for basal drain discharge from the Covered test pile over the three-year record between 2007 and 2009 are less distinct (**Figure 5-11**). However, the cover appears to attenuate an initial response resulting from increased moisture supplied by snowmelt. The cover results in a shift of the peak discharge from late August or September, observed at the Type I and Type III test pile, to mid to late October. Discharge steadily decreases following the peak, but continues drain for a longer duration than the uncovered piles. Over the 2009/2010 water year, discharge from the covered pile continues through spring 2010. As the low permeability cover will slow infiltration into the waste rock pile, water flow is interpreted to predominantly occur through the matrix.

The EC measured in the discharge can be used to assist with the understanding of flow mechanisms occurring within the test piles as the EC has a direct relationship with the total dissolved solids. Discharge with high EC is indicative of matrix-dominated flow since the longer residence time permits greater interaction with mineral surfaces. Discharge with lower EC suggests flow through preferential flow paths, which reflect the speed of transit through the pile resulting in less time for interaction with exposed mineral surfaces, as well as passage across less surface area. Large magnitude or intensity rainfall events that trigger water flow through preferential pathways are expected to result in discharge at the base of the test piles containing lower concentrations of dissolved solids and thus exhibit a lower EC. Flow-through cells with automated EC measurement are part of the basal drain and basal collection

lysimeter drainage systems at the test piles and AZLs. Field analyses of EC was also performed when samples were collected for geochemical analyses. EC is temperature dependent, therefore for comparison purposes the EC was converted to specific conductance (SC), which is the EC normalized to 25ºC. EC was converted to SC by equation 5-1.

$$SC = \frac{EC}{1+m(T-25^{o}C)} \qquad 5\text{-}1$$

Where *m* is the slope of the temperature correction and was calibrated to 0.0245 (Neuner, 2009) and T is the water temperature at the time of measurement. Typical values of SC in rainwater range from 2 to 100 μScm^{-1} (Sanders, 1998). Typical SC of the drainage discharging from the test piles ranges between several 100 and several 1,000 μScm^{-1}.

The Covered test pile response was reviewed to provide insight to flow processes. Minimal discharge was observed in 2007 (0.5 m^3). In 2008, outflow from the Covered test pile began on August 26, immediately following the large storm event, referenced previously. On this date, 60.7 L of discharge was recorded from the basal drain. As discharge from the drain at the Covered pile initiated on the day of the storm event there is no pre-event SC data, however the available automated and manual measurements indicate approximately 2,000 μScm^{-1} on August 27, which increases to around 6,000 μScm^{-1} six days later (**Figure 5-12**). At the end of the 2007 active season (January 10, 2008), SC was about 5,000 $\mu Scm^{-1.}$ This suggests that infiltrating rainwater from the storm event contributed to discharge at the drain, along with mobilizing antecedent pore-water. This discharge suggests passage of freshwater rapidly through the cover, possibly permitted through a tension crack created following settlement of the cover, and may indicate activation of preferential flow paths or shorten flow paths through the matrix.

Similarly, the basal drain at the Type I pile responded to the August 26 storm event with a peak in discharge on August 27 at 7,270 L. Corresponding to this peak in discharge was a peak in the SC, at about 2,000 μScm^{-1}, which was an increase from prior to the storm event when the seven-day average was about 1,300 μScm^{-1} (**Figure 5-12**). This suggests that water reporting to the drain was mobilized pore-water that had time to interact with the surface of the waste rock material, which is reflected by the higher SC and not predominantly composed of recently infiltrated rainwater. Water short-circuiting

through shorter flow paths of the batters, or preferential flow paths, if any exist, did not provide sufficient quantity to lower the SC.

Discharge from the southern basal drain at the Type III test pile demonstrated a different response to this storm event. Instead, peak discharge on August 27 at 2,855 L corresponded with a decrease in SC from about 2,300 μScm^{-1}, the seven-day pre-event average, to about 1,400 μScm^{-1} (**Figure 5-12**). This response suggests either, activation of rapid macropore flow paths, or that the contribution of water flow through the shorter flow paths provided by the lower limits of the batters. Discharge from the northern basal drain at the Type III test pile also peaked on August 27, but change in SC between pre-event and post event was not as pronounced. The seven-day pre-event average SC was about 1,400 μScm^{-1} and on August 27, SC was about 1,150 μScm^{-1} (**Figure 5-12**). The difference between the two drains at the Type III pile is of note and may reflect the difference in the proportional contribution of batter area relative to pile core area in the discharge.

Interpretation from the SC of the drainage from the basal drains is limited because of the potential influence of water flow through the batters. The basal collection lysimeters provide discharge representative of flow through the entire height of the pile; even basal collection lysimeters located beneath the batters represent a longer flow path as these underlie portions of the batter that are relatively close to the pile crest. **Figure 5-13** presents the SC from the Type I and Type III basal collection lysimeters during periods of outflow in 2008 and 2009. The northern central basal collection lysimeter (3BNClys4E) was flowing prior to the August 25 event; the southern central basal collection lysimeter (3BSClys4E) began flowing on August 31. Pre-event SC from the northern basal collection lysimeter averaged 6,600 μScm^{-1} and following the event on August 28, during which daily discharge peaked at 91 L (within the maximum daily discharge the tipping bucket is capable of recording), the SC increased to 7,200 μScm^{-1}. This response suggests downward displacement of pore-water through the matrix rather than rapid infiltration of new water. At the southern central basal collection lysimeter, the SC averaged 130 μScm^{-1} until September 2 when it increased up to 8,000 μScm^{-1}. The low SC of the initial discharge suggests rainwater was delivered through preferential flow paths to the basal collection lysimeter and

consisted of the dominate portion of the outflow initially. Discharge appears to be dominated by water flow through the matrix by September 2 based on the high SC.

Overall, initial SC response from both the basal drain and basal collection lysimeters at the Type III test pile exhibits low conductance (less than 500 μScm^{-1}) and during the course of the active season the conductance increases (**Figure 5-12 and Figure 5-13)**. This is consistent with the interpretation that initial contribution of outflow is from melting snow on the batters reaching the basal drain more rapidly. During the summer a greater portion of outflow contribution is supplied from water travelling longer flow paths through the central portion of the piles after it has greater time to interactive with exposed minerals surfaces. This interpretation is confounded with the seasonal evolution of pore-water geochemistry. Bailey (2013) documents how alkalinity in the pore-water is replenished over the winter and depleted during the active season which will exhibit a similar geochemical signal on the SC.

Monitoring EC in the drainage at the base of the test piles provides one means to interpret flow processes within the test piles. Since the AZLs are not influenced by water flow through shorter flows paths (e.g., water flow through batters), the temperature corrected EC in the discharge was also reviewed. **Figure 5-14** presents the SC at the Type I and Type III AZLs during periods of outflow in 2008 and 2009. The response exhibited at the AZLs is different from that described in the preceding discussion on the test piles. At the AZLs, annually the SC of the initial drainage is between 3,000 and 5,000 $\mu S \cdot cm^{-1}$ and increases as outflow continues until about the peak discharge, after which it reaches between 10,000 and 12,000 $\mu S \cdot cm^{-1}$. Following this peak, the SC gradually decreases through the remaining outflow season. This is somewhat unexpected, as drain down conditions are expected to consist of water flow through the matrix and therefore contain higher loads of dissolved solids (Smith and Beckie, 2003). In both 2008 and 2009, following a stoppage in outflow after an initial period of discharge the SC was further elevated (**Figure 5-14**). This is consistent with flushing of water with a sufficient residence time to interact with the waste rock; for example, water from the previous season pushed by snowmelt infiltration or early season rainfall. Pore-water that resides in the AZLs during periods without discharge interacts with reactive minerals on waste rock surfaces, which resulted in elevated SC when outflow resumed. Due to the smaller volume of rock available for interaction and because of the shorter travel distance, the AZLs do

not maintain elevated SC over the entire active season, unlike the test piles, which generate larger loadings.

5.3 Thermal Controls

The thermal regime experienced at the site results in the creation of an active layer (Pham et al., 2013), which affects the hydrologically active volume of the test piles. This section looks at the relationship between the thermal and hydrologic regime to identify the effect of thermal controls on test pile hydrology and to quantify changes in the depth of the active layer. The active layer does not only advance vertically, from the top surface inwards, but also upwards from the frozen subsurface, and horizontally through the pile batters.

As noted in Neuner et al. (2013) between about October and May, heat transfer between the atmosphere and the pile is influenced by snow deposits, wind speed and direction, and density-driven convection. To explore the effects of the thermal regime on the hydrological regime estimates of the thermal state of the Type I and Type III test pile were made with the following methods relying on unfrozen area estimates from Face 1 through Face 4 provided by Pham (personal communication, 2010). These estimates of the unfrozen volume within the test piles are based on thermistor data, and assumes conditions are similar through-out the zone represented by thermistors on the specific face of the test pile. This may not be the case due to heterogeneities within the piles, which create isolated areas that respond differently to thermal controls. Within the Type III test pile there are 12 thermistors strings located on Face 1, Face 2 and Face 4 which extend to a depth of 12 m below the top surface of the test pile. On each of these tip-faces there are two thermistor strings along the face, located 5 m, north and south of the pile centre line and two thermistor strings extending along the north and south batter, beginning 5 m from the centre line (Pham et al., 2013). The positioning of the thermistor string is the same in the Type I pile, except the orientation of the pile centre is perpendicular to the Type III test pile. Thermal data was not available for the 3 m gap near the base of the test piles. Linear interpolation was performed between each of the instrumented faces (e.g., Face 1 and Face 2) to estimate unfrozen area between interior faces. Then estimates of unfrozen area on exterior faces were calculated by extrapolating from Face 1 to Face 0 (the ramp) and Face 4 to Face 5 (exterior face). Estimates of unfrozen volume were determined from an

average representative length between each face. **Table 5-6** presents the estimated peak percentage of active volume of the Type I and Type III test piles for 2007, 2008 and 2009 based on this approach.

To determine the percentage of active volume, the volume of the test piles was calculated in Surfer version 8.0 by Golden Software, Inc. Surfer relies upon three numerical integration algorithms to calculate volume (i.e., Extended Trapezoidal Rule, Extended Simpson's Rule and Extended Simpson's 3/8 rule) which come from Press et al., (1988). To calculate the volume, triangulated irregular networks (TINs) from as-built terrain models extracted from AutoCAD files, provided by FDA Engineering, were imported to Surfer. In Surfer, a surface of the test pile and a surface of the base of the test pile was created. Using the built-in volume calculation function, the volume was determined by subtracting the test pile surface shape from the base shape. The three methods result in values within 1 m^3 of each other. Test pile volumes determined by this method are reported in **Table 5-6**. The volume of the Type I test pile was calculated to be slightly greater than the Type III test pile.

Through 2009, the active layer of the Type I and Type III test piles extends the entire depth although there may be areas within the core that remain frozen (Pham, 2013). Support for this conclusion is also presented in terms of drainage detected from basal collection lysimeters located beneath the central portion of test pile (3BNClys, 3BnClys, 3BSClys, 1BEClys, 1BWClys) in either 2008 or 2009, or both, and from basal collection lysimeters located beneath the batters of the test pile (3BNBlys, 1BWBlys) in either 2008 or 2009, or both (**Section 5.2.3**).

Normalized discharge as outflow flux ($m^3 \cdot s^{-1} \cdot m^{-2}$) is a useful means of reporting outflow for comparison when discharge areas are different. For sites were the hydrologic regime is as affected by the thermal regime as is the case this experiment located in the Canadian Arctic however, normalized discharge to the active volume ($L \cdot d^{-1} \cdot m^3$) may allow more representative comparison of discharge between piles and provide greater insight into the flow processes. **Figure 5-15** and **Figure 5-16** provide the estimates for the unfrozen pile volume for the Type III and Type I test piles. **Figure 5-9** and **Figure 5-10** present normalized discharge to unfrozen pile volume along with measured discharge and near-surface test pile temperature for the Type III and Type I test piles. **Figure 5-17** and **Figure 5-18** present normalized

discharge to unfrozen pile volume plotted against Julian day to allow annual comparison for the Type III and Type I test piles.

Hydrographs of outflow from the basal drains at the Type I and Type III test piles normalized to unfrozen volume show a peak discharge initially and rapid decline followed by a somewhat more stable outflow period for the remainder of the active season for both piles and all years (**Figure 5-9 and Figure 5-10**). Discharge plotted in this manner contrasts the bi- or multi-modal shape of the hydrograph of the directly observed discharge, as shown in the middle plots on Figure 5-9 and 5-10. The change in discharge over the summer is proportionate with the change in active volume of the pile contributing to outflow. This is indicated by the stable, or flat, part of the normalized hydrograph between about July and October, when compared to direct discharge, which increases and decreases. Normalized discharge at the Type I test pile in 2008 exhibits more variation during the otherwise more stable period, indicating that the proportion of discharge increased relative to the proportion of active volume. The first peak follows the large storm event that ended on August 26; the second peak occurs on October 14, no rainfall occurred over the previous 14 days. The August 26 rainfall event is discernible in the normalized outflow regime for Type III test pile but no increase in discharge was observed in October when the pile starts to freeze.

Normalized outflow to unfrozen volume indicates that the highest outflow occurs during initial spring melt. These plots help to emphasize the importance of the outflow through the batters, which occurs at the beginning of thaw, before the interior of the pile contributes to discharge. The peak active volume is not reached until early to late August in 2007 and 2008 and not until mid to late September in 2009 (**Figure 5-15 and Figure 5-16**).

As temperatures decrease, the discharge ceases, even while a portion of pile remains unfrozen (**Figure 5-9 and Figure 5-10**). The base and the exterior of the pile freeze first, followed by the core of the pile (Pham, 2013). During this period reaction products will potentially build-up in areas of the pile exposed to liquid water and some redistribution of water within the piles may occur.

Initially, in 2007, the Type I test pile thaws earlier and to a greater extent than the Type III test pile; however by 2009, the Type I test pile was thawing to a slightly lesser extent than the Type III test pile and

remained thawed for a shorter duration (**Figure 5-15 and Figure 5-16**). Over the period between 2007 and 2009, each year the duration that discharge occurs from the pile has shortened and the total volume that thaws has been reduced.

Appendix D provides an assessment of the effect of high solutes concentration during freezing. To evaluate if there was a change with time (and geochemistry) that delayed the freezing of a portion of the pore-water with high solute concentration the pore-water EC is reviewed against the time the TDR probes stop recording liquid water. As noted in Section 5.2.1, VMC recorded when temperatures reach greater than 0°C the following spring/summer was generally higher than compared to the VMC recorded prior to the onset of freezing conditions. The analyses provided in Appendix D attempts to identify if the change in VMC at TDR probes observed before and after freezing was a result of a change in solute concentration, or if infiltration and redistribution processes within the matrix surrounding the probes could describe this change.

5.4 Freezing Front Migration

In the fall, the onset of freezing conditions is expected to propagate from the surface of the test pile downwards towards the base, as well as inwards from the pile batters. In addition, as the piles are located on permafrost, the freezing front is also be expected to propagate upwards from the base of the pile. The permeability of the waste rock composing the Type I and Type III test piles permits advective air movement to penetrate and quickly cool the interior (Pham, 2013). As noted by Neuner (2009) the development of a frost layer under freezing conditions can act to redistribute pore-water towards the ice, either in response to a matric suction gradient created as the media dries in response to freezing (Black and Tice, 1989) or in response to a thermal gradient that can transport moisture in a liquid or vapor phase (Cary, 1965; Dirksen and Miller, 1966). Neuner (2009) observed such an upward effect at the AZL on October 6, 2007. A gradient of 2.0 was measured between the tensiometers installed at 0.3 and 0.6 m as the waste rock above these instruments began to freeze. The thermal gradient at the same time was relatively low, between 0.01 and 0.08 $^{o}C \cdot cm^{-1}$, leading Neuner to conclude that the upward redistribution of moisture was driven by capillarity due to the penetrating frost, and not the thermal gradient.

In 2008, beginning on October 7, air temperatures were regularly below 0ºC. Temperature at 0.3 mbg, as recorded by the ECHO probe at the AZLs, remains above 0ºC until sometime after October 20. During this period, the tensiometers remained in operation by covering and heating the exposed stick-ups with a light bulb to prevent damage to the instruments. A transition from a downward moisture flux past 0.45 m to an upward moisture flux was recorded in response to the advance of the freezing front (**Figure 5-19**). During this period, a total of 0.1 mm of rainfall was recorded, and that was received on October 16. The thermal gradient during this period is upwards except during a brief warming period on Oct.11/12. On October 16/17, the surface temperature falls rapidly by 5ºC which results in a large thermal gradient (approximately $30ºC \cdot m^{-1}$) and one day after this increase in the thermal gradient, the upwards flux from 0.6 to 0.3 m increases steadily. Daily average solar radiation has diminished to 0.2 $W \cdot m^{-2}$, and the upward redistribution of water is attributed the large thermal gradient; however, the response is likely also a result of the capillarity due to the penetrating frost front. On October 19, upward flux from 0.6 to 0.3 m was 0.74 $mm \cdot d^{-1}$; this compares to the rate of approximately 0.4 $mm \cdot d^{-1}$ reported by Neuner (2009) on the final day of observation in 2007.

In 2009, due to the drier conditions, the flux is upwards throughout September and October and any influence from the capillarity in response to the freezing front or thermal gradients on upward moisture redistribution to the penetrating frost front is difficult to distinguish.

5.5 Flow Mechanisms - Conclusion

Infiltration into waste rock placed at less than field capacity will be held in the matrix until drainage occurs. Under drier conditions and in response to lower infiltration rates, infiltrating water will move through the matrix domain. At higher infiltration rates, water flow may enter coarser-grained macropores and move through the waste rock at greater velocity. Data reviewed in preceding section tracked the progression of the VMC in the waste rock, year to year, and in response to individual rainfall events. Drainage of infiltrated water that moved through the test pile was recorded and its geochemical signature was used to understand water flow mechanism through the pile. Influence of thermal conditions and water flow in response to temperature changes was discussed. Key observations from this data are reviewed in the following.

In-situ instrumentation installed within matrix material of the test piles record moisture content and provide an opportunity to track the wetting front through the test piles, until the moisture discharges from the base of the pile and is recorded by the basal drain or basal collection lysimeter. Average matrix moisture content of the three test piles in 2008 range from 18.5% (about 74% saturation) for the Type III test pile, 6.9% (about 28% saturation) for the Type I test pile and 11.2% (45% saturation) for the Covered test pile. The Type I test pile and the Covered test pile were in the process of matrix wet-up through 2009, whereas the Type III test pile appears to have reached a dynamic equilibrium. The moisture content in all three piles was lower in 2009 as drain down occurred and low net percolation did not replenish the moisture lost.

The initial wetting front in the Type III test pile appeared to advance at approximately 7.5 $m \cdot yr^{-1}$. The wetting front advanced to 5 m in 2007, to 7 m by July 2008 and 9 m by August 2008. Drainage began to report at several basal collection lysimeters located under the central portion of the test pile in August and September 2008. Although limited data are available from the Type I test pile, the initial wetting front appeared to advance at approximately 6 $m \cdot yr^{-1}$, but during 2009 the advance has stopped due to drier conditions. The initial wetting front in the Covered test pile appeared to advance at approximately 5 $m \cdot yr^{-1}$. The wetting front advanced to about 6 or 7 m by the fall of 2008 and to 10 m in the winter of 2008/2009. No discharge was recorded from the basal collection lysimeters. The advance of the wetting front in the Covered test pile was more variable through different regions of the pile, in contrast to the more uniform advance at the Type III test pile. Note despite the cover on the Covered test pile the wetting front has advanced similar to the rate observed at the Type I test pile.

The preceding discussion (**Section 5.2.2**) attempted to assess whether water movement within the test pile in response rainfall events could be observed to identify flow mechanisms within the waste rock by describing the wetting front response to different magnitude and intensity rainfall events. This review showed that only the largest events produce a discernible response at depth; however, there is limited data to draw this conclusion. The geochemical signature, as represented by the SC of the drainage from the test pile, suggests water flow through the matrix is the dominate flow mechanism under average rainfall conditions (lower infiltration rates). Only in response to large storm events did water flow through

preferential flow paths appear to occur (e.g., in response to the greatest rainfall event observed during the study period which delivered 35.8 mm over 24.8 hours), and although preferential flow was observed, it was not the dominant flow mechanism.

Through 2009, the active layer of the Type I and Type III test piles extends the entire depth of the pile, although there may be areas within the core that remain frozen. Each year the period the piles discharge has shortened and the total active volume of the test piles has decreased, consistent with an overall cooling of the lower central core of the test piles. Normalized outflow to unfrozen volume shows highest outflow occurs during initial spring melt, before the interior of the test pile is contributing. As the interior of the pile thaws, the discharge increases proportionately with the active volume. During the fall, at the onset of freezing conditions, interior portions of test piles still have liquid water, however discharge has stopped, allowing reaction products to build-up and for redistribution of water within the piles. The freezing front migration was observed to generate an upward flux in response to the thermal gradient. In 2008, in response to a large thermal gradient (approximately 30 $^{o}C \cdot m^{-1}$) upward flux past 0.45 m was observed as 0.7 $mm \cdot d^{-1}$.

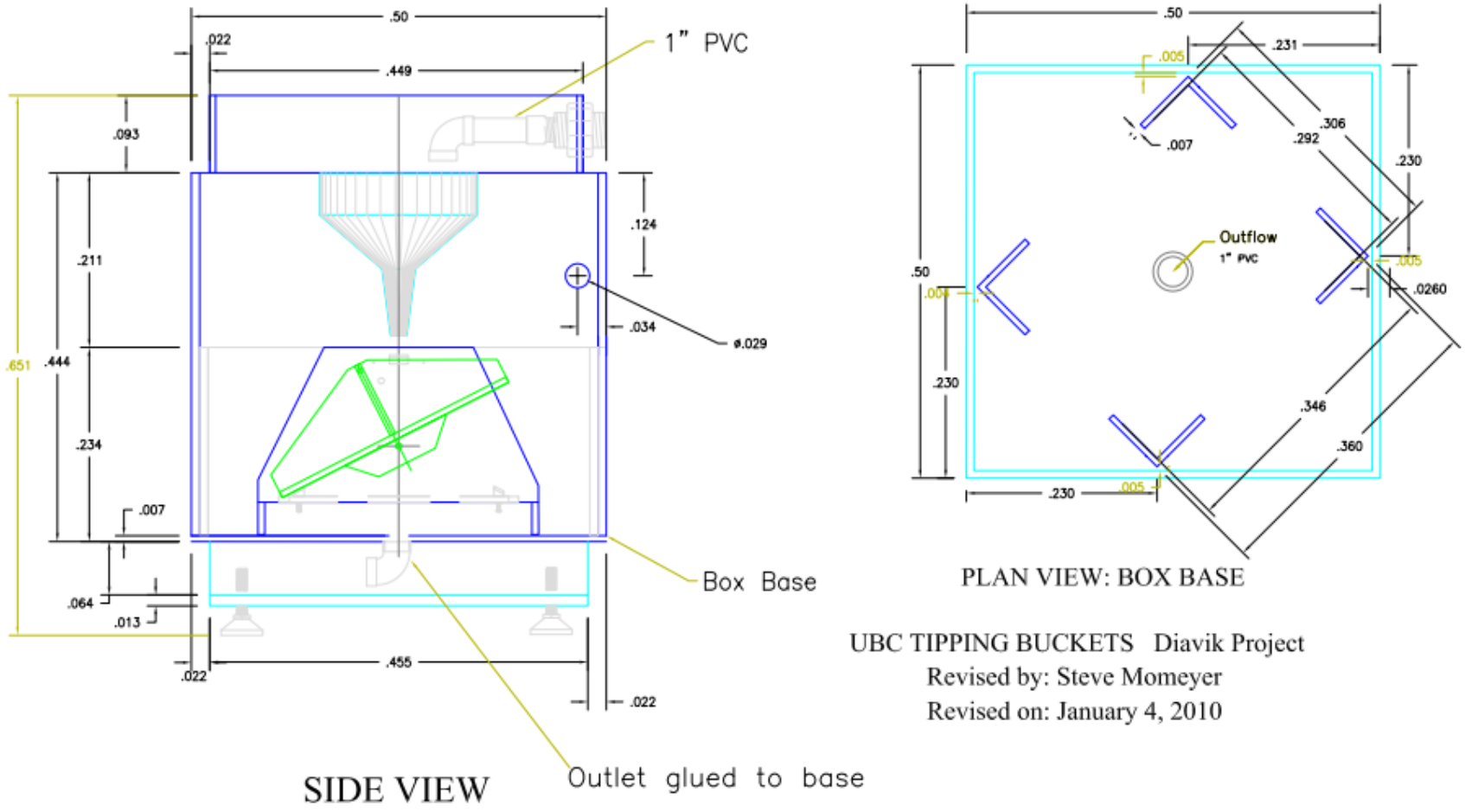

Figure 5-1: Custom built tipping bucket. All measurements in mm.

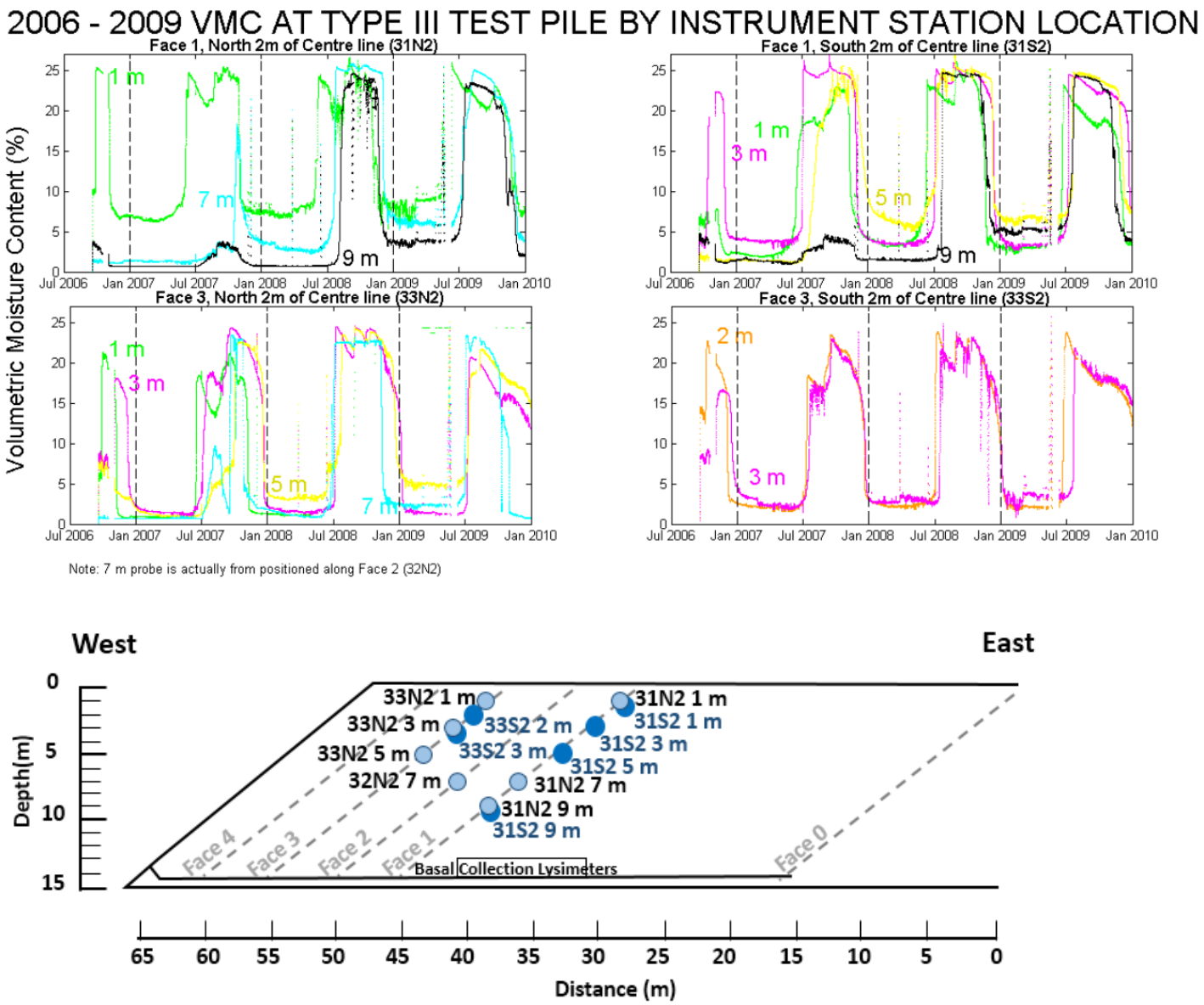

Figure 5-2: 2006 to 2009 VMC at the Type III test pile organized by instrument station location.

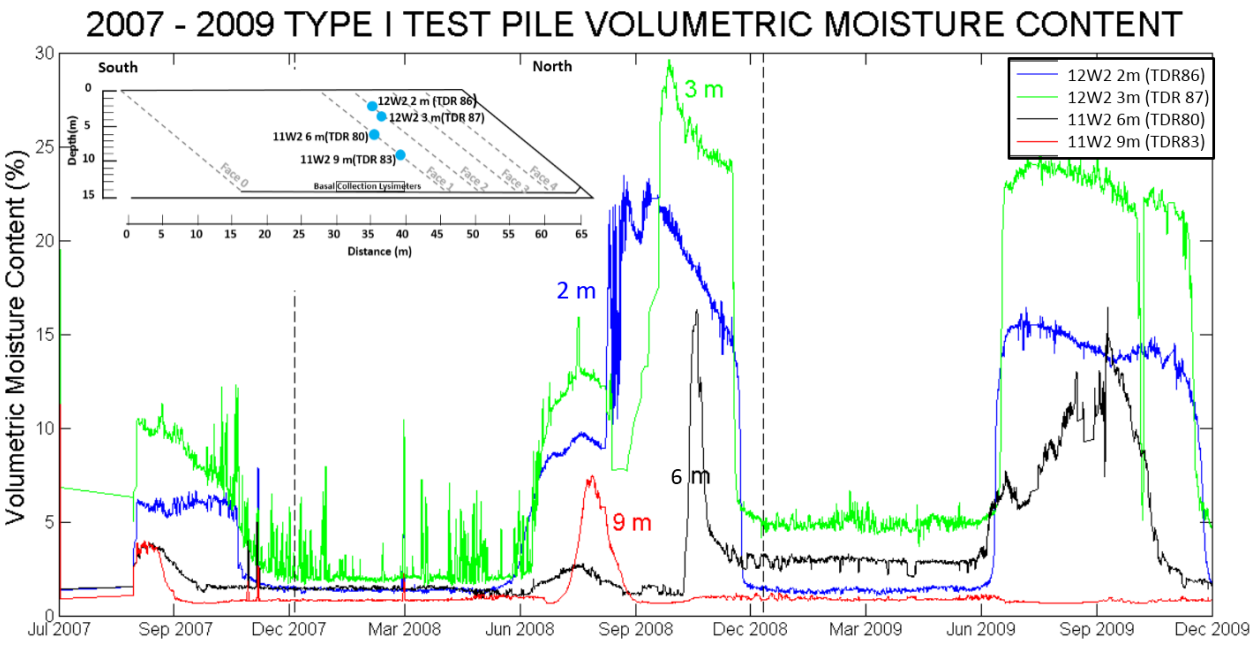

Figure 5-3: 2007 to 2009 VMC at the Type I test pile organized by instrument station location.

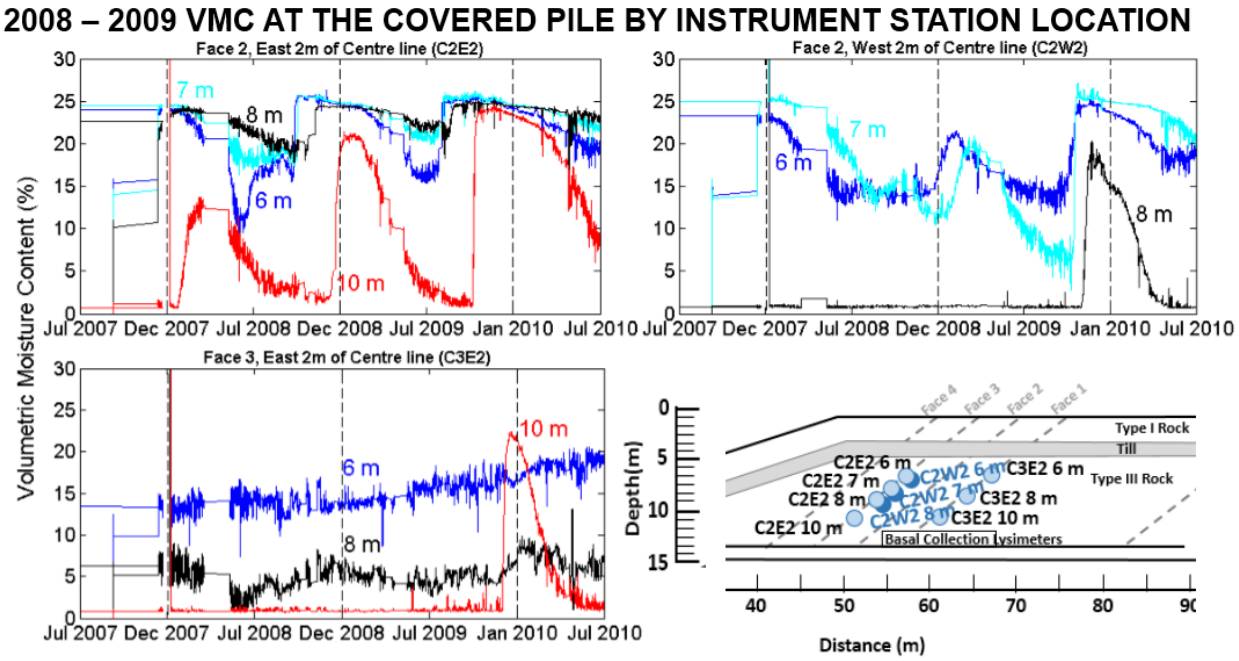

Figure 5-4: 2008 to 2009 VMC at the Covered test pile organized by instrument station location.

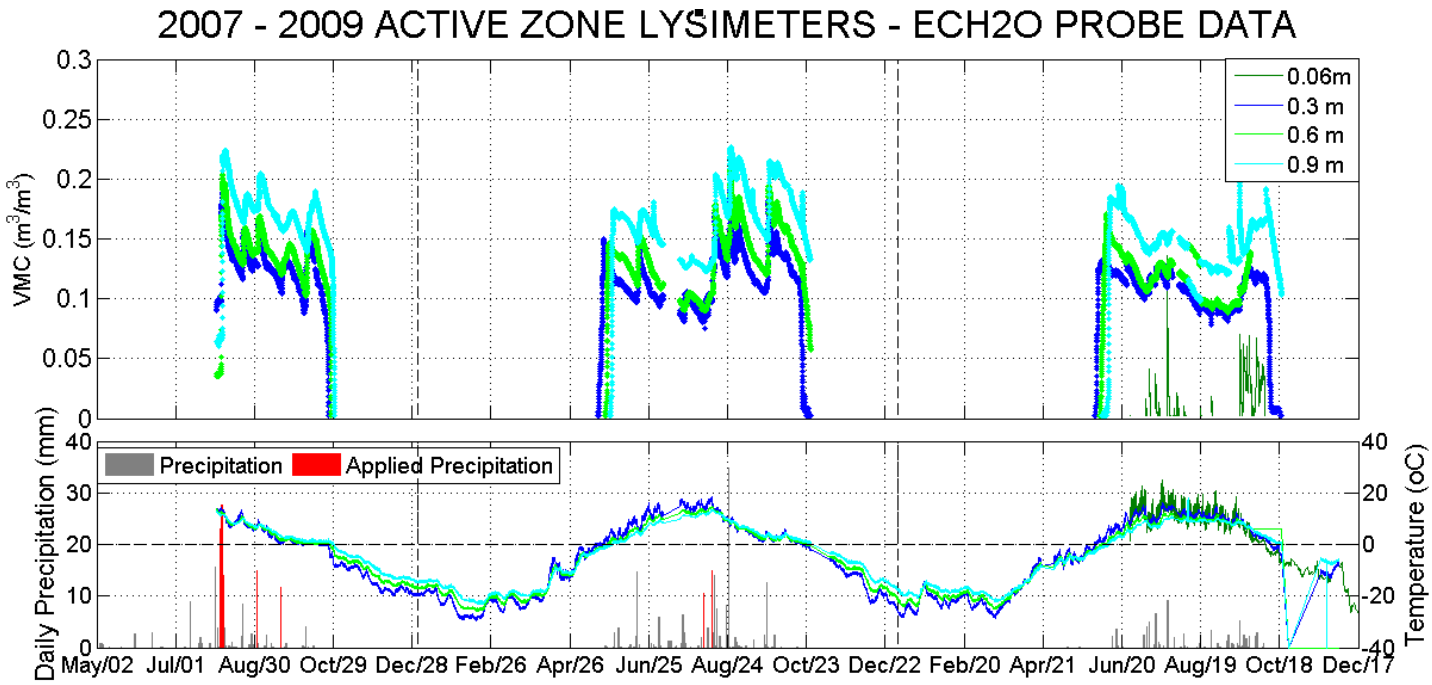

Figure 5-5: 2007 to 2009 VMC recorded by the ECH$_2$O probes adjacent to the Type III AZLs.

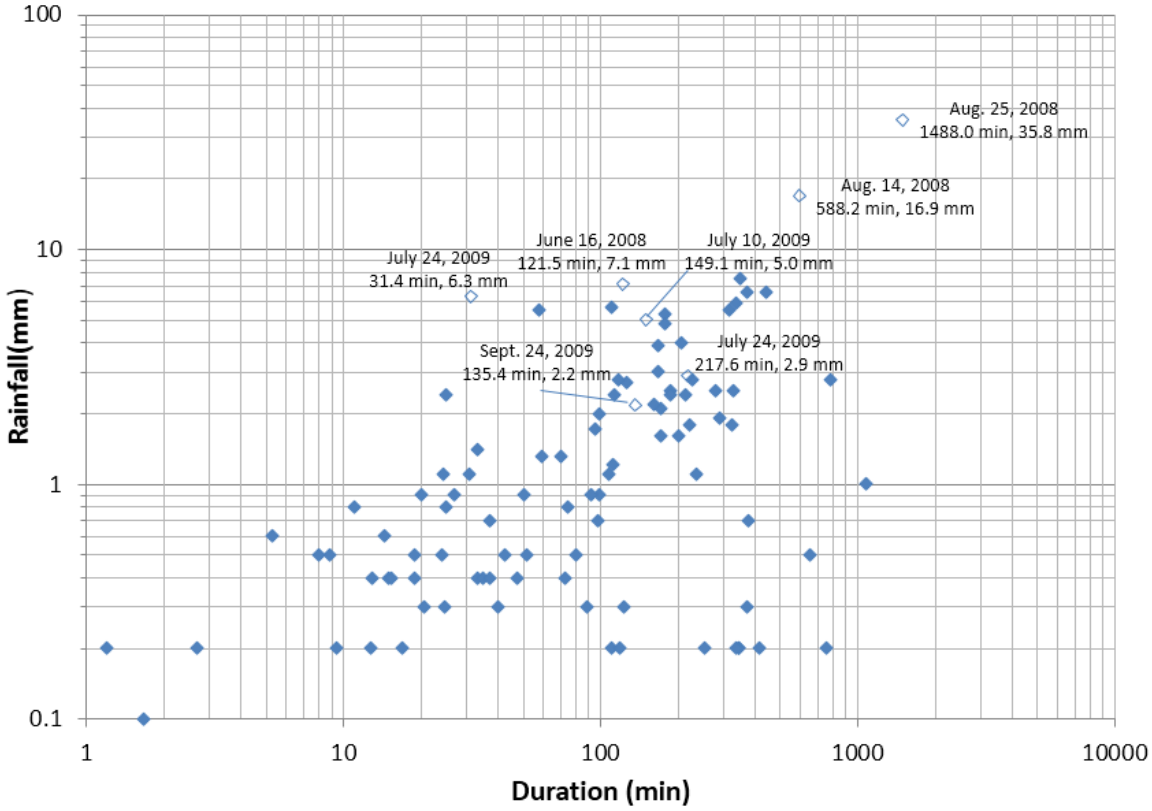

Figure 5-6: Rainfall event magnitude compared to event duration of all rainfall in 2008 and 2009. Rainfall events discussed in text and reported on Table 5-1 are shown with open symbols and labelled with the event date, duration and rainfall magnitude.

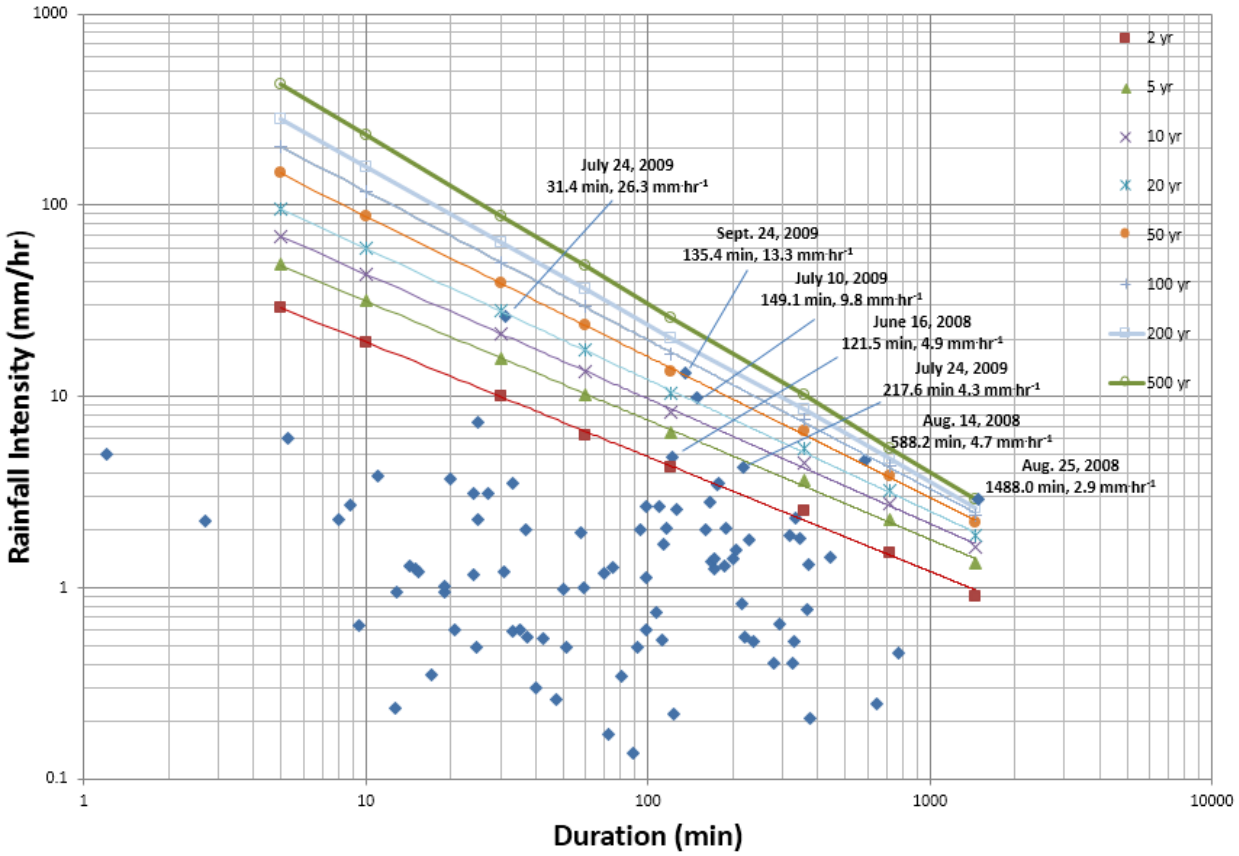

Figure 5-7: Intensity duration frequency curves for rainfall at Lac De Gras from Golder (2008), overlain with intensity duration data for individual rainfall events in 2008 and 2009 from the site. Rainfall events discussed in text and reported on Table 5-1 are labelled with the event date, duration and rainfall intensity.

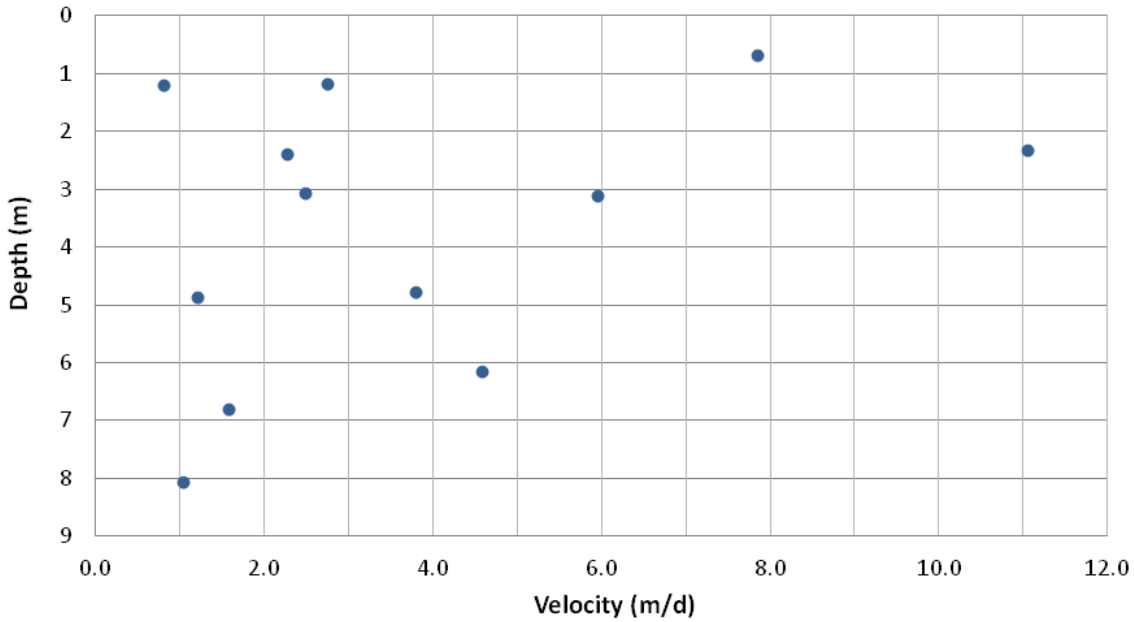

Figure 5-8: Velocity of wetting front response detected at the Type III TDR probes in response to large magnitude rainfall event that initiated on August 25, 2008.

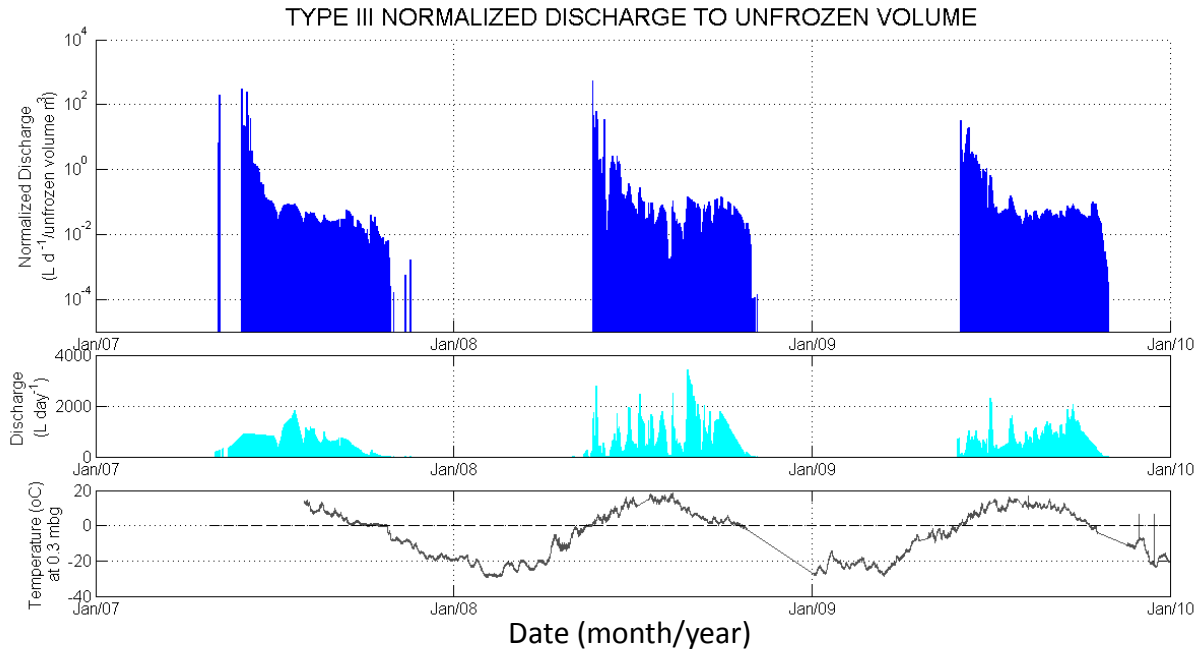

Figure 5-9: Discharge normalized to unfrozen pile volume for the Type III test pile between 2007 and 2009.

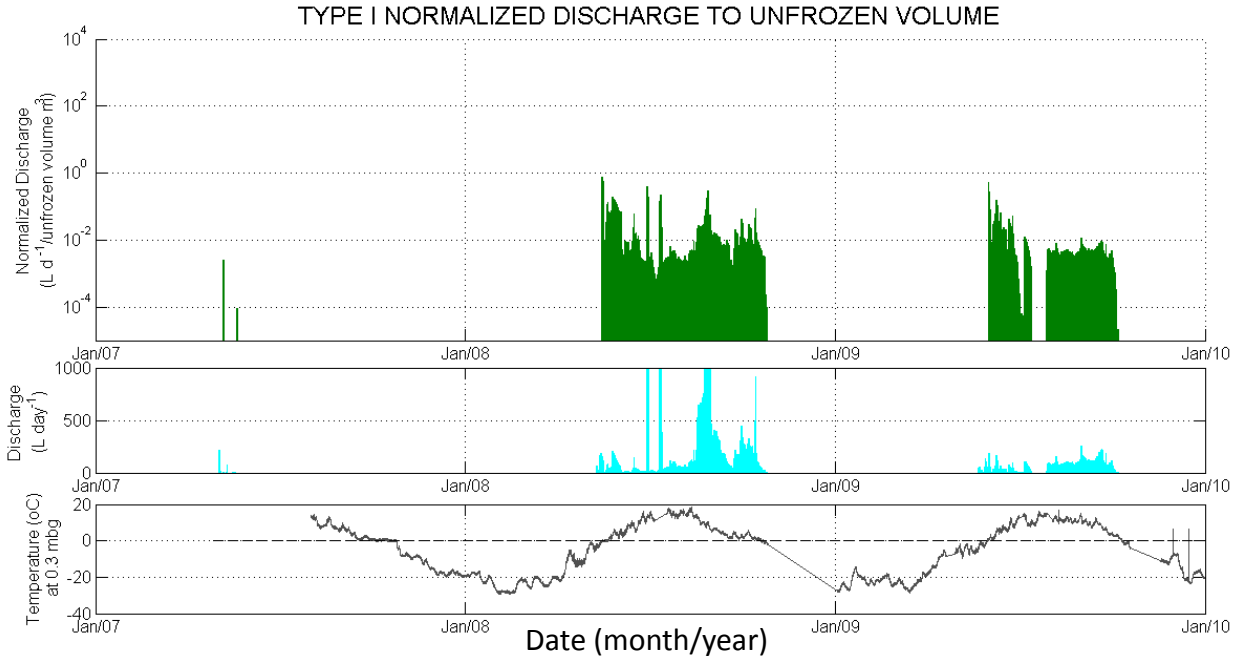

Figure 5-10: Discharge normalized to unfrozen pile volume for the Type I test pile between 2007 and 2009.

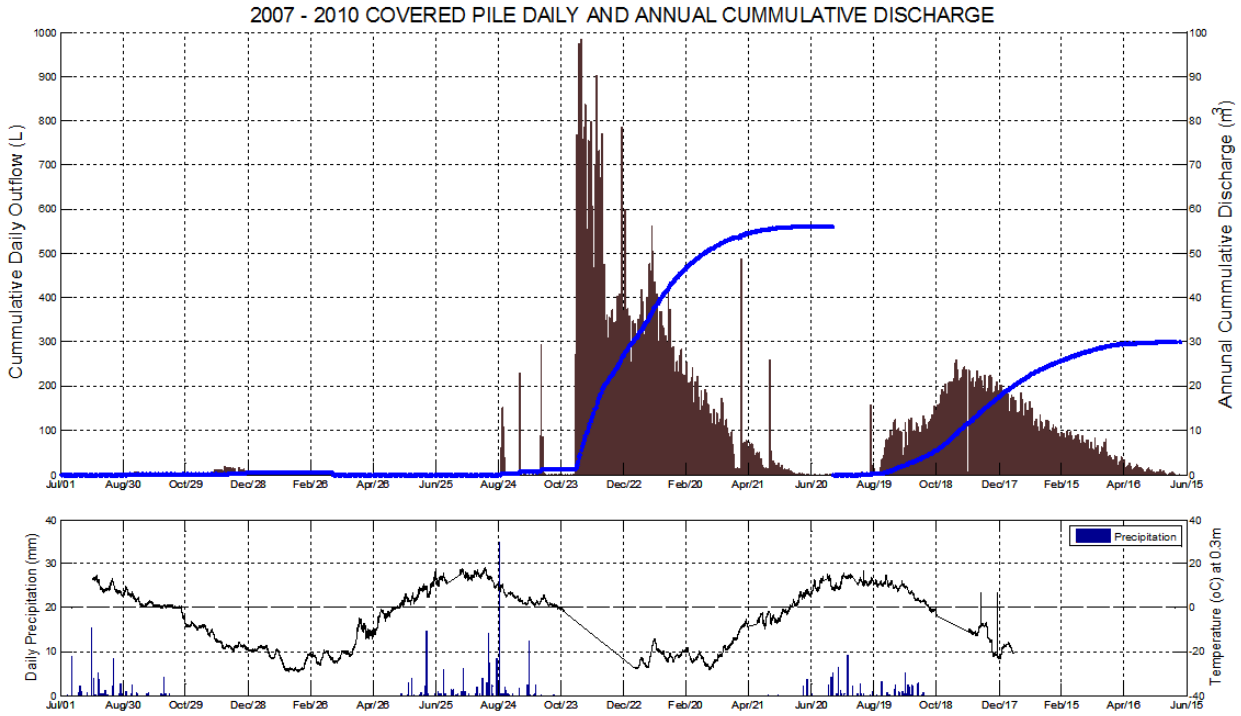

Figure 5-11: Discharge from the Covered test pile between 2007 and spring 2010.

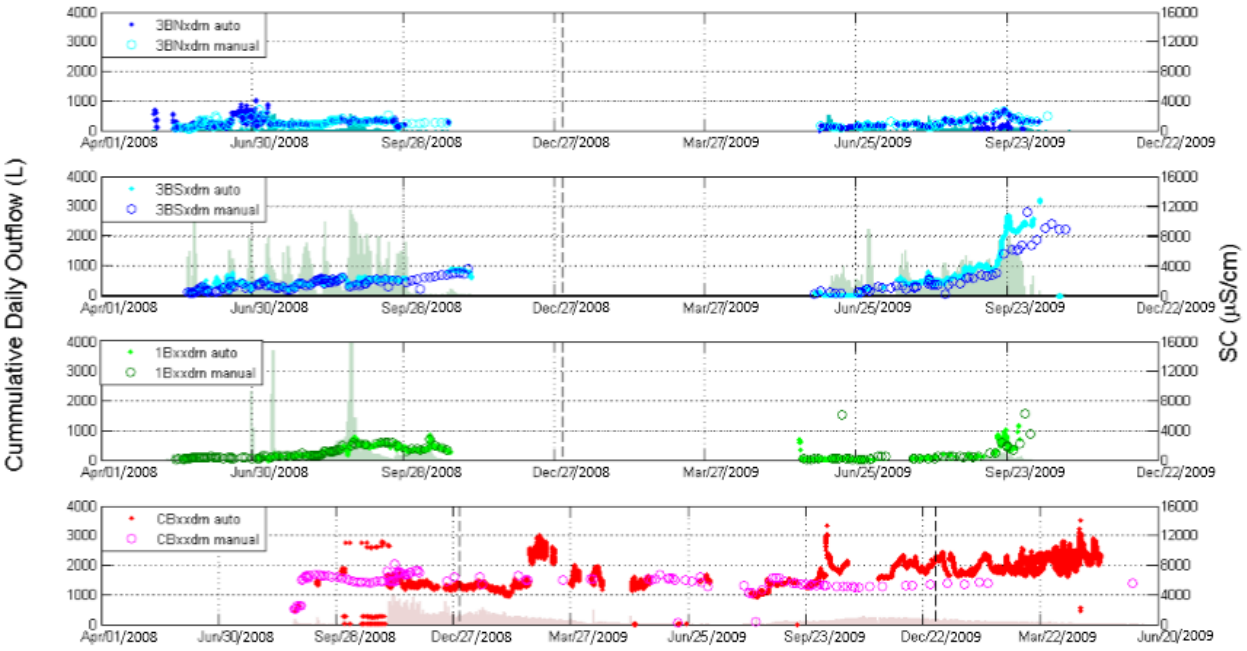

Figure 5-12: Specific conductance compared to daily discharge from the Type I, Type III and Covered test piles for 2008 and 2009. Markers indicate specific conductance and bars represent cumulative daily outflow.

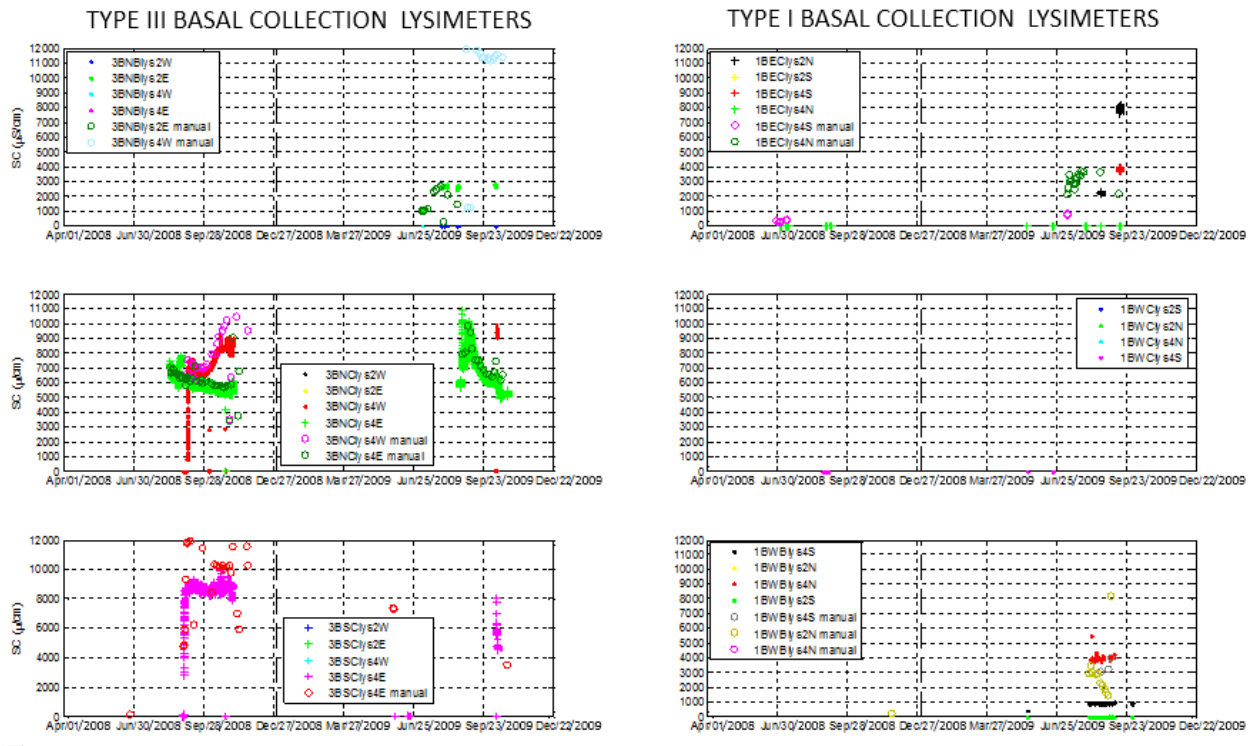

Figure 5-13: Specific conductance during periods discharge from the Type I and Type III basal collection lysimeters in 2008 and 2009.

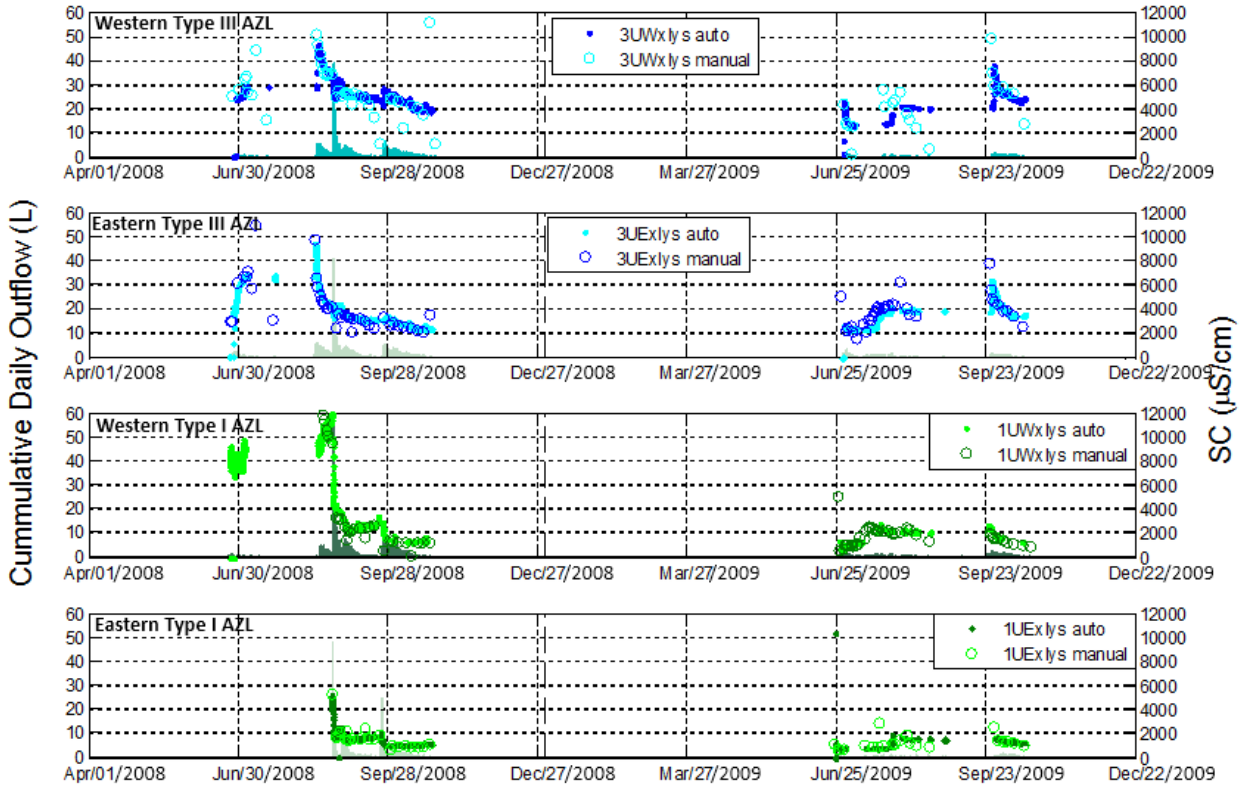

Figure 5-14: Specific conductance compared to daily discharge from the AZLs for 2008 and 2009. Markers indicate specific conductance and bars represent cumulative daily outflow.

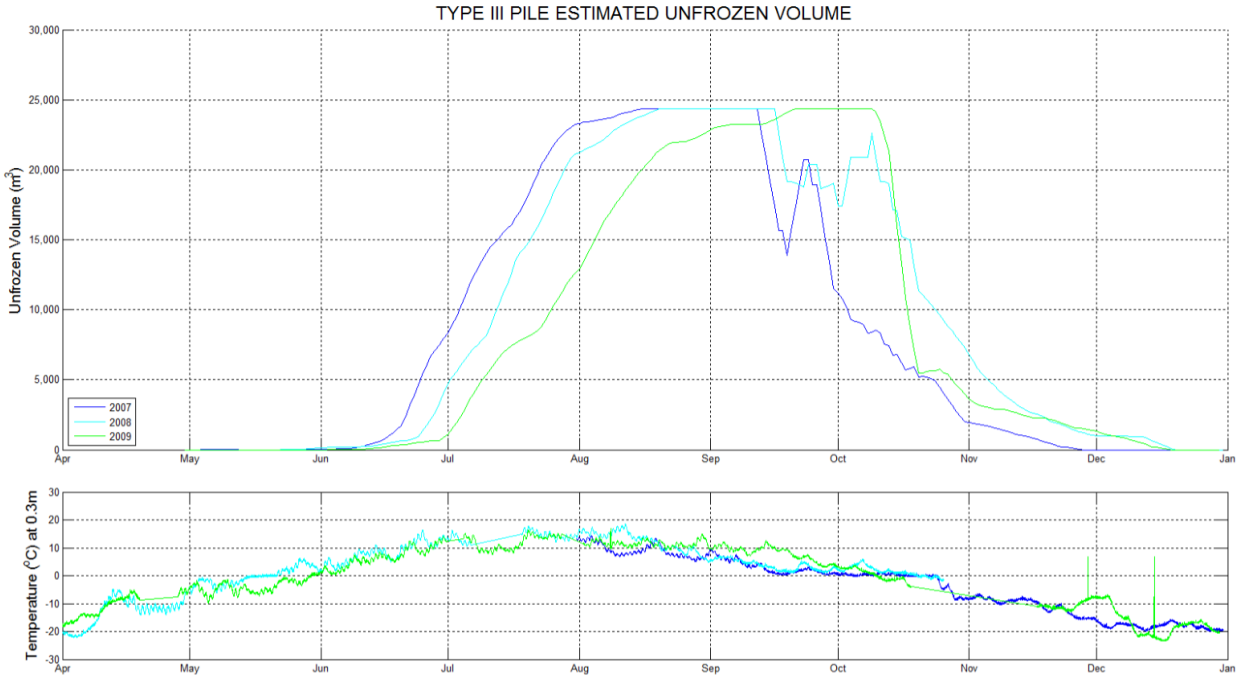

Figure 5-15: Estimated unfrozen Type III test pile volume for 2007, 2008, and 2009 plotted against Julian day for annual comparison. Moving average filter (7-day) applied to unfrozen volume data to remove signal noise.

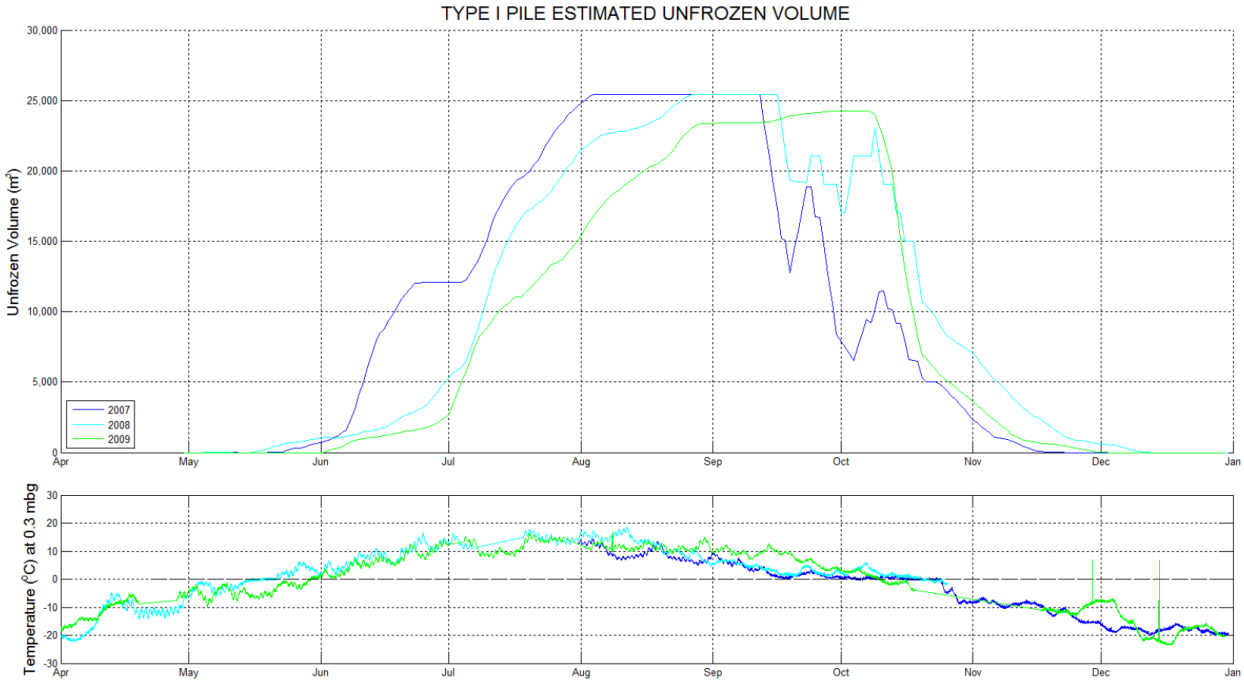

Figure 5-16: Estimated unfrozen Type I test pile volume for 2007, 2008, and 2009 plotted against Julian day for annual comparison. Moving average filter (7-day) applied to unfrozen volume data to remove signal noise.

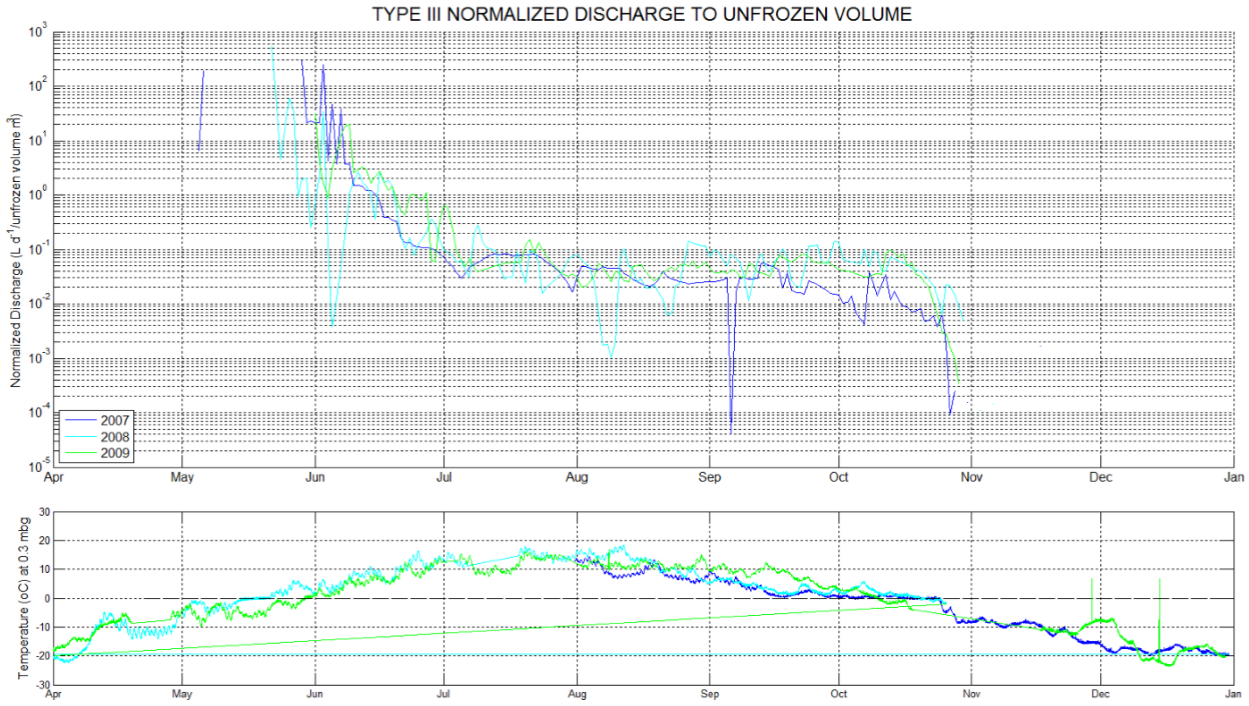

Figure 5-17: Discharge normalized to unfrozen pile volume for the Type III test pile plotted against Julian day for annual comparison.

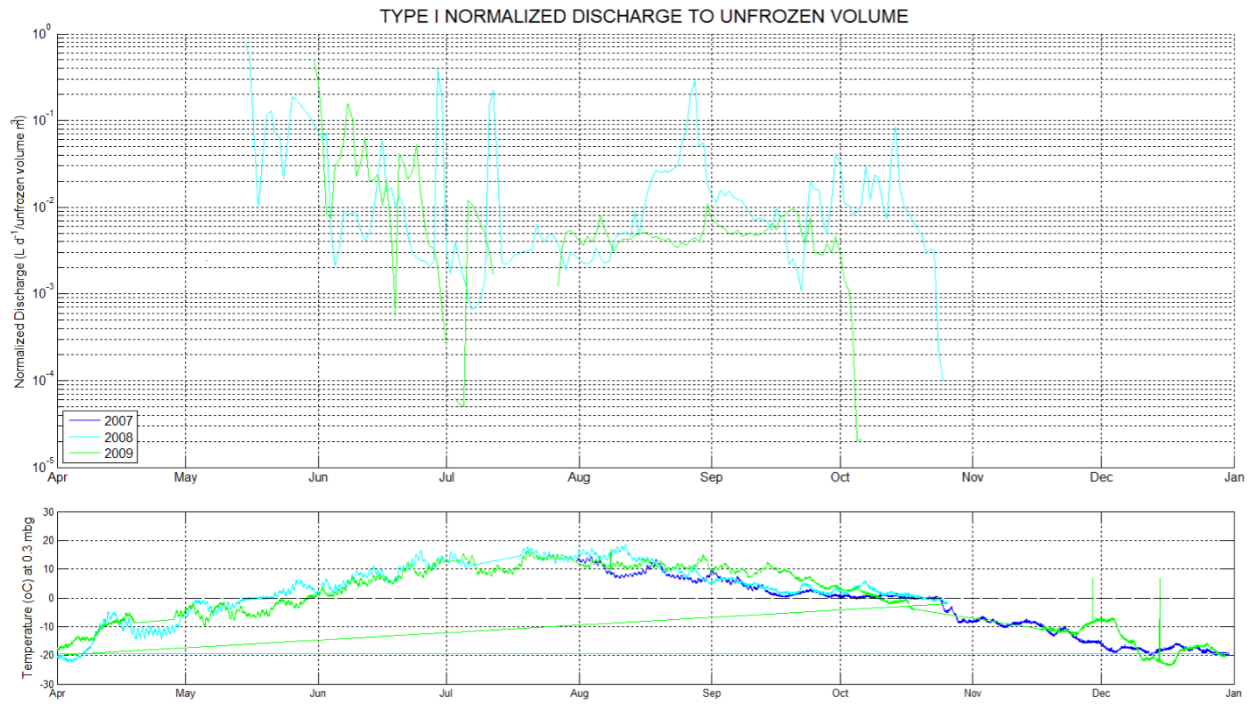

Figure 5-18: Discharge normalized to unfrozen pile volume for the Type I test pile plotted against Julian day for annual comparison.

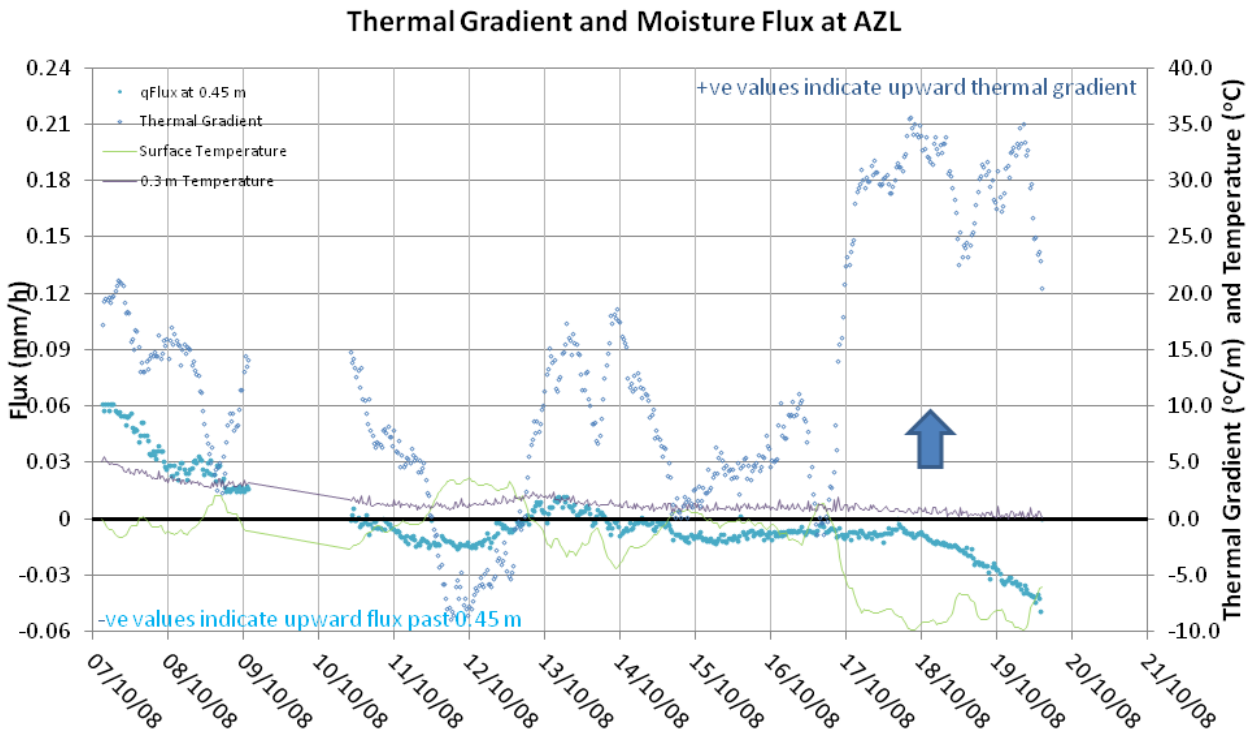

Figure 5-19: Temperature, thermal gradient and moisture flux observed at surface of the AZLs at onset of freezing conditions in 2008.

Year	Annual Average VMC (%)	Active Season Average VMC (%)	Active Season Average VMC as % Matrix Saturation
Type III test pile			
2007	7.9	16.9	68
2008	11.0	20.6	82
2009	11.7	18.9	76
Type I test pile			
2007	3.8	5.2	21
2008	4.1	9.1	36
2009	5.3	10.8	43
Covered test pile			
2008	13.0	15.6	62
2009	14.1	16.9	68

Table 5-1: Long term average annual volumetric moisture contents for test piles between 2007 and 2009.

	Median Time of Event	Duration (min)	Intensity ($mm \cdot hr^{-1}$)	Recorded Magnitude (mm)	Average Velocity of Wetting Front ($m \cdot d^{-1}$)	Standard Deviaton	Average Velocity of Wetting Front by ECH2O at AZL ($m \cdot d^{-1}$)	Standard Deviaton
<2 yr recurrence	June 16, 2008 02:36	121.5	4.9	7.1	0.0	0.0	1.0	0.1
2 to 5 yr recurrence	July 24, 2009 13:41	217.6	4.3	2.9	-	-	-	-
10 to 20 yr recurrence	July 24, 2009 18:13	31.4	26.3	6.3	0.0	0.0	2.3	0.8
10 to 20 yr recurrence	July 10, 2009 15:12	149.1	9.8	5.0	0.0	0.0	6.6	8.8
20 to 50 yr recurrence	August 14, 2008 03:40	588.2	4.7	16.9	0.0	0.0	0.1	0.0
50 to 100 yr recurrence	September 24, 2009 12:30	135.4	13.3	2.2	0.4	0.6	1.0	0.1
>100 yr recurrence	August 25, 2008 15:55	1488.0	2.9	35.8	3.8	3.2	1.1	0.3
	25% of all rainfall events are greater than 2 mm in magnitude (75th percentile) 10% of all rainfall events are greater than 3.9 mm in magnitude (90th percentile)							

Table 5-2: Wetting front velocity in response to various intensity rainfalls. Recurrence interval based on data from Golder (2008), provided for relative comparison of event size.

	Location	Date Discharge Began	Date Discharge Stopped	Days Thawed/ Flowing	Recorded Discharge Volume (m^3)	Interpolated Discharge Volume [not recorded] (m^3)	Uncertainty (m^3)
2007	Type I	May 01, 2007	not known	not known	0.3	unknown	0.02
	Type III	May 03, 2007	Nov 01, 2007	182	40	70	2
	Covered	Sep 08, 2007	Jan 10, 2008	124	0.5	-	0.02
2008	Type I	May 10, 2008	Oct 25, 2008	168	50	1	5
	Type III	May 02, 2008	Oct 30, 2008	181	130	20	5
	Covered	Aug 26, 2008	Jul 10, 2009	318	55	120	10
2009	Type I	May 22, 2009	Oct 06, 2009	137	10	0.5	1
	Type III	May 29, 2009	Oct 30, 2009	154	100	17	2.5
	Covered	Aug 06, 2009	Jun 08, 2010	306	30	0.1	4

Notes:

1.The discharge from the Covered pile occurs over a water year, defined as the period from when outflow starts, to when it stops, which occurs from the summer over the winter, stopping the following summer.

2. Date discharge stopped was determined from the last tip recorded (could be small amounts of flow that allowed sampling for longer).

3. Interpolated volume [not recorded] includes discharge volume interpolated during periods when the datalogger was malfunctioning (linear interpolation) and manual measurements, made at a specific time during a day, extrapolated to be constant over the course of the day.

4. Estimated discharge volume uncertainty reports measurement error from the tipping bucket.

5. Volume of water applied through irrigation events during 2006 and 2007 to the Type III test pile: 70 m^3; Type I and Covered test piles did not recieve applied rainfall.

Table 5-3: Discharge from test piles basal drains between 2007 and 2009.

		Location	Date Discharge Began	Date Discharge Stopped	Recorded Discharge Volume (m^3)	Estimated Sample Volume Removed (m^3)	Uncertainty (m^3)
2008	Type III	3BNBlys2E	no flow	-	-	-	-
		3BNBlys4W	no flow	-	-	-	-
		3BNClys4W	Sep 06, 2008	Nov 04, 2008	1	0.01	0.1
		3BNClys4E	Aug 16, 2008	Nov 04, 2008	1	0.02	0.1
		3BSClys4E	Aug 31, 2008	Nov 04, 2008	0.2	0.02	0.02
	Type I	1BWBlys Cluster	no flow	-	0.002	0.002	-
		1BWClys Cluster	Aug 27, 2008	Sep 03, 2008	0.003	0.000	0.0004
		1BEClys Cluster	Jun 29, 2008	Sep 06, 2008	0.02	0.003	0.0001
2009	Type III	3BNBlys2E	Jul 06, 2009	Oct 07, 2009	0.1	0.01	0.01
		3BNBlys4W	Jul 07, 2009	Oct 22, 2009	0.3	0.01	0.03
		3BNClys4W	Jul 07, 2009	Oct 10, 2009	0.001	0.00	0.0001
		3BNClys4E	Jul 07, 2009	Oct 17, 2009	0.2	0.01	0.02
		3BSClys4E	Jul 07, 2009	Oct 11, 2009	0.01	0.00	0.001
	Type I	1BWBlys Cluster	Jul 07, 2009	Sep 29, 2009	0.1	0.01	0.01
		1BWClys Cluster	Jul 07, 2009	Jul 10, 2009	0.001	0.001	0.00002
		1BEClys Cluster	Jul 07, 2009	Sep 29, 2009	0.1	0.01	0.01

Notes:

1. Date discharge began was determined from the first instance of consecutive days of outflow. Date discharge stopped was determined from the last tip recorded (could be small amounts of outflow that allowed sampling for longer).
2. Sampling Volume (L) is the volume of water removed from the flow-through cell by sampling and therefore did not report to the tipping bucket. In 2008 the volume was estimated, in 2009, the volume was typically recorded.
3. Estimated uncertainty reports measurement error from the tipping bucket.
4. Volume of water applied through irrigation events during 2006 and 2007 to the Type III test pile: 70 m^3; Type I and Covered test piles did not receive applied rainfall.

Table 5-4: Discharge from the test pile basal collection lysimeters between 2007 and 2009.

	Location	Date Discharge Began	Date Discharge Stopped	Days Thawed/ Flowing	Recorded Discharge Volume (m^3)	Estimated Sample Volume Removed (m^3)	Uncertainty (m^3)
2007	Eastern Type III AZL	Aug 25, 2007	Nov 10, 2007	77	0.03	0.009	0.01
	WesternType III AZL	Aug 28, 2007	Oct 10, 2007	43	0.04	0.008	0.004
	Eastern Type I AZL	no flow	no flow	-	-	-	-
	WesternType I AZL	no flow	no flow	-	-	-	-
2008	Eastern Type III AZL	Jun 26, 2008	Oct 21, 2008	117	0.2	0.02	0.00
	WesternType III AZL	Jun 27, 2008	Oct 23, 2008	118	0.2	0.02	0.00
	Eastern Type I AZL	Aug 25, 2008	Oct 23, 2008	59	0.2	0.01	0.01
	WesternType I AZL	Aug 17, 2008	Oct 21, 2008	65	0.3	0.02	0.01
2009	Eastern Type III AZL	Jun 28, 2009	Oct 25, 2009	119	0.04	0.02	0.02
	WesternType III AZL	Jul 01, 2009	Oct 25, 2009	116	0.02	0.01	0.01
	Eastern Type I AZL	Jun 26, 2009	Oct 15, 2009	111	0.02	0.01	0.01
	WesternType I AZL	Jun 26, 2009	Oct 15, 2009	111	0.07	0.02	0.01

Notes:
1. Date discharge began was determined from the first instance of consecutive days of outflow. Date discharge stopped was determined from the last tip recorded (could be small amounts of outflow that allowed sampling for longer).
2. The collection area of the Type III AZL is 2.09 m^2 whereas the the Type I AZL is 3.60 m^2.
3. Estimated uncertainty reports measurement error from the tipping bucket.
4. Volume of water applied through irrigation events during 2007 and 2008 to the Type III AZL was 240 L (190 L in 2007 and 50 L in 2008); the Type I AZL did not recieve any applied rainfall events.

Table 5-5: Discharge from AZLs between 2007 and 2009.

		Type I test pile		Type III test pile	
Total Volume (m^3)		26,240		24,980	
Peak Unfrozen Volume (m^3)	2007	25,500	30-Jul. to 13-Sept.	24,400	11-Aug. to 13-Sept.
	2008	25,500	20-Aug. to 15-Sept.	24,400	13-Aug. to 11-Oct.
	2009	24,200	22-Sept. to 6-Oct.	24,400	14-Sept. to 8-Oct.

Table 5-6: Estimated peak unfrozen volume for the Type I and Type III test piles.

6 CONCLUSIONS

Hydrologic processes of three unsaturated waste rock test piles and four active zone lysimeters located in a semi-arid continuous permafrost environment were studied. These approximately 15 m high test piles each covering a footprint of about 3,000 m^2 are well instrumented with a series of monitoring devices designed to collect geochemical, thermal and hydrological data. Specific instrumentation installed within the piles to collect hydrology related data included: TDR probes for VMC determination; commercial TDR ECH_2O probes also for determining VMC as well as temperature, and bulk soil EC; and tensiometer probes for monitoring matric suction. Outflow discharge and geochemistry parameters (pH, EC, temperature) are continuously monitored from infiltration reaching the base of the test piles and AZL. Hydrologic processes including infiltration, evaporation, wetting front movement, moisture storage and redistribution, discharge, and thermal interaction were examined from the growing dataset established by the research project. In addition, mean residence time was estimated from a tracer test conducted at the AZL scale and bulk hydrologic properties of waste rock were characterized on a 27 m^3 field permeameter. Key conclusions from the dataset available between 2006 and 2009 are:

- Water flow through this unsaturated waste rock is dominated by passage through the matrix material and is therefore controlled by capillary forces despite a grain size distribution with less than 18% of the waste rock composed of the finer than 5 mm fraction. The significance of this is, that the longer residence time in contact with the finer grain sized fraction will allow greater reaction time and dissolution of weathering products and should allow for better prediction from laboratory based testing which generally only includes the finer grain size fraction. Based on solute transport at AZLs the average advective velocity, during the active flow period, is between 7 and 10 $mm \cdot d^{-1}$ or 1.0 and 1.4 $m \cdot yr^{-1}$. Mean residence time was between 169 and 229 days, this is equivalent to between 1.2 and 1.7 years residence time, when corrected for the average 137 days annual active period.
- The rate of initial wetting front advancement under average precipitation was tracked at the Type III test pile as about 7.5 $m \cdot yr^{-1}$ and under drier conditions at the Type I test pile as 6 $m \cdot yr^{-1}$, but during 2009 the advance has stopped due to drier conditions. Despite a low permeability till cover

on the Covered test pile attenuating infiltration, the wetting front has advanced at a rate similar to the rate observed at the Type I test pile and reached greater depths.

- Normalized outflow to unfrozen volume shows highest outflow occurs during initial spring melt, before the interior of the test pile is contributing to discharge. As the interior of the pile thaws, the discharge increases proportionately with the active volume. During the fall, at the onset of freezing conditions, interior portions of test piles still have liquid water, however discharge has stopped, allowing reaction products to build-up and for redistribution of water within the piles.
- The geochemical signature, as represented by the SC of the drainage from the test pile, suggests water flow through the matrix is the dominate flow mechanism under average rainfall conditions (lower infiltration rates). Only in response to large storm events did water flow through preferential flow paths appear to occur (e.g., in response to a large magnitude and intensity duration rainfall event which delivered 35.8 mm over 24.8 hours, in August 2008).
- Detailed discharge measurements of drainage from the base of the test piles is key for mass loadings estimates as there is diurnal and day-to-day fluctuations in outflow that would not be observed from periodic or instantaneous snap-shot measurements.
- Evaporation determined by the extended Penman-Monteith model provided good agreement to evaporation estimated by a water balance on the AZLs, with an absolute difference less than 8 mm or 10% of the rainfall. This comparison demonstrates the model as a valid technique to estimate evaporation at this northern latitude and net percolation, in the absence of run-off. These modelled evaporation estimates indicate that for a year with mean average precipitation approximately 50% evaporated. Modelled evaporation estimated 85%, 49% and 94% of the natural rainfall evaporated in 2007, 2008 and 2009, respectively. Snowmelt infiltration across the top surface of a waste rock dump in a semi-arid arctic environment provides a minimal amount of net infiltration. As seen in the VMC data from the Type I test pile, in this semi-arid environment greater than 3 years was required to wet-up the matrix of a 15-m high waste rock test pile. Infiltration into waste rock placed at less than field capacity will be held in the matrix until drainage occurs. In this northern environment, under natural rainfall conditions a significant amount of time

will be required for full-scale waste rock stockpiles to reach a dynamic equilibrium state, during which moisture may freeze.

- In-situ measurements of wetting front propagation made with TDR probes provided good prediction of the timing of matrix wet-up which corresponded with the initiation of drainage from the basal collection lysimeters at the Type III pile; however this was not the case at the Type I test pile where drainage from the basal collection lysimeters occurred in 2008 and 2009 while moisture content indicated that the wetting front had not reached below 9 m. This may be a result of poor spatial coverage of TDR probes within the Type I test pile where only 4 instruments survived or it may be a reflection of the difficultly of in situ monitoring of water movement through heterogeneous waste rock material.
- Net percolation/evaporation in northern waste rock piles is influenced by seasonal changes with respect to solar radiation and the timing and magnitude of individual rainfall events. Water movement across the waste rock surface is restricted to between about May and October, and by late August or early September, evaporation is energy-limited. Rainfall received after net radiation peaked in June, and available energy was a limiting factor for evaporation, permitted greater infiltration. In 2007, 2008 and 2009 between 35% and 50% of the rainfall fell between late August and when freezing conditions set-in, in mid-October, coincident with declining or energy-limited evaporation stage therefore allowing significant rainfall infiltration to occur during this period. Strong seasonal variation on net percolation/evaporation necessitates consideration of seasonality, at a monthly or finer scale, when determining and applying evaporation estimates to waste rock piles in a northern environment. Annual net percolation/evaporation as a percentage of annual rainfall varied significantly with variation in annual rainfall.
- Based on characterization experiments on two sample sizes (16 m^3 and 27 m^3 field permeameter) bulk porosity of the waste rock produced by open pit mining operations at Diavik ranges between 24% and 31.5%. The bulk saturated hydraulic conductivity of the same material ranges between $3x10^{-3}$ and $1x10^{-2}$ $m \cdot s^{-1}$.
- The cold climate at the test pile research site located in the Canadian subarctic and the permeability of the waste rock permits advective air movement to penetrate and cool the interior

of the test piles. Each year discharge from the test piles occurs for a shorter period and less of the pile volume thaws, consistent with an overall cooling of the lower central core of the test piles. However through 2009, the active layer of the Type I and Type III test piles extends the entire depth of the pile, although there may be areas within the core that remain frozen. Freezing of stockpiled mine wastes provides one measure to mitigate effects of AMD as long as future climatic conditions remain similar.

7 REFERENCES

Adams, E.E., Gelhar, L.W., 1992. Field study of dispersion in a heterogeneous aquifer: 2. Spatial moments analysis. Water Resources. Research. 28, 3293–3307. doi:10.1029/92WR01757

Agricola, G., Hoover, H.C., Hoover, L.H., 1950. De Re Metallica (1556). Dover Publications Inc. New York.

Allen, R.G., Pereira, L.S., Raes, D., Smith, M., 1998. Crop Evapotranspiration (guidelines for computing crop water requirements), FAO Irrigation and Drainage Paper. No. 56. Food and Agriculture Organization of the United Nations, Rome, Italy.

Amos, R.T., Blowes, D.W., Smith, L., Sego, D.C., 2009. Measurement of wind-induced pressure gradients in a waste rock pile. Vadose Zone Journal. 8, 953–962. doi:10.2136/vzj2009.0002

Andrina, J., Wilson, G.W., Miller, S., 2009. Behavior of water flow and geochemical mixing in layered waste rock stockpiles: a meso-scale experiment., in: Proceedings of the 8th International Conference on Acid Rock Drainage. Skelleftea, Sweden.

Andrina, J., Wilson, G.W., Miller, S., Neale, A., 2006. Performance of the acid rock drainage mitigation waste rock trial dump at Grasberg mine, in: Proceedings of the 7th International Conference on Acid Rock Drainage. American Society of Mining and Reclamation, St. Louis, Missouri.

ASTM International, 2010a. Test Methods for Measurement of Hydraulic Conductivity of Saturated Porous Materials Using a Flexible Wall Permeameter. ASTM International.

ASTM International, 2010b. Test Methods for Laboratory Determination of Water (Moisture) Content of Soil and Rock by Mass. ASTM International.

Azam, S., Wilson, G., Herasymuik, G., Nichol, C., Barbour, L., 2007. Hydrogeological behaviour of an unsaturated waste rock pile: a case study at the Golden Sunlight Mine, Montana, USA. Bulletin of Engineering Geology and the Environment. 66, 259–268. doi:10.1007/s10064-006-0077-7

Bailey, B.L., 2013. Geochemical and microbiological characterization of effluent and pore water from low-sulfide content waste rock (Ph.D. dissertation). University of Waterloo.

Bailey, B.L., Smith, L.J.D., Blowes, D.W., Ptacek, C.J., Smith, L., Sego, D.C., 2013. The Diavik Waste Rock Project: Persistence of contaminants from blasting agents in waste rock effluent. Applied Geochemistry. 36, 256–270. doi:10.1016/j.apgeochem.2012.04.008

Bay, D.S., 2009. Hydrological and Hydrogeochemical Characteristics of Neutral Drainage from a Waste Rock Test Pile (M.Sc. dissertation). University of British Columbia, Vancouver, B.C.

Bear, J., 1988. Dynamics of fluids in porous media. Courier Dover Publications.

Bellehumeur, T.M., 2001. Mechanisms and spatial variability of rainfall infiltration on the Claude waste rock pile. (M.Sc. dissertation). University of British Columbia, Vancouver, B.C.

Beven, K., Germann, P., 1981. Water Flow in Soil Macropores II. A Combined Flow Model. Journal of Soil Science. 32, 15–29. doi:10.1111/j.1365-2389.1981.tb01682.x

Black, P.B., Tice, A.R., 1989. Comparison of soil freezing curve and soil water curve data for Windsor sandy loam. Water Resource Research. 25, 2205–2210.

Blowes, D., Moncur, M., Smith, L., Sego, D., Bennet, J., Garvie, A., Linklater, C., Gould, D., Reinson, J., 2006. Construction of two large-scale waste rock piles in a continuous permafrost region, in: Proceedings of the 7th International Conference on Acid Rock Drainage. American Society of Mining and Reclamation, St. Louis, Missouri.

Blowes, D.W., Ptacek, C.J., 1994. Acid-neutralization mechanisms in inactive mine tailings. The environmental geochemistry of sulfide mine-wastes, short course handbook. 22, 271–292.

Blowes, D.W., Ptacek, C.J., Jambor, J.L., Weisner, C., 2003. The Geochemistry of Acid Mine Drainage, in: Lollar, B.S. (Ed.), Treatise on Geochemistry. Elsevier, Amsterdam; Heidelberg [u.a.], pp. 149–204.

Carey, S.K., Barbour, S.L., Hendry, M.J., 2005. Evaporation from a waste-rock surface, Key Lake, Saskatchewan. Canadian Geotechnical Journal. 42, 1189–1199.

Cary, J.W., 1965. Water Flux in Moist Soil: Thermal Versus Suction Gradients. Soil Science. 100, 168–175.

Chi, X., 2011. Characterizing low-sulfide instrumented waste-rock piles: image grain-size analysis and wind-induced gas transport (M.Sc. dissertation). University of Waterloo.

Christensen, J.H., 1942. Irrigation by Sprinkling. Bulletin 670. Agricultural Experimental Station. University of California, Berkley.

Corazao Gallegos, J.C., 2007. The Design, construction, instrumentation and initial response of a field-scale waste rock test pile. (M.Sc. dissertation). University of British Columbia, Vancouver, B.C.

Decker, D.L., Tyler, S.W., 1999. Evaluation of Flow and Solute Transport Parameters for Heap Leach Recovery Materials. Journal of Environment Quality. 28, 543. doi:10.2134/jeq1999.00472425002800020020x

Diodato, D.M., Parizek, R.R., 1994. Unsaturated Hydrogeologic Properties of Reclaimed Coal Strip Mines. Ground Water 32, 108–118. doi:10.1111/j.1745-6584.1994.tb00618.x

Dirksen, C., Miller, R.D., 1966. Closed-System Freezing of Unsaturated Soil. Soil Science Society of America Journal. 30, 168–173. doi:10.2136/sssaj1966.03615995003000020010x

Domenico, P.A., Schwartz, F.W., 1998. Physical and Chemical Hydrogeology. Wiley.

Elberling, B., 2001. Environmental controls of the seasonal variation in oxygen uptake in sulfidic tailings deposited in a permafrost-affected area. Water Resource Research. 37, PP. 99–107. doi:200110.1029/2000WR900259

Elberling, B., 2005. Temperature and oxygen control on pyrite oxidation in frozen mine tailings. Cold Regions Science and Technology. 41, 121–133. doi:10.1016/j.coldregions.2004.09.004

Elboushi, I.M., 1975. Amount of water needed to initiate flow in rubbly rock particles. Journal of Hydrology. 27, 275–284. doi:10.1016/0022-1694(75)90060-8

Eriksson, N., Destouni, G., 1997. Combined effects of dissolution kinetics, secondary mineral precipitation, and preferential flow on copper leaching from mining waste rock. Water Resource. Research. 33, 471–483.

Eriksson, N., Gupta, A., Destouni, G., 1997. Comparative analysis of laboratory and field tracer tests for investigating preferential flow and transport in mining waste rock. Journal of Hydrology. 194, 143–163. doi:10.1016/S0022-1694(96)03209-X

Fala, O., Molson, J., Aubertin, M., Bussière, B., 2005. Numerical modelling of flow and capillary barrier effects in unsaturated waste rock piles. Mine Water Environment. 24, 172–185.

FDA Engineering Ltd., 2008. Test Piles Project. 2006 Construction Summary.

Fines, P.E., 2006. Hydrologic characterization of two full-scale waste rock piles. (M.Sc. dissertation). University of British Columbia.

Flerchinger, G., Lehrsch, G., McCool, D., 2004. Freezing and thawing processes. Encyclopedia of Soils in the Environment. 104–110.

Fretz, N.M., 2013. Multi-year hydrologic response of experimental waste-rock piles in a cold climate : active-zone development, net infiltration, and fluid flow (M.Sc. dissertation). University of British Columbia.

Freyberg, D.L., 1986. A natural gradient experiment on solute transport in a sand aquifer: 2. Spatial moments and the advection and dispersion of nonreactive tracers. Water Resource Research. 22, 2031–2046. doi:10.1029/WR022i013p02031

Garabedian, S.P., LeBlanc, D.R., Gelhar, L.W., Celia, M.A., 1991. Large-scale natural gradient tracer test in sand and gravel, Cape Cod, Massachusetts: 2. Analysis of spatial moments for a nonreactive tracer. Water Resource Research. 27, 911–924. doi:10.1029/91WR00242

Gerke, H.H., 2006. Preferential flow descriptions for structured soils. Journal of Plant Nutrition and Soil Science. 169, 382–400. doi:10.1002/jpln.200521955

Gerke, H.H., van Genuchten, M.T., 1993. A dual-porosity model for simulating the preferential movement of water and solutes in structured porous media. Water Resource Research. 29, 305–319. doi:10.1029/92WR02339

Godwalt, R.C., Biggar, K.W., Sego, D.C., 1999. AMD Generation at sub-zero temperatures, in: Proceedings of Symposium on Assessment and Remediation of Contaminated Sites in Arctic and Cold Climates. Edmonton, Canada, pp. 75–82.

Golder Associates, 2008. 2007 Review of Baseline Climate and Surface Water Hydrology for the Diavik Diamond Mine (No. RPT-602 Ver.0). Burnaby, BC.

Golder Associates Ltd., 1989. Report to Environment Canada on the drilling program at the Mt. Washington mine site, British Columbia (No. Report 882-1441).

Gould, W.D., Kapoor, A., 2003. The microbiology of acid mine drainage, in: Jambor, J.L., Blowes, D.W., Ritchie, A.I.M. (Eds.), Environmental Aspects of Mine Wastes. Mineralogical Association of Canada.

Granger, R., n.d. Partitioning of Energy During the Snow-Free Season at Wolf Creek Research Basin, in: Wolf Creek Research Basin: Hydrology, Ecology and Environment. Environment Canada, Saskatoon, Saskatchewan, pp. 33–44.

Granger, R.J., Gray, D.M., 1989. Evaporation from natural nonsaturated surfaces. Journal of Hydrology. 111, 21–29. doi:10.1016/0022-1694(89)90249-7

Gray, D.M., Granger, R.J., 1986. In situ measurements of moisture and salt movement in freezing soils. Can. J. Earth Sci. 23, 696–704.

Han, S., Hu, H., Yang, D., Tian, F., 2011. A complementary relationship evaporation model referring to the Granger model and the advection–aridity model. Hydrological Processes. 25, 2094–2101. doi:10.1002/hyp.7960

Hannam, S., 2012. Diavik Waste Rock Project: Geochemical and mineralogical investigations of waste-rock weathering (M.Sc. dissertation). University of Waterloo.

Harries, J.R., Ritchie, A.I.M., 1983. Runoff fraction and pollution levels in runoff from a waste rock dump undergoing pyritic oxidation. Water, Air, and Soil Pollution. 19, 155–170. doi:10.1007/BF00211802

Harvey, C., Gorelick, S.M., 2000. Rate-limited mass transfer or macrodispersion: Which dominates plume evolution at the macrodispersion experiment (MADE) site? Water Resource Research. 36, 637–650. doi:10.1029/1999WR900247

Harvey, C.F., Gorelick, S.M., 1995. Temporal Moment-Generating Equations: Modeling Transport and Mass Transfer in Heterogeneous Aquifers. Water Resource. Research. 31, 1895–1911. doi:10.1029/95WR01231

Heikkinen, P.M., Räisänen, M.L., Johnson, R.H., 2009. Geochemical Characterisation of Seepage and Drainage Water Quality from Two Sulphide Mine Tailings Impoundments: Acid Mine Drainage versus Neutral Mine Drainage. Mine Water Environment. 28, 30–49. doi:10.1007/s10230-008-0056-2

Hilhorst, M.A., 2000. A Pore Water Conductivity Sensor. Soil Science Society of America Journal. 64, 1922. doi:10.2136/sssaj2000.6461922x

Hillel, D., 1980. Fundamentals of soil physics. Academic Press.

Holubec, I., 2004. Covers for reactive tailings located in permafrost regions review (No. MEND Report 1.61.4). Mine Environment Neutral Drainage (MEND), Ottawa.

INAP, 2011. Global Acid Rock Drainage Guide.

Indian and Northern Affairs, 1993. Guidelines for Acid Rock Drainage Prediction in the North (No. R71-50/1E). Government of Canada Publications.

Janowicz, J.R., Hedstrom, N.R., Granger, R.J., 2008. Investigation of Anvil Range Mining Corporation (Faro) Waste Dump Water Balance: Vangorda Trial Covers Water Balance.

Jury, W.A., Stolzy, L.H., Shouse, P., 1982. A field test of the transfer function model for predicting solute transport. Water Resource. Research. 18, 369–375. doi:10.1029/WR018i002p00369

Kool, J.B., Parker, J.C., van Genuchten, M.T., 1985. Determining Soil Hydraulic Properties from One-step Outflow Experiments by Parameter Estimation: I. Theory and Numerical Studies. Soil Science Society of America Journal. 49, 1348–1354. doi:10.2136/sssaj1985.03615995004900060004x

Kuipers, J., Maest, A.S., MacHardy, K.A., Lawson, G., 2006. Comparison of Predicted and Actual Water Quality at Hardrock Mines: The Reliability of Predictions in Environmental Impact Statements. Earthworks.

LeBlanc, D.R., Garabedian, S.P., Hess, K.M., Gelhar, L.W., Quadri, R.D., Stollenwerk, K.G., Wood, W.W., 1991. Large-scale natural gradient tracer test in sand and gravel, Cape Cod, Massachusetts: 1. Experimental design and observed tracer movement. Water Resource Research. 27, 895–910. doi:10.1029/91WR00241

Lefebvre, R., Hockley, D., Smolensky, J., Gélinas, P., 2001. Multiphase transfer processes in waste rock piles producing acid mine drainage: 1: Conceptual model and system characterization. Journal of Contaminate Hydrology. 52, 137–164.

Malmström, M.E., Destouni, G., Banwart, S.A., Strömberg, B.H., 2000. Resolving the scale-dependence of mineral weathering rates. Environ. Sci. Technol. 34, 1375–1378.

Marcoline, J.R., 2008. Investigations of water and tracer movement in covered and uncovered unsaturated waste rock (Ph.D. dissertation). University of British Columbia.

Martin, V., Aubertin, M., Bussiere, bruno, Chapuis, R., 2004. Evaluation of Unsaturated Flow in Mine Waste Rock. Presented at the 57th Canadian Geotechnical Conference.

Meldrum, J.L., Jamieson, H.E., Dyke, L.D., 2001. Oxidation of mine tailings from Rankin Inlet, Nunavut, at subzero temperatures. Canadian Geotechnical Journal. 38, 957–966.

Meteorological Service of Canada, Environment Canada Government of Canada, 2001. Canadian Climate - Canadian Climate Normals - 1971-2000 [WWW Document]. URL http://climate.weatheroffice.gc.ca/climate_normals/index_e.html (accessed 7.21.13).

Meteorological Service of Canada, Environment Canada Government of Canada, 2009. National Climate Data and Information Archive - Intensity-duration-frequency Statistics [WWW Document]. URL http://climate.weatheroffice.gc.ca/prods_servs/index_e.html (accessed 7.21.13).

Moncur, M.C., Ptacek, C.J., Blowes, D.W., Jambor, J.L., 2005. Release, transport and attenuation of metals from an old tailings impoundment. Applied Geochemistry. 20, 639–659. doi:10.1016/j.apgeochem.2004.09.019

Morin, K., Gerencher, E., Jones, C., Konasewich, D., 1991. Critical Literature Review of Acid Drainage from Waste Rock (No. MEND Project 1.11.1).

Morin, K.A., Jones, C.E., van Dyk, R.P., 1994. Internal hydrogeologic monitoring of an acidic waste-rock dump at Westmin Resources' Myra Falls Operations, British Columbia, in: Proceedings of the International Land Reclamation and Mine Drainage Conference and the Third International Conference on the Abatement of Acidic Drainage. pp. 355–364.

Neuner, M., 2009. Water Flow Through Unsaturated Mine Waste Rock in A Region of Permafrost (M.Sc. dissertation). University of British Columbia, Vancouver, B.C.

Neuner, M., Smith, L., Blowes, D.W., Sego, D.C., Smith, L.J.D., Fretz, N., Gupton, M., 2013. The Diavik waste rock project: Water flow through mine waste rock in a permafrost terrain. Applied Geochemistry. 36, 222–233. doi:10.1016/j.apgeochem.2012.03.011

Newman, L.L., Herasymuik, G.M., Barbour, S.L., Fredlund, D.G., Smith, T., 1997. The hydrogeology of waste rock dumps and a mechanism for unsaturated preferential flow, in: Proceedings of 4th International Conference on Acid Rock Drainage, ICARD. pp. 551–566.

Nichol, C., Smith, L., Beckie, R., 2003. Time domain reflectrometry measurements of water content in coarse waste rock. Canadian Geotechnical Journal. 40, 137–148. doi:10.1139/t02-097

Nichol, C., Smith, L., Beckie, R., 2005. Field-scale experiments of unsaturated flow and solute transport in a heterogeneous porous medium. Water Resource. Research. 41, n/a–n/a. doi:10.1029/2004WR003035

Nichol, C.F., 2002. Transient flow and transport in unsaturated heterogneous media: Field experiments in mine waste rock (Ph.D. dissertation). University of British Columbia, Vancouver, B.C.

Nichols, R.S., 1986. Rock segregation in waste dumps, in: Flow-through Rock Drains: Proceedings of the International Symposium Convened at the Inn of the South, Cranbrook, BC.

Nordstrom, D.K., Alpers, C.N., 1999. Geochemistry of acid mine waters, in: Plumlee, G.S., Logsdon, M.J. (Eds.), The Environmental Geochemistry of Mineral Deposits. Society of Economic Geologists, pp. 133–160.

Okane Consultants, 2004. Design, construction and performance monitoring of cover systems for waste rock and tailings (No. MEND 2.21.4).

Pham, H.N., 2013. Heat transfer in waste-rock piles constructed in a continuous permafrost region (Ph.D. dissertation). University of Alberta.

Pham, N.H., Sego, D.C., Arenson, L.U., Blowes, D.W., Amos, R.T., Smith, L., 2013. The Diavik Waste Rock Project: Measurement of the thermal regime of a waste-rock test pile in a permafrost environment. Applied Geochemistry. 36, 234–245. doi:10.1016/j.apgeochem.2013.05.007

Press, W.H., Teukolsky, S., Vetterling, W.T., Flannery, B.P., 1988. Numerical Recipes in C. Cambridge University Press.

Price, W.A., 2003. Challenges posed by metal leaching and acid rock drainage, and approaches used to address them, in: Jambor, J.L., Blowes, D.W., Ritchie, A.I.M. (Eds.), Environmental Aspects of Mine Wastes. Mineralogical Association of Canada.

Ptak, T., Piepenbrink, M., Martac, E., 2004. Tracer tests for the investigation of heterogeneous porous media and stochastic modelling of flow and transport—A review of some recent developments. Journal of Hydrology. 294, 122–163.

Rasmussen, T.C., Baldwin, R.H., Dowd, J.F., Williams, A.G., 2000. Tracer vs. Pressure Wave Velocities through Unsaturated Saprolite. Soil Science Society of America Journal. 64, 75. doi:10.2136/sssaj2000.64175x

Rohde, T.K., Williams, D.J., 2009. Early Hydrological Monitoring of Cadia's Instrumented Trial Waste Rock Dump, in: Proceedings of the 8th International Conference on Acid Rock Drainage. Skelleftea, Sweden.

Roscoe Postle Associates Inc., 2005. Diavik Diamond Mine Mineral Reserve and Mineral Resource Audit. NI 43-101 Report.

Rykaart, M., Hockley, D., 2009. Mine waste covers in cold regions (No. MEND Report 1.61.5a). Mine Environment Neutral Drainage (MEND), Ottawa.

Rykaart, M., Hockley, D., 2010. Cold Regions Cover Research - Phase 2 (No. MEND Report 1.61.5b). Mine Environment Neutral Drainage (MEND).

Sanders, L.L., 1998. A manual of field hydrogeology. Prentice Hall.

Schincariol, R.A., Schwartz, F.W., Mendoza, C.A., 1994. On the generation of instabilities in variable density flow. Water Resource Research. 30, 913–927. doi:10.1029/93WR02951

Šimůnek, J., van Genuchten, M.T., 2008. Modeling Nonequilibrium Flow and Transport Processes Using HYDRUS. Vadose Zone Journal. 7, 782. doi:10.2136/vzj2007.0074

Slater, B., Moodie, S., 2008. Investigation of Predictions for Acidic Drainage at the Vangorda Plateau, Faro Mine Complex (Faro, YT) (No. MEND Report 1.70.1). MEND Report 1.70.1.

Smith, L., Beckie, R., 2003. Hydrologic and geochemical transport processes in mine waste rock, in: Jambor, J.L., Blowes, D.W., Ritchie, A.I.M. (Eds.), Environmental Aspects of Mine Wastes. Mineralogical Association of Canada.

Smith, L., Lopez, D.L., Beckie, R., Morin, K., Dawson, R., Price, W.A., 1995. Hydrogeology of waste rock dumps. British Columbia Ministry of Energy, Mines and Petroleum Resources and CANMET.

Smith, L.J.., Blowes, D.W., Jambor, J.L., Smith, L., Sego, D.C., Neuner, M., 2013. The Diavik Waste Rock Project: Particle size distribution and sulfur characteristics of low-sulfide waste rock. Applied Geochemistry. 36, 200–209. doi:10.1016/j.apgeochem.2013.05.006

Smith, L.J.D., 2009. Building and characterizing low sulfide instrumented waste rock piles: Pile design and construction, particle size and sulfur characterization, and initial geochemical response (M.Sc. dissertation). University of Waterloo, Waterloo, Ontario.

Smith, L.J.D., Moncur, M.C., Neuner, M., Gupton, M., Blowes, D.W., Smith, L., Sego, D.C., 2013. The Diavik Waste Rock Project: Design, construction, and instrumentation of field-scale experimental waste-rock piles. Applied Geochemistry. 36, 187–199. doi:10.1016/j.apgeochem.2011.12.026

SRK Consulting, Mehling Environmental Management Inc., 2006. Update on Cold Temperature Effects on Geochemical Weathering (No. MEND Report 1.61.6). Mine Environment Neutral Drainage (MEND).

Stockwell, J., Smith, L., Jambor, J.L., Beckie, R., 2006. The relationship between fluid flow and mineral weathering in heterogeneous unsaturated porous media: A physical and geochemical characterization of a waste-rock pile. Applied Geochemistry. 21, 1347–1361.

Swanson, D.A., Savci, F., Danzinger, G., Williamson, A., Barnes, C., 2000. Unsaturated hydrologic assessment of waste rock stockpiles in semi-arid climates, in: Proceedings of the 5th International Conference on Acid Rock Drainage. pp. 1273–1282.

Tami, D., Rahardjo, H., Leong, E.-C., Fredlund, D.G., 2004. Design and laboratory verification of a physical model of sloping capillary barrier. Canadian Geotechnical Journal. 41, 814–830.

Tokunaga, T.K., Wan, J., 1997. Water film flow along fracture surfaces of porous rock. Water Resour. Res. 33, 1287–1295.

Tremblay, G.A., Hogan, C.M., 2009. The Canadian MEND Program, in: Proceedings of the 8th International Conference on Acid Rock Drainage. Skelleftea, Sweden.

University of Saskatchewan, Department of Civil Engineering, Unsaturated Soils Group, 1999. Placer Dome cover and waste rock research programs: 1993-1999. Unsaturated Soils Group, Dept. of Civil Engineering, University of Saskatchewan, Saskatoon, Sask.

Van Dam, C.J., Stricker, J.N.M., Droogers, P., 1992. Inverse Method for Determining Soil Hydraulic Functions from One-Step Outflow Experiments. Soil Science Society of America Journal. 56, 1042–1050. doi:10.2136/sssaj1992.03615995005600040007x

Van den Daele, G.F.A., Barker, J.A., Connell, L.D., Atkinson, T.C., Darling, W.G., Cooper, J.D., 2007. Unsaturated flow and solute transport through the Chalk: Tracer test and dual permeability modelling. Journal of Hydrology. 342, 157–172. doi:10.1016/j.jhydrol.2007.05.021

Van Genuchten, M.T., Wierenga, P.J., 1976. Mass transfer studies in sorbing porous media I. Analytical solutions. Soil Science Society of America Journal. 40, 473–480.

Velbel, M.A., 1993. Constancy of silicate-mineral weathering-rate ratios between natural and experimental weathering: implications for hydrologic control of differences in absolute rates. Chemical Geology. 105, 89–99. doi:10.1016/0009-2541(93)90120-8

Wagner, K., 2004. Characterization of the geochemistry of discharge waters, pore waters, primary and secondary minerals of an experimental waste rock pile, Cluff Lake mine, Saskatchewan, Canada. (M.Sc. dissertation). University of British Columbia, Vancouver, B.C.

Wilson, G.W., Fredlund, D.G., Barbour, S.L., 1994. Coupled soil-atmosphere modelling for soil evaporation. Canadian Geotechnical Journal. 31, 151–161. doi:10.1139/t94-021

Yazdani, J., Barbour, L., Wilson, W., 2000. Soil water characteristic curve for mine waste rock containing coarse material., in: Proceedings of the Sixth Environmental Engineering Specialty Conference of the Canadian Society of Civil Engineers. London ON. Canada.

Yilmaz, E., 2011. Advances in reducing large volumes of environmentally harmful mine waste rocks and tailings. Gospodarka Surowcami Mineralnymi. T. 27, z. 2, 89–112.

Zachmann, D.W., DuChateau, P.C., Klute, A., 1981. The Calibration of the Richards Flow Equation for a Draining Column by Parameter Identification. Soil Sci. Soc. Am. J. 45, 1012–1015. doi:10.2136/sssaj1981.03615995004500060002x

Zhang, H., Schwartz, F.W., Wood, W.W., Garabedian, S.P., LeBlanc, D.R., 1998. Simulation of variable-density flow and transport of reactive and nonreactive solutes during a tracer test at Cape Cod, Massachusetts. Water Resource Research. 34, 67–82. doi:10.1029/97WR02918

Zinn, B., Harvey, C.F., 2003. When good statistical models of aquifer heterogeneity go bad: A comparison of flow, dispersion, and mass transfer in connected and multivariate Gaussian hydraulic conductivity fields. Water Resource Research. 39, SBH4.1–SBH4.18.

APPENDIX

Appendix A Instrument Location and Calibration

Appendix A documents the specific instruments used to monitor hydrology related data presented in this thesis. Instruments include:

- Custom-built TDR probes for VMC measurement in the test piles (Table A-1);
- Tipping buckets for discharge measurement from the base from the test piles and AZLs (Table A-2);
- Tipping buckets for recording rainfall received on top of the test piles (Table A-2);
- Commercial ECH_2O probes for monitoring VMC, EC and temperature adjacent to the AZLs (Table A-3); and
- Tensiometers for measurement of matric tension within the upper surface of the Type III test pile and the AZLs (Table A-4).

Figure A-1 documents calibration equations relating the time between tips and flow rate for the tipping buckets monitoring drainage from the waste rock. Calibration was performed in 2009 on all basal drain tipping buckets to check that each tipping bucket was properly balanced and to confirm the relationships for tip time to flow rate.

	Data Array ID	Location	Instrument ID	Northing (m)	Easting (m)	Elevation (m)	Depth (vertical) (m)
Type III Test Pile	51	TDR_1	31N2TDR01	7,151,165.6	533,357.5	451.131	0.7
	52	TDR_2	31N2TDR07	7,151,165.6	533,349.1	445.615	6.2
	53	TDR_3	31N2TDR09	7,151,166.1	533,347.3	443.713	8.1
	54	TDR_4	31S2TDR01	7,151,159.7	533,356.4	450.571	1.4
	55	TDR_5	31S2TDR03	7,151,160.8	533,354.5	449.326	2.6
	56	TDR_6	31S2TDR05	7,151,160.9	533,351.6	446.993	4.9
	57	TDR_7	31S2TDR09	7,151,160.5	533,346.7	442.868	9.1
	59	TDR_9	33N2TDR01	7,151,164.7	533,350.7	450.163	1.6
	60	TDR_10	33N2TDR03	7,151,166.4	533,349.1	449.035	2.7
	61	TDR_11	33N2TDR05	7,151,164.0	533,346.0	446.545	5.2
	58	TDR_8	32N2TDR07	7,151,166.0	533,343.8	444.910	6.8
	62	TDR_12	33S2TDR02	7,151,160.0	533,342.3	449.298	2.5
	63	TDR_13	33S2TDR03	7,151,161.2	533,341.2	448.559	3.2
Type I Test Pile	86	TDR_36	12W2TDR02	7,151,228.0	533,420.7	449.417	2.6
	87	TDR_37	12W2TDR03	7,151,228.9	533,421.0	448.742	3.3
	80	TDR_30	11W2TDR06	7,151,226.1	533,419.6	445.949	6.1
	83	TDR_33	11W2TDR09	7,151,231.0	533,418.5	442.895	9.1
Covered Test Pile	90	TDR_39	C2E2TDR06	7,150,973.9	533,423.2	448.362	5.1
	91	TDR_40	C2E2TDR07	7,150,973.3	533,423.1	447.966	5.5
	92	TDR_41	C2E2TDR08	7,150,971.6	533,423.0	446.559	6.9
	93	TDR_42	C2E2TDR10	7,150,969.5	533,421.7	444.804	8.7
	94	TDR_43	C2W2TDR06	7,150,974.0	533,417.6	448.249	5.2
	95	TDR_44	C2W2TDR07	7,150,972.7	533,417.7	447.296	6.1
	96	TDR_45	C2W2TDR08	7,150,971.8	533,418.0	446.273	7.2
	96	TDR_46	C2W2TDR10	7,150,969.8	533,417.8	444.191	9.2
	97	TDR_47	C3E2TDR06	7,150,965.7	533,416.8	447.528	5.7
	98	TDR_48	C3E2TDR08	7,150,964.0	533,417.1	446.100	7.2
	99	TDR_49	C3E2TDR10	NS	NS	NS	10.0

Table A-1: Location of functioning TDR probes. NS indicates not surveyed.

	Data Array ID	Location	Instrument ID	Descripton
Type III Test Pile	14	TB_14	3BNXdrn15	Northern basal drain
	15	TB_15	3BSXdrn15	Southern basal drain
	1	TB_1	3BNBlys2W/3BNBlys2E	Basal collection lysimeter underlying batter
	2	TB_2	3BNBlys4W	Basal collection lysimeter underlying batter
	3	TB_3	3BNBlys4E	Basal collection lysimeter underlying batter
	4	TB_4	3BNClys2W/3BNClys2E	Basal collection lysimeter underlying crest
	5	TB_5	3BNClys4W	Basal collection lysimeter underlying crest
	6	TB_6	3BNClys4E	Basal collection lysimeter underlying crest
	7	TB_7	3BSClys2W/3BSClys2E	Basal collection lysimeter underlying crest
	8	TB_8	3BSClys4W	Basal collection lysimeter underlying crest
	9	TB_9	3BSClys4E	Basal collection lysimeter underlying crest
Type I Test Pile	13	TB_13	1BXXdrn13	Basal drain
	10	TB_10	1BWBlys cluster	Basal collection lysimeter underlying batter
	11	TB_11	1BWClys (all)	Basal collection lysimeter underlying crest
	12	TB_12	1BEClys cluster	Basal collection lysimeter underlying crest
Covered Test Pile	19	TB_27	CBXXdrn15	Basal drain
	16	TB_24	CBBClys (all)	Basal collection lysimeter underlying batter
	17	TB_25	CBWClys (all)	Basal collection lysimeter underlying crest
	18	TB_26	CBEClys (all)	Basal collection lysimeter underlying crest
AZL	20	TB_16	3UW3lys02	Basal drain at Western Type III AZL
	21	TB_17	3UE3lys02	Basal drain at Eastern Type III AZL
	22	TB_18	1UW3lys02	Basal drain at Western Type I AZL
	22	TB_19	1UE3lys02	Basal drain at Eastern Type I AZL
3Ta	24	TB_24	T3 rain gauge	Rain gauge on top of Type III test pile
1Ta	25	TB_25	T1 rain gauge	Rain gauge on top of Type I test pile
CTa	26	TB_26	TC rain gauge	Rain gauge on top of Covered test pile

Table A-2: Locations of tipping buckets to measure discharge and rainfall.

	Data Array ID	Location	Instrument ID	Depth (mbg)	Descripton
Type III AZL	113	ECHO_1mc	3UX0ech.3	0.3	ECH_2O probe - VMC
	113	ECHO_1ec	3UX0ech.3	0.3	ECH_2O probe - EC
	113	ECHO_1t	3UX0ech.3	0.3	ECH_2O probe - temperature
	113	ECHO_2mc	3UX0ech.6	0.6	ECH_2O probe - VMC
	113	ECHO_2ec	3UX0ech.6	0.6	ECH_2O probe - EC
	113	ECHO_2t	3UX0ech.6	0.6	ECH_2O probe - temperature
	113	ECHO_3mc	3UX0ech.9	0.9	ECH_2O probe - VMC
	113	ECHO_3ec	3UX0ech.9	0.9	ECH_2O probe - EC
	113	ECHO_3t	3UX0ech.9	0.9	ECH_2O probe - temperature
	113	Tension_1	3UX0ten.3	0.3	Matric tension (kPa)
	113	Tension_2	3UX0ten.6	0.6	Matric tension (kPa)
	113	Tension_3	3UX0ten.9	0.9	Matric tension (kPa)
Type III Test Pile	121	Tension_4	3TN2ten.6	0.6	Matric tension (kPa)
	121	Tension_5	3TN2ten01	1.2	Matric tension (kPa)
	121	Tension_6	3TS2ten.6	0.6	Matric tension (kPa)
	121	Tension_7	3TS2ten01	1.2	Matric tension (kPa)

Table A-3: Instrumentation installed adjacent to the Type III AZL and Type III test pile to record VMC, EC, temperature and matric tension.

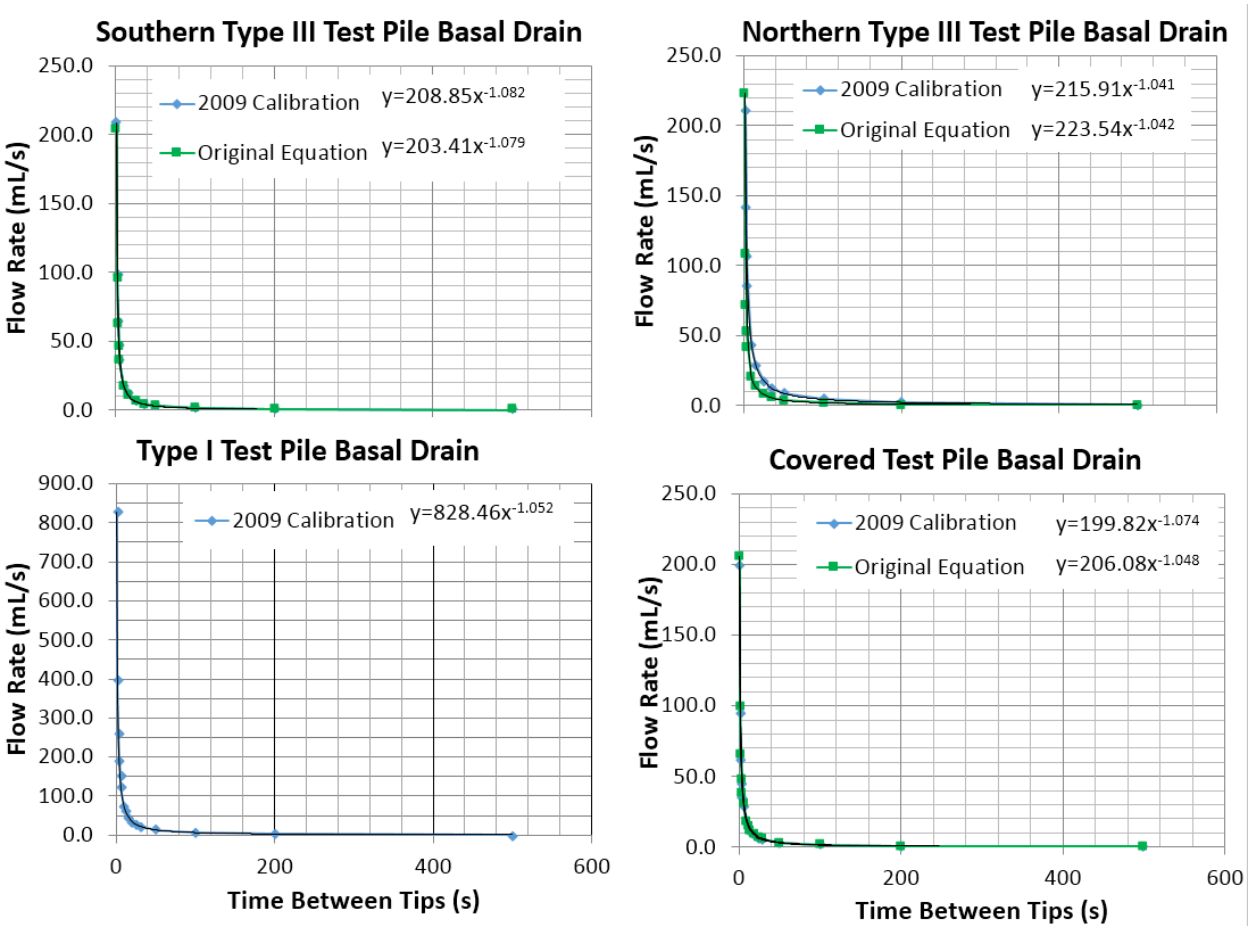

Location	Date Range From	To	Equation	Notes
1Bxxdrn13	1-May-07	1-Aug-07	$Q=6.717 \cdot t^{-1.0526}$	small grey TB, larger than Young model 52202
	1-Aug-07	1-Jan-09	$Q=206.08t^{-1.0483}$	original TB
	1-Jan-09	24-May-09	$Q=2.6425t^{-1.1124}$	temporary small Young model TB
	24-May-09	31-May-09	$Q=203.41t^{-1.0792}$	TB from Southern Type III test pile
	31-May-09	-	$Q=828.46t^{-1.052}$	new custom built TB
3BNxdrn15	1-Aug-07	-	$Q=223.54t^{-1.0421}$	
	calibration check		*$Q=215.91t^{-1.041}$*	
3BSxdrn	1-Aug-07	16-Jun-10	$Q=203.41t^{-1.0792}$	TB replaced in 2010, see Fretz, 2013.
	calibration check		*$Q=208.85t^{-1.082}$*	
CBxxdrn13	1-May-07		$Q=2.6425t^{-1.1124}$	R.M. Young model 52202
	6-Nov-08	-	$Q=206.08t^{-1.0483}$	TB moved from Type I drain
	calibration check		*$Q=199.82t^{-1.074}$*	
All Basal Collection Lysimeters and AZL drains	1-Jul-06	-	$Q=2.6425t^{-1.1124}$	R.M. Young model 52202
	calibration check		*$Q=2.9177t^{-1.1111}$*	

Notes:
Q is discharge rate in $mL \cdot s^{-1}$ and t is time between tips in seconds.
TB - tipping bucket

Figure A-1:Tipping bucket calibration.

Appendix B Permeameter Work Plan

DIAVIK TEST PILES RESEARCH PROJECT

SUMMER 2009

Work Program for
Construction and Testing of a
Field Permeameter

DRAFT

DATE: JUNE 10, 2009

EXECUTIVE SUMMARY

In 2007 a field permeameter was constructed to perform field scale saturated hydraulic conductivity testing, estimate porosity and evaluate average flow velocity and specific yield of 16 m^3 sample of waste rock (Neuner, 2009). This work plan provides a summary of the previous investigation and outlines the methods and procedures for up-scaling the field permeameter to evaluate a 32 m^3 sample in an attempt to overcome limited hydraulic head differences observed in the previous study. The field investigation work plan has been prepared to provide Diavik staff, University project supervisors and field personnel with details of the required pre-field and field activities and to assist with the identification of hazards during a pre-field risk assessment. The scope of the proposed field and pre-field activities includes: (a) acquiring necessary construction materials; (b) conducting a job specific risk assessment with key personnel involved in the permeameter project and undertaking any addition safety training deemed necessary, by the risk assessment; (c) construction/placement of the base platform and the field permeameter, including placement of a liner within a wooden frame and installation of the necessary plumbing; and (d) conducting porosity, saturated hydraulic conductivity and drain-down testing. The objective of this field activity is to: (a) determine a porosity measurement of a 32 m^3 waste rock sample to compare to the previous measurement (25%); (b) estimate a saturated hydraulic conductivity value; and (c) depending on the results of ‘a’ and ‘b’ measure several parameters during drainage of the sample.

TABLE OF CONTENTS

INTRODUCTION

This work plan was prepared to assist in the pre-field and field activities related to the design, construction and testing of a field permeameter. The outline of tasks will assist with a thorough risk assessment prior to proceeding with construction and testing. The work plan provides a brief review of the previous field permeameter experiment performed by M. Neuner (2009) as part of the test piles research project and outlines several of the difficulties with the previous experiment which warrant a second experiment to be conducted. This is followed by a proposed schedule of field activities and a listing of the key personnel/departments involved in the project. Section 2 of the work plan provides an overview of the pre-field activities including the health and safety plan and a consideration of the equipment required to commence construction. Section 3 of the work plan provides construction details, followed by an outline of the testing program (Section 4). Appended to the work plan are proposed drawings of the field permeameter.

Scope of Work

The field permeameter program will consist of the following activities:

- Investigation and acquisition of the necessary materials and supplies;
- Risk assessment with key personnel involved with the construction and testing of the permeameter;
- Construction of the field permeameter; and
- Testing of the field permeameter.

Background

In 2007 a 16 m^3 Type 1 waste rock sample was tested in a field permeameter (measuring 4 m x 4m by 1 m high) to measure porosity, saturated hydraulic conductivity, flow velocity and specific yield. For the sample size tested (16m^3) the appropriate maximum clast size to include in testing is 0.5 m^3. A summary of results obtained from the tests conducted by M. Neuner (2009) on the field permeameter are:

- Porosity: 25-26%;
- Saturated hydraulic conductivity: >1x10^{-2} m/s;
- Rapid draining specific yield: 19%
- Maximum flow velocity: 10m/h; and
- Average flow velocity: 1m/h.

Difficulties encounter with the field permeameter experiment concern measurement of very small hydraulic head variation over the length of the sample and small changes in the flow rate, likely due to restriction in the lower drain (inflow).

The following work plan outlines the proposed re-visitation of the field permeameter incorporating increased height of the sample (4x4m by approximately 2 m high) in an attempt to overcome the limited change in hydraulic head measurement. Changes to the drain inflow will also be made, as a greater flow rate will increase the change in head over the length of the sample. However, flow through the sample will be maintained at rates which do not result in turbulent flow within the sample.

In the previous experiment a drain down test was performed and measurement of flow velocity was made by applying a rhodamine dye tracer on the water surface. Collection of outflow samples was done through a ½" tube restricting discharge from the sample. This portion of the experiment may or may not be repeated depending on the results of the first to tests.

Schedule

The following schedule is proposed for the field activities (Table 1). Currently an additional co-op student has been schedule to assist with the activities from June 16 to 30. It is anticipated that the construction and testing of the field permeameter will require approximately 2 weeks. As noted in item number 8 of Table 1, additional time has been allotted for additional preparation, timing of equipment and material availability and external changes in scheduling as well as unexpected events.

Table 1: Estimated Schedule for Construction and Testing of a Field Permeameter

item no.	Description	Estimated Time Required (days)
1	Construct base with 2" crush and grade with 0.1 m sand	1
2	Install plumbing and lower drain	1
3	Build 4x4 m plywood frame approx. 2 m height	1
4	Installation of pre-fabricated Enviroliner 4040	1-2
5	Placement of porous layer (3/8" crush) and level	1
6	Placement of waste rock and standpipes	1
7	Installation supply tanks and plumbing	1
8	Miscellaneous prep, timing and unexpected occurrences	3
9	Porosity Testing	1
10	Constant head permeameter testing	1
11	Drain down testing	1

a. Principal Personnel

The following personnel will be involved in the field permeameter project:

Name	Affiliation	Telephone No./Radio
Steve Momeyer	UBC Graduate Student	604-822-XXXX
Lianna Smith	Diavik Project Manager	867-765-XXXX
Clarence Choban	Diavik – Liaison (cross-shift)	867-766-XXXX/ Ch. 7
Dave Mohler	Diavik - Liaison (cross-shift)	867-766-XXXX/ Ch. 7
Co-op Student	UW co-op student	
Raw Water	Diavik – Site Services	867-766-XXXX/ Ch.5
Water Pump	Diavik – Site Services	867-766 -XXXX/ Ch.5
Scott Falkenberg	Layfield (Enviroliner)	780-732-XXXX
	G&G Expediting Ltd.	867-669-XXXX

PRE-FIELD ACTIVITIES

The following section outlines the pre-field activities, which includes the health and safety preparation and acquisition of the necessary materials required to build the permeameter.

H&S Plan and Risk Assessment

A Health, Safety and Environment Plan (HSE) (Test Piles Research Group, 2008) has been produced for the monitoring phase of the test piles project to cover general site activities and specific routine procedures. This safety plan been read by all researchers (graduate students, co-op students and professors) and all activities will be in conformance with its direction. In addition, since the field permeameter experiment is outside the normal routines covered by the HSE, a job specific risk assessment will be conducted. Regular safety meetings in the form of job hazard analysis (JHA) will be conducted with the personnel to be completing the task to address the steps about to occur and to identify the obvious and hidden hazards. Safety toolbox meetings will be held daily at the beginning of each day. Lastly, personal 'Take 5 and keep it on T.R.A.C.K.' books will be completed by individuals prior to undertaking tasks.

A risk assessment will be conducted with the relevant personnel involved in the project. The risk assessment process steps through the required activities to identify the associated safety concerns with each task and corresponding measures to reduce or eliminate the hazards identified. Several key hazards to be addressed include:

- Working at heights (permeameter > 1.8m) during measurement of manometers, placement and adjustment of the constant head vessel;

- Working inside the plywood frame (confined space) during drain installation and liner placement;
- Working with hand tools;
- Working with power tools;
- Operation of gasoline powered equipment (water pumps);
- Working around equipment and vehicles;
- Working on uneven ground; and
- Working in areas where wildlife could be present;

Specific Training Requirements

Should the risk assessment identify additional training requirements, or should the proposed control measures not be sufficient, (for example working at heights) specific training will be completed by the required staff before proceeding with the work.

Equipment and Materials Required

As part of the pre-field activities, the arrangements for all required materials and equipment will be made. Table 3 provides a list of the materials (Table 3a), and heavy equipment (Table 3b) required for the construction of the permeameter.

Table 3a: Materials

Item no	Description	Est. Quantity	Units	Comments
1	Type 1 or III Waste rock	38	m^3	$32m^3$ for interior (sample), max clast 0.5 m^3
2	Type I Waste Rock	275	m^3	build up around outside for support (3:1 slope)
3	2" Crush base	12	m^3	0.5 m thick base (4.5 x 4.5m base)
4	Clean sand base	4	m^3	10 cm thick base graded (extra included for sand settlement)
5	Plywood – 4x8 ft	18	sheets	for permeameter frame
6	Lumber – 4x4x8 ft	4	ea	corner posts
7	Lumber – 2x4x8 ft	28	ea	for framing
8	Enviroliner 4040	1	ea	10x10 m prefabricated box
9	Geotextile liner	1	Ea	4x4 m sheet as overlay to protect liner (non-woven 540 g/m2)
10	PVC and fittings	TBD	TBD	connections from supply tanks to lower drain and upper drains
11	Compression fittings	4	ea	seal drains to liner
12	Silicone caulk	1	Pack	miscellaneous connections
13	3/8" Clean Gravel Crush base	5	m^3	$16m^2$ by average of 0.15 m height
14	1" PVC pipe	3	ea	manometers10ft sections with 5 cm slot section
15	Rope or twine	1	Roll	tie manometers in place during construction
16	1000L storage tank	1	ea	on site or move 4000 L storage tank from T3
17	Water level tape	1	ea	
18	20 L pail	1	ea	
19	Stop watch	1	ea	
20	Rake	1	ea	grading sand at permeameter base
21	Reciprocating saw	1	ea	to cut hole in liner for drain (or drill with door knob bit)
22	Hack saw	1	ea	
23	Measuring tape	1	ea	
24	Rhodamine Dye	1	ea	For drain down test
25	Water Pump	1	ea	
26	Misc. PVC supplies	TBD	TBD	PVC primer and glue, valves, wicking tape, wrenches
27	10 ft extension ladder	2	ea	Provide ingress and egress to the permeameter
28	Rock sample bags	1	Pack	*Collection of grain size and moisture content samples*
				all items include a 10-20% buffer

Notes:
1. TBD – indicates 'to be determined'
- to be supplied by Diavik

Table 3b: Equipment Supplied by Diavik

item no				Description
1	Track hoe	1-2	day	placement of rock in and around
2	Rubber tire backhoe	1-2	day	prep of base and gravel layer
3	Haul truck	1	day	deliver waste rock
4	Water Truck	1-2	day	for filling storage tank during testing
5	Fork lift/loader	1	day	to move 4000 L water tank from top of T3 and shipped liner to work site
6	Pick-up truck	14	day	for collecting miscellaneous supplies during construction and testing

INSTALLATION PLATFORM AND PERMEAMETER CONSTRUCTION

The permeameter will consist of an installation platform utilized to install the plumbing required and to provide an underlay to the Enviroliner 4040. Sitting on the base with a plywood frame, lined with a low permeability liner and filled with waste rock. Coincident with filling the plywood frame, waste rock will be placed exterior to the frame to provide structural support. Additional plumbing will complete the permeameter. Drawings documenting the proposed construction of the field permeameter are provided at the end of the work plan report (Drawing 3.1 through 3.5). The proposed location of the field permeameter is in the area adjacent to the covered pile, north of the instrumentation trailer called ‘Alabama’ (Drawing 3.1).

Installation Platform

The installation platform will provide a base for the plywood frame and it will form the base for the main water supply and constant head supply reservoirs (Drawing 3.2). In addition the platform will be sufficiently large to place waste rock surrounding the exterior of the plywood frame to provide support. It is proposed that the slopes will be shaped at 3:1 (i.e. similar to the covered pile) to allow safe access to the top of the permeameter, to control the hazard of working at heights. As indicated in drawing 3.2b, a platform with a base of 25.7 m x 22.3 m will be required to facilitate the sloping of the batters. The installation platform shall consist of the following materials (Drawing 3.2a):

- 4.5 m x 4.5 m, 2” crushed rock base, 0.5 m thick to support the plywood frame (12 m^3); and
- Clean sand, graded towards the location of the lower drain, with average thickness of 0.10 m (4 m^3, allowing for settlement within the crush).

It is anticipated that the construction of the platform will require approximately 1 day and it will utilize material and a track hoe excavator (or similar) provided by Diavik.

Permeameter Basal Plumbing

There will be a lower drain which enters the permeameter at the base, beneath the waste rock and liner. Two inch (2") PVC will be directed from the constant head supply reservoir to the base of the permeameter and will terminate at the lower drain, a 2" slotted PVC. Slot size utilized will be greater than in the previous experiment to eliminate the issue of restricted flow. The drain will be located at the lowest end of the permeameter (Drawing 3.2a).

It is anticipated that the construction of the plumbing and drain will require 1 day and it will be completed by university graduate and co-op students.

Permeameter walls and liner

Following the placement of the installation platform and basal plumbing, a plywood frame for the permeameter will be constructed on top of the platform (Drawing 3.2a). The base of the plywood frame will measure approximately 4 m by 4 m and the sides will rise approximately 2 m.

Assuming 1.2m x 2.4 m sheets of plywood, a total of 16 sheets will be required. The plywood frame will be supported by 4x4" by 1.8 m posts at the corners; and will be framed by 2x4s along the sides (Drawing 3.3). A base will not be required. Plywood and posts will be cut to between 2.0 and 2.2 m to maintain a convenient working height.

For ease of access during construction and installation of the liner, three of the four sides of the plywood box will be constructed. Then a portion of the liner placement, drain placement and 3/8" clean crush placement could be performed to eliminate some of the time otherwise spent working in a confined space.

An Enviroliner 4040 (supplied by Layfield) measuring 4 m x 4 m (i.e. pre-fabricated box) shall be fitted into the plywood frame to provide a durable low permeability barrier. The Enviroliner is a flexible polyethylene liner which can be welded before delivery and folded for transport. Once placed on top of the permeameter base the liner will be unfolded and fixed to the plywood walls. It may be necessary to install an overlay sheet of durable geotextile fabric (nonwoven 540g/m^2, available on site) to provide addition abrasion resistance for the true liner. The installation of the liner may require equipment support to lift the liner onto the pad (135 lbs).

Access to the interior of the permeameter will be required to complete the plumbing and to fit the liner to the corners of the permeameter. Access will occur via ladders secured to the exterior and interior of the permeameter to permit ingress and egress. Alternatively a sloped ramp of waste rock could provide access to the top of the exterior of the permeameter and a ladder utilized in the interior.

Following the placement of the liner, an upper drain will be installed on one side, as close to the top of the wall as practical. The upper drain will be connected and sealed with a rubber gasket compression fitting. The upper drain will report flow back to the main supply tank and will contain a discharge port for flow measurement.

The lower drain will be sealed to the liner with a rubber gasket compression fitting and then covered with 3/8" clean crushed gravel and leveled at the surface to provide a high permeability base to evenly distribute inflowing water. Thickness of 5 cm to 25 cm as required to level (Drawing 3.2a).

Prior to placement of the waste rock, manometers consisting of 1" PVC with 5 cm slotted section will be situated at the base of the waste rock and held in place by tying to the sides of the permeameter from opposing directions.

It is anticipated that the construction of the plywood frame will require 1 day and installation of the liner and plumbing of the upper drain will require 1 to 2 days. These activities will be predominantly conducted by university students however additional support may be required with placement of a prefabricated box liner. Placement of the 3/8" crush will require 0.5 days and it will utilize material and a track hoe excavator (or similar) provided by Diavik.

Surveying

Subsequent to installation of the upper and lower drain and placement of the clean crush, the dimensions of the interior of the field permeameter will be determined. Surveying activities will be completed by university students and will be completed over an hour or two.

Waste Rock Placement

The previous experiment was conducted on Type 1 waste rock. Type 1 and Type 3 waste rock have a similar grain size distribution however the distribution Type 3 rock is finer (ie. less gravels). Results of other experiments conducted on the project will provide hydraulic conductivity values for comparison from Type 3 waste rock. Either Type 1 or Type 3 waste

rock could be utilized. However to meet additional research objectives, it has been suggest that Type 3 waste rock be utilized.

To allow precise determination of the volume of water required to saturate the waste rock sample, as well as to test the integrity of the liner and operation of the plumbing and drain, the 3/8" gravel base will be saturated before loading waste rock. In the previous experiment approximately 650 L of water was required to saturate the base. A period of approximately 1 hour will be allowed to pass while the water level is monitored to evaluate the condition of the liner. The valve will be shut on the lower drain, to maintain the saturated base while the rock is loaded into the permeameter.

Prior to placement of the waste rock material it will be necessary to sort the waste rock with a track-mounted excavator or similar to remove clasts larger than 0.5 m^3 (0.8m x 0.8m x 0.8m). Approximately 5 hand samples (material finer than 100 mm) and matrix samples (material finer than 5mm) will be collected for grain size distribution and moisture content determination.

Following the saturation of the gravel base the waste rock material shall be placed by track-mounted excavator or similar equipment. It is anticipated that the placement of the waste rock will require one to two days to complete. As the waste rock is placed in the permeameter it shall be coincidently placed outside the plywood frame to provide structural support to the sides of the permeameter (Drawing 3.2b). Care shall be taken during the placement of the waste rock to preserve the integrity of the liner and the standpipes. The batters of the exterior support shall be sloped at 3H:1V to allow for safe access to the top of the permeameter. The slopes will result in a field permeameter with a footprint of 25.7 by 22.3 m (Drawing 3.4). Alternatively to sloping the batters, fall protection procedures could be put into place or construction in stages may be possible.

Permeameter Plumbing

Following placement of the waste rock the permeameter plumbing will be completed (Drawing 3.5). A large supply vessel will be placed and used as the main water supply tank. Due to the volumes of water required, it would be worthwhile to move the 4000 litre tank from atop the type 3 pile for use in the permeameter. A smaller 200L drum (or similar) will be used as a constant head supply reservoir. A gasoline powered pump will also be used to conduct the experiment over a range of flow rates. Pipe and fittings will be required to connect the supply tank to the constant head bucket or to a pump and connect to the lower drain. The upper drain will be connected to return flow back to the main supply tank, and will include values to stop the return flow and direct flow towards a sampling point to determined discharge flow rate. The lower drain will also have a valve in line, to prevent unwanted drainage.

It is anticipated that the plumbing of the supply tanks to the permeameter will require approximately 1 day. The majority of this work will be performed by the university students; however relocation of the 4000 L tank from the top of the T3 pile will require the assistance of Diavik equipment.

PERMEAMETER TESTING PROCEDURES

Testing proposed for the field permeameter includes porosity testing, saturated hydraulic conductivity determination, and potentially flow velocity and specific yield measurement. The following provides an overview of the steps required to complete the proposed testing.

Porosity Testing

Porosity testing consists of recording the volume of water required to saturate the full sample volume. Several activities which accompany the porosity testing are to collect samples from the waste rock to determine the initial moisture content and to increment the main supply tank for determination of volume of water required to saturate the sample. Raw water delivery will be required from Diavik.

Constant Head Permeameter Testing

From Darcy's Law (K = Q/iA), by measuring the discharge flowing through a sample of length (L~2m) and cross sectional area (A~16m^2), determining the hydraulic gradient across the sample will allow the saturated hydraulic conductivity to be determined. Constant flow rate will be created with the use of a constant head water supply. Optimal evaluation can be made if the testing is conducted over a range of flow rates. It is anticipated that the range of the flow rates capable from the constant head water supply will be limited; therefore a water pump will also be utilized to drive flow into the permeameter. Flow rates will be maintained such that no turbulent flow is initiated within the sample. During testing measurements of the discharge will be made regularly along with measurements of the hydraulic head in the manometers. The hydraulic head at the top of the sample can be measured from the phreatic surface, determined by the level of the upper drain above the datum.

Drain Down Testing

During the previous permeameter experiment, a rhodamine dye tracer was applied to measure flow velocity and observe whether macropore flow was initiated on a 1 m sample. Also the volume of rapid draining water was accounted. The plumbing was such that the discharge was directed through ½" tubing restricting the discharge rate, but allowing detailed collection of samples and discharge volume. Depending on the results of the initial two experiments this portion of the experiment may or may not be completed.

References

Neuner, M., 2009. Water flow through unsaturated mine waste rock in a region of permafrost. M.Sc. thesis. University of British Columbia, Vancouver, Canada.

Test Piles Research Group, 2008. Work plan and health, safety, and environment (HSE) plan for the monitoring phases of the test pile project. University of Waterloo, Ontario, Canada.

DRAWINGS

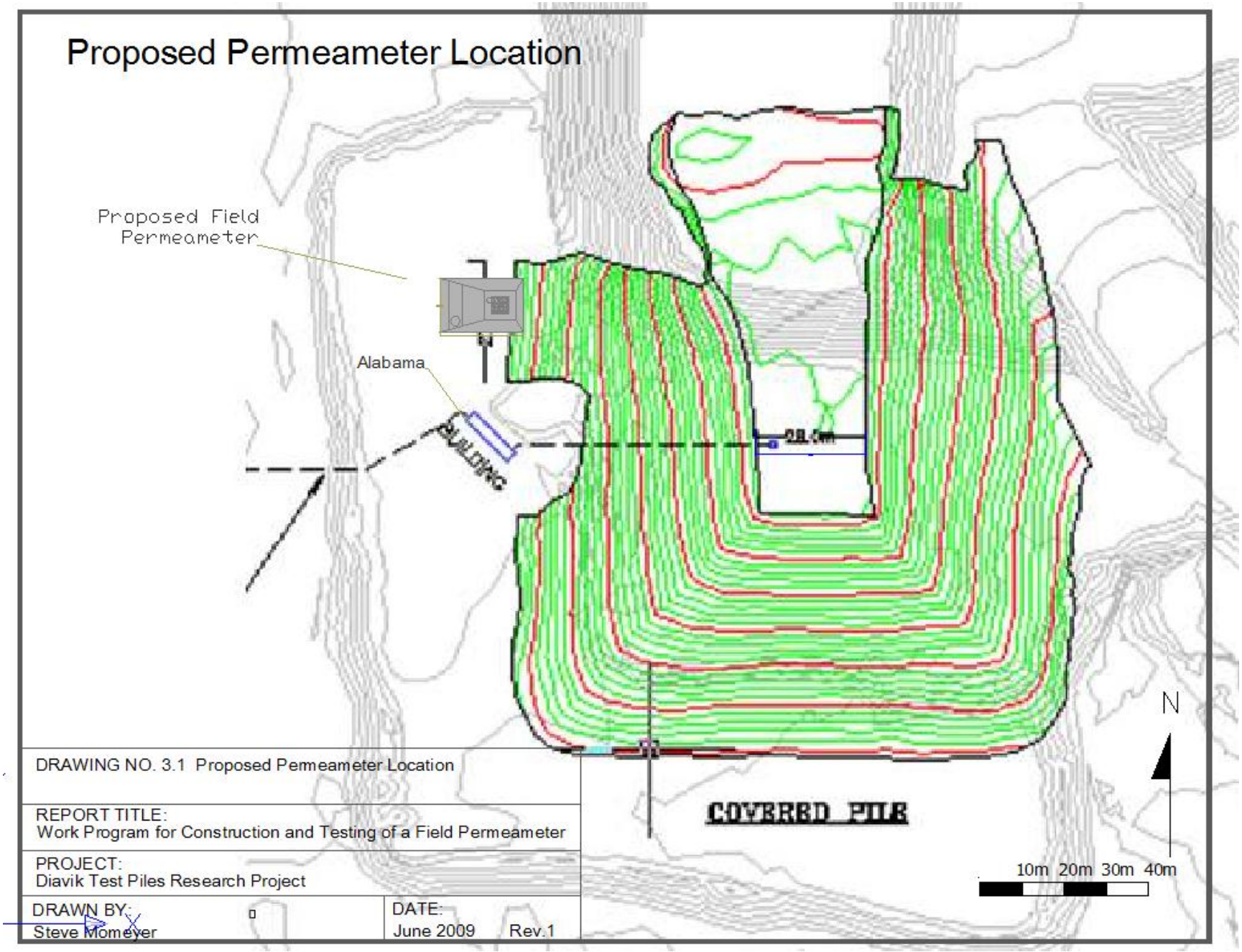
Proposed Permeameter Location
Proposed Field Permeameter
Alabama
BUILDING
COVERED PILE
N
10m 20m 30m 40m
DRAWING NO. 3.1 Proposed Permeameter Location
REPORT TITLE:
Work Program for Construction and Testing of a Field Permeameter
PROJECT:
Diavik Test Piles Research Project
DRAWN BY:
Steve Momeyer
DATE:
June 2009
Rev.1

Cross Section of Permeameter

1. Construct 0.5 m thick base with 2" crush
2. Place 0.1 m thick clean sand base
3. Install inflow plumbing and lower drain
4. Build 4mx4m plywood box by 2 m height
5. Install Enviroliner
6. Add 0.10 to 0.25 m thick clean $\frac{3}{8}$" gravel crush base (covering the lower drain)

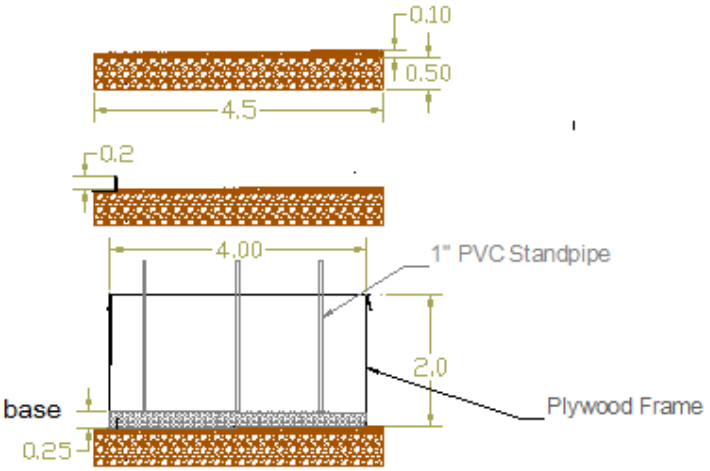

DRAWING NO. 3.2a Cross-Section View of Field Permeameter	
REPORT TITLE: Work Program for Construction and Testing of a Field Permeameter	
PROJECT: Diavik Test Piles Research Project	
DRAWN BY: Steve Momeyer	DATE: May 2009

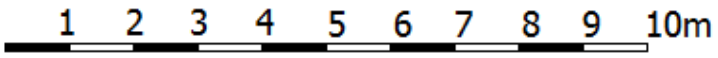

Cross Section of Permeameter

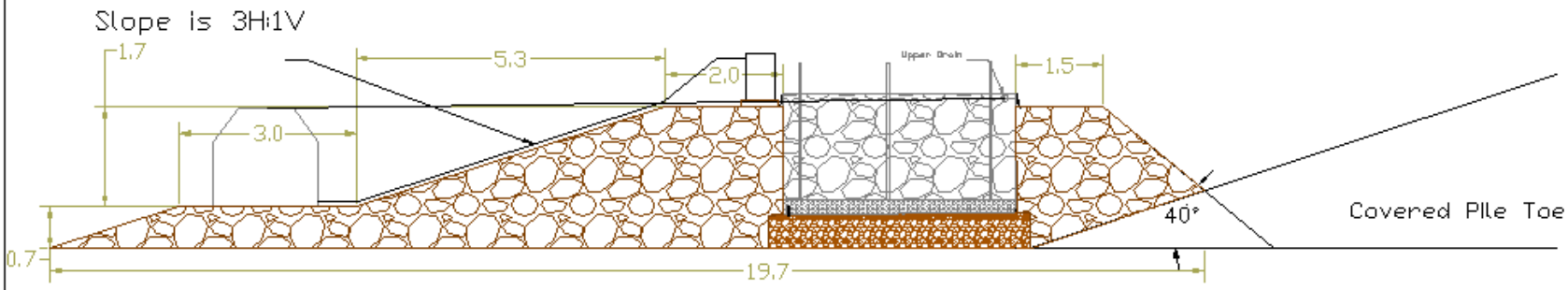

⑦ Fill plywood box with Type 1 or 3 waste rock and build up waste rock surrounding the permeameter to provide support to the permeameter

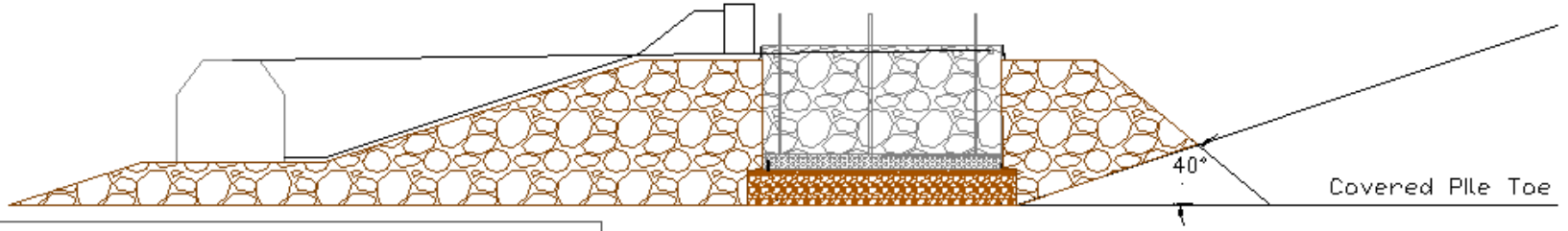

DRAWING NO. 3.2b Cross-Section View of Field Permeameter	
REPORT TITLE: Work Program for Construction and Testing of a Field Permeameter	
PROJECT: Diavik Test Piles Research Project	
DRAWN BY: Steve Momeyer	DATE: June 2009 Rev.1

⑧ Placement of main water supply reservoir and constant head supply tank and connection of all remaining plumbing.

1 2 3 4 5 6 7 8 9 10m

Construction of Plywood Box

Plan View

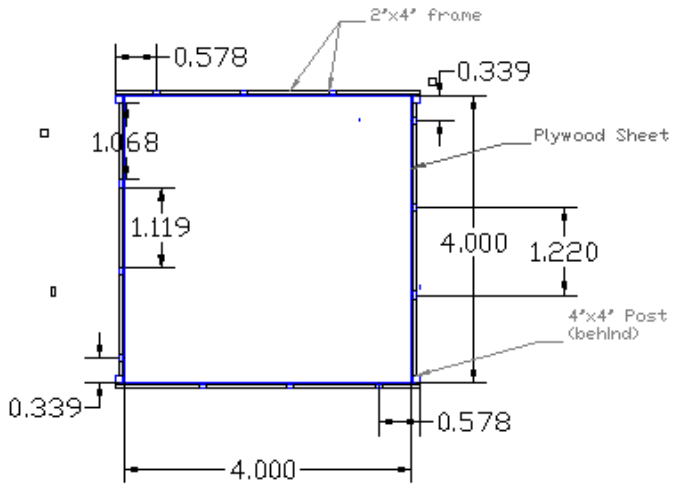

4 Plywood sheets per side joined with 2x4" and supported at corner with 4x4" post (with 2x4" framing removed for clarity)

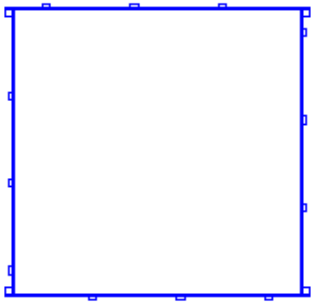

Cross Section View

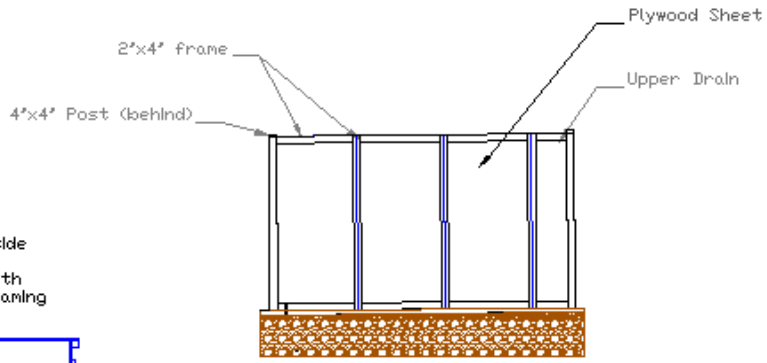

DRAWING NO. 3.3 Cross-Section View of Plywood Box	
REPORT TITLE: Work Program for Construction and Testing of a Field Permeameter	
PROJECT: Diavik Test Piles Research Project	
DRAWN BY: Steve Momeyer	DATE: June 2009

1 2 3 4 5 6 7 8 9 10m

Plan View of Field Permeameter

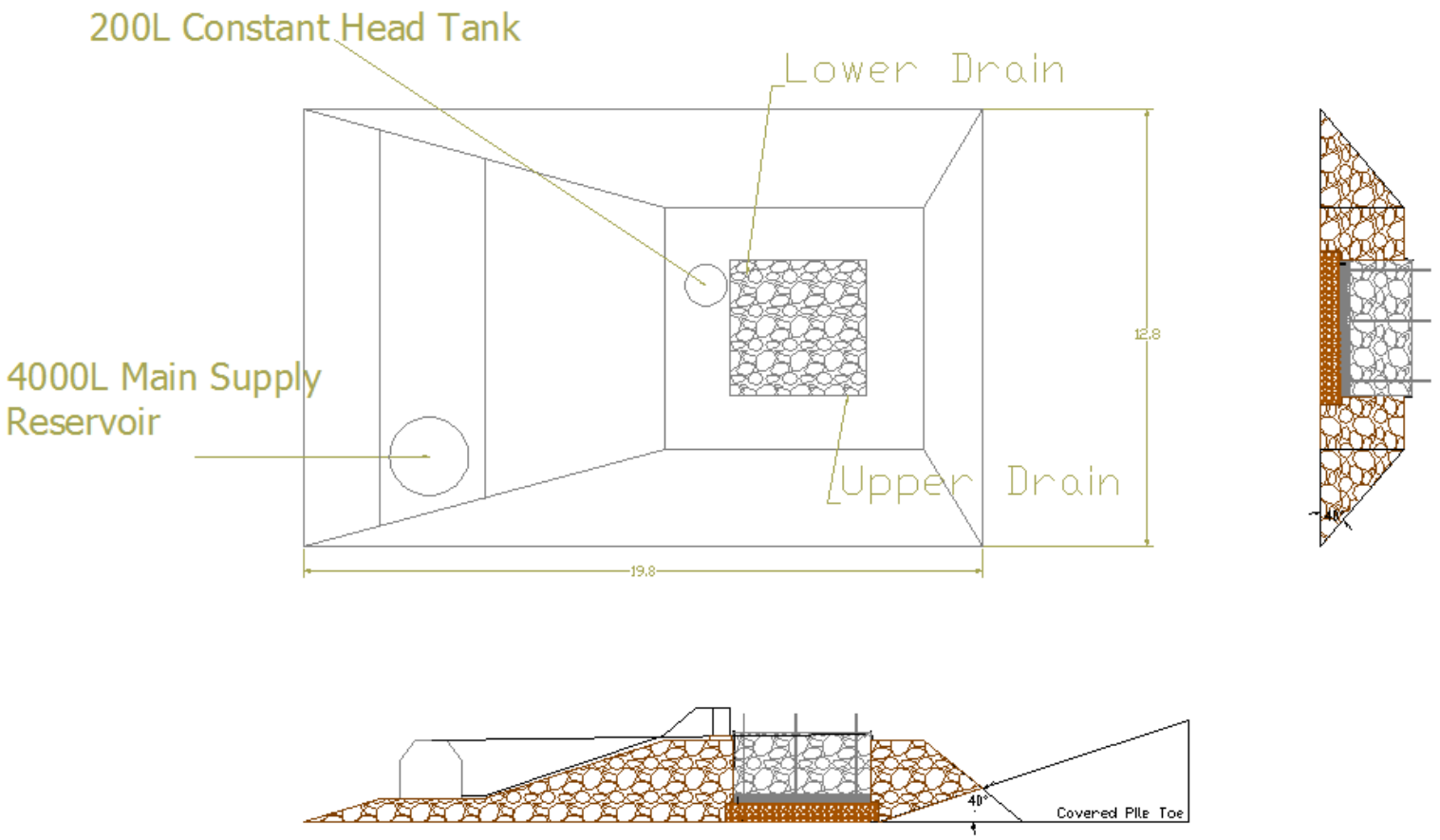

DRAWING NO. 3.4 Plan View of Permeameter	
REPORT TITLE: Work Program for Construction and Testing of a Field Permeameter	
PROJECT: Diavik Test Piles Research Project	
DRAWN BY: Steve Momeyer	DATE: June 2009 Rev.1

Detailed Conceptual Configuration of Permeameter Plumbing

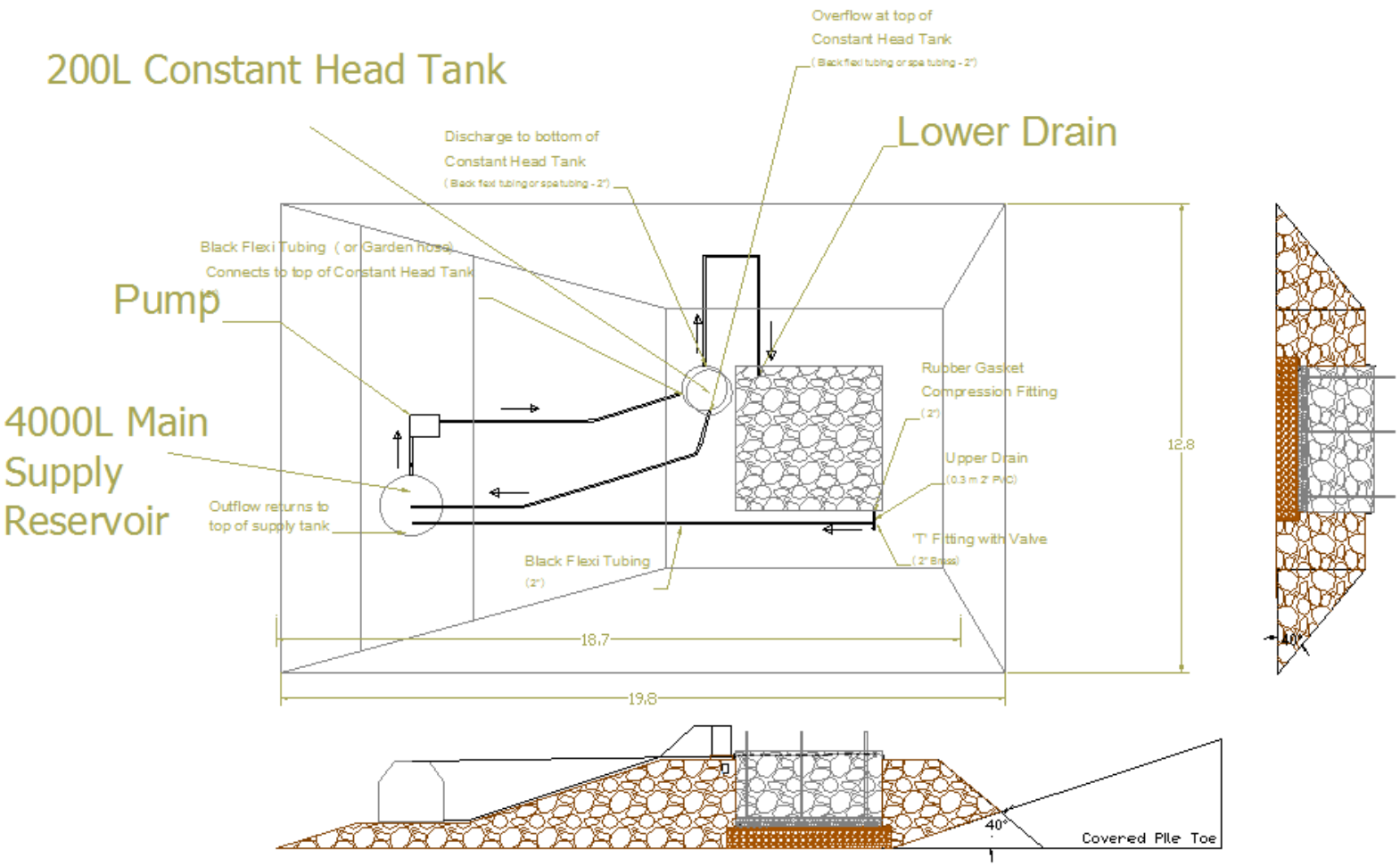

DRAWING NO. 3.5 Conceptual Configuration of Permeameter Plumbing (Plan View)	
REPORT TITLE: Work Program for Construction and Testing of a Field Permeameter	
PROJECT: Diavik Test Piles Research Project	
DRAWN BY: Steve Morneyer	DATE: June 2009 Rev.1

Appendix C New Covered Test Pile Datalogger Program

```
'ECHO probe from Colin Campbell
'most of the flesh from Matt and Davey
'revised dmj eos ubc june 2007

'revised by andre july 08
'removed data interval from tipping tables and the rest of the tables
'changed sampling for totalize to sample to output the exact number on the counter
'added a total tips variable to record the total number of tips since the program was
started
'sampled total tips

'revised by steve momeyer March 09 for Diavik Covered Pile
'removed ECHO probe logging and TDR logging
'added pH probe logging


'revised by steve momeyer and andre wilde May 09
'troubleshooting

' STATION:      CBa
' LOCATION:     West side base of TC waste rock pile

' Serial Numbers:
' PS-100                # 5274
' CR1000                # 10931 (11231)
' AM16/32 (1)           # 9170
' AM16/32 (2)           # 9171
' TIPPING BUCKETS       # TB_24 to TB_27  ' these do not agree with Array Id spreadsheet
but used for historical purposes as this is what Mike G called them
' EC probes             # EC_32 to EC_44
' pH probes             # pH_20 to pH 21 (expandable to pH_32)


'Requirements:
'Covered waste rock pile flow, geochemistry, and temperature.
' Flow:3 Young's tipping bucket rain gauges for basal lysimeters; 1 Custom TB for basal
drain
' Geochemistry: Electrical conductivity sensors (13) -  EC corrected for thermistor in
cell
' pH probes (up to 13) - pH corrected for temperature
' Temperature:  Thermistors located in the three basal lysimeter clusters, near the heat
trace and in waste rock near the lysimeter (6) all EC cells (13), and one in 'the
instrument shack (1).

'1 wire thermistors(SE voltage measurement from half Bridge), 2 wire pH (voltdiff) and 6
wire conductivity(6wire Full Bridge)

' Conductivity is on one mux set as 4x16
' 1 EC probe can be measured in each mux cycle (4 or 6 wire) ???
' Thermistors and pH are on the second mux, set as 4x16
' 4 thermistors can be measured each mux address cycle (1 wire)
' 2 pH measurement can be made for each cycle (2 wire)
' Half Bridge Resistor = 2255 ohms
```

```
'Port Usage (see wiring diagram Datalogging Scheme:
'CR1000 SN11231 (10931)
'P1 TB_24   Array id 16    TC Basal lysimeter Cluster 1
'P2 TB_25   Array id 17    TC Basal lysimeter Cluster 2
'C1 'AM32 #9170 RES   EC
'C2 'AM32 #9170 CLK   EC
'C3 'AM32 #9171 RES   Therm
'C4 'AM32 #9171 CLK   Therm
'C5 --
'C6 TB_26   Array id 18    TC Basal lysimeter Cluster 3
'C7 TB_27   Array id 19    TC Basal Drain
'AG Jumper to SE2, Brown pH probe leads, all EC and therm grounds
'C8 --
'  SE1 Diff 1   EC COM AM16/32 #9170 ODD  H Red w/ 470 Ohm to AG and jumper to SE2
'  SE2 Diff 1   EC COM AM16/32 #9170 ODD  L Jumper to SE1 and AG
'  SE3 Diff 2   EC COM AM16/32 #9170 EVEN H White
'  SE4 Diff 2   EC COM AM16/32 #9170 EVEN L Green
'  SE5 Diff 3   Th COM AM16/32 #9171 ODD  H Black 10k Ohm to AG
'  SE6 Diff 3   Th COM AM16/32 #9171 ODD  L Red 10k Ohm to AG
'  SE7 Diff 4   Th COM AM16/32 #9171 EVEN  H White 10k Ohm to AG
'  SE8 Diff 4   Th COM AM16/32 #9171 EVEN  L Green 10k Ohm to AG
'  SE9 Diff 5
'  SE10 Diff 5
'  SE11 Diff 6
'  SE12 Diff 6
'  E1 Excites thermistors. Red
'  E2 Excites EC probes.   Black
'  E3 --
'  5V TB 26 and 27, 5V only req'd when using a control port for a pulse signal

'  AM16/32 9170 4x16 COM
'  Odd High EC Black
'  Odd Low EC Red
'  Even High EC White
'  Even Low EC Green

'  AM16/32 9171 4x16 COM
'  OH therm Black
'  OL therm Red
'  EH therm White
'  EL therm Green
'


' #####
'  Pulse Channel 1 (switch closure only) TC Basal Lysimeter Cluster 1 Tipping Bucket
'  Pulse Channel 2 (switch closure only) TC Basal Lysimeter Cluster 2 Tipping Bucket
'  Pulse Control Port 6 (switch closure only) TC Basal Lysimeter Cluster 3 Tipping Bucket
'  Pulse Control Port 7 (switch closure only) TC Basal Drain Tipping Bucket
'
' ######
' ELECTRICAL CONDUCTIVITY
'  Set Control Port 1 High RESET: Activate AM16/32 9170 by setting Control Port 1 high
'  Pulse Control Port 2 CLOCK: Switches through the 13 EC cells
'  Set Control Port 1 low RESET: De-activate AM16/32 9170 by setting Control Port 1 low
' TEMPERATURE MEASUREMENTS
'  Set Control Port 3 High RESET: Activate AM16/32 9171 by setting Control Port 3 high
```

```
'  Pulse Control Port 4 CLOCK: Switches through the 20 basal thermistors
'  Set Control Port 3 Low RESET: De-activate AM16/32 9171 by setting Control Port 3 low
' pH MEASUREMENTS
'  Voltdiff Channel 5 on CR1000
' End of program

' OUTPUT TABLES:
'
' ### CBa_TB_Cluster 1 ###
' ARRAY ID: 16 TC Basal Lysimeter Cluster 1 Tipping Bucket
'  Real Time Year,Mo,Day, (midnight = 0000)
'  Record No.
'  Array Id
'  Minute into current day
'  Time Seconds
'  Sample 1 rep TB_24
' ### CBa_TB_Cluster 2 ###
' ARRAY ID: 17 TC Basal Lysimeter Cluster 2 Tipping Bucket
'  Real Time Year,Mo,Day, (midnight = 0000)
'  Record No.
'  Array Id
'  Minute into current day
'  Time Seconds
'  Sample 1 rep TB_25
' ### CBa_TB_Cluster 3 ###
' ARRAY ID: 18 TC Basal Lysimeter Cluster 3 Tipping Bucket
'  Real Time Year,Mo,Day, (midnight = 0000)
'  Record No.
'  Array Id
'  Minute into current day
'  Time Seconds
'  Sample 1 rep TB_26
'### CBa_TB_Basal_Drain ###
' ARRAY ID: 19 TC Basal Drain Tipping Bucket
'  Real Time Year,Mo,Day, (midnight = 0000)
'  Record No.
'  Array Id
'  Minute into current day
'  Time Seconds
'  Sample 1 rep TB_27
'
' ### TABLE CBa_EC_volt ###
' ARRAY ID: 32 volt
' Resolution High
'  Real Time Year,Mo,Day, (midnight = 0000)
'  Record No.
'  Array Id
'  Minute into current day
'  Seconds
'  Sample 13 Reps V2V1_1

' ARRAY ID: 33
'  Sample 13 Reps Rs_1

' ARRAY ID: 34
'  Sample 13 Reps EC_32
```

```
' ### TABLE CBa_EC_Tcorr ###
' ARRAY ID: 35
'  Real Time Year,Mo,Day, (midnight = 0000)
'  Record No.
'  Array Id
'  Minute into current day
'  Seconds
'  Sample 13 Reps EC25C

' ### TABLE CBa_Temp_mv ###
' ARRAY ID: 40
'  Real Time Year,Mo,Day, (midnight = 0000)
'  Record No.
'  Array Id
'  Minute into current day
'  Sample 20 Reps TRatio

' ARRAY ID: 41
'  Sample 20 Reps Rth

' ### TABLE CBa_Temperature ###
' ARRAY ID: 42
'  Real Time Year,Mo,Day, (midnight = 0000)
'  Record No.
'  Array Id
'  Minute into current day
'  Sample 20 Reps Temp_C

' ### TABLE CBa_pH_volt ###
' ARRAY ID: 247
' Resolution High
'  Real Time Year,Mo,Day, (midnight = 0000)
'  Record No.
'  Array Id
'  Minute into current day
'  Seconds
'  Sample 13 Reps pHV_1
'  Sample 13 Reps pH_1

''''''''''''''''''''''''''''''''''''''''''''''''''''''''''''''''''''''''''''''''''''''''''
'

'Declare Constants: Const constant name  = expression
' constants cannot be changed while the program is running, unlike variables
' must be declared before they are called
Const OFF = 0
Const ON = 1

Const CR1000SN = 11231 ' label indicates 10931, but dev config called it 11231

Const TB_scanRate = 200 'millisec; old program 125 ms, but multiple of 10ms, max
resolution 10 ms
Const MainScanRate = 30 ' minutes collects all

Const ECReset = 1 'control port 1 AM16/32 #9170 for EC
Const ECClock = 2 'control port 2 AM16/32 #9170 for EC
Const TReset = 3 'control port 3 AM16/32 #9171 for therm
```

```
Const TClock = 4 'control port 4 AM16/32 #9171 for therm

' coefficients for Steinhart-Hart equation based on temp range expected to minimize
errors (-10, 0, 10 celsius)
'Steinhart, J.S. and S.R. Hart, Deep Sea Res. 15, 497-503(1968)
' 1/T = A + B*ln(R) + C*(ln(R)^3)  where T is in Kelvins and R = resistance(ohms)
Const A = 0.001286798
Const B = 0.000235938
Const C = 0.000000094

Const VExcit = 2.5 'v
Const RValue = 10000 'ohms

Const mV_conversion = -0.016941  ' converts from mV to pH = pHV_1/(RT*ln(10)/F) - const
'where R = gas const; T = temp in K; F = faraday; const = offset
'Const offSet_1 = 5.657 ' calibration offset from June 15, 2008 for basal drain pH probe
'Const offSet_2 = 7.169
Const offSet = 7.0 'for now use a generic offset

const nPH = 2 'number of pH probes
''''''''''''''''''''''''''''''''''''''''''''''''''''''''''''''''''''''''''''''''''''''''

'Declare Public variables: Public variable name(size, size) 'optional' as Type
'  Public variables are available for outputting to a table
' (size, size) allows the creation of an array, size by size
' Public Drain(3) would create Drain(1), Drain(2), Drain(3)

'TIPPING BUCKET vars
Public TB_24 ' counts tips per sec in sublysimeter flow gauges (TB_24, TB_25, TB_26)
Public TB_24_total as long
Public TB_25
Public TB_25_total as long
Public TB_26
Public TB_26_total as long
Public Drain     ' counts tips per sec in basal drain (TB_27)
Public Drain_total as long

'THERMISTOR vars
' 6x basal lysimeters: each 1 near heat trace, 1 in waste rock;
' Basal lysimeter EC cells have one thermistor each (12)- 3x4 sample cells
' The basal drain has one thermistor in EC cell (1) and 1 located in instrument hut
Public Temp_C(20) 'thermistor
Public TRatio(20)
'Public RValue(20) ' re-instate constant Rvalue, above
Public TResist 'temp var for calculating temperature resistance
Public LnR ' temp var for calc natural log of temp resistance (Steinhart-Hart)
Public Kelvin 'temp var to convert from degrees Kelvin to degrees Celsius

'ELECTRICAL CONDUCTIVITY vars
Public Full(13) 'conductivity full bridge output
Public EC_V2_V1(13)
Public EC_Rs(13) 'resistance through the water sample
Public EC(13) 'Electrical Conductivity of the water sample
Public EC25C(13) 'Electrical Conductivity of water sample temperature corrected

Const EC_Rf = 470 ' Reference resistor [Ohms] (SE1 to SE2) for EC sensor
Const k = 1.884   'Cell constant for EC sensor [m^-1]
```

```
'k is determined by the equation k=(2/pi^2*d)(ln((4a+pi*d)/(4a+pi*d/2)) from Won (1987).

'pH vars
Public pHV_(2) 'pH reading in mV
Public pH_(2)  'pH converted from mV

Public Batt

'ECHO vars - deleted

Public x, i as float  ' declares two variables as float, x and i
Public cch ' conductivity counter
Public tch ' thermistor counter
Public ich 'Celcius counter
Public ipH 'pH counter
Public iipH 'pH counter

'DIM vars
'Dim declares variables, but unlike Public these variables cannot be viewed
Dim modThing
Dim count

''''''''''''''''''''''''''''''''''''''''''''''''''''''''''''''''''''''''''''''''''''''''

'Declare Units; Units variable name = unit label
'  sets units to be displayed in output table
Units Drain=tip
Units TB_24=tip
Units TB_25=tip
Units TB_26=tip
Units EC()=mS/cm
Units Temp_C()=deg C
Units pH_() = pH

''''''''''''''''''''''''''''''''''''''''''''''''''''''''''''''''''''''''''''''''''''''''

'Declare DataTables
'used to define the name, trigger condition and size of an output table
'(Name: used to call the DataTable,
'TrigVar: const or var to test for triggering DataTable,
'Size: const to define number of records that should be allocated; -1 divides memory
between tables)
'-deleted rain data table

DataTable (CBa_TB_Cluster_1,True,-1) 'TB_24 cluster 1 CBWBlys
  sample(1,TB_24,FP2)
'sample - stores the current value of the variable
'sample(reps, source, dataType) - reps, if >1 then an array must be specified for source,
source = variable, dataType = saved format, IEEE$, FP2, String, Boolean
  sample(1,TB_24_total,long)
EndTable

DataTable (CBa_TB_Cluster_2,True,-1) 'TB_25 cluster 2 CBWClys
  sample(1,TB_25,FP2)
  sample(1,TB_25_total,long)
EndTable
```

```
DataTable (CBa_TB_Cluster_3,True,-1) 'TB_26 Cluster 3CBEClys
  sample(1,TB_26,FP2)
  sample(1,TB_26_total,long)
EndTable

DataTable (CBa_TB_Basal_Drain,True,-1)
  sample(1,Drain,long)
  sample(1,Drain_total,long)
EndTable

'&&&&&&&&&&&&&&&&&&&&&&&&&&&&&&&&&&&&&&&&&&&&&&&&&&
DataTable (CBa_Temperature,True,-1)
'  DataInterval(0,30,Min,0)
'  Sample (1,Batt,FP2)
'  Sample (20, TRatio,IEEE4)
  Sample(20,Temp_C(),IEEE4)
EndTable

DataTable (CBa_Temp_mv,True,-1)
  Sample (1,Batt,FP2)
  Sample (20, TRatio,IEEE4)
EndTable

DataTable (CBa_EC_Tcorr,True,-1)
'  DataInterval(0,30,Min,0)
'  Sample (1,Batt,FP2)
'  Sample (13,EC_V2_V1(),IEEE4)
  Sample (13,EC25C(),IEEE4)
EndTable

DataTable (CBa_EC_volt,True,-1)
  Sample (13,EC_V2_V1(),IEEE4)
EndTable


DataTable (CBa_pH_volt,True,-1)
'  DataInterval(0,30,Min,0)
      Sample (2,pHV_(),IEEE4)
  Sample (2,pH_(),IEEE4)
  EndTable

'-Deleted Echoprobe dataTable

'&&&&&&&&&&&&&&&&&&&&&&&&&&&&&&&&&&&&&&&&&&&&&&&&&&&&&&&&&&&&&&&&&&&&&&&&&&&&&&&&&&&&&&&&&&
&

'SubRoutines
'-deleted Sub InitEcho()

'-deleted Sub GetEcho(); Echo probes

'-deleted Sub SplitString(); Moisture contents, TDR

Sub GetTherm()
    ''''''''''''get Temperatures readings (20 measurements)'''''''''''''''
    PortSet(TReset,ON) 'turn on AM16/32 #9171; PortSet(port, state)
```

```
    Delay (0,150,mSec)  ' Delay(option, delay, units) option: 0=measurement task
sequence; 1 = processing
    'clock mux NOTE first pulse sets to ADDRESS 0 then each pulse clocks
    For tch = 1 to 20 step 4
        PortSet(TClock,ON) ' TClock pulse this to advance channel (while mux activated)
        Delay (0,20,mSec)
        PortSet(TClock,OFF)
        Delay (0,200,mSec)  '>>> add delay July 3, 2009
        'get a thermistor readings
        'BrHalf applies an excitation voltage, delays then makes a single ended voltage
measurement
        'BrHalf(Dest, Reps, Range, SEChan, ExChan, MeasPEx, ExmV, RevEx, Settling Time,
Integ, Mult, Offset)
        'SEChan - single ended channel first measurement made, cycles through for reps
       'for a BrHalf in CR1000, output is ratio of the measured voltage divided by the
excitation voltage
        BrHalf (TRatio(tch),4,mv2500,5,VX1,4,2500,True,0,250,1,0)

        'BrHalf (TRatio(tch),4,mv2500,5,VX1,4,2500,false,0,250,1,0) ' June 21 try program
without reversing excitation.
        Delay (0,500,mSec)
    Next tch
    PortSet(TReset,OFF) 'turn off AM16/32
 Endsub

Sub CalcCelsius()
    'convert Voltage ratios to Temperature
    'apply Stienhart-Hart equation
    For ich = 1 to 20
        'calculate resistance of thermistor
        'need to multiply output by Vexcit first as output is ratio of the measured
voltage divided by the excitation voltage (July 3, 2009)
        TResist =((VExcit*RValue)/(TRatio(ich)*VExcit))-RValue  'use this conversion
(2009-06-04)
         'TResist = RValue*TRatio(ich)/(1-TRatio(ich))
        'now apply Stienhart Hart eq
        'log = ln in CR1000
        LnR = LOG(TResist)
        Kelvin = 1/(A + B*LnR + (C*LnR*LnR*LnR))
        Temp_C(ich) = Kelvin - 273.15
    Next ich
Endsub

Sub GetCond()
    ''''''''''''get Conductivity readings (13 measurements) ''''''''''''
    PortSet(ECReset,ON) 'turn on AM16/32 #9170
    Delay (0,100,mSec)
    'clock mux NOTE first pulse sets to ADDRESS 0 then each pulse clocks

    PortSet(ECClock,ON)   '<---Add this clock to advance to read channel 1 (2009-06-04)
    Delay (0,20,mSec)
    PortSet(ECClock,OFF)
    Delay (0,200,mSec)   '>>> add in this delay 2009-07-02 and change from 20 msec to 200
msec (ie, same as between cch)
     'do each channel twice (one as half bridge and one as Full Bridge) <<-- APPEARS TO
BE CHANGED, ONLY FULL BRIDGE
    ' DIAVIK OLD PROGRAM, FULL BRIDGE EXCITATION ONLY
```

```
    For cch = 1 to 13
    '6 wire full bridge measurement: applies excitation voltage and makes two
differential voltage measurements; sequential channels
    '=1000*V2/V1 (V2 - voltage on second channel, V1 - voltage on first channel)
    'BrFull6W(Dest, Reps, Range1, Range2, DiffChan, ExChan, MeasPEx, ExmV, RevEx,
RevDiff, SettlingTime, Integ, Mult, Offset)
        BrFull6W (Full(cch),1,AutoRange,AutoRange,1,VX2,1,2500,True,True,0,250,1.0,0)
        Delay (0,200,mSec)
       'BrHalf4W (Half(cch),1,mV2500,mV2500,1,Vx1,1,2500,True ,True ,0,250,1.0,0)
        'Delay (0,200,mSec)  '>>>>> removes this second delay 2009-07-02
       'clock to next channel
        PortSet(ECClock,ON)
        Delay (0,20,mSec)
        PortSet(ECClock,OFF)
        Delay (0,200,mSec)
    Next cch
    PortSet(ECReset,OFF) 'turn off AM16/32 #9170
Endsub

'''''Convert voltage reading to EC reading
' Resistance of the solution around the probe is determined by the following equation;
' Rs=RfV2/V1 [Ohms]
' Electrical conductivity [S/m]=cell constant(k)/resistance of solution.
' k is determined by the equation k=(2/pi^2*d)(ln((4a+pi*d)/(4a+pi*d/2)) from Won (1987).
' For the Diavik probes, k = 1.884 [m^-1]
' This output is 1000 times the ratio between the potential measured by the central
electrodes
' in the water and the potential measured by the outer electrodes in the solution,
' in series with the reference resistor.
' Multiplying by the reference resistance (470 Ohms)
' yields the resistance in the flow-through cell.
' Multiplied by 0.001 for [mV] to [V] and Rf=470 Ohms
Sub CalcEC()
    'convert Full Bridge output to EC in mS/cm
    For cch = 1 to 13
        EC_V2_V1(cch) = Full(cch)*0.001 'output is 1000*V2/V1
        EC_Rs(cch) = EC_V2_V1(cch)*EC_Rf 'EC_Rf = Resistance en ohmns
        EC(cch) = (k/EC_Rs(cch))*10000*3.963 ' Units conv. [S/m] to [uS/cm] and
Calibration Fact. [add brackets (k/EC_Rs)*...
        'Calibration Factor :  This factor was derived to make EC probes output EC
expected based on five different molar concentration laboratory-prepared KCl solutions.
     'delete Select Case and place unit conversion and calibration factor into for
statement
     'Temperature Correction
     ' EC25C=EC_32/(0.8703*(1+(0.0213*(Temp_C_19-18))))
     ' Temperature of thermistor 19 (basal drain) chosen for all corrections
            ' In case other thermistors fail as did thermistor 18
           EC25C(cch) = EC(cch)/(0.8703*(1+(0.0213*(Temp_C(19)-18))))
     Next cch
Endsub

'Sub InitTherms()
    'Delete unique bridge values; Rvalue is constant = 10000 ohms


'''''''''''''''Take pH reading'''''''''''''''
Sub GetpH()
```

```
'VoltDiff(Dest, Reps, Range, DiffChan, RevDiff, SettlingTime, Integ, Mult, Offset)
'July 6 move pH probes to CR1000 diff channel 5 (CBxx) and ch 6 (spare)

VoltDiff(pHV_(),2,mV2500,5,true,0,250,1,0)

'     PortSet(TReset,ON) 'turn on AM16/32 #9171; PortSet(port, state)
 '   Delay (0,150,mSec)  ' Delay(option, delay, units) option: 0=measurement task
sequence; 1 = processing
    'clock mux NOTE first pulse sets to ADDRESS 0 then each pulse clocks
  '         PortSet(TClock,ON) ' TClock pulse this to advance channel need to advance to
ch 13 - AM16/32 set to 4x16(while mux activated)
   '     Delay (0,20,mSec)
    '    PortSet(TClock,OFF)
     '   Delay (0,20,mSec)
      ''  PortSet(TClock,ON) ' 1
        'Delay (0,20,mSec)
        'PortSet(TClock,OFF)
        'PortSet(TClock,ON) ' 2
        'Delay (0,20,mSec)
        'PortSet(TClock,OFF)
        'Delay (0,20,mSec)
        'PortSet(TClock,ON) ' 3
        'Delay (0,20,mSec)
        'PortSet(TClock,OFF)
        'Delay (0,20,mSec)
        'PortSet(TClock,ON) ' 4  add extra clocks, 4 - 6 July 5, 2009
        'Delay (0,20,mSec)
        'PortSet(TClock,OFF)
        'Delay (0,20,mSec)
        ' PortSet(TClock,ON) ' 5
        'Delay (0,20,mSec)
        'PortSet(TClock,OFF)
        'Delay (0,20,mSec)
        ' PortSet(TClock,ON) ' 6
        'Delay (0,20,mSec)
        'PortSet(TClock,OFF)
        'Delay (0,20,mSec)

   ' For ipH = 1 to nPH step 2
                  '     PortSet(TClock,ON) ' TClock pulse this to advance channel to
start at ch17 (while mux activated)
     '   Delay (0,20,mSec)
      '     VoltDiff(pHV_(ipH),2,mV2500,1,true,0,250,1,0) 'july 5, change diff channel to
3 from 5 (but maybe shoul be 1) integration to 60 hz from 250, as per manual for pH probe
(CSIM-11)
            'PortSet(TClock,OFF)
            'Delay (0,500,mSec)
      'next ipH
  '  PortSet(TReset,OFF) 'turn off AM16/32
Endsub


Sub CalcpH()
      For iipH = 1 to nPH
      'convert from mV to pH based on Nerst equation
            pH_(iipH) =  mV_conversion*pHV_(iipH)
            'could add offset for each probe or can be corrected afterwards....
```

```
            pH_(iipH) = pH_(iipH) + offSet
      next iipH
Endsub


Sub getData()

        'deleted calls to ECHO programs

        GetTherm
        CalcCelsius

        GetCond
        CalcEC

        GetpH
        CalcpH

        Battery (Batt)
EndSub

'&&&&&&&&&&&&&&&&&&&&&&&&&&&&&&&&&&&&&&&&&&&&&&&&&&&&&&&&&&&&&&&&&&&&&&&&&&&&&&&&&&&&&&&&&

'Main Program
SequentialMode

BeginProg

 'InitTherms ' NO LONGER NEEDED?
 count = 0
modThing = MainScanRate*60000/TB_scanRate ' 15000 counts (15000*0.12s/60min/s = 30 min)
'modThing = MainScanRate*2000/TB_scanRate ' 15000 counts (15000*0.12s/60min/s = 1 min)
faster scan time for testing

'''Flow Gauges''''''''''''''''
'Scan(Interal, Units, BufferOption, Count)
 Scan (TB_scanRate,mSec,1,0)
      'delete Rain Gauge

      'Sublysimeters
      'PulseCount(Dest, Reps, PChan, PConfig, POption, Mult, Offset) - control port
configured as a switch closure input
      PulseCount (TB_24,1,1,2,0,1.0,0)  'P1 = TB_24 (sublysimeter 1)
      TB_24_total=TB_24_total+TB_24
      If TB_24 >0 then
          CallTable CBa_TB_Cluster_1
      Endif

      PulseCount (TB_25,1,2,2,0,1.0,0)  'P2 = TB_25 (sublysimeter 2)
      TB_25_total=TB_25_total+TB_25
      If TB_25 >0 then
         CallTable CBa_TB_Cluster_2
      Endif

      PulseCount (TB_26,1,16,2,0,1.0,0) 'C6 = TB_26 (sublysimeter 3)
      TB_26_total=TB_26_total+TB_26
      If TB_26 >0 then
```

```
         CallTable CBa_TB_Cluster_3
      Endif

      'Basal Drain
      PulseCount (Drain,1,17,2,0,1.0,0) 'C7 = TB_27 (whole pile outflow)
      Drain_total=Drain_total+Drain
      if Drain >0 then
         CallTable CBa_TB_Basal_Drain
      endif

        count = count + 1
        if count > modThing
            Call getData()
      Calltable CBa_Temperature
      Calltable CBa_Temp_mv
      Calltable CBa_EC_Tcorr
      Calltable CBa_EC_volt
      Calltable CBa_pH_volt
            count = 0
        EndIf

NextScan
```

Appendix D - Effect of High Solute Concentration During Freezing

High solute concentrations of the pore-water can result in a delay in the onset of freezing conditions by freezing point depression (Godwalt et al., 1999; Elberling, 2001; Elberling, 2005). Water residing in the piles for longer durations, are expected to contain higher concentrations of dissolved constituents due to greater interaction with exposed mineral surfaces. This may be observed by the presence of fluid pore-water beyond the onset of freezing conditions. Analyzing VMC, indicated by the TDR probes, coincidently with the temperatures from nearby thermistors, should indicate fluid pore-water if the TDR probes continued reading after thermistors began recording temperatures below freezing. Results of this comparison between VMC and thermistor readings are presented in **Figures D-1** through **Figure D-8** and described below. The EC measured from adjacent, or nearby, soil water solution samplers (SWSS) is also plotted to correlate the EC of the pore-water with presence of fluid as indicated by the VMC.

Water with higher EC can cause interference with TDR readings due to loss of signal amplitude and the introduction of a higher imaginary permittivity component, which can be neglected up to 5,000 $\mu S \cdot cm^{-1}$ (Nichol, 2002). Dissolved ions in pore-water act to decrease permittivity of the water (which would suggest lower moisture content by TDR) however the increase in the imaginary component acts to increase permittivity (which would suggest higher moisture content by TDR) (Nichol 2002). The high resistance coating on the central rod of the three-rod design can be used with pore-water electrical conductivities at least as high as 70,000 $\mu S \cdot cm^{-1}$and still allow waveforms to be interpreted. Nichol (2002) found a 0.4 nano-second (ns) delay in travel time between solutions of 1 and 70,000 $\mu S \cdot cm^{-1}$ (i.e., in higher EC pore-water, the shorter travel time without correction would suggest lower water content).

From this comparison, there was no evidence of pore-fluids that remained in a liquid state following the onset of freezing temperatures. No location continued to record VMC once temperatures decreased below zero degrees Celsius. Several notes regarding the plots are provided in the following:

- At Type III test pile on Face 3, 2 m south of the centre line (33S2) in 2007 it appears that water remained fluid following the onset of freezing (**Figure D-4**), where TDR continued to record VMC for about 40 days after the temperature fell below zero degrees Celsius. However, as the nearest

thermistor is actually from Face 2, and TDR are on Face 3 (i.e., TDR closer to the exterior of the test pile as compared to the thermistors); therefore, this provides a weak comparison. The EC at around this depth was recorded as 26 $mS \cdot cm^{-1}$, and other areas have been noted with higher EC without the TDR probes continuing to record VMC (e.g., at Type III test pile on Face 1, 2 m south of centre (31S2)).

- At the Covered test pile, on Face 2, 2 m east of centre (C2E2) at 6 m depth, although it appears that the TDR probe is still recording moisture content when temperature is below zero, the actual temperature experienced is not below zero. The thermistor is from a shallower depth (5 m) as compared to the TDR probe depth (6 m) (**Figure D-5**).

The VMC from TDR probe readings coupled with temperature data were not successful in identifying solute controlled freezing point depression. Although the results were not successful, the analysis should not be interpreted as suggesting that no relationship exists; instead more robust methods or data, or both, are needed to observe the effect.

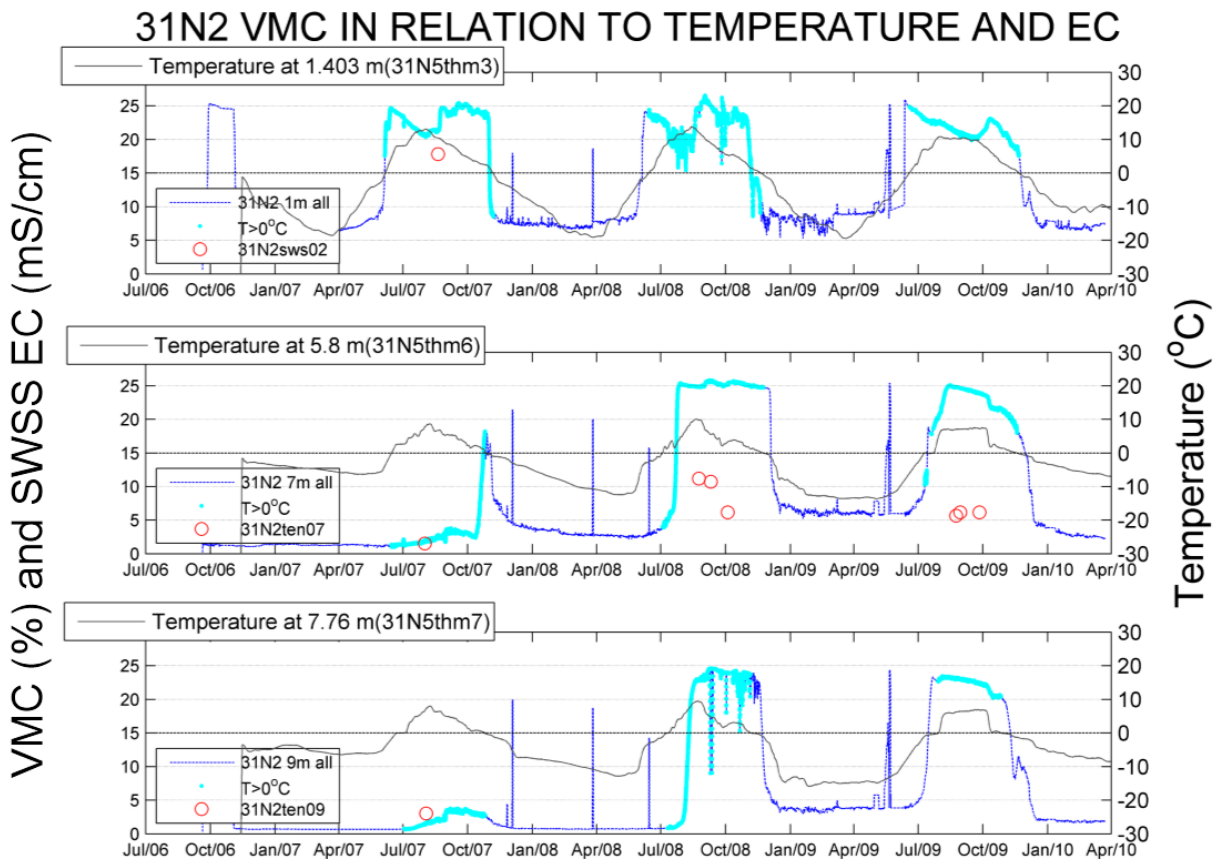

Figure D-1: Observed relationship between VMC, temperature and EC for instruments installed within the Type III test pile on Face 1 (interior) north of the pile centerline.

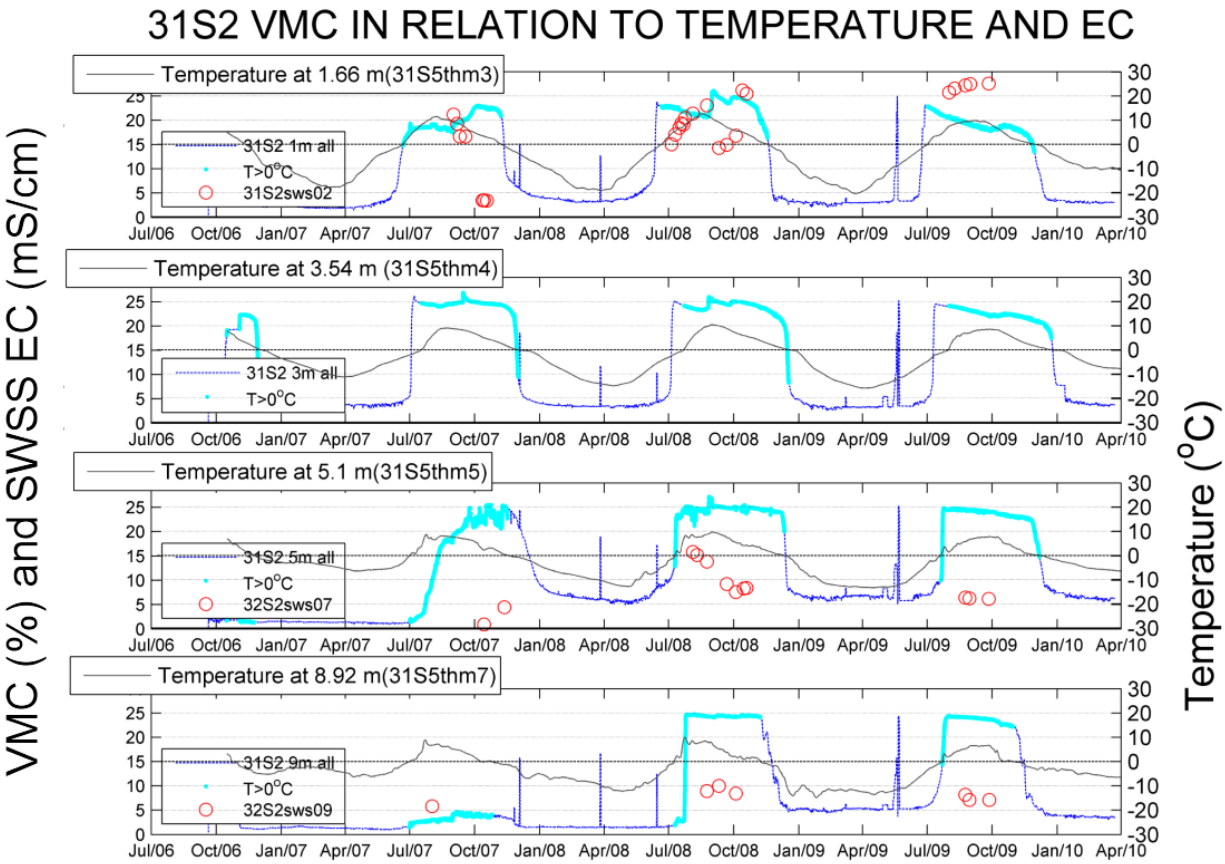

Figure D-2: Observed relationship between VMC, temperature and EC for instruments installed within the Type III test pile on Face 1 (interior) south of the pile centerline.

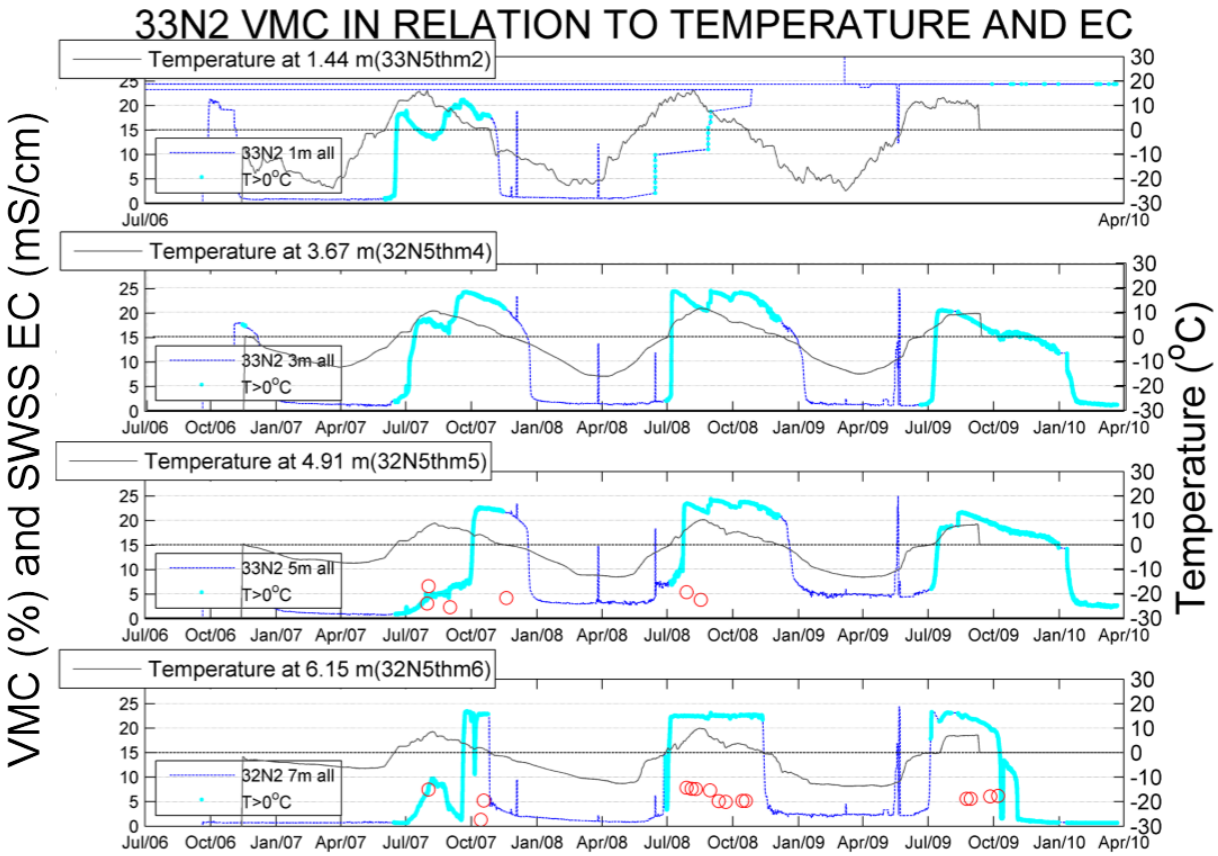

Figure D-3: Observed relationship between VMC, temperature and EC for instruments installed within the Type III test pile on Face 3 (central) north of the pile centerline.

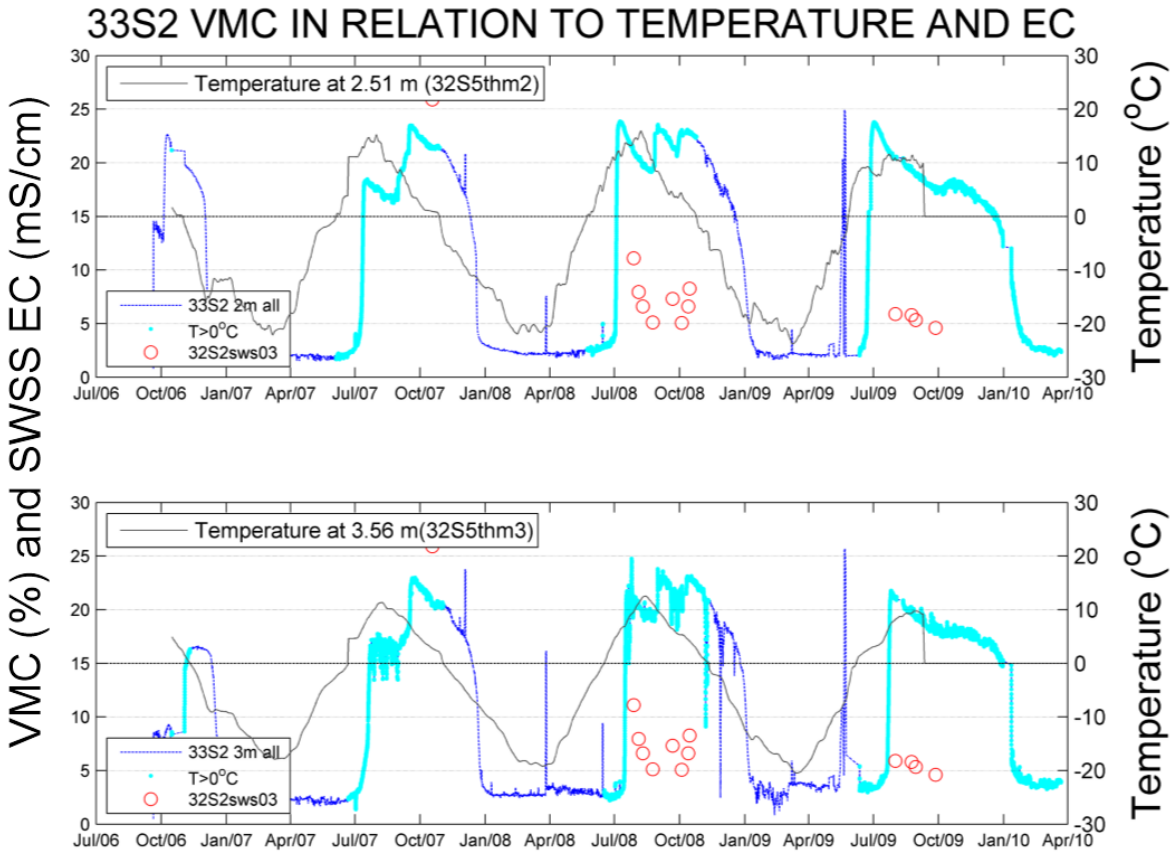

Figure D-4: Observed relationship between VMC, temperature and EC for instruments installed within the Type III test pile on Face 3 (central) south of the pile centerline.

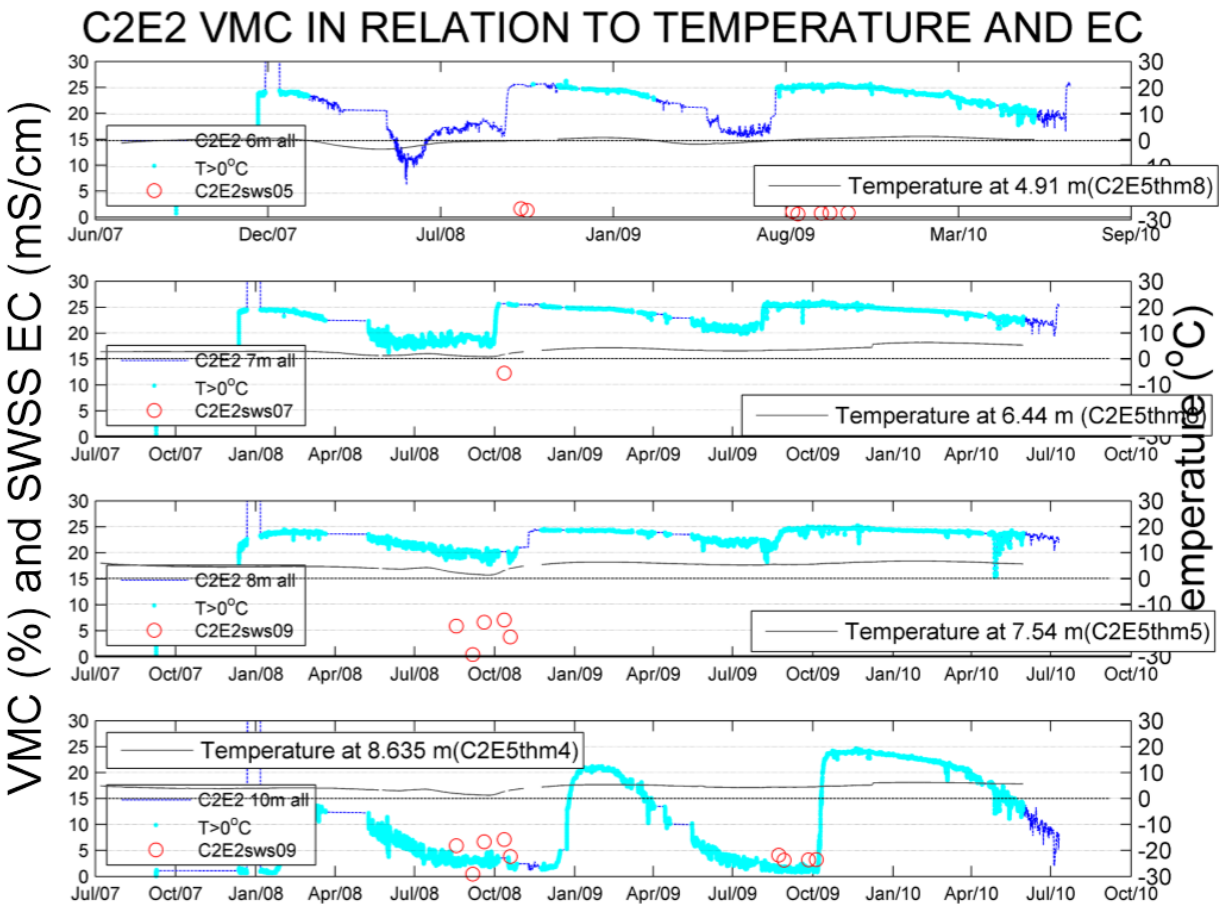

Figure D-5: Observed relationship between VMC, temperature and EC for instruments installed within the Covered test pile on Face 2 (central) east of the pile center line.

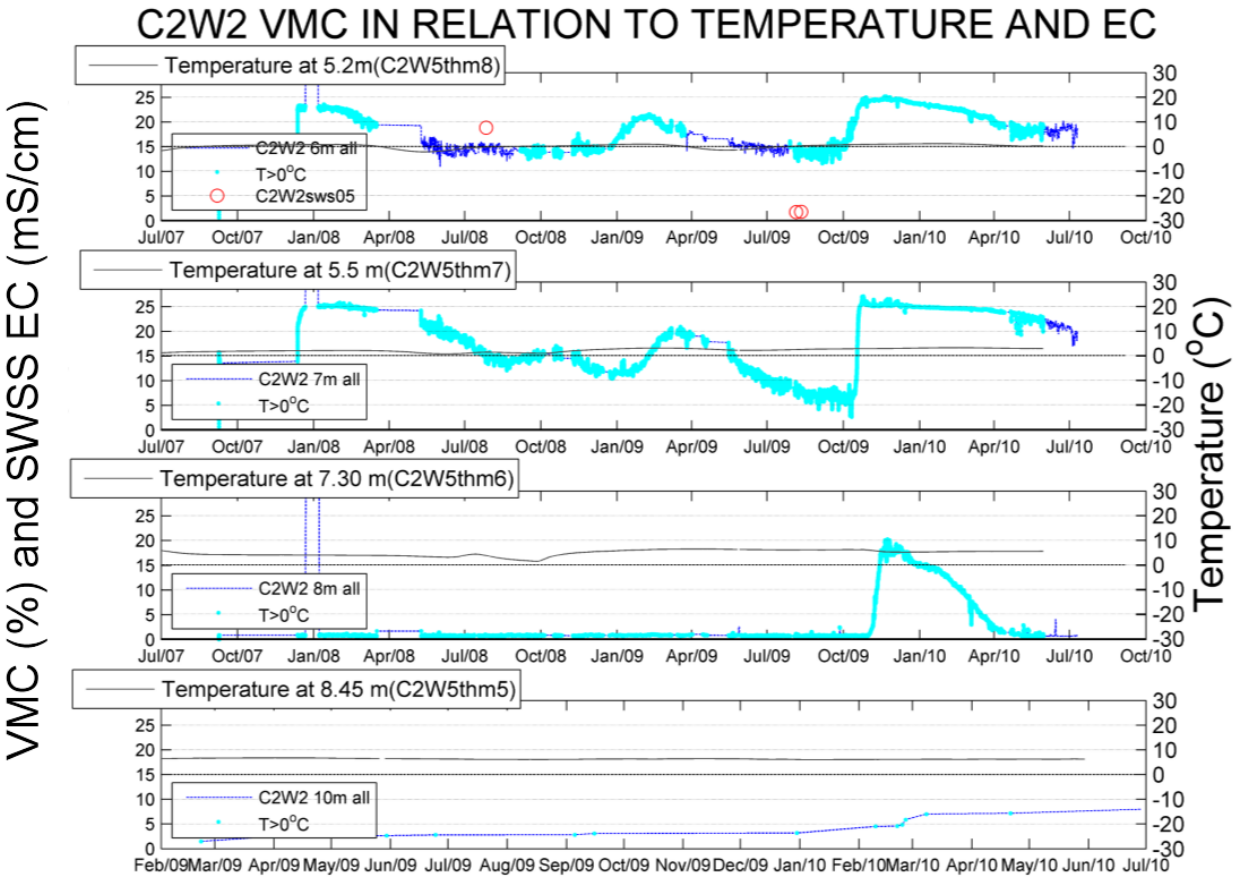

Figure D-6: Observed relationship between VMC, temperature and EC for instruments installed within the Covered test pile on Face 3 (central) west of the pile center line.

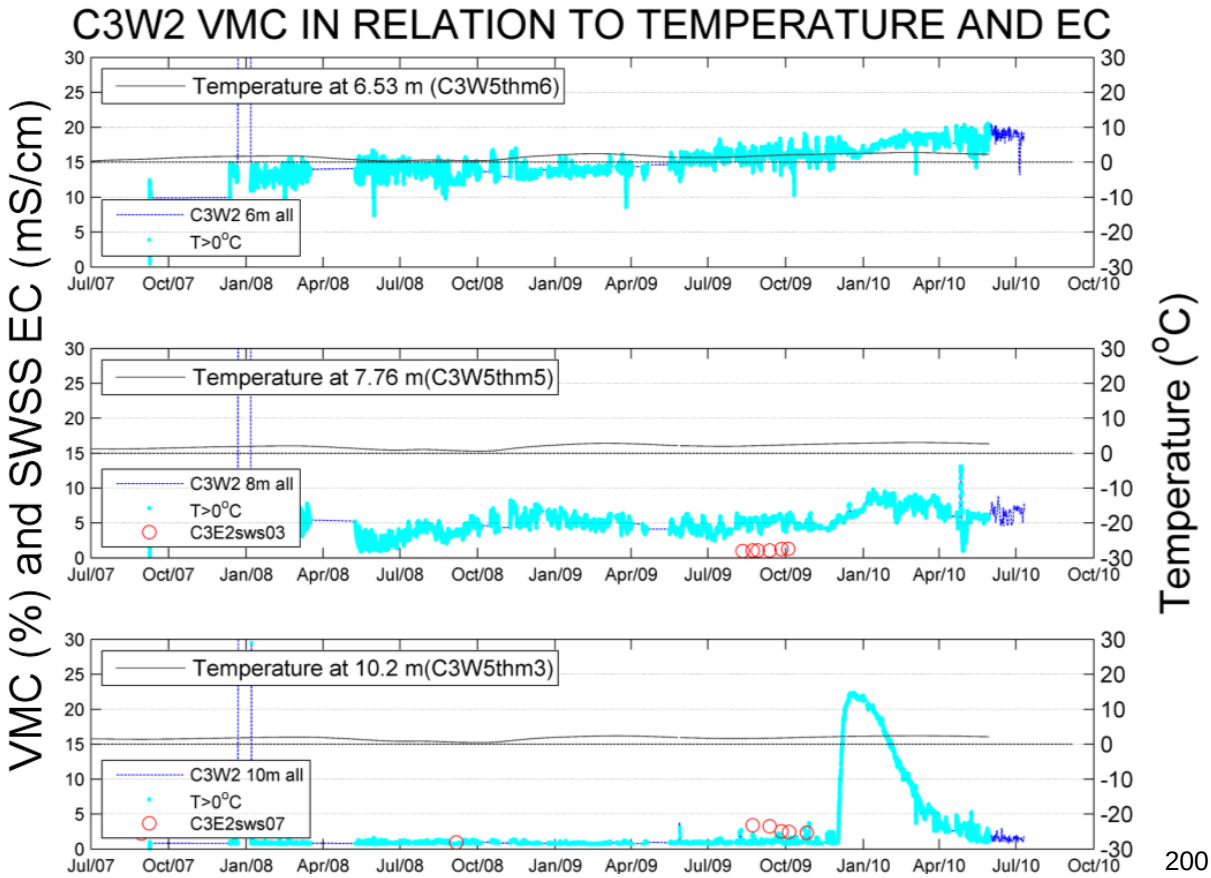

Figure D-7: Observed relationship between VMC, temperature and EC for instruments installed within the Covered test pile on Face 3 (central) west of the pile center line.

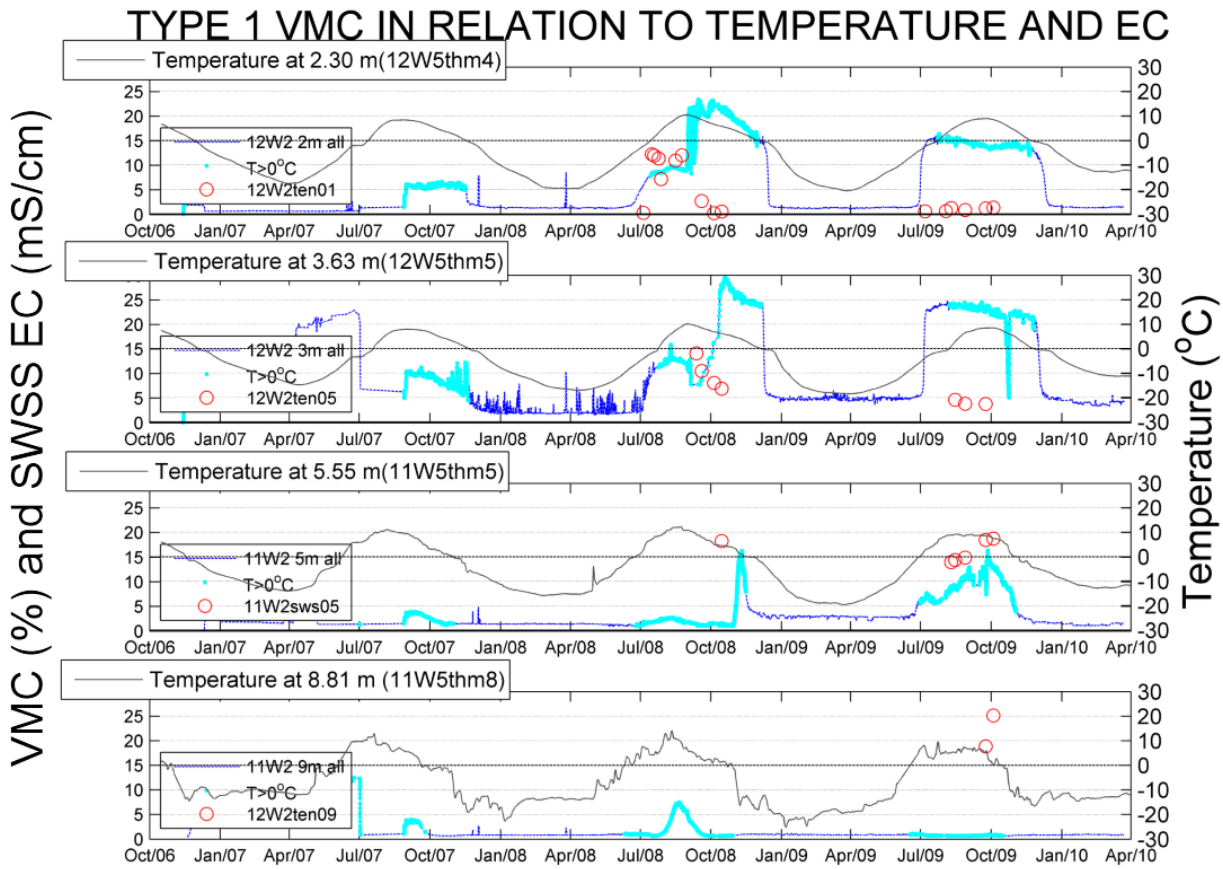

Figure D-8: Observed relationship between VMC, temperature and EC for instruments installed within the Type I test pile on Face 1 and 2 west of the pile center line.

Appendix E - Drainage Differences

Drainage Differences for Type I and Type III Test Piles

The volumetric discharge recorded at the Type III test pile in 2008 and 2009 is 3.8 times greater than the discharge recorded at the Type I test pile. The volume of water applied through irrigation events during 2006 and 2007 to the Type III test pile totals 70 m^3. The difference in the discharge volume between the two piles, 170 m^3, is 2.4 times the volume accounted for directly by applied rainfall events. In each of 2008 and 2009 only a fraction (39% and 10%) of the volume of outflow that reported to the basal drain at the Type III test pile reported to the basal drain at the Type I test pile.

This also may be the case for 2007, however due to the uncertain volume of outflow that occurred from the Type I test pile in 2007, it is unknown how discharge volumes compare for 2007. The discharge stopped flowing from the basal drain due to problems related to thermal expansion of the basal drain plumbing system.

Several possible reasons for the difference observed in the 2008 and 2009 dataset are reviewed. The following will look at the rationale and likelihood of each.

In Fretz's synthesis of data between 2007 and 2011, he provides a review of the difference in outflow between the Type I and Type III piles. Fretz provides several explanations for the differences in discharge. Identified in his work as potential contributors include:

- Basal drain orientation differences
- Different crush materials utilized at the base of the test piles
- Snow accumulation and infiltration differences on the batters
- Net rainfall infiltration differences
- Preferential flow differences
- Leakage from the base of the Type I test pile.

This discharge difference was evident for the data record to 2009; therefore, some additional discussion on this topic is warranted here.

Prior to 2008 there were several irrigation events, both labeled and unlabeled, on the Type III test pile (Neuner, 2009). From these rainfall events, the Type III test pile has received an additional 118.2 mm of infiltration as compared to the Type I test pile, with 57.9 mm applied in 2006 and 60.3 mm applied in 2007. This contribution of applied events was delivered to the top surface of the test pile, with an estimated wetted area footprint of, 20 m by 30 m (i.e., not the entire surface area). Therefore, the total volume of water applied to the test piles was 34.7 m^3 and 36.2 m^3 in 2006 and 2007, respectively. Applied rainfall events were performed in the central portion on the top surface of the test pile and hence water from these events must travel flow paths that are the full height of the test pile, or non-vertical flow paths along depositional faces. Consider the unlikely scenario in which all of the applied rainfall has reported to the basal drain at the Type III test pile (70.9 m^3), the applied events account for 42% of the difference between Type I and Type III total basal drain discharge for 2008 and 2009. More likely, 40 to 60% of this applied rainfall evaporated (**Section 4.2.2**), and the applied events account for between 17 and 25% of the difference between Type I and Type III discharge. The difference in reported basal drain discharge for the Type I and Type III piles are therefore not directly attributable to the manual application of water to the top surface of the test pile.

As Fretz points out, crush material used at the base of the Type I test pile includes fines, whereas the Type III test pile used 50.8 mm clean crush, which has been screened to remove grain sizes smaller than 50.8 mm. The fines within the crush may hold water that drains from the 50.8 mm clean crush. As reported by (FDA Engineering Ltd., 2008) a total of 952 m^3 of crush was used in the Type I test pile, therefore up to between 95 and 140 m^3 of water is required to raise the moisture content from the initial placement content to the field capacity within the fines, assuming a field capacity of 0.10 to 0.15 m^3/m^3.

Between 135 and 210 m^3 of water is accounted for from the 70 m^3 of water potentially sourced from the irrigation event and between 95 and 140 m^3 of water potentially retained in the fines upon wetting. Therefore, these two processes may account for the difference in outflow volume observed between the Type I and Type III test piles. However, at the estimated low end, 35 m^3 of discharge is unaccounted. Other differences in the test piles that may account for the discharge discrepancy include orientation,

basal drain configuration, test pile surface area, active zone development, and the unsaturated hydraulic conductivity of the material.

It was suspected that pile orientation might contribute to the outflow difference. The centerline of the Type III test pile is located in an east/west alignment; whereas the centerline of the Type I test pile is north/south. The construction of the piles from a central ramp creates exposed aspects that face the south, west and north at the Type III test pile whereas the Type I test pile has aspects to the west, north and east. Based on this orientation, snow accumulates on the north side of the Type III test pile due to sheltering by the position of the Type I and Type III test piles. Field observation in the winter and spring of 2010 indicates that snow accumulation is greatest on north facing slopes (**Figure 4-1 and Figure 4-2**). Due to the orientation of the test piles, about 46.7 m wide face of Type I test pile faces north, whereas, about a 53.6 m long face of the Type III is orientated northward. The southerly and western aspects receive more intense solar radiation, which results in additional sublimation. Wind direction varies so snow is scoured and redistributed from the top and batters of the test pile but the north slope of the Type III test pile is potentially more sheltered by the surroundings than the Type I test pile. However this does not appear to provide adequate explanation for the discrepancy in discharge volumes. **Figure E-1** presents individual discharge from the north and south basal drains at the Type III test pile. The design of the Type III test pile divides the basal drainage area between the north drain and the south drain, although it is uncertain as to the proportion of the catchment directed to each drain. Evident from a comparison of the discharge occurring during the spring melt is that the drainage from the north drain does not control the volumes of discharge from the Type III test pile (**Figure E-1**). Without the contribution from the Type III north drain, which appears to be dominated by snowmelt contribution, the discharge from the Type III test pile in 2008 and 2009 would still be 3.7 times that of the Type I test pile. In 2008 early season discharge (May and June) from the Type III north basal drain accounts for approximately 6 m^3 and in 2009 for approximately 4 m^3. Therefore snow accumulation on the north side of the Type III test pile does not account for the difference.

Drainage piping installed at the base of the two piles is different (Fretz, 2013; Smith et al., 2013), with the Type I test pile plumbing being placed diagonally across the base and the Type III test pile plumbing

aligned along the perimeter. The Type I liner slopes to the southwest corner at a grade of about 1.4%; whereas the Type III liner slopes at about 0.5% towards the outside edges of the test pile and drains to low points in both the southwest and northwest corners (Smith et al., 2013). The difference in the collection systems may affect drainage when the center of the test pile freezes while the perimeter remains active. That is, the Type I test pile, with the main drain orientated diagonally across the base of the test pile is potentially affected to a greater degree by gradual cooling of the test pile core, than the Type III test pile drain, situated near the perimeter of the test pile and exposed to a greater degree to seasonal temperature fluctuations.

The catchment area (surface area) of the Type I test pile is about 5,443 m^2 and approximately 5,564 m^2 for the Type III test pile; in other words the Type I test pile has 97.8% of the surface area of the Type III test pile. The estimate of surface area was determined in the commercially available computer program, Surfer, a surface mapping system, by Golden Software Inc. From the as-built drawings produced by FDA Engineering Ltd (2008), it appears that the HDPE lined basal area of the Type I test pile is 3,325 m^2 and 3,295 m^2 for the Type III test pile. Therefore, this difference in catchment area may contribute to, but does not make up the outflow difference.

Differences in the active test pile volume will influence the portion of test pile contributing to the discharge. The active volume contributing to test pile discharge was discussed in more detail in **Section 5.3**, but is briefly considered here in relation to the difference in discharge between the Type I and Type III test piles. A cooling trend between 2007 and 2009 in the Type I test pile, as compared to the Type III test pile has been observed. **Table E-1** and **Figure E-2** provide a tabulated and graphical comparison of the active volume of the test piles that contribute discharge. In 2007, the portion of unfrozen volume of the Type I test pile thawed earlier and to a greater extent than the Type III test pile. In 2008, the Type I test pile thawed to a greater extent but the duration the test pile remained at peak unfrozen volume was less than the Type IIII test pile. In 2009, the Type I test pile thawed later than the Type III test pile, remained thawed for a shorter duration and the extent of the thaw was slightly less than the Type III test pile. In 2007, the active volume of the test pile did not contribute to the discrepancy in outflow between the two piles, however in 2008 and 2009 it could provide a potential influence. As described below in **Section 5.3**

on thermal controls, when outflow was normalized to active portion of the test pile, normalized discharge at the Type III test pile remained greater than normalized discharge at the Type I test pile.

Eight thermistors located in the 4 by 4 m lysimeters in the Type III test pile, and two thermistors in Type I test pile lysimeters, show distinct seasonal changes indicating their location is not controlled by heat trace located at the base of the lysimeters. Whereas, the thermistors located in the 2 by 2 m lysimeters fluctuate around a similar value to the heat trace setting, indicating their locations is controlled by the heat trace in the vicinity. Based on a comparison between 2008 and 2009 with eight Type III locations and two Type I locations, the date the lysimeters, or area around the thermistor in each lysimeters, reached a temperature greater than 0^{o}C increased by an average of 18 days at the Type III test pile compared to 44.5 days at the Type I test pile (**Table E-2**). The central lysimeters thawed an average of approximately 8 to 9 days later in 2009 compared to the lysimeters situated under the batters. A portion of the volumetric difference in discharge reporting to the basal drain could be due to the increased water storage in a solid state. Though areas of the Type I test pile may have remained below zero for a longer duration in 2009 pathways are observed to be available for water flow. For example, the central 16 m^2 eastern Type I basal collection lysimeter and batter 4m^2 western Type I basal collection lysimeter (1BEClys4N and 1BWBlys2N, respectively) recorded discharge in late June and July/August.

Although outside of the period of this study, the basal drain at the Type I test pile did not begin to report outflow in 2010 until July 27. Drainage began following after an upward adjustment of the temperature setting on the heat trace buried within the pile. No such adjustment was performed (or required) in the Type III test pile. A difference in grain size, aspect/orientation, or convection, may promote the cooling of the Type I test pile base/core, causing infiltrated moisture to be stored in a solid state and reducing discharge.

The difference in outflow volumes could be also be explained by increased evaporation from the Type I test pile relative to the Type III test pile. The lower VMC of the Type I test pile will result in it having an effectively lower unsaturated hydraulic conductivity than the Type III test pile given a similar grain size distribution. The result will be a slower downward movement of the water migrating through the matrix following a rainfall event, therefore facilitating a greater portion of water available for evaporation within

the upper 0.5 m of the waste rock. The grain size of the two piles is similar, however the matrix material of the Type I rock is slightly finer grained (Neuner et al., 2013; Smith et al., 2013), which controls the movement of moisture through the piles. Estimates of the saturated hydraulic conductivity have been made on 18 samples of the finer than 5 mm fraction (Neuner et al., 2013). The geometric mean of the saturated hydraulic conductivity determined from the samples from the Type I test pile is 7.8×10^{-6} $m \cdot s^{-1}$ as compared to 9.7×10^{-6} $m \cdot s^{-1}$ from the Type III test pile samples. Under similar conditions the piles are expected to inherently have similar hydraulic properties, although the less than 5 mm fraction in the Type I test pile has a slightly lower average saturated hydraulic conductivity. The drier material will exhibit an even lower unsaturated hydraulic conductivity. Slower moving infiltrating moisture will be exposed to greater evaporative losses. As the Type III test pile was "wet-up" with artificial rainfall events in 2006 and 2007, it remains at a state with higher moisture content. There is no VMC data within the upper 0.5 or 1 m of the Type I test pile, so instead a comparison of VMC at 2 m depth indicates the average VMC in the Type I test pile (TDR probe 11W2 2m), during the active season is 3.7, 10.4 and 9.7 $m^3 \cdot m^{-3}$ in 2007, 2008 and 2009. The average VMC at the 2 m depth in the Type III test pile (TDR probe 33S2 2m), during the active season is 1.4, 15.6 and 16.7 $m^3 \cdot m^{-3}$ in 2007, 2008 and 2009.

The difference in outflow volume observed between the Type I and Type III test piles may be accounted for between the applied rainfall events and the fluid retained in the fine-grained material contained in the crush material backfilled around the pluming for the basal drain in the Type I test pile. Additional influences that may account for the discrepancy in discharge include orientation, basal drain configuration, test pile surface area, active zone development, and the unsaturated hydraulic conductivity of the material.

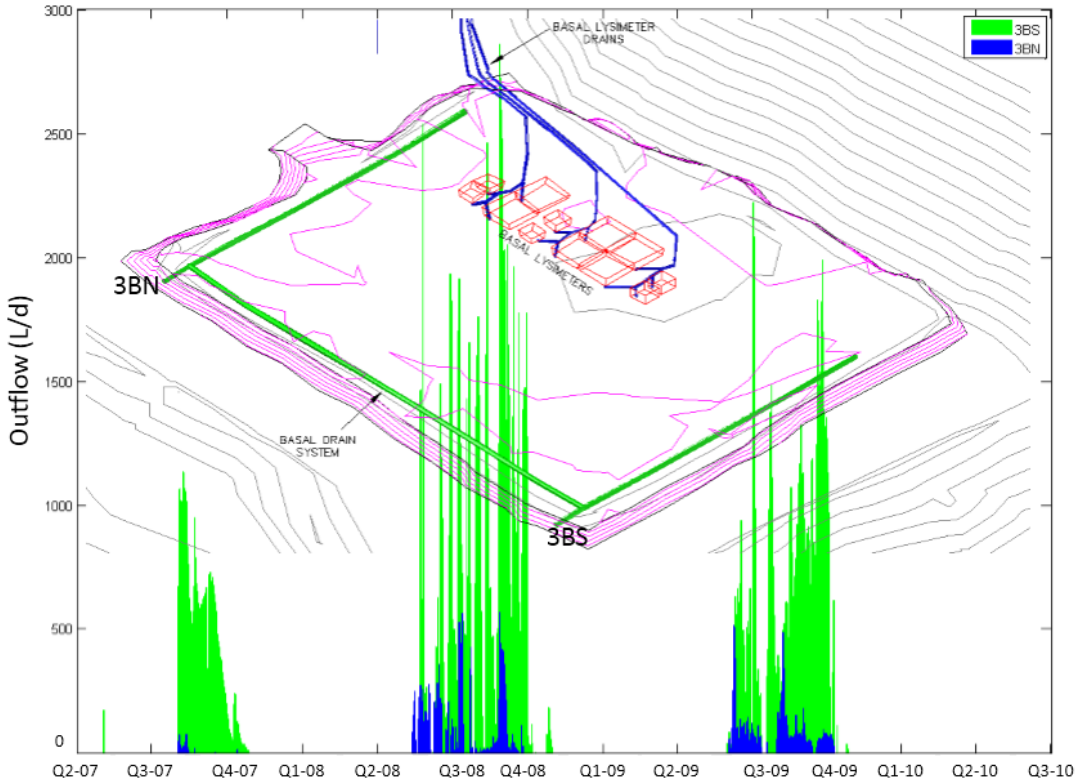

Figure E-1: Comparison of discharge volume between the north (3BN) and south (3BS) basal drains at the Type III test pile for 2007 through 2009.

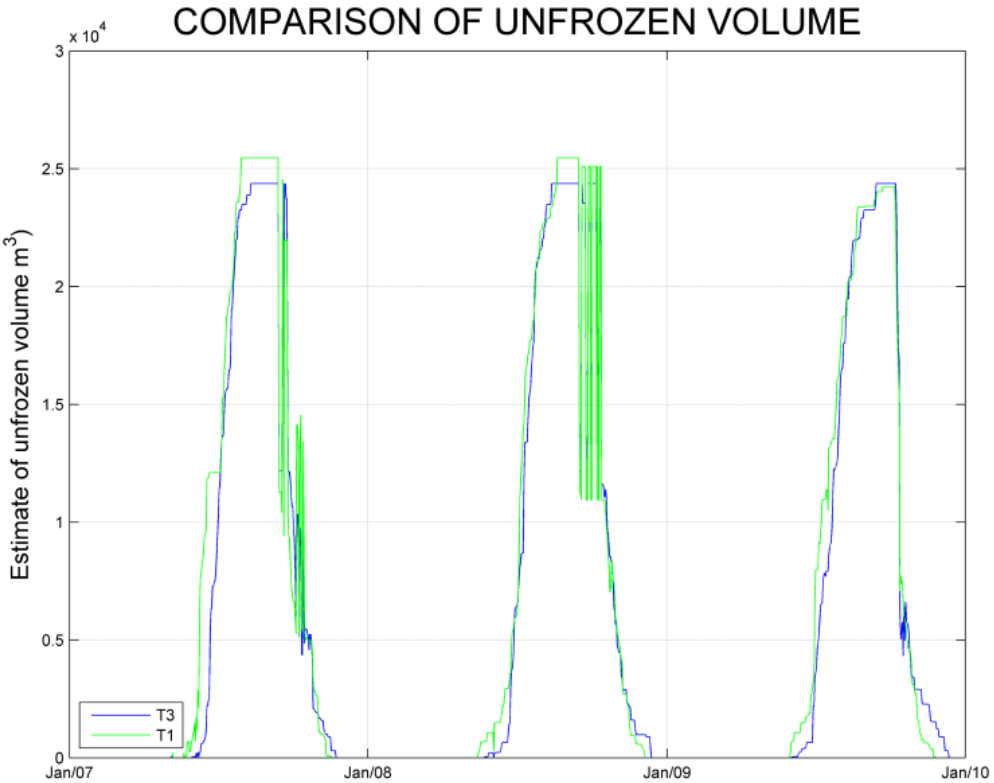

Figure E-2: Comparison of estimated unfrozen volume between Type I and Type III test pile between 2007 and 2009. Note that units on y-axis are x104.

	Calculated Pile Volume (m^3)	Estimated Peak Active Volume As Percent of Pile Volume (%)		
		2007	2008	2009
Type III test pile	24,980	98	98	98
Type I test pile	26,240	97	97	92

Table E-1: Estimated peak active volume of the test piles for 2007 through 2009.

Lysimeter Location	2008 Date Temperature Recorded Above 0°C	2009 Date Temperature Recorded Above 0°C	Days Difference Between 2008 and 2009
Type III			
3BNBlys4E	Aug. 6, 2008	Aug. 23, 2009	17
3BNBlys4W	Aug. 8, 2008	Aug. 21, 2009	13
3BNBlys4E	Aug. 7, 2008	Aug. 23, 2009	16
3BNBlys4W	Aug. 6, 2008	Aug. 16, 2009	10
3BNClys4W	Aug. 14, 2008	Sept. 8, 2009	25
3BNClys4E	Aug. 21, 2008	Sept. 15, 2009	25
3BNClys4W	Aug. 20, 2008	Sept. 5, 2009	16
3BNClys4E	Aug. 27, 2008	Sept. 21, 2009	25
Type I			
T1	Before July 1, 2008	Aug. 13, 2009	>43
T1	Aug. 18, 2008	Oct. 3, 2009	46

Table E-2: Timing that basal collection lysimeters became active in 2008 and 2009 based on thermistor readings located beyond the influence of installed heat trace.

Drainage Differences Between Eastern and Western Type I AZLs

The Type I eastern AZL consistently reports lower volumetric discharge suggesting the grain size difference visible in **Figure 1-6** affects infiltration. It is postulated that the finer-grained surficial material at the eastern lysimeter reduces the rate of infiltration. This increases the portion of precipitation which evaporates as compared to the coarser-grained surface at the western lysimeter. In contrast, the coarser-grained surface at the western lysimeter is interpreted to facilitate infiltration, and therefore reduce evaporation, as the infiltrating wetting front will percolate to greater depths more rapidly as compared to the eastern lysimeter. This positive feedback loop reinforces itself, as drier soil will comparatively have a lower unsaturated hydraulic conductivity than wetter soil with the same grain size distribution. Soil with lower unsaturated hydraulic conductivity will slow water migrating through the matrix, allowing additional time for evaporation therefore keeping the soil drier.

During construction of the western Type I AZLs, the container split near its top end and was subsequently repaired (Neuner, 2009). This tear may permit infiltration to follow a route that does not report to the drainage collection system. This is not believed to be the case based on the quantity of discharge following the August 25/26, 2008 rainfall event. Checks were made on the accuracy of the tipping bucket to rule out equipment malfunctions affecting the recorded outflow.